TRANSCRIPTIONAL REGULATION BY DFOS AND BMP-SIGNALING SUPPORT TISSUE INVASION OF *DROSOPHILA* IMMUNE CELLS

by

Stephanie Wachner

April, 2022

A thesis presented to the
Graduate School
of the
Institute of Science and Technology Austria, Klosterneuburg, Austria
in partial fulfillment of the requirements
for the degree of
Doctor of Philosophy

Committee in charge:
Mario de Bono, Chair
Daria Siekhaus
Anna Kicheva
Michael Sixt
Rik Derynck

The thesis of Stephanie Wachner, titled *Transcriptional regulation by Dfos and BMP-signaling support tissue invasion of Drosophila immune cells*, is approved by:

Supervisor: Daria Siekhaus, IST Austria, Klosterneuburg, Austria

Signature: _____

Committee Member: Anna Kicheva, IST Austria, Klosterneuburg, Austria

Signature: _____

Committee Member: Michael Sixt, IST Austria, Klosterneuburg, Austria

Signature: _____

Committee Member: Rik Derynck, UCSF, San Francisco, USA

Signature: _____

Exam Chair: Mario de Bono, IST Austria, Klosterneuburg, Austria

Signature: _____

signed page is on file

IST Austria Thesis, ISSN: 2663-337X

I hereby declare that this dissertation is my own work and that it does not contain other people's work without this being so stated; this thesis does not contain my previous work without this being stated, and the bibliography contains all the literature that I used in writing the dissertation.

I declare that this is a true copy of my thesis, including any final revisions, as approved by my thesis committee, and that this thesis has not been submitted for a higher degree to any other university or institution.

I certify that any republication of materials presented in this thesis has been approved by the relevant publishers and co-authors.

Signature: _____

Stephanie Wachner

April 14, 2022

signed page is on file

Abstract

The infiltration of immune cells into tissues underlies the establishment of tissue-resident macrophages and responses to infections and tumors. However, the mechanisms immune cells utilize to collectively migrate through tissue barriers *in vivo* are not yet well understood. In this thesis, I describe two mechanisms that *Drosophila* immune cells (hemocytes) use to overcome the tissue barrier of the germband in the embryo. One strategy is the strengthening of the actin cortex through developmentally controlled transcriptional regulation induced by the *Drosophila* proto-oncogene family member Dfos, which I show in Chapter 2. Dfos induces expression of the tetraspanin TM4SF and the filamin Cher leading to higher levels of the activated formin Dia at the cortex and increased cortical F-actin. This enhanced cortical strength allows hemocytes to overcome the physical resistance of the surrounding tissue and translocate their nucleus to move forward. This mechanism affects the speed of migration when hemocytes face a confined environment *in vivo*.

Another aspect of the invasion process is the initial step of the leading hemocytes entering the tissue, which potentially guides the follower cells. In Chapter 3, I describe a novel subpopulation of hemocytes activated by BMP signaling prior to tissue invasion that leads penetration into the germband. Hemocytes that are deficient in BMP signaling activation show impaired persistence at the tissue entry, while their migration speed remains unaffected.

This suggests that there might be different mechanisms controlling immune cell migration within the confined environment *in vivo*, one of these being the general ability to overcome the resistance of the surrounding tissue and another affecting the order of hemocytes that collectively invade the tissue in a stream of individual cells.

Together, my findings provide deeper insights into transcriptional changes in immune cells that enable efficient tissue invasion and pave the way for future studies investigating the early colonization of tissues by macrophages in higher organisms. Moreover, they extend the current view of *Drosophila* immune cell heterogeneity and point toward a potentially conserved role for canonical BMP signaling in specifying immune cells that lead the migration of tissue resident macrophages during embryogenesis.

Acknowledgments

I would like to thank the Austrian Academy of Sciences (DOC fellowship, code 24800), the IST Graduate School, the Erasmus placement initiative, and the Ludwig Boltzmann Society (Expert Internship fellowship from the Career Center) for funding.
Additionally, I would like to thank the following for reagents: The *Drosophila* Genomics Resource Center supported by NIH grant 2P40OD010949-10A1 for plasmids, K. Brückner, G. Pyrowolakis, F. Schweisguth, D. Andrew, B. Stramer, M. Uhlirova, O. Schuldiner, the Bloomington *Drosophila* Stock Center supported by NIH grant P40OD018537 and the Vienna *Drosophila* Resource Center for fly stocks, FlyBase (Thurmond et al., 2019) for essential genomic information, and the BDGP *in situ* database for data (Tomancak et al., 2002, 2007). For antibodies, I thank the Developmental Studies Hybridoma Bank, which was created by the Eunice Kennedy Shriver National Institute of Child Health and Human Development of the NIH, and is maintained at the University of Iowa. I thank the Vienna BioCenter Core Facilities for RNA sequencing and analysis and the Life Scientific Service Units at IST Austria for technical support and assistance with microscopy and FACS analysis.

I thank Daria Siekhaus for giving me the opportunity to perform the research projects in her group, and all past and present members of the Siekhaus group, as well as all co-authors for their collaboration, and my committee members for discussion of the research projects.

I would also like to thank my manager Dr. Christian Lenz and my mentor Dr. Sylvia Nanz at Pfizer for their support and encouragement.

On a more personal note, I would like to thank my family and friends for their love and support throughout all these years. I am very grateful for all wonderful and inspiring people I met during my PhD. However, there are special souls that I would like to highlight here. Big thanks go to my PhD buddies Sina and Shamsi as well as my Heidelberg crew Doro, Marleen and especially Christian, who helped with proof-reading. I thank Anni and Sabrina for their friendship throughout all these years. Moreover, I would like to thank my one and only pack from Polearts, especially my instructors Desi and Fanny, who created the time and space to allow my brain to not think about cell migration. Moreover, from the bottom of my heart, I thank my boyfriend Manuel for standing by my side during these very challenging times.
Moreover, I would like to express my gratitude for the people in my life, who left this world far too young and without whom I would not have grown into the person I am today: Matthias, Steffi, and Katja. Thank you!

Lastly, unconventionally, I thank my younger self for choosing these challenges and working through them.

About the Author

Stephanie Wachner completed a BSc in Biosciences and a MSc in Molecular Biosciences at the University of Heidelberg, Germany, before joining IST Austria Graduate School in September 2015. Her main research interests include cellular mechanisms that govern immune cell migration in a living organism and the underlying genetics. She worked on the research project “Fos regulates macrophage infiltration against surrounding tissue resistance by a cortical actin-based mechanism in *Drosophila*”, and has published these results as a shared first-author in the journal *PLOS Biology* in 2022. During her PhD studies, Stephanie has also presented her research results in an oral presentation at the *European Drosophila Research Conference (EDRC)* in Lausanne in 2019, and through poster presentations at regional and international research meetings. In summer 2021, Stephanie performed an Expert internship in the medical department of Pfizer. Since December 2021, she works as a Vaccines Manager Medical Lead at Pfizer Corporation in Austria.

List of Publications Appearing in Thesis

1. Belyaeva, V.*, Wachner, S.*, Gyoergy, A.*, Emtenani, S., Gridchyn, I., Akhmanova, M., Linder, M., Roblek, M., Sibilia, M., & Siekhaus, D. (2022). Fos regulates macrophage infiltration against surrounding tissue resistance by a cortical actin-based mechanism in Drosophila. **PLoS Biology**, 20(1), e3001494. https://doi.org/10.1371/JOURNAL.PBIO.3001494

2. Gyoergy, A., Roblek, M., Ratheesh, A., Valoskova, K., Belyaeva, V., Wachner, S., Matsubayashi, Y., Sánchez-Sánchez, B. J., Stramer, B., & Siekhaus, D. E. (2018). Tools allowing independent visualization and genetic manipulation of Drosophila melanogaster macrophages and surrounding tissues. **G3: Genes, Genomes, Genetics**, 8(3). https://doi.org/10.1534/g3.117.300452

3. Wachner, S., Cattenoz, P., Bykov, A., György, A., Belyaeva, V., Giangrande, A., Cochella, L., Siekhaus, D. E. (2022) BMP activates a subpopulation of macrophages that lead efficient tissue infiltration in *Drosophila* embryos. Manuscript in preparation.

* These authors contributed equally.

Table of Contents

List of Figures by Chapter

Chapter 1: INTRODUCTION

Chapter 2: FOS REGULATES MACROPHAGE INFILTRATION AGAINST SURROUNDING TISSUE RESISTANCE BY A CORTICAL ACTIN-BASED MECHANISM IN *DROSOPHILA*

Chapter 3: BMP ACTIVATES A SUBPOPULATION OF MACROPHAGES THAT LEAD EFFICIENT TISSUE INFILTRATION IN *DROSOPHILA* EMBRYOS

List of Tables

List of Symbols/Abbreviations

Actβ	Activinβ
AGM	aorta gonad mesonephros
AML	acute myeloid leukemia
AMP	anti-microbial peptide
Babo	Baboon
BDGP	Berkeley Drosophila Genome Project
BLAST	Basic Local Alignment Search Tool
BMP	bone morphogenetic protein
CAF	cancer associated fibroblasts
cdc42	cell division protein 42
cDNA	complementary DNA
CIL	contact inhibition of locomotion
CNS	central nervous system
Col IV	Collagen type IV
Crq	croquemort
dad	Daughters against dpp
daw	dawdle
DE-Cad	Drosophila ectodermal-Cadherin
DEG	differentially expressed gene
Dfos	Drosophila Fos proto-oncogene
Dia	Diaphanous
DN-Cad	Drosophila neuronal-Cadherin
Dpp	Decapentaplegic
E(spl)C	enhancer of split complex
ECM	extracellular matrix
EGF	Epidermal growth factor
EMT	epithelial to mesenchymal transition
FACS	Fluorescence-activated cell sorting
Fas2 and Fas3	Fasciclin2 and Fasciclin3
FGF	fibroblast growth factor
FOG	Friend of GATA
GATA	GATA-binding transcription factor family
gb	germband
gbb	glass bottom boat
gcm	glial cells missing
GEF	Guanine nucleotide exchange factors
GFP	green fluorescent protein
Hemo	hemocyte
Hes1/Hey	Hairy And Enhancer Of Split 1/ Hes Related Family BHLH Transcription Factor with YRPW Motif
HSC	hematopoietic stem cell
ICAM	intercellular adhesion molecule
ID1	Inhibitor of DNA binding 1
if	Inflated
IMD	immune deficiency

I-Smad	inhibitory Smad
JAK/STAT	Januskinase/Signal Transducers and Activators of Transcription
KLF4	Krüppel-like factor 4
LE	leading edge
Lz	Lozenge
mac	macrophage
Mad/ P-Mad	Mothers against dpp/ phosphorylated Mad (active)
mav	maverick
M-CSF	macrophage colony stimulating factor
Med	Medea
Mipp1	Multiple inositol polyphosphate phosphatase 1
MMP	matrix metalloproteases
mRNA	Messenger RNA
myo	myoglianin
mys	myospheroid
nls	nuclear localization signals
PDGF	platelet-derived growth factor
PL	plasmatocyte
PPO	Prophenoloxidas
PSC	posterior signaling center
put	punt
Pvf	PDGF- and VEGF-related factor
PVR	PDGF- and VEGF-receptor related
RNA	ribonucleic acid
RNAi	RNA interference
R-Smad	receptor Smad
sax	saxophone
scw	screw
Smox	Smad on X
srp	serpent
TAM	tumor associated macrophages
TGFβ	transforming growth factor β
Tkv/Tkv^{DN}/Tkv^{CA}	thickveins/thickveins $^{\text{dominant negative}}$/ thickveins $^{\text{constitutively active}}$
TNF	tumor necrosis factor
TRiP	Transgenic RNAi Project
Tsp	Tetraspanin
ush	u-shaped
VCAM	vascular cell adhesion molecule
VDRC	Vienna Drosophila Resource Center
VEGF	vascular endothelial growth factor
vkg	viking
vnc	ventral nerve cord
WB	western blot
wit	wishful thinking

1 Introduction

1.1 THE RELEVANCE OF CELL MIGRATION IN DEVELOPMENT AND DISEASE

1.1.1 Mechanisms of cell migration during development

The formation of a complex multicellular organism relies on the well-orchestrated and controlled organization of cell masses. According to the famous biologist Lewis Wolpert, it is not birth, marriage, or death, but gastrulation which is truly the most important time in your life. Without the ability of cells to migrate, this formation of the three germ layers could not happen. Furthermore, during the subsequent phases of embryonic development, cells interact with each other and move individually or collectively, giving rise to organs composed of complex cellular identities and functions. While we are surrounded by a plethora of different life forms, it is astonishing that basic mechanisms allowing cells to actively move from one place to another are similar within all of them.

For this migration to occur, cells use a combination of protrusion formation in the front, contraction in the back, and transmission of internally generated forces to their outside environment (Trepat et al., 2012). The formation of cell protrusions relies on the growth of an internal network of the cytoskeletal protein actin (Abercrombie et al., 1970; Cramer, 1997; Svitkina, 2018). This polymerization of actin at the leading edge is regulated via Rho-GTPases (Rac1 and CDC42) and signaling lipid phosphatidylinositol triphosphate (PIP3) (Ridley, 2015; Ridley et al., 1995; C. Y. Wu et al., 2014). In the back of the cell, non-muscle myosin causes contraction of the trailing edge, which is regulated by Rho-ROCK pathways (Etienne-Manneville, 2008; Ridley, 2015). There are three main modes of migration: mesenchymal, amoeboid, and lobopodial (a mix of the other two modes) (Yamada & Sixt, 2019).

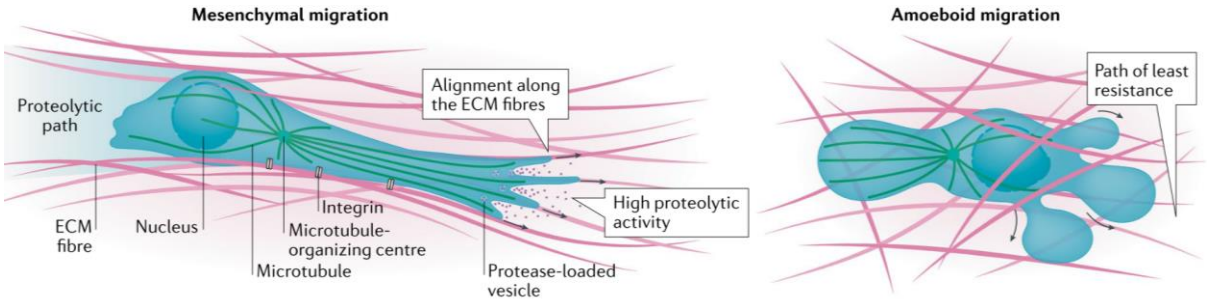

Chapter 1 Fig 1. Modes of cell migration

Mesenchymal migrating cells extend protrusions at their leading edge and align along fibers of extracellular matrix (ECM) components. They digest the ECM by secreting proteases, leaving behind a proteolytic path. The nucleus is located in the back of the cell behind the microtubule-organizing center. Integrin adhesion proteins link the cell to the outside environment. In contrast, integrin-independent amoeboid migrating cells form blebs and migrate through the pores of the ECM. They localize their nucleus in front of the microtubule-organizing center. Adapted from Yamada and Sixt, 2019.

In mesenchymal migration, cells couple their rearward internal flow of actin to the outside extracellular matrix (ECM) components via adhesion proteins such as Integrin. Integrins can associate with other adhesion proteins creating focal adhesion sites, which can form signaling clusters at the cell membrane and translate the retrograde actin flow, leading to the forward movement of the cell in 3D environments. Most cellular migration during development takes place in the context of cell collectives, in which cells interact with each other and with components of the ECM; I will describe examples of such interactions later in this section.

Another mode of migration is amoeboid migration, which does not rely on integrin-mediated adhesion and can be distinguished by rounded blebs growing out from the cell membrane due to high acto-myosin contractility and hydrostatic pressure (Paluch & Raz, 2013). Integrin-independent migration is utilized by germ cells during embryonic migration (Blaser et al., 2006; Kunwar et al., 2006). During zebrafish development, primordial germ cells migrate in an amoeboid mode, and the localization of blebs in the cell front is controlled by E-Cadherin to allow directional persistence (Grimaldi et al., 2020). In addition, zebrafish mesoderm progenitors were shown to alternate between blebs and actin-rich protrusions, and their proportion affects directional persistence (Diz-Muñoz et al., 2016). This migration strategy is also used by fast-moving leukocytes, which can migrate under high confinement and change their shape highly dynamically while still keeping their front-rear polarity (Friedl & Weigelin, 2008; Lämmermann et al., 2008; Paluch & Raz, 2013; Reversat et al., 2020). The protrusions of amoeboid migrating cells are not proteolytic, and these cells can use their nucleus to measure the space they are migrating in by nuclear positioning in the front of the cell (Lomakin et al., 2020; Renkawitz et al., 2019). This is contrary to situations in which the large nucleus localized in the cell back creates a bottleneck effect of cell migration in tight spaces, and changing nuclear deformability by alternated lamin A/C levels supports cellular squeezing (Calero-Cuenca et al., 2018).

The third migration mode that combines aspects of mesenchymal and amoeboid migration is lobopodial migration. In lobopodial migrating cells, the actin cortex breaks due to hydrostatic pressure, causing blebs at the leading edge, while at the same time, adhesion proteins allow a tight coupling to the surrounding ECM (Yamada & Sixt, 2019).

During development, cells receive signals from their environment, such as mechanical stimuli, or they interact with externally-bound molecules or soluble factors (chemokines or growth factors) that regulate their oriented migration. While long-range chemotaxis regulates the global migration of single cells, which respond to external stimuli individually, collectively migrating cells also interact with and influence each other (Khalil & Friedl, 2010; Scarpa & Mayor, 2016). Depending on their cellular identity, cells can either migrate collectively as a cohesive tissue with stable adherens adhesions and apicobasal polarity as epithelial sheets or as a mesenchymal cell collective with transient cell-cell connections (Scarpa & Mayor, 2016; Theveneau & Mayor, 2010). However, in all cases, collectively migrating cells are mechanically connected.

Examples of epithelial collective migrations are *Drosophila* tracheal morphogenesis and angiogenesis in the mouse retina, as well as *Drosophila* border cell and zebrafish lateral line migration (Scarpa & Mayor, 2016). During tracheal formation in *Drosophila*, leading tip cells are induced by the highest concentration of the chemokine *branchless* (*Drosophila* Fibroblast Growth factor, FGF), which leads to protrusion formation and initiation of collective migration. Tip cells express high levels of the ligand Delta that activates the Notch receptor in following stalk cells, leading to lateral inhibition and formation of only very small protrusions. Whereas leader cells actively migrate forward, follower cells passively intercalate and thereby

elongate the tube (Caussinus et al., 2008; Ghabrial & Krasnow, 2006; Lebreton & Casanova, 2014). A similar Delta-Notch-dependent mechanism regulates angiogenesis in mouse retina via the ligand Vascular Endothelial Growth Factor A (VEGF-A) (Hellström et al., 2007; Suchting et al., 2007). In other examples of developmental collective cell migrations, all cells within the group are actively migrating. Zebrafish lateral line morphogenesis is regulated by the chemokine CXCL12/SDF-1. Leading cells appear to undergo mesenchymal migration with a large protrusion and front-rear polarity; they only express the receptor Cxcr4b. Trailing cells are epithelial and express Cxcr4b and Cxcr7 (Valentin et al., 2007), leading to the generation of a chemokine gradient by Cxcr7 acting as a sink (Donà et al., 2013). Another example is that of *Drosophila* border cells, which migrate as an isolated epithelial cluster surrounded by nurse cells. Border cells utilize alternating leader cells, which extend protrusions that are regulated by the guidance receptor Pvr (Prasad & Montell, 2007). Similarly, the position of leader cells during neural crest migration is also transient (Kuriyama et al., 2014). Neural crest cells arise from the neural tube via epithelial to mesenchymal transition (EMT), and contact inhibition of locomotion (CIL) was shown to control differences in protrusion sizes between leader and follower cells during their migration (Carmona-Fontaine et al., 2008; Theveneau & Mayor, 2010). In addition, the complement fragment C3a controls mutual cell attraction in the front of the cell collective (Carmona-Fontaine et al., 2011). This cell-cell interaction makes migration of the collective more effective than chemotaxis of individual neural crest cells following the same chemokine (SDF-1) (Theveneau & Mayor, 2010). These examples highlight the importance of well-orchestrated cellular mechanisms within the cell collective that allow efficient migration.

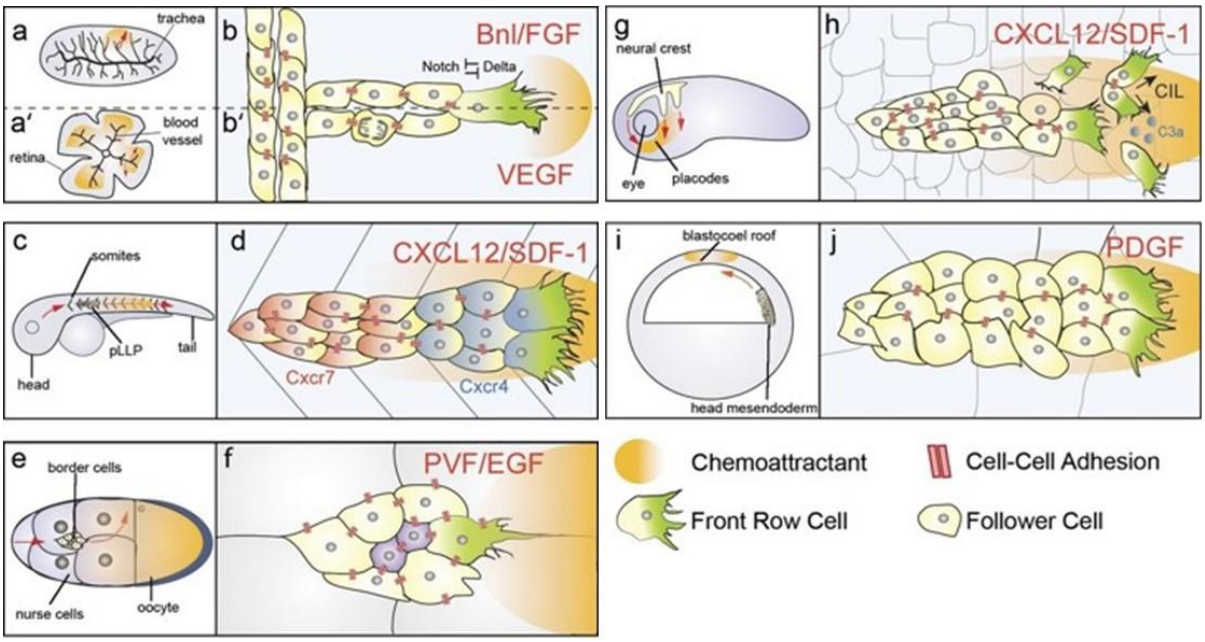

Chapter 1 Fig 2: Collective cell migration during development

(a and b) Branching morphogenesis of Drosophila trachea and during angiogenesis in mouse retina are guided by chemokines branchless (Bnl/FGF) and VEGF, which induce large protrusions in leading cells, and cause lateral cell inhibition of protrusions in follower cells through Delta-Notch signaling. **(c and d)** Leading cells of the lateral line primordium in zebrafish express receptor Cxcr4 sensing the chemokine CXCL12/SDF1, whereas cells in the back of the collective also express Cxcr7, which acts as a sink for the ligand, creating a chemokine gradient. **(e and f)** Border cells migrate through the *Drosophila* egg chamber as an epithelial cluster with two polar cells inside. The leading border cell extends protrusions between nurse cells in response to the highest concentration

of PVF and EGF chemokines. **(g and h)** Neural crest cells in *Xenopus* delaminate from the head mesoderm and migrate in response to CXCL12/SDF1. Contact inhibition of locomotion (CIL) and mutual cell attraction induced by the complement fragment C3a in the leading front allow efficient forward migration of the collective. **(i and j)** *Xenopus* mesoderm cells extend protrusions in leader cells towards the PDGF chemokine secreted by the blastocoel roof, and the rest of the collective follows via cell-cell contacts. Adapted from Scarpa and Mayor, 2016.

In this thesis, I investigated mechanisms controlling the migration of embryonic blood cells, which delaminate from the procephalic mesoderm and migrate collectively as individual cells interacting with each other. Before providing detailed insight into the regulation of their migration in section 1.3, I will give an overview of their origin, highlighting conserved factors in hematopoiesis from fly to man. As I will also discuss conserved mechanisms in immune cell tissue invasion, I will give a brief overview of tissue invasion in immune cells and cancer cells.

1.1.2 Cell migration as a crucial function of the immune system

Immune cells crucially rely on their ability to migrate in the complex 3D environment of the organism to reach sites of infection. During infection, the exit of leukocytes from the bloodstream is induced by pro-inflammatory cytokines and damage signals, which lead to leukocyte rolling along the vascular endothelium. This process is regulated by the binding of selectins. Leukocytes then attach via Integrin to adhesion molecules of the endothelial cells, such as VCAM-1 and ICAM-1. Leukocytes additionally rely on endothelial permeability by E-Cadherin modulation. Through proteolytic cleavage of ECM components, they are then able to migrate through interstitial tissues (Friedl & Weigelin, 2008; Nourshargh et al., 2010).
Moreover, during early embryonic development, blood cells colonize the organisms to establish tissue reservoirs of specialized immune cells, which not only function in the immune response but also assist normal development of tissues and help maintain tissue homeostasis (Nobs & Kopf, 2021). Tissue-resident macrophages were shown to play a role in tissue remodeling of the mammary gland epithelium during development and pregnancy (Dawson et al., 2020; Ingman et al., 2006; Y. Wang et al., 2020) and promote branching morphogenesis in kidney and alveolar development (Jones et al., 2013; Rae et al., 2007).
Examples of tissue-resident macrophages are microglia of the brain and Langerhans cells in the skin (Davies et al., 2013; Lenz & Nelson, 2018). Embryonic microglia have been shown to affect the wiring of the embryonic brain, synaptic pruning, and the size of the neuronal precursor pool in mammals (Cunningham et al., 2013; Paolicelli et al., 2011; Squarzoni et al., 2014). Langerhans cells constantly surveil their environment for pathogens while maintaining tissue integrity through tight junctions with surrounding keratinocytes in the skin (Kubo et al., 2009). The engulfment of dying cells by Langerhans cells in a steady state and after infection allows local immune tolerance to self-antigens (West & Bennett, 2018).
Therefore, tissue-resident immune cells play important roles during normal development and in maintaining tissue integrity.

1.1.3 Leader cells in collective cancer cell migration

Cancer cells exploit similar mechanisms and modes of migration to those I described in the first section for cells during normal developmental processes. Cancer cells can perform amoeboid or mesenchymal single-cell invasion, multicellular streaming, or collective invasion (Friedl & Alexander, 2011). The formation of leader cells from solid tumors, which form actin-

rich protrusions and can remodel the tumor environment, can be caused by genetic heterogeneity, epigenetic states, and cell-cell interactions with the tumor stroma (Vilchez Mercedes et al., 2021). Leader cells in cancer progression create paths for other cells to follow through ECM deposition, physical remodeling, or proteolysis, and they biochemically or biomechanically coordinate the motion of follower cells. In addition to tumor-derived leader cells are stroma-derived leader cells, such as cancer-associated fibroblasts (CAFs) and tumor-associated macrophages (TAMs) (Vilchez Mercedes et al., 2021). Tumor-derived leader cells can have characteristics of mesenchymal cells after an epithelial to mesenchymal transition (EMT) with the ability to invade through ECM. However, these leader cells can also arise from partial EMT, showing expression of both E-cadherin and N-Cadherin along with other mesenchymal markers (vimentin, ZEB1, SNAIL, and TWIST), which allows them to interact with shared adhesion proteins expressed on follower cells with only epithelial marker expression (Quan et al., 2020). CAFs can act as leader cells via secretion of soluble factors, metabolic effects, or matrix remodeling (Sahai et al., 2020). They can form tracks for cancer cells to disseminate from the original tumor and lead the migration of follower cancer cells via interaction through N-cadherin (Labernadie et al., 2017). Tumors can induce TAMs through the secretion of cytokines like IL-10, transforming growth factor β (TGFβ), and macrophage colony stimulating factor (M-CSF, or CSF1) (Hollmén et al., 2016; Sousa et al., 2015). TAMs show similar characteristics to immunosuppressive M2 macrophages and physically remodel ECM to create paths for following cancer cells (Afik et al., 2016). They can also produce cytokines, chemokines, and growth factors to induce invasive migration of cancer cells (Y. Lin et al., 2019).

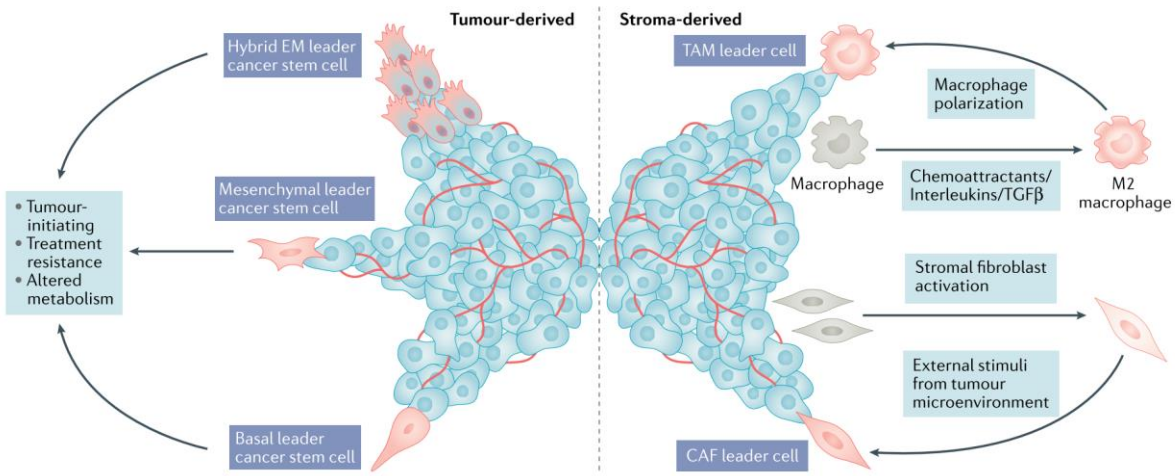

Chapter 1 Fig. 3: Leader cells in cancer invasion
Leader cells can originate from the tumor itself or from the surrounding stroma. Tumor-derived leader cells can either show characteristics of complete epithelial to mesenchymal transition, resemble an epithelial-mesenchymal (EM) hybrid state, or show epithelial markers (basal leader cancer cell). Tumors can induce macrophage polarization into the pro-invasive M2 state, promoting cancer cell invasion through assistance of tumor-associated macrophages (TAMs). Additionally, tumor cells can induce stromal fibroblasts to become cancer-associated fibroblasts (CAFs) that lead cancer cell invasion. Adapted from Vilchez Mercedes et al., 2021

These findings highlight the role of macrophages with M2 characteristics in guiding the invasion of follower cells. In the following section, I will explain the immune system of flies and describe our current knowledge of embryonic immune cells and their ability to invade into tissues.

1.2 THE IMMUNE SYSTEM OF DROSOPHILA MELANOGASTER

1.2.1 Major types of immune cells in *Drosophila* melanogaster

There are three major types of *Drosophila* blood cells or hemocytes. Plasmatocytes make up approximately 90-95% of all *Drosophila* hemocytes, whereas crystal cells comprise a much smaller amount, only 2-5% (Banerjee et al., 2019; Lebestky et al., 2000; Paladi & Tepass, 2004). In contrast, large lamellocytes can only be observed upon infection with a parasitic wasp egg (Rizki & Rizki, 1992). Lamellocytes were shown to be rich in β-Integrin, which allows them to encapsulate large invaders (Irving et al., 2005). Additionally, they express the Prophenoloxidase 3 (PPO3) and can be visualized using a marker line for the gene *misshapen* (Dudzic et al., 2015; C. J. Evans et al., 2003).

Plasmatocytes play a crucial role during embryonic development and are highly similar to macrophages in higher organisms. They secrete and remodel components of the extracellular matrix (ECM) such as Laminin and Collagen IV, engulf apoptotic cells, and assist proper development (Bunt et al., 2010; Olofsson & Page, 2005; Sánchez-Sánchez et al., 2017). By secretion of Collagen IV, plasmatocytes were shown to indirectly affect the development of renal organs (Malpighian tubules) through local enrichment of the ligand Decapentaplegic (dpp), leading to forward movement of the anterior-most cells within the tube (Bunt et al., 2010). Plasmatocytes can be distinguished at embryonic stage 10 when they begin to form highly dynamic actin protrusions and start to migrate throughout the embryo (Tepass et al., 1994; Wood et al., 2006).

Crystal cells got their name from their internal crystalline structures, and they express high levels of PPO1 and PPO2, contributing to the melanization process upon septic or sterile injury, an important feature of the innate immune response in flies (Dudzic et al., 2015). They do not actively migrate and can be identified as a small sessile cell population within the embryo (de Velasco et al., 2006).

1.2.2 Hematopoiesis throughout the lifespan of *Drosophila*

Similar to vertebrates, there are two waves of hematopoiesis in the fly, with the first wave resembling primitive hematopoiesis in the embryo and the second wave inside the lymph gland, the hematopoietic organ of the larva, giving rise to stem cell-like progenitors (Fig. 4; (Banerjee et al., 2019; Gold & Brückner, 2014; Makhijani et al., 2011). Embryonic hemocytes originate in the procephalic mesoderm and relate to the erythro-myeloid lineage of tissue-resident macrophages in vertebrates (de Velasco et al., 2006; Gold & Brückner, 2014; Tepass et al., 1994). They are specified by the expression of the transcription factor *Serpent* (*Srp*) as early as embryonic stage 5 (Lebestky et al., 2000; Tepass et al., 1994). In 2004, Brückner and colleagues generated a fly line with a hemocyte-specific promoter “SrpHemo” that has been used since then as an early driver and marker for hemocytes (Brückner et al., 2004). As those early hemocytes could not be distinguished by differences in marker gene expression, they were referred to as pro-hemocytes, which can differentiate into macrophage-like plasmatocytes and non-migratory crystal cells (de Velasco et al., 2006; Lebestky et al., 2000). The genes *glial cell missing* (*gcm*) and *glial cell missing 2* (*gcm2*) are direct targets of *Srp* and additional regulators of plasmatocyte specification in the embryo (Alfonso & Jones, 2002; Bernardoni et al., 1997). Crystal cell differentiation relies on the downregulation of *gcm* and

gcm2 and the expression of the Runx-family marker *lozenge* (lz) (Bataillé et al., 2005; Lebestky et al., 2000). Further, in hemocytes that express *srp* and *gcm*, *u-shaped* (*ush*) induces plasmatocyte differentiation and suppresses crystal cell fate (Fossett et al., 2003; Muratoglu et al., 2006; Waltzer et al., 2003). During embryogenesis, hemocytes undergo four rounds of cell division until the end of stage 11, leading to approximately 700 plasmatocytes and 36 crystal cells (C. J. Evans et al., 2003; Tepass et al., 1994).

The lymph gland lineage originates from cardiogenic mesoderm, which is more similar to hematopoietic stem and progenitor cells of the vertebrate aorta-gonad-mesonephros (AGM) (Mandal et al., 2004). While lymph gland hemocytes are only released into circulation upon metamorphosis, embryonic hemocytes actively migrate via stereotyped routes (Siekhaus et al., 2010; Tepass et al., 1994). The lymph gland consists of four lobes, and most studies have examined the anterior primary lobe to investigate hematopoiesis (Banerjee et al., 2019). The primary lobe can be divided into different zones depending on the function of the zone. The posterior signaling center (PSC) serves as a niche maintaining hemocyte progenitors, and cells in the PSC express the markers *antennapedia*, *hedhehog*, and *collier* (Crozatier et al., 2004; C. J. Evans et al., 2007; Lebestky et al., 2000). Recently, the BMP ligand Dpp was found to be secreted from the PSC as a factor maintaining the stem cell-like features of preprogenitor hemocytes, which express *Notch* and its downstream component *Enhancer of split mβ (E(spl)mβ)* and can give rise to JAK/Stat receptor *dome*-expressing prohemocytes (Dey et al., 2016). The medullary zone (MZ) is populated by medially located progenitors expressing high levels of *dome* and its cytokine *unpaired3*, *cytotoxic reactive oxygen species* (*ROS*), *wingless*, *E-cadherin*, and very low levels of *collier* (Banerjee et al., 2019). The outside cortical zone (CZ) consists of maturing hemocytes. Mature plasmatocytes in the MZ are characterized by the expression of *hemolectin*, *eater*, *NimrodC*, and *peroxidasin* (Boulet et al., 2021; Jung et al., 2005; Kurucz et al., 2007; Letourneau et al., 2016).

1.2.3 Conservation of factors regulating immune cells from fly to man

Genes and signaling pathways regulating blood cell development and function are highly conserved from fly to man (Fig. 4; (C. J. Evans et al., 2003)). Similar to Srp in *Drosophila*, zinc finger transcription factors GATA1-3 are crucial for hematopoietic development in mice and the earliest regulators of primitive hematopoiesis (Belele et al., 2009; Fujiwara et al., 2004; Lebestky et al., 2000; Ohneda & Yamamoto, 2002; Tsai et al., 1994). Moreover, Srp interacts with the Friend of GATA (FOG) homolog Ush to induce plasmatocyte differentiation in *Drosophila* embryos, similar to the function of FOG in mice and zebrafish (Amigo et al., 2009; Fossett et al., 2003; Mancini et al., 2012; Tsang et al., 1997). The crystal cell fate regulator Lozenge belongs to the Runx transcription factor family and shows high conservation to human acute myeloid leukemia (AML)/Runx1, which is needed for maturation of primitive erythrocytes as well as for macrophage formation in mice (Bruveris et al., 2021; Daga et al., 1996; Yokomizo et al., 2001). Additionally, Runx1 can interact with GATA-1 to induce megakaryocyte differentiation in vitro (Elagib et al., 2003). While *gcm* and *gcm2* are conserved vertebrates, their possible role in hematopoiesis in higher organisms has not been identified (Wegner & Riethmacher, 2001). However, the human ortholog GCM1 has been shown to interact with GATA-3 in the regulation of invasive trophoblast migration (Chiu & Chen, 2016).

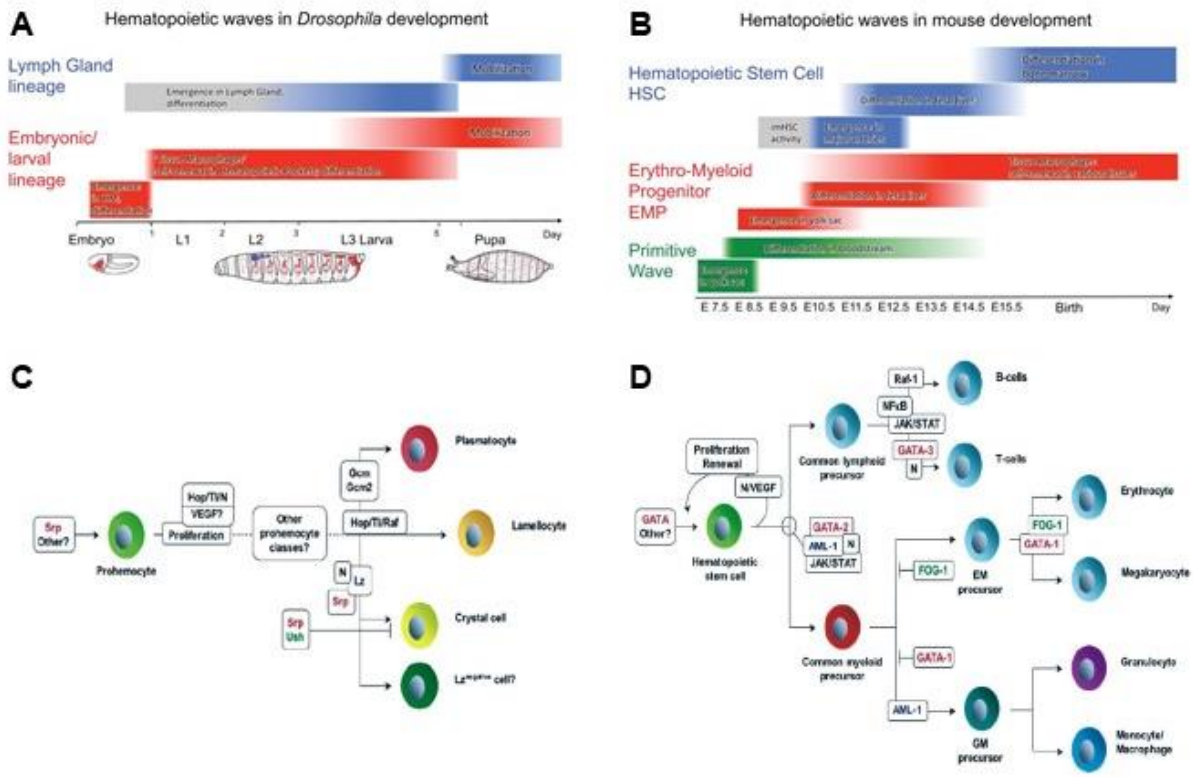

Chapter 1 Fig 4: Conservation of hematopoiesis in flies and mammals
(A) In *Drosophila*, there are two waves of hematopoiesis in the embryo (red) and the larval lymph gland (blue). **(B)** These waves share similarities with primitive and definite hematopoiesis in mammals. **(C)** Factors regulating blood cell development in *Drosophila*. The zinc finger GATA factor Srp is the earliest-identified marker defining prohemocytes. It interacts with the Friend of GATA (FOG) homolog Ush to induce plasmatocyte differentiation. Crystal cell differentiation is controlled by the Runx/AML transcription factor Lz and Notch signaling (N). **(D)** Several factors are conserved in mammalian hematopoiesis, such as GATA transcription factors, which can interact with Runx/AML transcription factors, Notch signaling regulating differentiation of hematopoietic stem cells, or FOG giving rise to erythrocytes and megakaryocytes. Adapted from Gold and Brückner, 2015 and Evans et al., 2003

1.3 DROSOPHILA EMBRYONIC MACROPHAGES AS A MODEL FOR TISSUE INVASION

1.3.1 Colonization of the embryo by hemocytes

After formation in the procephalic mesoderm, *Drosophila* hemocytes populate the whole organism. They migrate via three stereotypical routes from stage 10 onwards: (1a, 1b) up to and into the germband tissue, (2) along the segments of the developing ventral nerve cord (VNC), and (3) along the dorsal vessel (Fig. 5).
The migration of embryonic hemocytes is regulated by PDGF/VEGF-related ligands (Pvf) and their receptor Pvr, which is expressed in hemocytes (N. K. Cho et al., 2002; Heino et al., 2001; Parsons & Foley, 2013; Wood et al., 2006). While Pvf2 and Pvf3 are important for hemocyte migration, Pvf1 does not appear to play a role in this process (Brückner et al., 2004; N. K. Cho et al., 2002; Wood et al., 2006). However, Pvf1 induces hemocyte proliferation in a *Drosophila* tumor model (Parisi et al., 2014). In addition to its function for hemocyte migration, Pvr also controls cell survival, which has complicated the initial assumption that Pvr-Pvf signaling simply induces a chemotactic response guiding hemocytes along different routes (Brückner

et al., 2004; N. K. Cho et al., 2002; Sears et al., 2003). Moreover, individual Pvf ligands are not exclusively expressed along specific paths, and it is still unclear how hemocytes decide between them (N. K. Cho et al., 2002). In the absence of Pvr, Pvf2 and Pvf3 were shown to be crucial for germband invasion when cell survival was restored (Parsons & Foley, 2013; Wood & Jacinto, 2007). In contrast, migration from the origin in the head mesoderm up to the germband is Pvr-independent (N. K. Cho et al., 2002).
At the ventral side of the embryo, Pvf2 first facilitates hemocyte migration along the vnc midline, but a decrease in *pvf2* levels is needed for hemocyte lateral migration at stage 15, which relies on *pvf3* expression (Wood et al., 2006). Additionally, this lateral spreading of ventral hemocytes is regulated by zyxin-dependent contact inhibition of locomotion between individual hemocytes (Davis, Luchici, Mosis, et al., 2015). Such repulsive hemocyte-hemocyte interaction has not been shown for other routes.

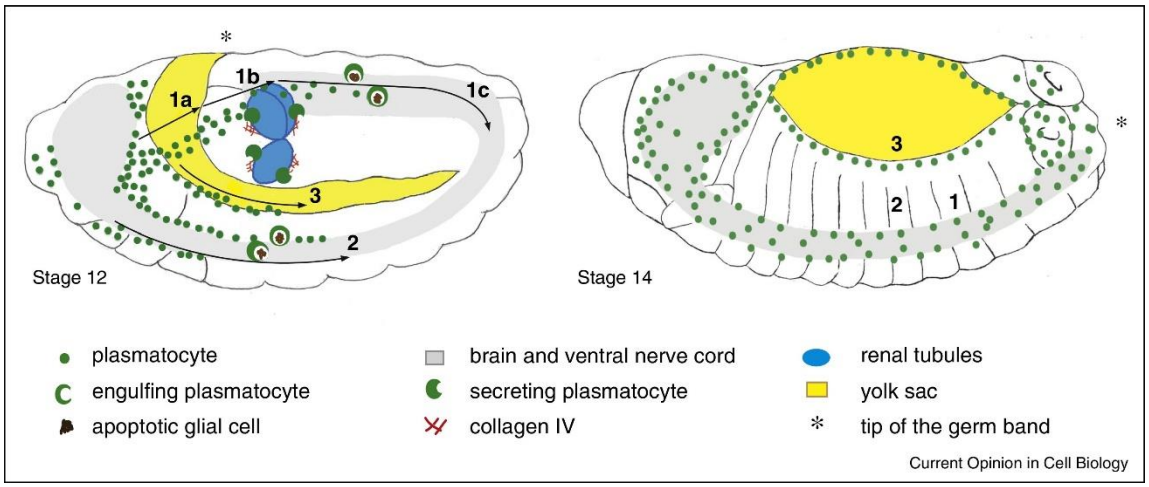

Chapter 1 Fig. 5: Hemocyte migration during Drosophila embryonic development
Schematic drawings of the *Drosophila* embryo in Stage 12, when hemocytes (green) have migrated out from their origin in the procephalic mesoderm to populate the embryo via three conserved routes: (1a, 1b) over the yolk (yellow) into the germband, (2) along segments of the vnc (grey), and (3) along the developing dorsal vessel. Arrows indicate the migration routes. Hemocytes support embryonic development by engulfing apoptotic cells and secreting ECM components such as collagen IV, which are crucial processes for the formation of organs such as renal tubules (also called Malpighian tubules, blue) and condensation of the vnc. In stage 14 embryos, hemocyte migration routes 1 and 2 have merged as the germband retracts posteriorly (*). Adapted by Ratheesh et al., 2015

The invasion of hemocytes into the germband tissue resembles mechanisms of mammalian immune cell penetration of the endothelial vasculature and the metastatic spread of cancer cells (Gout & Huot, 2008; Heyder et al., 2005; Nourshargh et al., 2010; Siekhaus et al., 2010). For this process to occur, hemocyte-specific RhoL was shown to control Rap1 localization, causing increased Integrin affinity at the leading edge of the invading hemocytes (Siekhaus et al., 2010). Hemocyte migration during this process is supported by the extracellular matrix (ECM) component Laminin and does not rely on matrix metalloproteases (MMPs) (Sánchez-Sánchez et al., 2017; Siekhaus et al., 2010; Valoskova et al., 2019). The recent identification and characterization of additional hemocyte-specific factors regulating germband penetration further demonstrated the conservation of immune cell tissue invasion in *Drosophila* and higher organisms. One study that O-glycosylation on the sulfhydryl oxidase Qsox1 is regulated by the conserved major facilitator superfamily member Minerva to allow

hemocyte germband invasion, and expression of the human ortholog *Msfd1* in the *minerva* mutant background can rescue the fly phenotype (Valoskova et al., 2019). Another study revealed the role of the conserved nuclear protein Atossa, which increases mitochondrial oxidative phosphorylation together with its transcriptional target *porthos* to provide sufficient energy for hemocyte tissue entry (Emtenani et al., 2021). Additionally, the stiffness at the germband entry side is controlled by the tumor necrosis factor (TNF) ortholog Eiger, causing decreased myosin activity and reduced apical tension in the germband ectoderm to facilitate hemocyte entry (Aparna Ratheesh et al., 2018). These findings highlight the conservation of mechanisms controlling immune cell migration in flies and higher organisms.

1.3.2 Differences in tissue environments colonized by macrophages

Hemocytes need to penetrate between closely apposed ectoderm and mesoderm cells during their invasion into the germband tissue. If the stiffness of the ectoderm is too high, hemocytes fail to enter the germband in time and accumulate in the area in front of the germband (Aparna Ratheesh et al., 2018). Very recently, the cell division of germband ectoderm cells was introduced as another crucial factor for hemocyte invasion, as it leads to the disassembly of integrin-mediated focal adhesion sites at the germband entry (Akhmanova et al., 2021). In our recently published study (Chapter 2 of this thesis), we showed that hemocytes rely on a strong actin cortex to overcome the tension of the germband tissue and that their nucleus becomes the limiting factor in the case of decreased cortical actin levels (Belyaeva et al., 2022). In contrast, hemocytes migrate in open channels along the vnc segments, which can be visualized by injections of dextran (Iwan Robert Evans & Wood, 2011). Loss of several factors that regulate germband invasion, such as RhoL, integrin, Minerva, Atossa, and Porthos, do not strongly affect general hemocyte migration in the relatively unconfined environment of the vnc (Emtenani et al., 2021; Siekhaus et al., 2010; Valoskova et al., 2019). In Chapter 2 and Chapter 3, I show similar effects for the transcriptional regulation induced by Dfos as well as for canonical BMP-signaling downstream of the receptor Thickveins (Tkv).

1.4 FUNCTIONS OF DFOS IN CELL MIGRATION AND IMMUNE CELLS

Fos family members are known oncogenes that drive the invasiveness of tumors (Milde-Langosch, 2005; Q. Wang et al., 2017). Similarly, Dfos can initiate the invasiveness of epithelial tumors and tumor cell dissemination, which is mainly linked to the breakdown of ECM components by expression of matrix metalloproteases (MMPs) (Benhra et al., 2018; Külshammer et al., 2015; Külshammer & Uhlirova, 2013; Uhlirova & Bohmann, 2006). Furthermore, Dfos regulates epithelial sheet migration during dorsal closure and wound responses and was shown to induce higher levels of the actin cytoskeleton interactors Profilin and Filamin (Belyaeva et al., 2022; Brock et al., 2012; Külshammer & Uhlirova, 2013; Riesgo-Escovar & Hafen, 1997). Together with DJun, Dfos is crucial for transcriptionally regulated processes during epithelial wound closure to induce stretching of leading edge cells as well as in more distal cells (Campos et al., 2010; Lesch et al., 2010; Pearson et al., 2009). In *Drosophila* immune cells, Dfos was shown to play a role in restricting lamellocyte differentiation, and knockdown of Dfos rescued the overproliferation phenotype of hemocytes expressing a dominant negative $Rab5/11^{DN}$ (Tokusumi et al., 2009; Yu et al., 2021). Moreover, RNAi-mediated knock-down of *Dfos* can block the expression of the antimicrobial peptides (AMPs)

Attacin and Drosomycin in *Drosophila* S2 cells (Kallio et al., 2005). Therefore, Dfos is an important regulator for immune cell function and cancer cell invasive migration.

1.5 BMP SIGNALING IN DROSOPHILA

There are three types of signaling pathways belonging to the TGFβ family: TGFβ, Activin, and BMP. For each signaling pathway, specific ligands bind as dimers to the extracellular part of a receptor complex consisting of two type I and two type II serine/threonine kinases. Upon ligand binding, the type II receptor phosphorylates the type I receptor with its intracellular kinase domain, leading to conformational changes in the type I receptor that can then bind and phosphorylate its associated transcriptional regulator Smad (also called receptor Smad, R-Smad) (Morikawa et al., 2016). Upon binding to a Co-Smad, activated R-Smad translocates into the nucleus to regulate transcription, which also activates a negative feedback loop by inducing the expression of an inhibitory Smad (I-Smad). In *Drosophila*, there are seven different ligands. The BMP-type ligands Decapentaplegic (Dpp, ortholog of BMP 2/4), Glass bottom boat (Gbb, ortholog of BMP5/6/7), and Screw (Scw, ortholog of BMP5) signal through the type I receptors Thickveins (Tkv) or Saxophone (Sax). Whereas the Activin/TGFβ-type ligands Activinβ (Actβ, ortholog of Inhibin), Maverick (Mav, ortholog of Nodal and GDF15), and Dawdle (Daw, ortholog of Activin) signal through different variants of the type I receptor Baboon (Babo). The type II receptors Punt (Put) and Wishful thinking (Wit) can act in both signaling pathways (Upadhyay et al., 2017) (Fig. 6). While there is only one Co-Smad in *Drosophila* (Medea, Med), there are two different R-Smads that are specific for binding to the type I receptors (Awasaki et al., 2008; T. Brummel et al., 1999; Nguyen et al., 2000; Upadhyay et al., 2017). Mothers against dpp (Mad) functions in BMP signaling and Smad on X (Smox) is downstream of Activin/TGFβ signaling. The only I-Smad in *Drosophila* is Daughters against dpp (Dad), which has been shown to block BMP signaling mediated by Tkv but not signaling downstream of Babo (H. Inoue et al., 1998; Kamiya et al., 2008; Tsuneizumi et al., 1997; Weiss et al., 2010a).
In Chapter 3, I focus on the role of BMP signaling for hemocyte invasion into an embryonic tissue, which is likely activated by dpp ligand close to the BMP^+ hemocytes.
During early embryonic dorso-ventral patterning, dpp plays a major role as a morphogen that regulates cell identity in a concentration-dependent manner (Ferguson & Anderson, 1992). Its diffusion and localization are tightly controlled by the extracellular factors Short gastrulation (Sog) and Twisted gastrulation (Tsg), which keep ligand dimers in an inactive complex, and the metalloprotease Tolloid (Tld), which leads to the release of active ligands (O'Connor et al., 2006).

BMP signaling is known to regulate hematopoiesis in higher organisms (Bhatia et al., 1999; Johansson & Wiles, 1995; Kirmizitas et al., 2017; Monteiro et al., 2016; Nakayama et al., 2000). In the *Drosophila* embryo, Dpp signaling regulates blood cell formation by controlling the formation of cardiogenic mesoderm that will later give rise to lymph gland tissue (Mandal et al., 2004). It also directly affects blood cell differentiation and proliferation in the PSC of larvae, and Dpp signaling activity in larval prohemocytes was recently shown to rely on Integrin (Dey et al., 2016; Khadilkar et al., 2020; Pennetier et al., 2012a).
Furthermore, Dpp has been shown to regulate the migration of epithelial sheets, such as during tracheal development and dorsal closure (Fernández et al., 2007; Riesgo-Escovar &

Hafen, 1997; Vincent et al., 1997; Zeitlinger et al., 1997). During dorsal closure, Dpp was proposed to act as a relay signal, as it is crucial for the regulation of cell shape changes in leader and follower cells, inducing stretching of the more ventral cells (Perkins et al., 1988). During larval histoblast formation, Dpp signaling is active in the outer leading edge cells, inducing their tissue invasion in an Integrin-dependent manner (Ninov et al., 2010). In Chapter 3, I show a novel role of Dpp signaling activation in a subpopulation of hemocytes, which are leaders of tissue invasion in the *Drosophila* embryo.
In *Drosophila* larvae, the receptor Put was shown to control hemocyte homing to hematopoietic pockets and hemocyte proliferation, which is dependent on the ligand Activinβ (Makhijani et al., 2017). The effect of Dpp signaling on embryonic hemocytes has not been investigated so far. In Chapter 3, I reveal that only a subpopulation of embryonic hemocytes shows BMP activation, and those BMP^+ hemocytes lead tissue invasion into the germband. These findings add to the body of knowledge about Dpp's function as a morphogen that regulates cell identity.

1.6 INTERACTIONS OF DFOS AND BMP SIGNALING IN DROSOPHILA

The AP1 complex consisting of Dfos and DJun, has previously been shown to interact with BMP signaling in *Drosophila*. During embryonic dorsal closure, leading edge (LE) cells of the migrating epithelial sheet secrete the BMP ligand Decapentaplegic (dpp) to induce cell shape changes in the follower cells in a Dfos-dependent manner, inducing a relay signal (Perkins et al., 1988; Riesgo-escovar & Hafen, 1997; Riesgo-Escovar & Hafen, 1997; Zeitlinger et al., 1997). Additionally, Dfos also regulates dpp target genes in a DJun-independent manner in the dorsal epithelium of the early embryo (Rusch & Levine, 1997). Moreover, a critical level of dpp signaling is needed for Dfos expression to control the morphological movements of follicle cells and subsequent development of respiratory appendages (Dequier et al., 2001). BMP signaling and Dfos also interact to induce the formation of the endoderm cell fate and the formation of *Drosophila* gut cells (Eresh et al., 1997; Szüts & Bienz, 2000). Canonical BMP is crucial for the expression of genes that regulate neuro-muscular junction growth and plasticity, including *Dfos*, the *cell adhesion molecule* (*CAM*) *Fasciclin III*, and the adenylyl cyclase *rutabaga* (Berke et al., 2013). Interestingly, in Chapter 3, we find *Fasciclin III* and *rutabaga* among the genes with higher expression in a novel BMP-activated hemocyte subpopulation, pointing towards a possible overlap of BMP activation and Dfos functions in *Drosophila* embryonic hemocytes. Moreover, BMP signaling activation and Dfos play a crucial role in tissue invasion of embryonic hemocytes, similar to the function of TGFβ-signaling and AP1 transcriptional regulation of breast cancer invasiveness (Belyaeva et al., 2022; Sundqvist et al., 2020).

1.7 SUBPOPULATIONS OF DROSOPHILA IMMUNE CELLS

For a long time, hemocytes in the early *Drosophila* embryo were thought of as progenitor-like cells, also called prohemocytes, which develop into plasmatocytes and crystal cells. However, data from Holz and colleagues have shown that the blastoderm embryo comprises two different hemocyte anlagen, with one of them giving rise to embryonic hemocytes and the other specifying lymph gland hemocytes (Holz et al., 2003). This study was followed by another description of hemocytes' origin from different zones of the procephalic mesoderm

between stages 7 and 11 (de Velasco et al., 2006). However, the recent rise of single-cell transcriptomics paved the way for in-depth analysis of hemocyte subpopulations. Utilizing single-cell RNA-Sequencing of larval hemocytes, three research groups identified previously unknown subpopulations in *Drosophila* immune cells, different states of hemocytes upon inflammation and immune challenge, and novel subtypes of crystal cells and lamellocytes enriched in the FGF-receptor *breathless* and the ligand *branchless*, which is crucial for parasite defense (Cattenoz et al., 2020; Fu et al., 2020; Tattikota et al., 2020). The very small population of primocytes was proposed as a novel hematopoietic precursor population labeled by the expression of transcription factors controlling cell fate specification and differentiation, including *Antennapedia*, *knot*, *hamlet*, *Mothers against dpp* (*Mad*), and *Z600* (Fu et al., 2020). However, a comparison between larval and embryonic hemocytes showed significant differences in gene expression and highlighted the need for in-depth characterization of hemocytes throughout embryonic development. Therefore, in an attempt to describe the embryonic hemocyte population during the time of their specification, transcriptome data from larval and embryonic single-cell RNA-Sequencing were used to generate a pseudo-transcriptome of embryonic hemocytes (Cattenoz et al., 2021). Procephalic mesoderm cells were thereby verified to express the earliest hemocyte-specific transcription factors g*cm* and the GATA factor s*rp*. The transcriptome profile of early undefined prohemocytes correlated strongly with the proliferative plasmatocyte subgroups of the larval lymph gland, indicating that proliferating embryonic hemocytes give rise to larval hemocytes (Cattenoz et al., 2021).

While these results point toward the existence of different hemocyte subpopulations in the embryo, their functional characteristics remain unclear. However, functionally distinct subpopulations were recently identified by a *Gal4* driver screen in late embryos at stage 15, a time when hemocytes have already dispersed through the embryo (Coates et al., 2021). The described subpopulations showed characteristics of pro-inflammatory M1 macrophages of vertebrates with a faster migration towards wounds, and they exhibited different localizations and dynamics throughout fly development, demonstrating the complexity of embryonic hemocytes. However, during early embryonic development, hemocytes face very different tissue environments and more closely resemble characteristics of M2-like macrophages that shape tissue development. In Chapter 3, I describe the characteristics of a novel subpopulation of BMP-activated hemocytes. Similar to anti-inflammatory M2 macrophages in higher vertebrates, BMP signaling activity was previously linked to hemocytes in the larva that did not produce anti-microbial peptides (AMPs) upon infection but showed pro-healing characteristics (Clark et al., 2011b). In our manuscript, we show that BMP-activated hemocytes lead tissue invasion into the germband. They have higher levels of putative target genes, which potentially regulate the interaction with non-BMP-activated hemocytes and become enriched in *E(spl)C* genes upon tissue invasion. While *E(spl)C* genes are known as downstream components of Notch signaling, hemocyte tissue invasion is Notch independent. We also find *E(spl)C* genes to be strong markers of novel hemocyte clusters identified by single-cell transcriptomic analysis. These findings suggest that *Drosophila* immune cells resemble different features during embryogenesis. They are similar to M1 macrophages in late-stage embryos and relate to M2 macrophages during earlier development. BMP signaling is potentially part of the M2 axis.

In our recent publication describing the role of Dfos in embryonic immune cell migration, we named them “macrophages” according to their functional similarity with their vertebrate counterparts (Belyaeva et al., 2022). However, given the recent identification of

subpopulations of plasmatocytes (i.e., macrophages) that might also resemble different activation states, I refer to *Drosophila* immune cells as hemocytes throughout the manuscript in Chapter 3 to avoid a potentially inaccurate definition (Cattenoz et al., 2021).

2 Macrophage Cortical Actin counteracts Tissue Resistance

Fos regulates macrophage infiltration against surrounding tissue resistance by a cortical actin-based mechanism in *Drosophila*

Vera Belyaeva[§1,2], Stephanie Wachner[§1], Attila Gyoergy[§1,3], Shamsi Emtenani[1], Igor Gridchyn[#1,4], Maria Akhmanova[#1], Markus Linder[5,6], Marko Roblek[1], Maria Sibilia[5], Daria Siekhaus[1*]

§: These authors contributed equally

#: These authors contributed equally

*- Corresponding author: daria.siekhaus@ist.ac.at

1 – Institute of Science and Technology Austria, Am Campus 1, 3400 Klosterneuburg, Austria

2 – Current address: Molecular Devices, Urstein Süd 17, 5412, Austria

3 – Current address: Campus-Vienna-BioCenter 1, 1030 Vienna, Austria

4 – Current address: TetraScience, Talstrasse 11, 87637, Seeg, Germany

5 – Institute of Cancer Research, Department of Medicine 1, Comprehensive Cancer Center, Medical University of Vienna, 1090 Vienna, Austria

6 – Current address: F. Hoffmann-La Roche Ltd., Grenzacherstrasse 124, 4070 Basel, Switzerland

2.1 ABSTRACT

The infiltration of immune cells into tissues underlies the establishment of tissue resident macrophages, and responses to infections and tumors. Yet the mechanisms immune cells utilize to negotiate tissue barriers in living organisms are not well understood, and a role for cortical actin has not been examined. Here we find that the tissue invasion of *Drosophila* macrophages, also known as plasmatocytes or hemocytes, utilizes enhanced cortical F-actin levels stimulated by the *Drosophila* member of the fos proto oncogene transcription factor family (Dfos, Kayak). RNA sequencing analysis and live imaging show that Dfos enhances F-actin levels around the entire macrophage surface by increasing mRNA levels of the membrane spanning molecular scaffold tetraspanin TM4SF, and the actin cross-linking filamin Cheerio which are themselves required for invasion. Both the filamin and the tetraspanin enhance the cortical activity of Rho1 and the formin Diaphanous and thus the assembly of cortical actin, which is a critical function since expressing a dominant active form of Diaphanous can rescue the *Dfos* macrophage invasion defect. *In vivo* imaging shows that Dfos enhances the efficiency of the initial phases of macrophage tissue entry. Genetic evidence argues that this Dfos-induced program in macrophages counteracts the constraint produced by the tension of surrounding tissues and buffers the properties of the macrophage nucleus from affecting tissue entry. We thus identify strengthening the cortical actin cytoskeleton through Dfos as a key process allowing efficient forward movement of an immune cell into surrounding tissues.

2.2 INTRODUCTION

The classical model of cell migration on a surface postulated in the 1980's by Abercrombie has been extended (Danuser et al., 2013) by studies showing that migrating cells utilize diverse strategies depending on the architecture and physical properties of their three dimensional (3D) surroundings (Paluch et al., 2016). Much of this work has been conducted *in vitro*, where variations in the environment can be strictly controlled. However most 3D migration occurs within the body, and much less research has elucidated the mechanisms used to efficiently move in these diverse environments, particularly into and through tissues. Such migration is crucial for the influence of the immune system on health and disease. Vertebrate macrophages migrate into tissues during development where they take up residence, regulating organ formation and homeostasis and organizing tissue repair upon injury (Ginhoux and Guilliams, 2016; Theret et al 2019). A variety of types of immune cells infiltrate into tumors, and can both promote or impede cancer progression (Greten and Grivennikov 2019; Sharma and Allison, 2015). Responses to infection require immune cells to traverse through the vascular wall, into the lymph node, and through tissues (Luster et al., 2005). Yet the mechanisms utilized by immune cells to allow migration into such challenging cellular environments *in vivo* are not well understood.

Migration in 2D and 3D environments requires actin polymerization to power forward progress. The assembly of actin at the leading edge, when coupled to Integrin adhesion to anchor points in the surrounding ECM, can allow the front of the cell to progress (Mitchison and Cramer, 1996). This anchoring also allows the contraction of cortical actin at the rear plasma membrane to bring the body of the cell forwards. But a role for crosslinked actin at the cell surface in assisting forward progress by helping to counteract the resistance of surrounding tissues and in buffering the nucleus has not been previously identified.

Our lab examines *Drosophila* macrophage migration into the embryonic germband (gb) to investigate mechanisms of immune cell tissue invasion. Macrophages, also called plasmatocytes or hemocytes, are the primary phagocytic cell in *Drosophila* and share striking similarities with vertebrate macrophages (Brückner et al., 2004; Evans & Wood, 2011; Lemaitre & Hoffmann, 2007; Ratheesh et al., 2015; Weavers et al., 2016). They are specified in the head mesoderm at embryonic stages 4-6 and by stage 10 start spreading along predetermined routes guided by platelet-derived growth factor- and vascular endothelial growth factor-related factors (Pvf) 2 and 3 (Cho et al., 2002; Brückner et al., 2004; Wood et al., 2006) to populate the whole embryo. One of these paths, the movement into the gb, requires macrophages to invade confined between the ectoderm and mesoderm (Ratheesh et al., 2018; Siekhaus et al., 2010). The level of tension and thus apparent stiffness of the flanking ectoderm is a key parameter defining the efficiency of macrophage passage into and within the gb (Ratheesh et al., 2018). Penetration of macrophages into the gb utilizes Integrin, occurs normally without MMPs (Siekhaus et al., 2010) and is even enhanced by ECM deposition (Valoskova et al., 2019; Sánchez-Sánchez et al., 2017) likely because the basement membrane has not yet formed at this stage (Matsubayashi et al., 2017; Ratheesh et al., 2018). Thus, *Drosophila* macrophage gb invasion represents an ideal system to explore the mechanisms by which immune cells and surrounding tissues interact with one another to aid the invasion process.

Here we sought to identify a transcription factor that could control immune cell tissue invasion and elucidate its downstream mechanisms. We identify a role for the *Drosophila* ortholog of the proto-oncogene Fos in initial entry and migration within the tissue. We find Dfos increases cortical macrophage F-actin levels through the formin Cheerio and a novel

target, the tetraspanin TM4SF, aiding macrophages to move forward against the resistance of the surrounding tissues while buffering the nucleus.

2.3 RESULTS

2.3.1 The transcription factor Dfos is required for macrophage germband invasion

To identify regulators of programs for invasion we searched the literature for transcription factors expressed in macrophages prior to or during their invasion of germband tissues (gb) (Fig 1A-B'). Of the 12 such factors (S1 Table, based on Hammonds et al., 2013) we focused on Dfos, a member of the Fos proto-oncogene family, assigned by the Roundup algorithm as being closest to vertebrate c-fos (Deluca et al., 2012; Thurmond et al., 2019) (Fig 1C). Dfos contains the basic leucine zipper domain (bZIP) shown to mediate DNA binding and hetero and homo dimerization (Glover and Harrison, 1995; Szalóki et al., 2015) with the third leucine replaced by a methionine, a position also altered in the *C. elegans* ortholog FOS-1A (Sherwood et al., 2005). Embryo *in situ* hybridizations reveal enriched expression of the gene in macrophages at early stage 11 (Fig 1D, arrow) which is attenuated by stage 13 matching what was seen in the BDGP *in situ* database https://insitu.fruitfly.org/cgi-bin/ex/report.pl?ftype=1&ftext=FBgn0001297. Antibody staining against Dfos protein appears in the nucleus in macrophages that are migrating towards the gb at stage 10-12 (Fig 1E-F' yellow arrowheads, G-G"' white arrows) and is still observed in stage 13 (S1A Fig). The *Dfos*^{1} null mutant that removes exon 1 including the translational start site (Riesgo-Escover and Hafen, 1997, Zeitlinger, et al., 1997) eliminates the signal in macrophages, indicating antibody specificity (Fig 1H). To determine if Dfos affects invasion, we examined the 70% of embryos that did not display developmental defects at these early stages from *Dfos*^{1} and the hypomorphic *Dfos*^{2} (Zeitlinger et al., 1997); we quantified macrophage numbers in the gb during a defined developmental period in early stage 12 (Fig 1M). Both Dfos mutants displayed significantly reduced numbers of macrophages in the gb compared to the control (Fig 1I-K, N) with normal numbers in the pre-gb zone for *Dfos*^{2} (S1B Fig) (S1 Data). Macrophage-specific expression of *Dfos* rescues the *Dfos*^{2} mutant (Fig 1L,N). Blocking Dfos function in macrophages with a dominant negative (DN) Dfos (Fig 1O-Q) that lacks the activation domain but retains the capacity to dimerize and bind DNA (Eresh et al., 1997) or two different RNAis against *Dfos* (Fig 1R) recapitulates the decrease in gb macrophages seen in the null while not affecting macrophage numbers in the whole embryo (S1C Fig), and along the ventral nerve cord (vnc) (S1D-E Fig). However, macrophages expressing DfosDN or the *Dfos* RNAis accumulate in the pre-germband area (S1F-G Fig), as if they are accumulating there when unable to progress further. These results argue that Dfos is required in macrophages for their migration into the gb.

The tool we chose to examine this capability was DfosDN for the following reasons. Dfos and DfosDN do not appear to inhibit other bZIP proteins at higher levels of expression: overexpressing DfosDN in the midgut does not inhibit another bZIP protein that acts there (Eresh et al., 1997) and overexpressing Dfos in macrophages does not change gb numbers (S1H Fig). DfosDN should exert a quicker effect than the RNAis. And finally, the *Dfos RNAi*s no longer exert an effect when a second UAS construct is simultaneously expressed (S1I Fig). Thus, our further experiments examining Dfos' role in enhancing macrophage germband invasion utilized mostly the DN form.

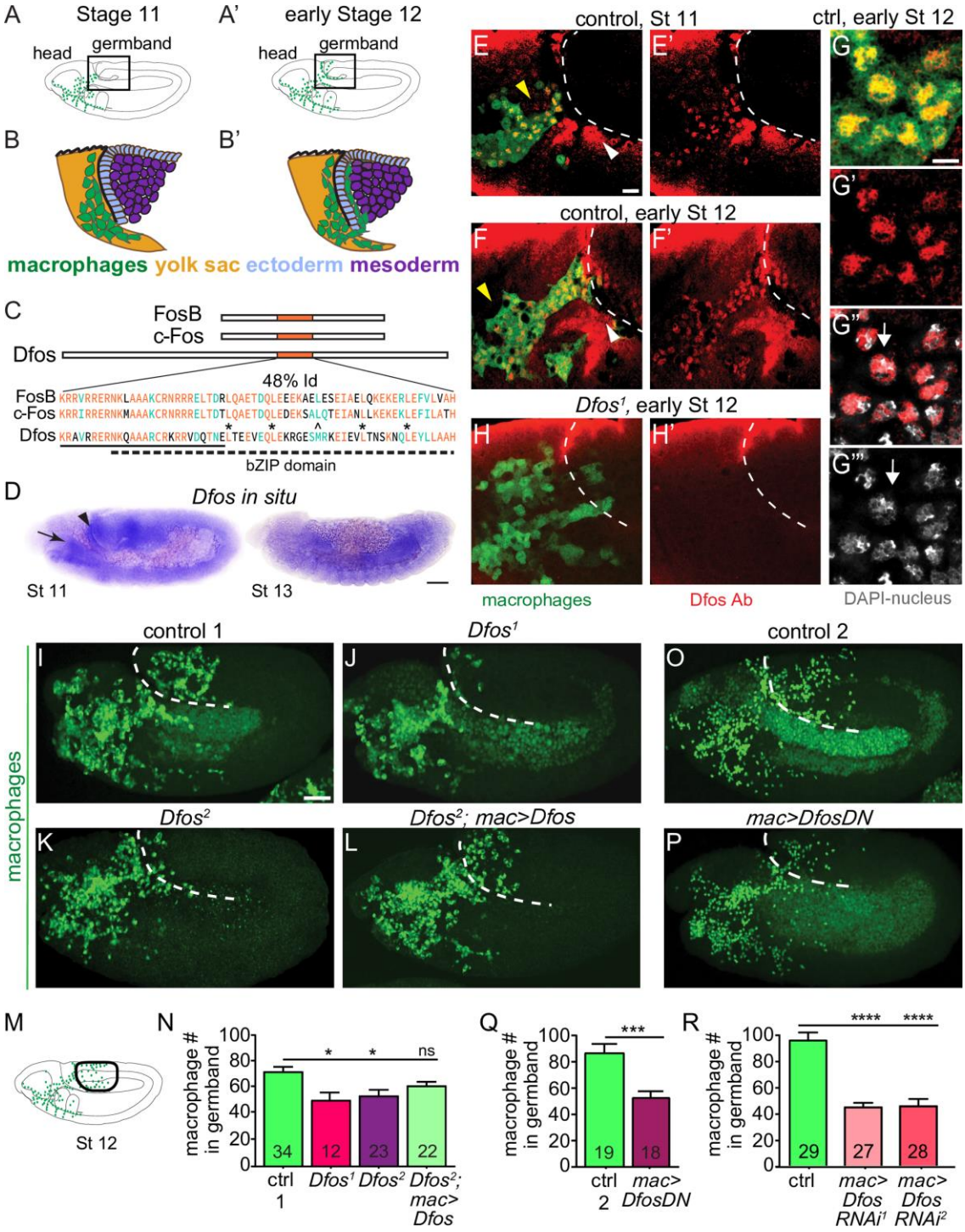

Chapter 2 Fig 1.The bZIP transcription factor Dfos acts in macrophages to facilitate their migration into the germband

Schematics of lateral (A) stage (St) 11 and (A') early St 12 embryos. The boxed region magnified below indicates where macrophages (green) invade the germband (gb) after moving there from the head (B-B'). Macrophages sit on the yolk sac (yellow) next to the amnioserosa (black line) and then invade between the ectoderm (blue) and mesoderm (purple). (C) Dfos protein aligned with its human orthologs c-Fos and FosB; orange outlines the bZIP region that has 48% identity to both proteins: identical amino acids shown in orange, conserved ones in green. Stars indicate Leucines in the zipper; ^ the third leucine which in Dfos is a methionine, a tolerated substitution (Garcia-Echeverria, 1997). The lower solid line indicates the basic domain and the dotted line the leucine zipper (ZIP). (D) *In situ* hybridization of St 11 and 13 embryos with a riboprobe for Dfos-RB (Fbcl0282531) which also detects all Dfos isoforms. *Dfos* RNA expression is enriched in macrophages (arrow) and the

amnioserosa (arrowhead) before gb invasion, but is gone thereafter. (E-H') Confocal images of the boxed region in A from fixed embryos expressing *GFP* in macrophages (green) stained with a Dfos Ab (red). (E-F', H-H') A white dashed line indicates the gb edge. (E-F) The Dfos Ab (yellow arrowheads) stains (E) macrophages moving towards the gb at St 11, and (F) early St 12, as well as the amnioserosa (white arrowheads). (G) Higher magnification shows Dfos colocalizing with the nuclear marker DAPI (white). (H) No staining is detected in macrophages or the amnioserosa in the null $Dfos^{1}$ mutant. (I-L) Lateral views of mid St 12 embryos from (I) the control, (J) the null allele $Dfos^{1}$, (K) the hypomorphic allele $Dfos^{2}$, and (L) $Dfos^{2}$ with *Dfos* re-expressed in macrophages. (M) Schematic of St 12 embryo, gb region indicated by a black oval outline. (N) Quantitation reveals that both *Dfos* alleles display fewer macrophages in the gb. Re-expression of *Dfos* in macrophages in the $Dfos^{2}$ hypomorph significantly rescues the defect. Control vs. $Dfos^{1}$ p=0.02 (30% reduction), Control vs. $Dfos^{2}$ p=0.017 (25% reduction), Control vs. $Dfos^{2}$*; mac>Dfos* p=0.334. (O-P) Lateral views of mid St 12 embryos from (O) the control, or (P) a line expressing a dominant negative (DN) form of Dfos in macrophages. (Q) Quantification of macrophage numbers in the gb (see schematic) in the two genotypes visualized in O-P. p=0.0002 (***) (40% reduction). Standard Deviation (SD): 25, 25. (R) Quantification of macrophage numbers in the gb of the control and two different lines expressing RNAi constructs against Dfos in macrophages. Quantification of macrophage numbers in the gb for lines expressing one of two different *UAS-Dfos RNAi* constructs in macrophages. Control vs. *mac>Dfos* $RNAi^{1}$ (TRiP HMS00254) or vs. *mac>Dfos* $RNAi^{2}$ (TRiP JF02804), p<0.0001 (54 or 52% reduction). SD: 32, 19, 29. The data in Q and R argue that Dfos is required within macrophages to promote gb tissue invasion. Embryos are positioned with anterior to left and dorsal up in all images and histograms show mean + standard error of the mean (SEM) throughout. Macrophages are labeled using *srp-Gal4* ("mac>") driving *UAS-GFP* in E-H, *UAS-GFP::nls* in I-L and *srpHemo-H2A::3xmCherry* in O-R. ***p<0.005, **p<0.01, *p<0.05. One-way ANOVA with Tukey post hoc was used for N and R, and unpaired t-test for Q. The embryo number analysed is indicated within the relevant column in the graphs. Scale bar: 50 μm in D, 5 μm in E-H and 10 μm in I-L, O-P. The data underlying the graphs in all Figures can be found in S1 Data.

2.3.2 Dfos promotes macrophage motility and persistence during tissue entry

To examine the dynamic effects of Dfos on tissue invasion, we performed live imaging and tracking of macrophages. We visualized macrophages with *srpHemo-H2A::3xmCherry* (Gyoergy et al., 2018) in either a wild type or *mac>DfosDN* background, capturing the initial stage of invasion (S1 Movie). The speed of macrophages moving in the area neighboring the germband prior to invasion was not significantly changed (pre-gb, Fig 2B,C). However, the first *mac>DfosDN* macrophage to enter is delayed by 20 min in crossing into the gb (Fig 2D). *mac>DfosDN* macrophages also displayed reduced speed and directional persistence during entering as well as while moving along the first 20μm of the ectoderm-mesoderm interface (gb entry, Fig 2E, S2A Fig). Macrophages in the $Dfos^{2}$ mutant largely mirrored this phenotype, but displayed slower movement in the pre-gb zone neighboring the amnioserosa in which Dfos is also expressed (Fig 1D-F), likely causing a non-autonomous effect (S2B-C Fig, S2 Movie) (Fig 1D, black arrowhead, E-F, white arrowheads). Macrophages expressing DfosDN moved with unaltered average speed as they spread out along the non-invasive route of the vnc (Fig 2F, Fig 2G, S3 Movie), albeit with reduced directional persistence (S2A Fig). We thus conclude from live imaging that Dfos in macrophages aids their initial invasive migration into the gb, increases their speed within the gb and does not underlie their progress along the vnc.

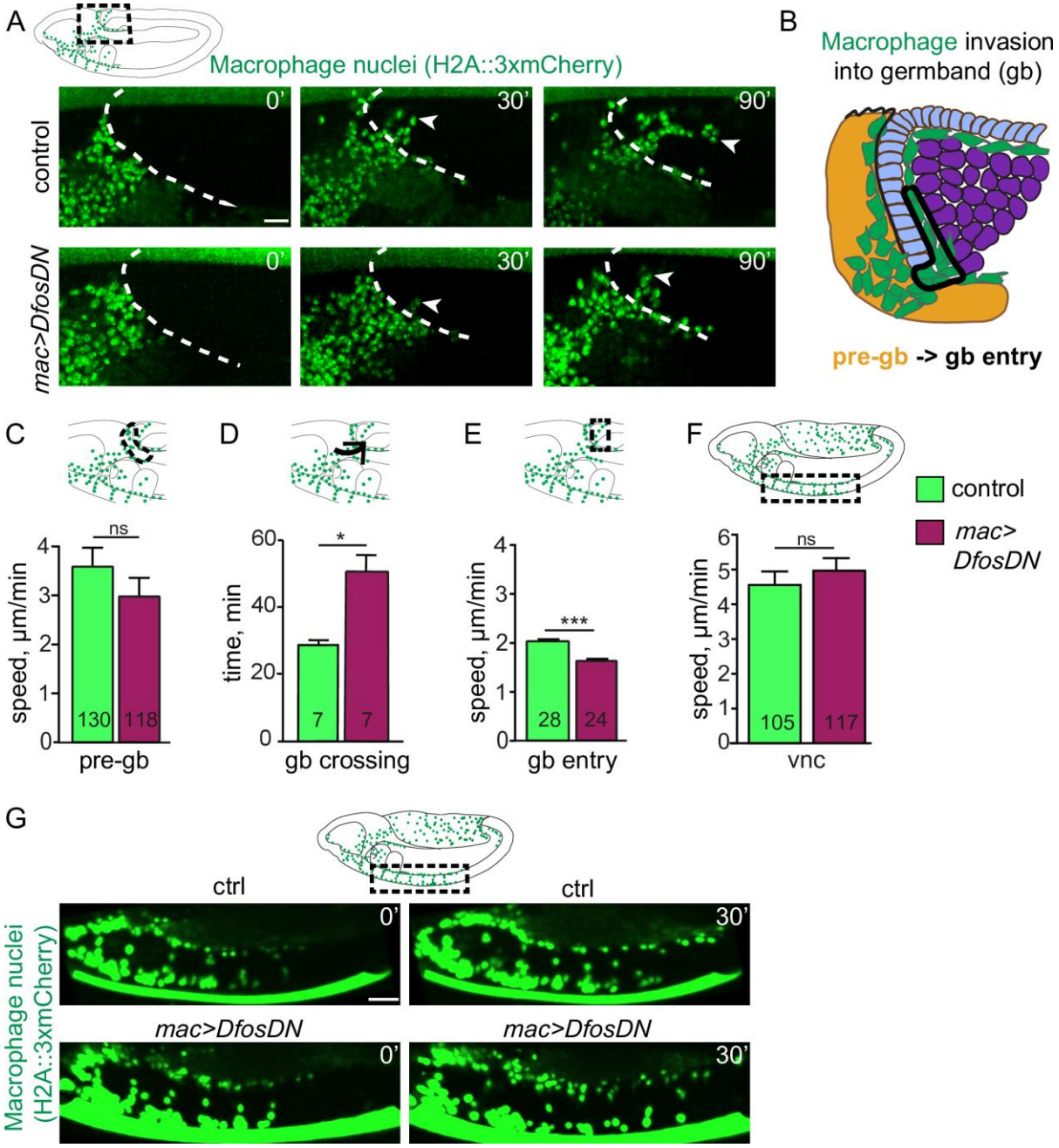

Chapter 2 Fig 2. *Dfos* facilitates the initial invasion of macrophages into the gb tissue
(A) Movie stills of control embryos and those expressing DfosDN in macrophages (green, labelled using *srpHemo-H2A::3xmCherry*). Area imaged corresponds to the black dashed square in the schematic above. The germband (gb) border is outlined with a white dashed line. The first entering macrophage is indicated with a white arrowhead, and time in minutes in the upper right corner. (B) Detailed schematic showing the different zones for which the parameters of macrophage gb invasion were quantified. The pre-gb area is shown in yellow, the gb entry zone is outlined in a solid line. (C) Macrophage speed in the pre-gb area was not significantly changed in macrophages expressing DfosDN (3.00 µm/min) compared to the control (3.61 µm/min), p= 0.58. (D) Quantification shows a 68% increase in the total gb crossing time of DfosDN expressing macrophages compared to the control. Total gb crossing time runs from when macrophages have migrated onto the outer edge of the gb ectoderm, aligning in a half arch, until the first macrophage has translocated its nucleus into the gb ecto-meso interface. p=0.008. SD: 4, 14. (E) DfosDN expressing macrophages displayed a significantly reduced speed (1.53 µm/min) at the gb entry zone compared to the control (1.98 µm/min), p= $1.11e^{-06}$. SD: 2, 2. (F) Macrophages expressing DfosDN in a Stage 13 embryo move with unaltered speed along the vnc in the region outlined by the dashed black box in the schematic above (4.93 µm/min), compared to the control (4.55 µm/min), p= 0.64. Corresponding stills shown in (G) Macrophages are labeled by *srpHemo-Gal4* driving *UAS-GFP::nls*.

***p<0.005, **p<0.01, *p<0.05. Unpaired t-test used for C-F, a Kolmogorov-Smirnov test for D. For each genotype, the number of tracks analysed in C and F, and the number of macrophages in D-E are indicated within the graph columns. Tracks were obtained from movies of 7 control and 7 *mac>DfosDN* expressing embryos in panel D, 3 each in C, F, and 4 each in E. Scale bar: 10 µm.

2.3.3 Dfos modulates Filamin and Tetraspanin to aid gb tissue invasion

To identify Dfos targets that promote macrophage invasion, we FACS isolated macrophages from wild type and *mac>DfosDN* embryos during the time when invasion has just begun, and conducted RNA-sequencing of the corresponding transcriptomes (Fig 3A, S1 Data). We first assessed reads that map to Dfos, which can correspond to both endogenous and DfosDN mRNA; we found a 1.6 fold increase in the presence of the one copy of DfosDN in this line, arguing that this transgene is expressed at levels similar to each endogenous copy of Dfos and is unlikely to produce extraneous effects (S2 Data). We then examined genes that displayed a $\log_2$ fold change of at least 1.5 with an adjusted P value less than 0.05 in the presence of DfosDN. Ten genes were down-regulated (Fig 3B, S3A-B Fig) and 9 up-regulated by DfosDN (S2 Table). Upregulated genes in DfosDN encoded mostly stress response proteins, consistent with the role previously demonstrated for fos in *C. elegans* in suppressing stress responses (Hattori et al., 2013). We concentrated on the downregulated class. Of these, we focused on the actin crosslinking filamin Cheerio (Cher) and the tetraspanin TM4SF from a group that can form membrane microdomains that affect signalling and migration (Razinia et al., 2012; Yeung et al., 2018). No known role for TM4SF had been previously identified in *Drosophila*. To determine if these Dfos targets were themselves required for invasion, we knocked down Cher and TM4SF through RNAi individually or simultaneously and observed significantly reduced macrophage numbers in the gb, particularly upon the knockdown of both targets simultaneously (Fig 3C-G) while not affecting macrophage numbers in the pre-gb zone (S3D Fig) or on the vnc (S3E Fig). Over-expression of Cher or TM4SF along with *DfosDN* in macrophages increased the mean macrophage numbers in the gb, and over-expression of TM4SF rescued the *DfosDN* macrophage invasion defect (Fig 3H-L). Expression of a GFP control did not restore macrophage invasion indicating that the rescue we observed through Cher or TM4SF expression was not due to promoter competition leading to reductions in DfosDN expression. We conclude that Dfos aids macrophage gb invasion by increasing the mRNA levels of the filamin actin crosslinker Cher and the tetraspanin TM4SF.

2.3.4 In murine osteosarcoma c-fos mRNA level increases correlate with those of Filamins and Tetraspanin-6

To determine if these Dfos targets in *Drosophila* could also be Fos targets in vertebrate cells, we utilized a well-established murine transgenic model that over expresses c-fos. In these mice transgenic c-fos expression from viral 3' UTR elements in osteoblasts (the bone forming cells) leads to osteosarcoma development accompanied by a 5 fold increase in c-fos mRNA expression (Fig 3M) (Linder et al., 2018).

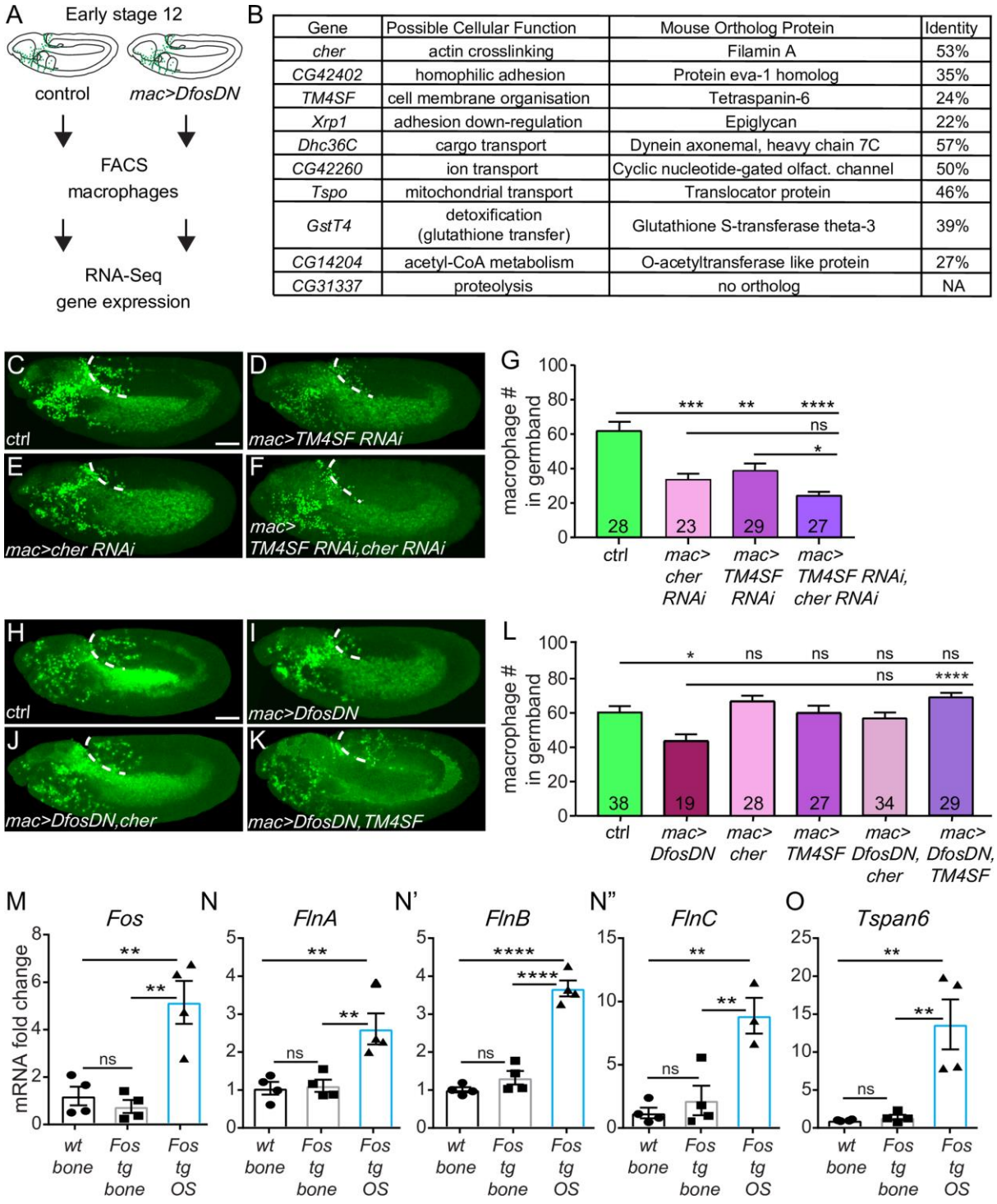

Gene	Possible Cellular Function	Mouse Ortholog Protein	Identity
cher	actin crosslinking	Filamin A	53%
CG42402	homophilic adhesion	Protein eva-1 homolog	35%
TM4SF	cell membrane organisation	Tetraspanin-6	24%
Xrp1	adhesion down-regulation	Epiglycan	22%
Dhc36C	cargo transport	Dynein axonemal, heavy chain 7C	57%
CG42260	ion transport	Cyclic nucleotide-gated olfact. channel	50%
Tspo	mitochondrial transport	Translocator protein	46%
GstT4	detoxification (glutathione transfer)	Glutathione S-transferase theta-3	39%
CG14204	acetyl-CoA metabolism	O-acetyltransferase like protein	27%
CG31337	proteolysis	no ortholog	NA

Chapter 2 Fig 3. *Dfos* regulates macrophage germband invasion through cytoskeletal regulators: the Filamin Cheerio and the tetraspanin TM4SF

(A) Schematic representing the pipeline for analyzing mRNA levels in FACS sorted macrophages. (B) Table of genes down regulated in macrophages expressing DfosDN. Genes are ordered according to the normalized p-value from the RNA-Sequencing. The closest mouse protein orthologs were found using UniProt BLAST; the hit with the top score is shown in the table. (C-F) Lateral views of representative St 12 embryos in which the two targets with links to actin organization, (D) the Tetraspanin TM4SF and (E) the Filamin Cheerio, have been knocked down individually or (F) together, along with the control (C). Scale bar: 50 µm. (G) Quantification shows that the number of macrophages in the germband is reduced in embryos expressing RNAi against either *cher (KK 107451*) or *TM4SF* (*KK 102206*) in macrophages, and even more strongly affected in the double RNAi of both. Control vs. *cher RNAi* p=0.0005 (46% reduction). Control vs. *TM4SF RNAi* p=0.009 (37% reduction), Control vs.

cher/TM4SF RNAi p>0.0001 (61% reduction). *cher RNAi* vs. *TM4SF RNAi* p=0.15. SD: 29, 23, 17, 12. (H-K) Lateral views of a representative St 12 embryo from (H) the control, as well as embryos expressing *DfosDN* in macrophages along with either (I) *GFP*, (J) *cher*, or (K) *TM4SF*. (L) Quantification shows that over-expression of *TM4SF* in *DfosDN* expressing macrophages restores their normal numbers in the gb. Over-expression of *cher* in this background shows a strong trend towards rescue, but did not reach statistical significance. Control vs. *DfosDN* p=0.015 (28% reduction); Control vs. *cher* p=0.74; Control vs. *TM4SF* p>0.99; *DfosDN* vs. *DfosDN cher* p=0.14; DfosDN vs. *DfosDN, TM4SF* p<0.0001; Control vs. *cher* p=0.97; Control vs. *TM4SF* p=0.35. SD: 22, 16, 16, 21, 22, 13. (M-O) q-PCR analysis of mRNA extracted from the bones of mice that are wild type, transgenic (tg) for *Fos* controlled by a Major Histocompatibility promoter and viral 3'UTR elements, and those in which such c-Fos transgenesis has led to an osteosarcoma (OS). Analysis of mRNA expression shows that higher levels of (M) *Fos* correlate with higher levels of (N-N") *FlnA-C*, and (O) *Tspan6* in osteosarcomas. p values = 0.86, 0.001, 0.003, SD: 0.7, 0.6, 0.3 in M, 0.98, 0.009, 0.007 and 0.4, 0.2, 1.5 in N, 0.39, < 0.0001, <0.0001 and 0.2, 0,3, 1.1 in N', 0.76, 0.005, 0.002 and 0.8, 2.3, 2.4 in N", 0.99, 0.004, 0.003 and 0.1, 0.2, 0.2 in O. Scale bar: 50 µm. Macrophages are labeled using either (C-F) *srp::H2A::3xmCherry* or (H-K) *srpHemo-Gal4* ("*mac>*") driving *UAS-mCherry::nls.* ***p<0.005, **p<0.01, *p<0.05. Unpaired t-test or one-way ANOVA with Tukey post hoc were used for statistics. Each column contains the number of analyzed embryos.

We examined by qPCR the mRNA levels of our identified Dfos targets' orthologs, comparing their levels in osteosarcomas (Fos tg OS) to neighboring, osteoblast-containing healthy bones from Fos tg mice (Fos tg bone) and control bones from wild-type mice (wt bone). We saw 2.5 to 8 fold higher mRNA levels of the three murine Filamin orthologs (Fig 3N-N") and a 15 fold increase in Tetraspanin-6 (Fig 3O) in osteosarcoma cells. mRNA levels of several of the orthologs of other Dfos targets we had identified showed less strong inductions or even decreases; the Glutathione S transferase Gstt3 and the Slit receptor Eva1c increased 4 and 2.8 fold respectively, while the mitochondrial translocator Tspo was 25% lower (S3F-I Fig). These results suggest that Dfos's ability to increase mRNA levels of two key functional targets for migration, a Filamin and a Tetraspanin, is maintained by at least one vertebrate fos family member.

2.3.5 Dfos increases assembly of cortical actin through Cheerio and TM4SF to aid macrophage invasion

We wished to determine what cellular properties Dfos could affect through such targets to facilitate *Drosophila* macrophage invasion. Given Cheerio's known role as an actin crosslinker, we examined actin in invading *mac>DfosDN* macrophages within live embryos.

To visualize actin in macrophages, we utilized a *srpHemo-moe::3xmCherry* reporter which marks cortical F-actin (Edwards et al., 1997; Franck et al., 1993) and observed a reduction of 53% (Fig 4A-D) in its signal in invading m*ac>DfosDN* macrophages. We saw no change by Western analysis in the levels of the Moe::3xmCherry protein itself upon *DfosDN* expression (Fig S4A-A'). We hypothesized that the changes in cortical actin we observed in the *mac>DfosDN* all could be due to the lower levels of Cheerio and/or TM4SF mRNA. Indeed, we observed reductions in Moe::3xmCherry all around the edge of invading macrophages in live embryos expressing RNAi against *cher* or *TM4SF* in macrophages (Fig 4E-H).

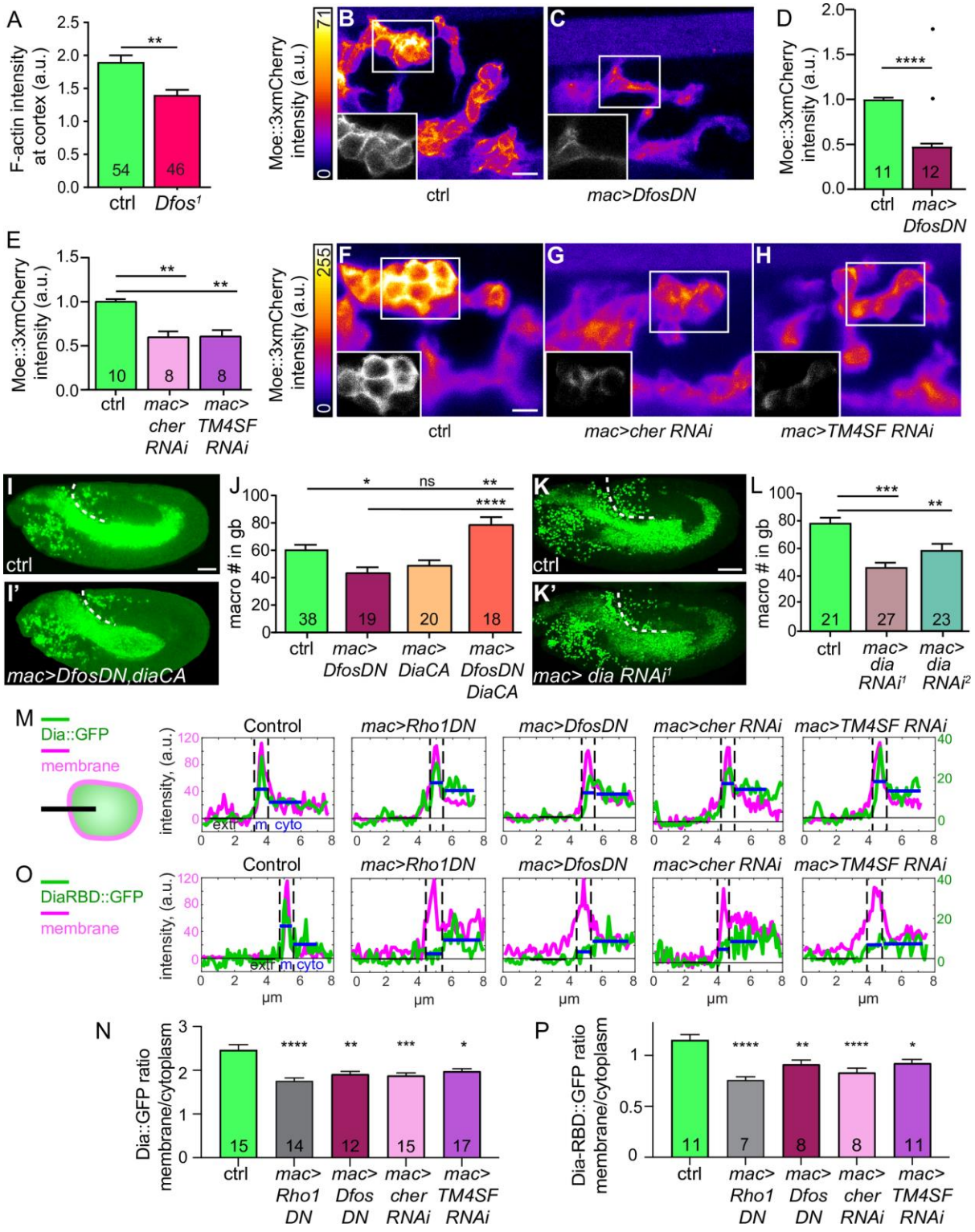

Chapter 2 Fig 4. Dfos regulates the actin cytoskeleton through Cher, TM4SF, and the formin Diaphanous
(A) Quantification of phalloidin intensity to detect F actin at the macrophage-macrophage contacts in Stage 11/12 *Dfos*^{1} embryos. F-actin is strongly reduced at these homotypic contacts. (B-C) Representative confocal images of live embryos expressing in invading macrophages the F-actin binding and homodimerizing portion of Moesin (*srpHemo-moe::3xmCherry)* to label F-actin, presented as a maximum z-projection. Relative Moe-3xmCherry intensity is indicated with a pseudo-color heat map as indicated on the left, with yellow as the highest levels and dark blue as the lowest as indicated in the calibration bar to the left. Insets in the bottom left corner of each panel show a grey-scale single z-plane corresponding to the white box in the main image. Embryo genotype indicated below. Strong reductions in cortical actin are observed in macrophages expressing DfosDN

compared to the control. (D-E) Quantification of the macrophage Moe:3xmCherry intensity as a measure of cortical F-actin, normalized to the average fluorescence intensity of the control per batch. (D) Quantification shows that macrophages expressing *DfosDN* display a 53% reduction in Moe::3xmCherry intensity compared to the control when the two outliers shown as single dots are excluded, 37% if they are included. Outliers identified by 10% ROUT. n of ROIs analysed = 650 for control, 687 for *DfosDN*. p=0.0007 for analysis including outliers (Kolmogorov-Smirnov) and p<0.0001 for analysis excluding outliers (Welch's t-test). SD: 0.2, 0.4. (E) Quantification reveals that macrophage expression of an RNAi against either *cher* or *TM4SF*, the two genes whose expression is reduced in *DfosDN*, also results in a decrease of Moe::3xmCherry intensity (by 40% each). n of ROIs analysed = 549 for control, 423 for *cher RNAi,* 306 for *TM4SF RNAi.* Control vs. *cher RNAi* p=0.006. Control vs. *TM4SF* p=0.003. SD: 0.2, 0.3, 0.2. (F-H) Images and representation as in B-C. Strong reductions in cortical actin are observed in macrophages expressing *cher RNAi* or *TM4SF RNAi* compared to the control. (I,I') Representative confocal images of St 12 embryos from the control and a line in which macrophages express *DfosDN* and a constitutively active (CA) form of the formin Dia to restore cortical actin polymerization. (J) Quantification shows that while macrophage expression of *DiaCA* does not significantly affect the number of macrophages in the gb, expressing it in a *DfosDN* background rescues macrophage gb invasion. Control vs. *DfosDN* p=0.017 (28% reduction), Control vs. *diaCA* p=0.18, Control vs. *DfosDN*, *diaCA* p=0.010, *DfosDN* vs. *DfosDN, diaCA* p<0.0001. SD: 22, 16, 16, 24. (K,K') Representative confocal images of St 12 embryos from the control and from a line expressing an RNAi against *dia* in macrophages. (L) Quantification of two RNAi lines against *dia* expressed in macrophages shows a 37% and 21% reduction in macrophage numbers in the gb compared to control. Control vs. *dia RNAi*^{1} (TRiP HMS05027) p<0. 0001; control vs. *dia RNAi*^{2} (TRiP HMS00308) p=0.0008. SD: 13, 20, 22. (M, O) Examples of line profiles used for the determination of the membrane-to-cytoplasmic ratio of Dia in panel N and DiaRBD in panel P. Line intensity profiles from fixed Stage 11 embryos of (M) Dia::GFP or (O) DiaRBD::GFP (green) and membrane myr::Tomato (magenta) across the outward facing edge of groups of macrophages sitting within ~ 40 µm of the germband that expressed either lacZ (Control), Rho1DN, DfosDN, *cher RNAi*, or *TM4SF RNAi* as shown in the schematic in M. Line length ~ 8 µm. Blue lines indicate mean GFP intensity on the membrane and in cytoplasm. (N, P) Quantification of membrane-to-cytoplasmic intensity ratio of (N) Dia::GFP or (P) DiaRBD::GFP expressed in macrophages under UAS control along with either lacZ (control, n=233 from 15 or n=158 line scans from 11 embryos), Rho1DN (n=212 from 14 or n=123 from 7), DfosDN (n=237 from 12 or n=135 from 8), *cher RNAi* (n=252 from 13 or n=128 from 8), *TM4SF RNAi* (n=279 from 17 or n=205 from 11). Control vs. Rho1DN ****p<0.0001 (29% (N), 34% (P) reduction), Control vs. DfosDN p=**0.0037 (23% (N), 21% (P) reduction), Control vs. *cher RNAi* ***p=0.0007 (24% (N), 28% (P) reduction), Control vs. *TM4SF RNAi* *p=0.024 or 0.026 (20% reduction). SD: 1.9, 0.9, 1.0, 0.9, 1.0 in N; 0.7, 0.5, 0.5, 0.5, 0.4 in P. Macrophages are labeled using either *srpHemo-Gal4* driving *UAS-mCherry::nls* (I-I'), *srpHemo-H2A::3xmCherry* (K-K'). *srpHemo-moe::3xmCherry*, *srpHemo-Gal4* (*mac>)* crossed to (B) *UAS-GFP* as a Control, (C) *UAS-DfosDN*, (F) *w*$^{-}$ Control, (G) *UAS-cher RNAi* (KK 107451), (H) *UAS-TM4SF RNAi* (KK 102206). *srpHemo-GAL4 UAS-Myr::tdTomato UAS-dia::GFP* (M, O) *or UAS-diaRBD::GFP* (N, P) crossed to *UAS-lacZ* as a Ctrl, *UAS-Rho1DN* or the lines indicated above. ***p<0.005, **p<0.01, *p<0.05. Unpaired t-test used for A. Welch's t test of normalized average mean intensity per embryo for D with the two indicated outliers excluded, for statistical assessment. One way ANOVA with Tukey post hoc for E, J, L. Kruskal-Wallis for N, P. The number of analyzed (A) macrophage-macrophage junctions, or (D-E, J, L, N, P) embryos is shown in each column. Scale bar 10µm in (B-C, F-H), 50µm in (I, K).

To test if a decrease in actin assembly could underlie the reduced tissue invasion of *mac>DfosDN* macrophages, we forced cortical actin polymerization by expressing a constitutively active version of the formin Diaphanous (*DiaCA*), in which Dia's inhibitory auto regulatory domain has been deleted, allowing active Dia to localize to the macrophage cortex (Davidson et al., 2019). Indeed, expressing *DiaCA* in macrophages completely rescued the *Dfos*^{1}, *Dfos*^{2} (Fig S4B), and *mac>DfosDN* invasion defect (Fig 4I-J). Given that Dia, like Dfos, does not affect general macrophage migratory capacities along the ventral nerve cord (Davis et al., 2015), we examined if Dia might normally play a role in invasion. We utilized two RNAis against Dia and observed decreased macrophage numbers in the gb in each (Fig 4K-L) with no effect on numbers in the pre-gb (S4C Fig) or on the vnc (S4D Fig). These results argue that

Dfos aids invasion by increasing levels of TM4SF and Cheerio to enhance assembly of actin around the surface of the macrophage.

2.3.6 Dfos stimulates the cortical activity of Rho1 and Diaphanous through its targets TM4SF and Cheerio

We hypothesized that Dfos and its targets enhance cortical actin assembly by affecting Dia. We had observed no increase in Dia's mRNA levels (S3C Fig) upon DfosDN expression, and thus examined localization of Dia protein. We expressed Dia::GFP (Homem and Peifer, 2008) in macrophages along with Myr::Tomato to mark the membrane and quantified intensity profiles of linescans across the membrane in various genetic backgrounds, assessing the ratio of membrane/ cytoplasmic mDia (Fig 4M). Dia's autoinhibition negatively regulates its cortical localization and activity in *Drosophila* macrophages (Davidson et al., 2019, Goode and Eck 2007). For mDia, binding to activated Rho GTPases as well as to other unknown membrane associated proteins can release this autoinhibition (Seth et al., 2006). *Drosophila* Rho1 has been shown to directly bind Dia lacking its autoinhibitory domain (Großhans et al., 2005). As predicted by these prior results, upon the expression of Rho1DN we observed a significant reduction, by 29%, in the enrichment of Dia at the cortex compared to the control (mem/cyto=2.46 in control, 1.76 for Rho1DN) (Fig 4N). We found that expressing either DfosDN, or RNAis against Cher or TM4SF resulted in a significant reduction of cortical Dia, 80, 83, and 70% respectively as strong as that seen upon Rho1DN expression (mem/cyto=1.9, 1.88, 1.97). To assess if this effect of the Dfos pathway on Dia could be due to an effect on Rho activity itself, we expressed a sensor of active Rho1, the Rho1 binding domain of Dia (DiaRBD::GFP) (Abreu-Blanco et al., 2014), in macrophages along with myristoylated Tomato to delineate the plasma membrane and quantified intensity profiles of linescans across the membrane in various genetic backgrounds as above (Fig 4O). To validate the assay we expressed Rho1DN and found, as expected, a significant reduction, by 34%, in the enrichment of DiaRBD at the cortex compared to the control (mem/cyto=1.15 in control, 0.76 for Rho1DN) (Fig 4P). Expressing either DfosDN, or RNAis against the filamin Cher or the tetraspanin TM4SF also resulted in a significant reduction of cortical DiaRBD, by 62, 82, and 59% respectively as much as that seen upon Rho1DN expression (mem/cyto=0.91, 0.83, 0.92 respectively). The lower Rho1 activity we observed in the absence of the Dfos pathway could be a result of reduced Rho1 GEF recruitment, as Filamin has been shown to bind the Rho GTPase GEFs Trio and Vav2 (Bellanger et al., 2000, Del Valle-Perez B., et al., 2010) and a Tetraspanin can recruit a Filamin (Brzozowski et al., 2018, Perez-Hernandez et al., 2013). Our data argue that higher levels of the Dfos targets TM4SF and Cheerio increase Dia localization at the cortex and thus stimulate cortical actin assembly, at least partially through increased Rho1 activity.

We examined what consequence these lower cortical F-actin levels had on the cellular behavior of macrophages during entry. Quantitation showed that the actin protrusion that macrophages initially insert between the ectoderm and mesoderm during invasion was actually longer in the *mac>DfosDN >LifeAct::GFP* macrophages than in the control (Fig 5A, S5A Fig, S4 Movie).

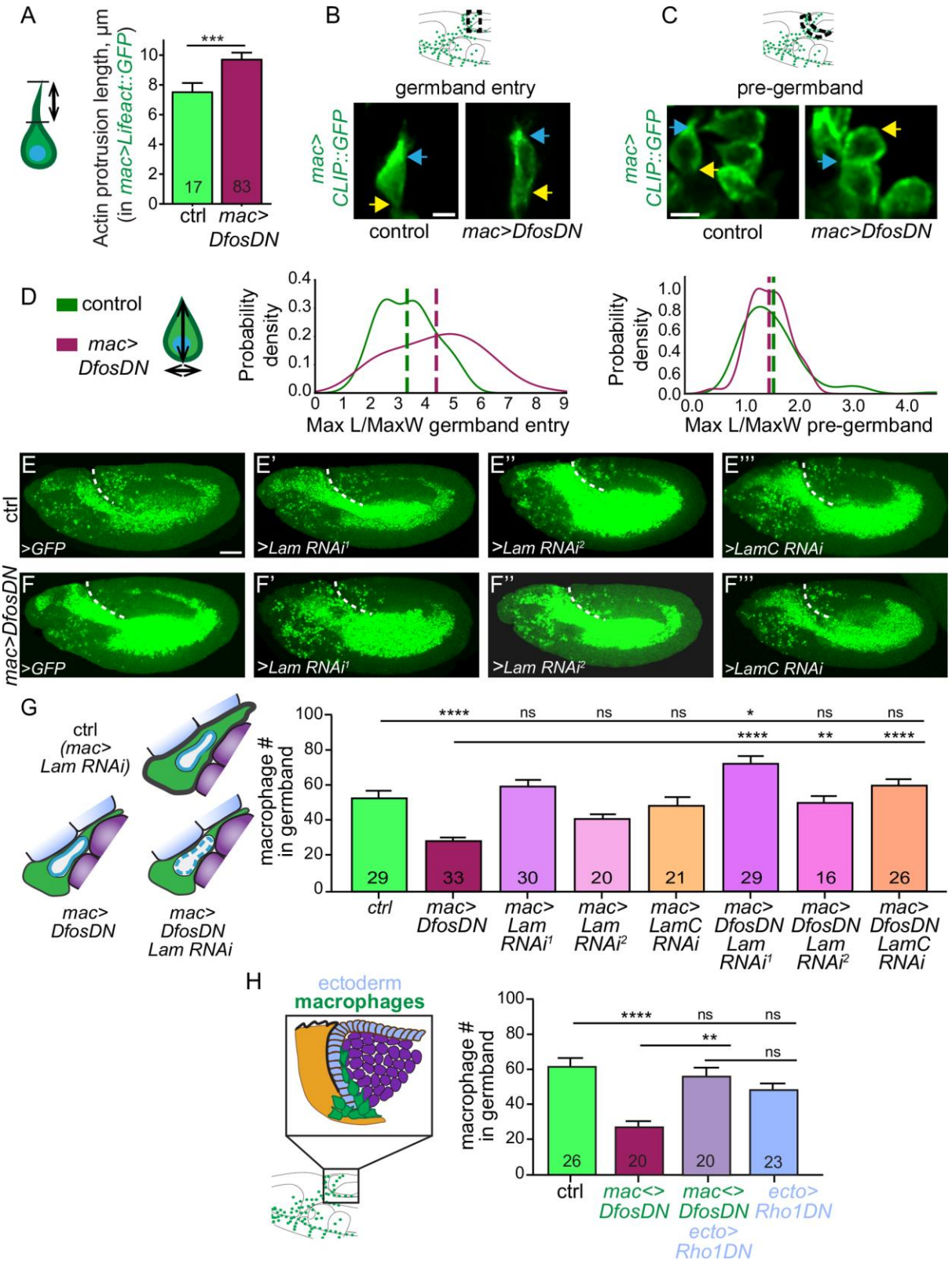

Chapter 2 Fig 5. Dfos aids macrophage gb invasion against the resistance of surrounding tissues and buffers the nucleus

(A) Quantification from live embryos shows that the length of the F-actin protrusion of the first entering macrophage is longer in macrophages expressing DfosDN. p= 0.011. The F-actin protrusion labelled with *srpHemo-Gal4* driving *UAS-LifeAct::GFP* was measured in the direction of forward migration (see schematic). SD: 2.4, 3.7. (B-C) Stills from 2-photon movies of St 11 embryos showing (B) the first macrophages entering the gb and (C) macrophages in the pre-gb zone in the control and in a line expressing *DfosDN* in macrophages.

Microtubules are labelled with *srpHemo-Gal4* driving *UAS-CLIP::GFP*. A blue arrow indicates the front and a yellow arrow indicates the rear of the macrophage. Schematics above indicate where images were acquired (D) Schematic at left shows macrophage measurements: vertical line for the maximum length and horizontal line for the maximum width. Histograms show the probability density distributions of the aspect ratios (maximum length over maximum width) of the first macrophage entering the gb (left) and macrophages in the pre-gb (right). Macrophages expressing *DfosDN* are more elongated the *mac>DfosDN* line. Control vs. *DfosDN* aspect ratios at gb entry p=0.0011, in pre-gb p=0.53. SD: in gb 1.0, 1.6; in pre-gb 0.5, 0.5. Confocal images of St 12 embryos expressing RNAi against Lamin or LaminC in macrophages in (E-E''') the control, or (F-F''') in embryos also expressing *DfosDN* in macrophages. *srpHemo-GAL4* used as drover. *Lam RNAi*^{1}: GD45636; *Lam RNAi*^{2}KK107419. *Lam C RNAi:* TRiP JF01406 (G) Macrophage RNAi knockdown of Lamins which can increase nuclear deformability did not affect macrophages numbers in the gb in the control. In embryos in which macrophages expressed *DfosDN*, *Lamin* knockdown rescues their reduced numbers in the gb. Control vs. *DfosDN* p<0.0001. Control vs. *Lam RNAi*^{1} p>0.99, vs. *Lam RNAi*^{2} p=0.83, vs. *LamC RNAi* p>0.99. Control vs. *DfosDN, Lam RNAi*^{1} p=0.024, vs. *DfosDN, Lam RNAi*^{2} p>0.99, vs. *DfosDN, LamC RNAi* p>0.99. *DfosDN* vs. *DfosDN, Lam RNAi*^{1} p<0.0001, vs. *DfosDN, Lam RNAi*^{2} p=0.0049, vs. *DfosDN, LamC RNAi* p<0.0001. SD: 22, 10, 19, 11, 21, 23, 16, 20. (H) Expressing *DfosDN* in macrophages reduces their number in the gb. Concomitantly reducing tissue tension in the ectoderm (light blue in schematic) through Rho1DN substantially rescues invasion. *srpHemo-QF QUAS* control (*mac<>)* governed macrophage expression and *e22C-GAL4* ectodermal (*ecto>*). Control vs. *mac<>DfosDN* p<0.0001 (56% reduction), vs. *mac<>DfosDN; ecto>Rho1DN* p>0.99, vs. *ecto>Rho1DN* p=0.11. *mac<>DfosDN* vs. *mac<>DfosDN; ecto>Rho1DN* p<0.0001, vs. *ecto>Rho1DN* p=0.0044. *mac<>DfosDN; ecto>Rho1DN* vs. *ecto>Rho1DN* p>0.99. SD: 23, 16, 21, 18.
Macrophages are labeled in B-C by *srp-Gal4* driving *UAS-CLIP::GFP,* and in E-F'" by *srpHemo-Gal4 UAS-mCherry-nls*. ***p<0.005, **p<0.01, *p<0.05. Unpaired t-test was used for A, one way ANOVA with Tukey post hoc for G-H. The number shown within the column corresponds to measurements in A, and analysed embryos in G-H. Scale bar 5µm in B-C, and 50µm in E-F'''.

We then performed live imaging of macrophages labeled with CLIP::GFP to visualize microtubules and thus cell outlines in both genotypes; we determined the aspect ratio (maximal length over width) that the first entering cell displays as it enters into the gb. The first DfosDN-expressing macrophage was extended even before it had fully moved its rear into the gb (S5B Fig). We carried out measurements, taking only cells that had entered the gb to be able to clearly distinguish the rear of the first macrophage from the tips of following cells (Fig 5B). We also avoided including in this measurement the forward protrusion and determined that the first macrophage inside the gb displays an average increase of 23% in the maximal length (L) of the cell body and a 12% reduction in the maximal width (W) (S5 Fig). Interestingly, in the pre-gb zone the aspect ratio (max L/W) of *mac>DfosDN* macrophages was not different from control macrophages (Fig 5C-D) although the *mac>DfosDN* cells were 9% smaller in both their length and width (S5D Fig). This suggested that the gb could impose resistance on the entering macrophage, an effect which *mac>DfosDN* macrophages have trouble overcoming due to their compromised cortical actin cytoskeleton.

2.3.7 Dfos promotes advancement of macrophages against the resistance of the surrounding tissues and buffers the nucleus

We therefore examined how the properties of the gb tissues and macrophages interact during invasion. We first investigated if the macrophage nucleus impedes normal invasion by varying levels of the two *Drosophila* Lamin genes, Lam and LamC, both equally related to the vertebrate lamins A and B1 (Muñoz-Alarcón et al., 2007) and both shown to affect nuclear stiffness and deformability (Wintner et al., 2020; Zwerger et al., 2013). Over-expressing Lam (S5E Fig) or knocking down either of these Lamins in macrophages through RNAi (Perkins et al., 2015) did not change macrophage numbers in the gb of wild type embryos (Fig 5E-E''', G),

suggesting that the properties of the macrophage nucleus are not a rate limiting parameter during normal tissue invasion into the narrow path between the ectoderm and mesoderm. This result also argues that Lamins' capacity to alter gene expression is not normally important for invasion (Andrés & González, 2009).
However in *mac>DfosDN* macrophages, knockdown of these Lamins was able to rescue the gb invasion defect (Fig 5E-G), supporting the conclusion that the properties of the nucleus affect invasion in the absence of the higher levels of cortical actin Dfos normally induces. To directly test if reducing the tension of surrounding tissues can counteract the absence of Dfos, we expressed Rho1DN in the ectoderm with the *e22C-GAL4* driver while expressing *QUAS-DfosDN* in macrophages with the GAL4-independent Q-system driver we had constructed, *srpHemo-QF2* (Gyoergy et al., 2018). Rho1 through ROCK is a key regulator of Myosin activity, epithelial tension and tissue stiffness (Warner & Longmore, 2009; Zhou et al., 2009); Myosin II is essential for actin contractility (Heer & Martin, 2017) and tension in the *Drosophila* gb ectoderm (Ratheesh et al., 2018). Indeed, we found that this reduction of ectodermal tension substantially rescued DfosDN expressing macrophage numbers in the gb (Fig 5H). Taken together our results argue that Dfos aids *Drosophila* macrophages in withstanding the resisting force of surrounding cells against the nucleus during invasion into tissues.

2.4 DISCUSSION

We identify the ability to tune the state of the cortical actin cytoskeleton as a key capacity for immune cells migrating into and within tissue barriers *in vivo*. We find that macrophages upregulate a program governed by the transcription factor Dfos to enable this. Dfos in *Drosophila* is known to regulate the movement during dorsal or wound closure of epithelial sheets (Brock et al., 2012; Lesch et al., 2010; Riesgo-Escovar & Hafen, 1997; Zeitlinger et al., 1997) as well as the development of epithelial tumors and their dissemination (Külshammer et al., 2015; Uhlirova & Bohmann, 2006; Külshammer & Uhlirova, 2013; Benhra et al., 2018). Here we define a different role, namely that Dfos enables a stream of individual immune cells to efficiently push their way into tissues, a process which is aided rather than hampered by the presence of the ECM (Sánchez-Sánchez et al., 2017; Valoskova et al., 2019). This function appears to be specifically required for invasion, as we observe no defects in *DfosDN* macrophages' migratory speed in open environments. *DfosDN* macrophages display decreased actin at the cell circumference and an elongated shape within in the confinement of the germband, suggesting a defect in the stiffness of the cortex. Strikingly, only in the presence of *DfosDN* does the state of the nucleus become relevant, with reductions in Lamins shown to underlie nuclear stiffness (Wintner et al., 2020) enhancing the ability of macrophages to invade. These findings along with the ability of a softened ectoderm to substantially rescue the *DfosDN* macrophages' germband invasion defect lead us to propose the model (Fig 6) that Dfos permits efficient initial translocation of the macrophage body under ectodermal reactive load by forming a stiff cortical actin shell that counteracts surrounding tissue resistance and protects the nucleus from undergoing high levels of mechanical stress during tissue entry.

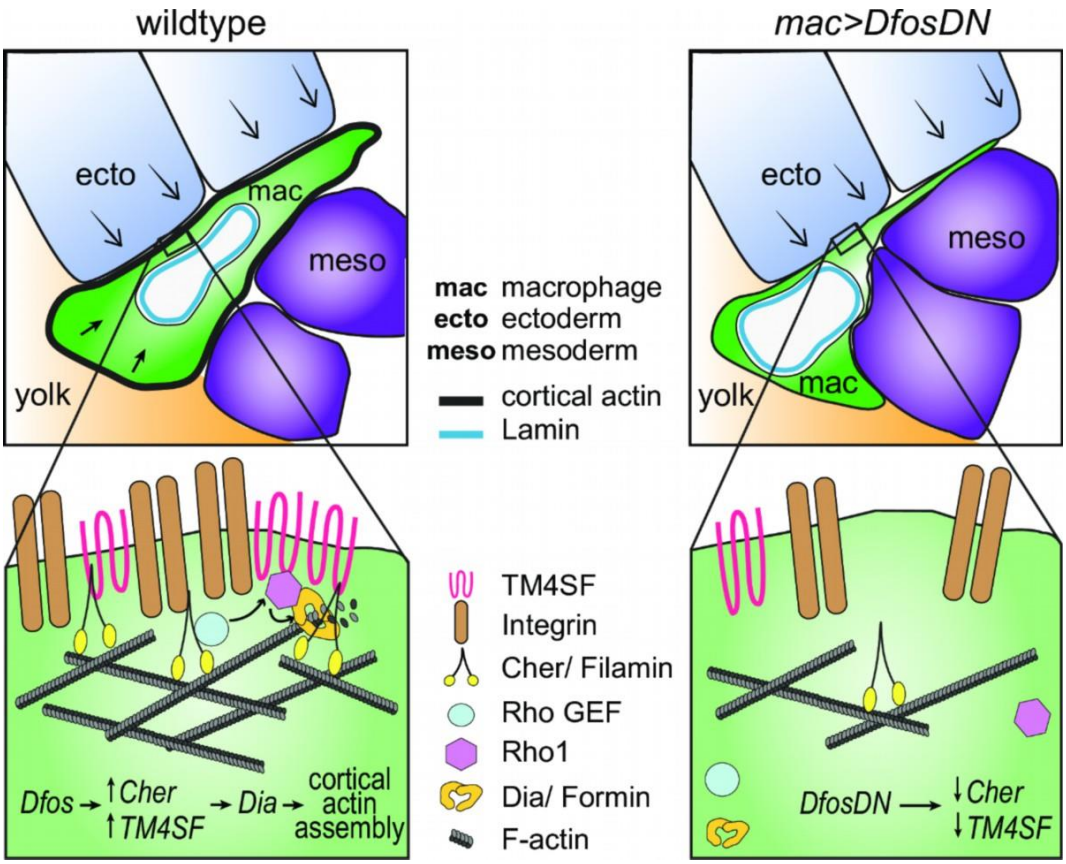

Chapter 2 Fig 6. Model: Dfos increases actin assembly and crosslinking through the tetraspanin TM4SF and the Filamin Cheerio to counter surrounding tissue resistance

We propose a speculative model for how Dfos tunes the cortical actin properties of *Drosophila* embryonic macrophages to aid their infiltration against the resistance of the surrounding germband tissue. We have shown that Dfos leads to an increase of the tetraspanin TM4SF and the Filamin Cheerio (Cher). Filamins cross-link actin and have been shown to bind to RhoGEFs; Tetraspanins bind to Integrins, Rho GTPases and Filamins in other systems (see Figure S6). Thus, we hypothesize that in *Drosophila* macrophages TM4SF and the Filamin Cheerio could form a network at the cell surface of Integrin, actin and upstream signaling molecules, recruiting Rho GEFs and leading to the activation of Rho1 GTPase and the actin polymerizing Formin Dia. Dia activation could occur through direct binding to active Rho1 and through direct interaction with TM4SF or Cheerio. Validation in *Drosophila* of all the protein interactions we propose awaits biochemical analysis. Through this pathway, a more crosslinked and dense F-actin network would form, aiding the macrophage in moving its cell body into the ecto-meso interface. The presence of Lamin around the nuclear membrane would not normally affect this process since the dense cross-linked cortical actin network would help macrophages withstand the load of the surrounding tissues. However, in the DfosDN-expressing macrophages, the loss of Cher and TM4SF would lead to reduced cross-linked actin levels at the cell cortex, making the stiffness of the nucleus the rate-limiting step for macrophage infiltration of the gb tissue.

2.4.1 A molecular program for tissue invasion that strengthens cortical actin

Crucial mediators of this process are two actin regulators, the filamin Cher, known to be a Dfos target in epithelia, and the previously uncharacterized membrane scaffold tetraspanin TM4SF. We show that both require Dfos for higher mRNA levels in macrophages and present correlative evidence that these classes of genes are also upregulated by vertebrate c-fos. Each of these Dfos targets is required for macrophage invasion; over-expression of TM4SF in macrophages can rescue the *DfosDN* tissue invasion phenotype. We propose that these targets act together to strengthen the actin cytoskeleton for tissue invasion. Higher Filamin

levels cross-link actin filaments into resilient and stiffer networks maintaining cell integrity during mechanical stress (Goldmann et al., 1997; Tseng et al., 2004; Fujita et al., 2012). This aids the distribution of forces from focal adhesions across the entire migrating cell body, since Filamins can bind directly to Integrin, and even more strongly under strain (Ehrlicher et al., 2011; Glogauer et al., 1998; Kumar et al., 2019; Razinia et al., 2012). Tetraspanins, self-associating multipass transmembrane proteins, also can bind Integrin, forming microdomains of adhesion molecules, receptors and their intracellular signaling complexes, including Rho GTPases (Termini & Gillette, 2017; Berditchevski & Odintsova, 1999, Zhuang et al, 2007, Delaguillaumie, et al., 2002, Hong et al., 2012; Tejera et al., 2013). Filamins similarly bind receptors, regulators of actin assembly, Rho GTPases and the Rho GEFs Trio and Vav2 (Popowicz et al., 2006; Stossel et al., 2001; Vadlamudi et al., 2002; Ohta et al., 1999; Bellanger et al., 2000, Del Valle-Perez, B., 2010). We observe reduced cortical levels of F-actin, active Rho1, and the actin polymerizing formin Diaphanous in the absence of either Dfos, the Filamin Cheerio or the Tetraspanin TM4SF. Thus our data supports the hypothesis that these Dfos targets enhance the cortical recruitment and activation of the formin Dia to stimulate actin polymerization at least in part through the recruitment of RhoGEFs which enhance GTP bound Rho1, which can activate Dia (Fig 6, S6 Fig) (Rose, et al, 2005; Rousso et al., 2013; Seth et al., 2006; Großhans et al., 2005; Williams et al., 2007; Vetter & Wittinghofer, 2001). Cheerio and/or Tetraspanin may also directly contribute to Dia activation, as Rho independent mechanisms of activation have been proposed (Homem and Peifer, 2009) and direct binding between Filamins and Formins has been observed (Hu et al., 2014; Lian et al., 2016). Full confirmation of our hypotheses requires future biochemical characterization of the interactions of these players in *Drosophila*. Dfos' upregulation of Cheerio and TM4SF could thus lead to a supra-network in which ECM-anchored FAs connect to a strong cross-linked cortical actin lattice, allowing Myosin contraction to be converted into cellular advancement despite resistance from the flanking ectoderm.

We demonstrate that the actin nucleating formin Dia is important for *Drosophila* macrophage invasion and capable of rescuing the defects in the *DfosDN* mutant. Unlike the formin Ena which mediates chemotaxis (Davidson et al., 2019), Dia is not required for general *Drosophila* macrophage migration, and instead allows macrophages to recoil away from one another (Davis et al., 2015). Dia could be required for macrophages specifically when they face resistance from their surroundings and need to increase their cortical tension. Modeling indicates that Dia1's regulation of cortical tension requires an optimal combination of actin cross-linking and intermediate actin filament length (Chugh et al., 2017). *Drosophila* Dia is a more processive nucleator than Ena (Bilancia et al., 2014) and thus could create the intermediate length actin filaments that enable higher levels of macrophage cortical tension and strain stiffening (Kasza et al., 2010) on all sides of the cell during their invasion.

Our findings thus demonstrate that there are commonalities in the molecular mechanisms by which *Drosophila* cells invade into either confluent tissues or the ECM. Dfos's upregulation of the Filamin Cheerio is also required in tumor cells and aneuploid epithelial cells to enhance ECM breaching (Külshammer & Uhlirova, 2013; Benhra et al., 2018). Both cell types displayed enhanced levels of cortical filamentous actin, which in the tumors is concomitant with Dia upregulation (Külshammer & Uhlirova, 2013). In the oocyte, Filamin is required for follicle cell intercalation and border cells display higher levels of Filamin and F-actin to maintain cellular integrity during migration between nurse cells (Sokol & Cooley, 2003; Somogyi & Rørth, 2004). The mediator of these increased F-actin levels, MAL-D, can be activated by Dia (Somogyi & Rørth, 2004). Thus while MMPs may be specific to ECM crossing, a denser and more cross

linked actin cortex due to increased levels of the filamin Cheerio and activity of the formin Dia could be a common feature of *Drosophila* cells moving through the resistance of either ECM or surrounding tissues. Determining if such shifts in cell surface actin properties underlie some vertebrate cancer cells' capacity to metastasize even in the presence of MMP inhibitors is an interesting area of inquiry (Butcher et al 2009; Kessenbrock et al 2010).

2.4.2 Implications for vertebrate immune cell migration

Our work also suggests a new perspective on the migration of some vertebrate immune cells. We find that altering lamin levels does not normally affect *Drosophila* macrophage tissue invasion. This contrasts with results showing that nuclear deformability from lower lamin levels underlies the migration of some immune cell types through narrow constrictions engineered from rigid materials (Davidson et al., 2014; Thiam et al, 2016). However, negotiation of such extremely challenging *in vitro* environments can lead to DNA damage (Raab et al., 2016) and higher nuclear flexibility caused by lower lamin levels is associated with increased cell death (Harada et al., 2014). A robust cell surface actin layer would allow long-lived cells or those not easily replenished to protect their genome as they move through resistant yet deformable environments. Embryonic *Drosophila* and vertebrate tissue resident macrophages migrate into tissues during development, survive into the adult, and serve as founders of proliferative hematopoietic niches (Holz et al., 2003; Makhijani et al., 2011; Bosch et al., 2019; Ginhoux and Guilliams, 2016; Theret et al 2019; Guilliams et al, 2020). Tissue resident memory T cells migrate in response to infection in mature animals, are long-lived and not easily renewed from the blood (Szabo et al., 2019). Thus the importance of nuclear mechanics for migration in challenging *in vivo* environments should be explored for a broader range of immune cells as well as the utilization of cortical actin as a strategy for genomic protection.

2.5 MATERIALS AND METHODS

2.5.1 Fly strains and genetics

Flies were raised on standard food bought from IMBA (Vienna, Austria) containing agar, cornmeal, and molasses with the addition of 1.5% Nipagin. Adults were placed in cages in a fly room or a Percival DR36VL incubator maintained at 25ºC and 65% humidity or a Sanyo MIR-153 incubator at 29ºC within the humidity controlled 25ºC fly room; embryos were collected on standard plates prepared in house from apple juice, sugar, agar and Nipagin supplemented with yeast from Lesaffre (Marcq, France) on the plate surface. Fly crosses and embryo collections for RNA interference experiments (7 hour collection) as well as live imaging (6 hour collection) were conducted at 29°C to optimize expression under GAL4 driver control (Duffy, 2002). All fly lines utilized are listed below.

2.5.2 Fly stocks

srpHemo-GAL4 (mac>) was provided by K. Brückner (UCSF, USA)(Brückner et al., 2004). Oregon R (control), P{CaryP}attP2 (control), P{CaryP}attP40 (control), kay^2 ($Dfos^2$), (UAS-Fra)2 (Dfos), UAS-Rho1.N19 Rho1DN), UAS-fbz (DfosDN), UAS-kayak RNAi (Dfos RNAi) TRiP HMS00254 and TRiP JF02804, UAS-dia RNAi TRiP HM05027, UAS-LamC RNAi TRiP JF01406 and

TRiP HMS00308, e22c-GAL4 (ecto>), Resille::GFP, UAS-GFP::nls, UAS-dia::EGFP, UAS-diaRBD::EGFP, UAS-mCherry::nls, UAS-CD8::GFP lines were obtained from the Bloomington Stock Center (Indiana, USA). kay^{1} (Dfos^{1}) line was provided by O. Schuldiner (WIS, Israel). UAS-dia::deltaDad::EGFP (diaCA) and srpHemo-GAL4 UAS-CLIP::GFP (mac>CLIP::GFP) lines were provided by B. Stramer (KCL, UK). UAS-cher::FLAG (cher) line was provided by M. Uhlirova (CECAD, Germany). w[1118] (control), UAS-cher RNAi KK107451, UAS-TM4SF RNAi KK102206, UAS-Lam RNAi^{1} GD45636, UAS-Lam RNAi^{2} KK107419 lines were obtained from the Vienna Drosophila Resource Center (Austria).

2.5.3 Extended genotypes:

Here we list the lines used in each Fig; we state first the name from FlyBase; in parentheses the name used in the Fig panels is provided.

Fig 1 and S1 Fig:
Fig 1D: *Oregon R.* Fig 1E-G: *srpHemo-GAL4, UAS-GFP (control).* S1A, F Fig: *srpHemo-Gal4, srpHemo-H2A::3xmCherry/P{CaryP}attP2 (control).* Fig 1H: *srpHemo-GAL4, UAS-GFP; kay^{1} (Dfos^{1}).* Fig 1I-L and S1B, G Fig: *srpHemo-GAL4, UAS-GFP::nls/+ (control 1).* Fig 1H, 1J, 1N: *srpHemo-GAL4, UAS-GFP/+; kay^{1} (Dfos^{1}).* Fig 1K, 1N and S1B: *srpHemo-GAL4, UAS-GFP::nls/+; kay^{2} (Dfos^{2}).* Fig 1L, 1N: *srpHemo-GAL4, UAS-GFP::nls/(UAS-Fra)2*; *kay^{2} (Dfos^{2};mac>Dfos).* Fig 1O, 1Q: *10XUAS-IVS-myr::GFP/+; srpHemo-Gal4, srpHemo-H2A*::3x*mCherry/+ (control 2 and control).* Fig 1P-Q: *UAS-DfosDN/+; srpHemo-Gal4, srpHemo-H2A*::3x*mCherry/+ (mac>DfosDN).* S1C, F Fig: *srpHemo-Gal4, srpHemo-H2A*::3x*mCherry/ UAS GFP::nls* (ctrl). *srpHemo-Gal4, srpHemo-H2A*::3x*mCherry/UAS-fbz (mac>DfosDN).* S1D Fig: *srpHemo-Gal4, srpHemo-H2A*::3x*mCherry /+* (ctrl). *srpHemo-Gal4, srpHemo-H2A*::3x*mCherry/UAS-DfosDN (mac>DfosDN).* Fig 1R and S1E, G, I Fig: *UAS-GFP; srpHemo-Gal4, srpHemo-H2A::3xmCherry (ctrl). UAS-Dfos RNAi HMS00254/srpHemo-Gal4, srpHemo-H2A::3xmCherry (mac>DfosRNAi^{1}). UAS-Dfos RNAi JF02804/srpHemo-Gal4, srpHemo-H2A::3xmCherry (mac>DfosRNAi^{2}).* S1H Fig: *srpHemo-GAL4, UAS-GFP::nls/+* or /(*UAS-Fra)2 (mac>Dfos).* S1I Fig: *UAS-GFP; UAS-Dfos RNAi HMS00254/srp-GAL4, srpHemo-Gal4, srpHemo-H2A::3xmCherry (mac>DfosRNAi^{1}+ GFP). UAS-GFP; UAS-Dfos RNAi JF02804/srpHemo-Gal4, srpHemo-H2A::3xmCherry (mac>DfosRNAi^{2}+ GFP).*

Fig 2 and S2 Fig:
Fig 2A, 2C-I and S2A-B, E Fig: *srpHemo-Gal4, srpHemo-H2A*::3x*mCherry/+ (control).* Fig 2D: *srpHemo-Gal4, srpHemo-H2A*::3x*mCherry/+* (3 movies) and *Resille::GFP/+; srpHemo-Gal4, srpHemo-H2A*::3x*mCherry/+* (4 movies, control) and *Resille::GFP/+; srpHemo-Gal4, srpHemo-H2A*::3x*mCherry/+* (3 movies) and *Resille::GFP/+; srpHemo-Gal4, srpHemo-H2A*::3x*mCherry/UAS-DfosDN (*4 movies, *DfosDN)* Fig 2A, 2C-I and S2A-B, E Fig: *srpHemo-Gal4, srpHemo-H2A*::3x*mCherry/UAS-fbz (mac>DfosDN).* S2C-D Fig: *srpHemo-GAL4, UAS-GFP.nls/+ (control).* S2C-D Fig: *srpHemo-GAL4, UAS-GFP.nls/+; kay^{2} (Dfos^{2}).*

Fig 3 and S3 Fig:
Fig 3C, G and S3D Fig: *UAS-Dicer2;; srpHemo-Gal4, srpHemo-H2A*::3x*mCherry/w^{1118} (control).* Fig 3D, 3G and S3D Fig: *UAS-Dicer2; UAS-TM4SF RNAi* KK10220*/+; srpHemo-Gal4, srpHemo-H2A*::3x*mCherry/+ (mac>TM4SF RNAi).* Fig 3E, G and S3D Fig: *UAS-Dicer2; UAS-cher RNAi* KK107451*/+; srpHemo-Gal4, srpHemo-H2A*::3x*mCherry/+ (mac>cher RNAi).* Fig 3F-G: *UAS-*

Dicer2; UAS-cher RNAi KK107451/*UAS-TM4SF RNAi* KK102206; *srpHemo-Gal4, srpHemo-H2A::*3x*mCherry/+ (mac>TM4SF RNAi, cher RNAi).* Fig 3H, L: *srpHemo-GAL4, UAS-mCherry::nls/UAS-mCD8::GFP (control).* Fig 3I, L: *srpHemo-GAL4, UAS-mCherry::nls/UAS-mCD8::GFP; UAS-fbz/+ (mac>DfosDN).* Fig 3J, L: *srpHemo-GAL4,UAS-mCherry::nls/UAS-cheerio::FLAG; UAS-fbz/+ (mac>DfosDN, cher).* Fig 3K-L: *srpHemo-GAL4,UAS-mCherry.nls/UAS-TM4SF; UAS-fbz/+ (mac>DfosDN, TM4SF).* Fig 3L: *srpHemo-GAL4, UAS-mCherry::nls/ UAS-TM4SF (mac>TM4SF).* Fig 3L: *srpHemo-GAL4, UAS-mCherry::nls/UAS-cher (mac>cher).* S3A-C Fig: *srpHemo-Gal4, srpHemo-*3x*mCherry/+ (control).* S3A-C Fig: *srpHemo-Gal4, srpHemo-*3x*mCherry/UAS-fbz (mac>DfosDN).*

Fig 4 and S4 Fig:

Fig 4A: *srpHemo-3xmCherry; kay[1] (Dfos[1]) and srpHemo-3xmCherry; +.* Fig 4B, D and S4A Fig: *srpHemo-Gal4, srpHemo-moe::*3x*mCherry/+;UAS-mCD8::GFP/+ (Control).* Fig 4C-D and S4A Fig: *srpHemo-Gal4, srpHemo-moe::*3x*mCherry/UAS-fbz (mac>DfosDN).* S4A Fig: *w[118].* Fig 4E-F: *srpHemo-Gal4, srpHemo-moe::*3x*mCherry/w[118] (Control).* Fig 4E, G: *srpHemo-Gal4, srpHemo-moe::*3x*mCherry/UAS-cher RNAi* KK107451 *(mac>cher RNAi).* Fig 4E, H: *srpHemo-Gal4, srpHemo-moe::*3x*mCherry/UAS-TM4SF RNAi* KK102206 *(mac>TM4SF RNAi).* Fig 4I-J: *srpHemo-GAL4, UAS-mCherry.nls/UAS-mCD8::GFP (control).* Fig 4I', J: *srpHemo-GAL4, UAS-mCherry.nls/UAS-DiaΔDad::EGFP; UAS-fbz/+ (mac>DfosDN, diaCA*). Fig 4J: *srpHemo-GAL4, UAS-mCherry.nls/UAS-mCD8::GFP; UAS-fbz/+ (mac>DfosDN)*. Fig 4J: *srpHemo-GAL4, UAS-mCherry.nls/ UAS-DiaΔDad::EGFP (mac>diaCA)*. S4B Fig: #1: *UAS-GFPnls; srpHemo-Gal4, srpHemo-H2A::3xmCherry*. #2: *UAS-GFPnls/srpHemo-Gal4, srpHemo-H2A::3xmCherry*; *Dfos[1]*. #3: *UAS-GFPnls/ srpHemo-Gal4, srpHemo-H2A::3xmCherry*; *Dfos[2]*. #4: *UAS-DiaDad::EGFP/srpHemo-Gal4, srpHemo-H2A::3xmCherry*; *Dfos[1]*. #5: *UAS-DiaΔDad::EGFP/srpHemo-Gal4, srpHemo-H2A::3xmCherry*; *Dfos[2]*. Fig 4K-L and S4C-D Fig: *UAS-Dicer2;; srpHemo-Gal4, srpHemo-H2A::*3x*mCherry/P{CaryP}attP40 (control).* Fig 4K', L and S4C-D Fig: *UAS-Dicer2;+; srpHemo-Gal4, srpHemo-H2A::*3x*mCherry/ UAS-dia RNAi* HM05027 *(mac>dia RNAi[1]).* Fig 4L and S4C-D Fig: *UAS-Dicer2;+; srpHemo-Gal4, srpHemo-H2A::*3x*mCherry/UAS-dia RNAi* HMS00308 *(mac>dia RNAi[2]).* Fig 4M-N and S4E Fig: *(control) UAS-dia::EGFP/+; UAS-nlacz/ srpHemo-Gal4, 10XUAS-IVS-myr::tdTomato. (mac>Rho1DN) UAS-dia::EGFP/+; UAS-Rho1N.19)/srpHemo-Gal4, 10XUAS-IVS-myr::tdTomato. (mac>DfosDN) UAS-dia::EGFP/+; UAS-fbz/srpHemo-Gal4, 10XUAS-IVS-myr::tdTomato. (mac>cher RNAi) UAS-dia::EGFP/+; UAS-cher RNAi KK107451/srpHemo-Gal4, 10XUAS-IVS-myr::tdTomato. (mac>TM4SF RNAi) UAS-dia::EGFP/+; UAS-TM4SF RNAi KK102206/srpHemo-Gal4, 10XUAS-IVS-myr::tdTomato.* Fig 4O-P and S4F Fig: *(control) UAS-diaRBD::GFP/+; srpHemo-Gal4, 10XUAS-IVS-myr::tdTomato/UAS-nlacZ. (mac>Rho1DN) UAS-diaRBD::GFP/+; srpHemo-Gal4, 10XUAS-IVS-myr::tdTomato/UAS-Rho1N.19. (mac>DfosDN) UAS-diaRBD::GFP/UAS-fbz; srpHemo-Gal4, 10XUAS-IVS-myr::tdTomato/+. (mac>cher RNAi) UAS-diaRBD::GFP/UAS-cher RNAi KK107451; srpHemo-Gal4, 10XUAS-IVS-myr::tdTomato/+. (mac>TM4SF RNAi) UAS-diaRBD::GFP/UAS-TM4SF RNAi KK102206; srpHemo-Gal4, 10XUAS-IVS-myr::tdTomato/+*.

Fig 5 and S5 Fig:

Fig 5A and S5A Fig: *srpHemo-Gal4 UAS-LifeActGFP UAS-RedStinger/ srpHemo-Gal4 UAS-LifeActGFP, UAS-RedStinger* control*; srpHemo-Gal4 UAS-LifeActGFP UAS-RedStinger/ srpHemo-Gal4 UAS-LifeActGFP UAS-RedStinger; UAS-DfosDN/UAS-DfosDN*. Fig 5B-D and S5B-D Fig: *srpHemo-Gal4, UAS-CLIP::GFP, UAS-RedStinger (control).* Fig 5B-D and S5B-D Fig:

srpHemo-Gal4, UAS-CLIP::GFP, UAS-RedStinger; UAS-fbz (mac>DfosDN). Fig 5E, G: *srpHemo-GAL4, UAS-mCherry.nls/UAS-mCD8::GFP (control).* Fig 5E'-E'', 5G: *srpHemo-GAL4, UAS-mCherry.nls/UAS-Lamin RNAi* GD45636, KK107419 *(mac>Lam RNAi*^{1} and *mac>Lam RNAi*^{2}*, respectively).* Fig 5E''', G: *srpHemo-GAL4, UAS-mCherry.nls/UAS-LaminC RNAi* TRIP JF01406 *(mac>LamC RNAi).* Fig 5F-G: *srpHemo-GAL4, UAS-mCherry.nls/UAS-mCD8::GFP; UAS-fbz/+ (mac>DfosDN).* Fig 5F',F'', G: *srpHemo-GAL4, UAS-mCherry.nls/UAS-Lam RNAi* (*Lam RNAi*^{1}=GD45636, *Lam RNAi*^{2}=KK107419)*; UAS-fbz/+ (mac>DfosDN, Lam RNAi*^{1} and *mac>DfosDN, Lam RNAi*^{2}*).* Fig 5F''', G: *srpHemo-GAL4, UAS-mCherry.nls/UAS-LaminC RNAi* TRIP JF01406*; UAS-fbz/+ (mac>DfosDN, LamC RNAi).* Fig 5H: *e22CGal4,srpHemo-H2A::*3x*mCherry/+ (control).* Fig 5H: *srpQF/ srpHemo-H2A::*3x*mCherry; QUAS-fbz/UAS-Rho1.N12 (mac<>DfosDN).* Fig 5H: *e22CGal4, srpHemo-H2A::*3x*mCherry/srpQF; +/ UAS-Rho1.N12 (ecto>Rho1DN).* Fig 5H: *srpQF/ e22C-Gal4, srpHemo-H2A::*3x*mCherry; UAS-Rho1N12/QUAS-fbz (mac<>DfosDN, ecto>rho1DN).* S5E Fig: *+;UAS-GFP::nls, srpHemo-GAL4 (control). +;UAS-GFP::Lamin, srpHemo-GAL4.*

2.5.4 Cloning and generation of QUAS-DfosDN line

The fragment was amplified from genomic DNA of the published *UAS-fbz (UAS-Dfos DN)* line (Eresh, Riese, Jackson, Bohmann, & Bienz, 1997) using primers encompassing a 5' consensus translation initiation sequence followed by the bZIP fragment and containing BglII and XhoI restriction sites: 5'-GAAGATCTATTGGGAATTCAACATGACCCCG-3' and 5'-CCCTCGAGTCAGGTGACCACGCTCAGCAT-3'. The resulting fragment was cloned into the pQUASt vector, a gift from Christopher Potter (Addgene plasmid # 104880). The final construct was sequenced and injected into the attP2 landing site by BestGene (Chino Hills, CA, USA).

2.5.5 Cloning and generation of UAS-TM4SF line

The TM4SF open reading frame was amplified from the DGRC GH07902 cDNA clone (#3260, Fbcl0121651), using primers acagcgGAATTCATGGCATTGCCGAAGAAAAT and acagcgTCTAGATTAAAAGCTAATCGTCTGTCATT. The PCR product and the pUASt-aTTB vector (DGRC plasmid #1419) were digested with EcoRI and XbaI, and ligated. After sequencing, the construct was injected into the landing site line, (*y*^{1} *M{vas-int.Dm}ZH-2A w**; *M{3xP3-RFP.attP}ZH-51D*, BL 24483), to produce second chromosome inserts. All male survivors were crossed to *w*; *Sp/CyO*; *PrDr/TM3Ser* virgins. Transformants were recognized by eye color and crossed again to *w*; *Sp/CyO*; *PrDr/TM3Ser* virgins to get rid of the X chromosomal integrase.

2.5.6 Embryo staging

Laterally oriented embryos with complete germband (gb) extension and the presence of stomadeal invagination were staged based on gb retraction from the anterior as a percentage of total embryo length. Embryos with no gb retraction were classified as Stage 11, 30% retraction early Stage 12, 60% retraction Stage 12, and 70% Stage 13. Imaged embryos are shown throughout paper in a lateral orientation with anterior to the left and dorsal up.

2.5.7 *In situ* hybridization and immunofluorescence

Embryos were dechorionated by 5 min treatment with 50% Chlorox bleach. After extensive washing with water, embryos were fixed with 3.7% formaldehyde/heptane for 20 min followed by methanol devitellinization for *in situ* hybridization and visualization of 3xmCherry or tdTomato. The *Dfos* cDNA clone SD04477 was obtained from the DGRC. T7 or T3 polymerase-synthesized digoxigenin-labelled anti-sense probe preparation and *in situ* hybridization was performed using standard methods (Lehmann & Tautz, 1994). Images were taken with a Nikon-Eclipse Wide field microscope with a 20X 0.5 NA DIC water Immersion Objective. Embryos were mounted after immunolabeling in Vectashield Mounting Medium (Vector Labs, Burlingame, USA) and imaged with a Zeiss Inverted LSM700 and LSM800 Confocal Microscope using a Plain-Apochromat 20X/0.8 Air Objective or a Plain-Apochromat 63X/1.4 Oil Objective as required.

Table 2-1: Antibodies used in this study (Chapter 2)

Antibody	Source animal	Dilution	Provided by
Anti-Dfos	Rabbit	1:50	J. Zeitlinger (Stowers Institute, USA)
Anti-GFP	Chicken	1:500	Abcam (ab13970)
Anti-mCherry	Goat	1:200	Invitrogen (M11217)

2.5.8 Dfos antibody

The Dfos rabbit polyclonal antibody was produced for the lab of Julia Zeitlinger. It was raised by Genescript (Piscataway, NJ, USA) against the C-terminal end of *Drosophila* Kayak found in all isoforms and was purified against an N terminally His tagged antigen corresponding to aa 73 to 595 of Kay isoform A. The internal Genescript order number is 163185-30, and in the Zeitlinger lab is referred to as anti-kay/fos Ab.

2.5.9 Western Blot

Cages were prefed on fresh yeast plates for two days. Late stage 11/ early Stage 12 embryos were hand picked using a Leica M205 fluorescent microscope on ice-cold apple juice plates. They were transferred to RIPA buffer (50mM Tris, 150mM NaCl, 1% NP-40, 1mM EDTA, 0.5% Na-Deoxycholate, 0.1% SDS) with a Halt Protease/Phosphatase inhibitor cocktail (ThermoFisher, #78440) and lysed. After a 30 min incubation on ice, they were centrifuged 15 min at 4°C at 15,000 g. 10 µg of the cleared lysate were separated by SDS-PAGE using 4%-15% Mini-PROTEAN TGX Precast Protein gels (Bio-Rad, #4561085) and blotted onto a Amersham Protran Premium Western blotting nitrocellulose membrane (Sigma, #GE10600003). The nitrocellulose membrane was blocked with Pierce Clear Milk blocking buffer (ThermoFisher, #37587) and incubated in blocking buffer with anti-mCherry (Novus Biologicals, #NBP1-96752) at 1:1000, and anti-Profilin (DSHB, #chi 1J) at 1:50 antibodies over night at 4°C. The membrane was washed three times for 10 minutes with 1x PBS and incubated with Goat Anti-Mouse IgG (H+L)-HRP Conjugate (BioRad, #172-1011). Chemiluminescence was induced by incubation with SuperSignal West Femto Maximum Sensitivity Substrate (ThermoFisher, #34096) and recorded with a ChemieDoc MP (BioRad) molecular imager. Densitometric quantification of bands was done with ImageJ.

2.5.10 Time-Lapse Imaging

Embryos were dechorionated in 50% bleach for 5 min, washed with water, and mounted in halocarbon oil 27 (Sigma) on a 24x50mm high precision coverslip (Marienfeld Laboratory Glassware, No. 1.5H) between two bridges (~0.5 cm high) of coverslips glued on top of each other, or mounted in halocarbon oil 27 (Sigma) between a 18x18mm coverslip (Marienfeld Laboratory Glassware, No. 1.5H) and an oxygen permeable membrane (YSI). The embryo was imaged on an upright multiphoton microscope (TrimScope, LaVision) equipped with a W Plan-Apochromat 40X/1.4 oil immersion objective (Olympus). GFP and mCherry were imaged at 860 nm and 1100 nm excitation wavelengths, respectively, using a Ti-Sapphire femtosecond laser system (Coherent Chameleon Ultra) combined with optical parametric oscillator technology (Coherent Chameleon Compact OPO). Excitation intensity profiles were adjusted to tissue penetration depth and Z-sectioning for imaging was set at 1µm for tracking. For long-term imaging, movies were acquired for 60 - 150 minutes with a frame rate of 25-45 seconds. A temperature control unit set to 29°C was utilized for all genotypes except *kay*^{2} for which the setting was 25°C.

2.5.11 Image Analysis

Macrophage cell counts: Autofluorescence of the embryo revealed the position of the germband (gb) for staging of fixed samples. Embryos with 40% (±5%) gb retraction (Stage 12) were analysed for macrophage numbers in the pre-gb, within the germband, along the ventral nerve cord (vnc) and in the whole embryo. For the kay RNAi.embryos with 70% gb retraction (Stage 13) were used for vnc counts. The pre-gb zone was defined based on embryo and yolk autofluorescence as an area on the yolk sac underneath the amnioserosa with borders defined posteriorly by the gb ectoderm and anteriorly by the head. Macrophages were visualized using confocal microscopy with a Z-stack step size of 2 µm and macrophage numbers within the gb or the segments of the vnc were calculated in individual slices (and then aggregated) using the Cell Counter plugin in FIJI. Total macrophage numbers were obtained using Imaris (Bitplane) by detecting all the macrophage nuclei as spots.

Macrophage Tracking, Speed, Persistence. Mode of Migration and Macrophage gb crossing Analysis

Embryos with macrophage nuclei labelled with *srpHemo-H2A::3xmCherry* and the surrounding tissues with *Resille::GFP,* or with only macrophages labelled by *srpHemo-H2A::3XmCherry, or srpHemo>GFP.nls* were imaged and 250x250x40µm^{3} 3D-stacks were typically acquired with ~0.2x0.2x1µm^{3} voxel size every 39-41 seconds for ~2 hours. For imaging macrophages on vnc frames were acquired at every 40-43 seconds for 30 min after macrophages started spreading into abdominal segment 2 (see Fig 2G). Multiphoton microscopy images were initially processed with ImSpector software (LaVision Bio Tec) to compile channels, and exported files were further processed using Imaris software (Bitplane) for 3D visualization.

Each movie was rotated and aligned along the embryonic AP axis for tracking analysis. For analysis of migration in the pre-gb and gb in the control and *kay*^{2} mutant, embryos were

synchronized using the onset of germ and retraction. For vnc migration analysis, macrophages were tracked for 30 minutes from when macrophages started moving into the second abdominal segment. Only macrophages migrating along the inner edge of the vnc were analyzed.
Gb crossing time was calculated from when the macrophages align in front of the gb ectoderm in a characteristic arc, until the first macrophage had transitioned its nucleus inside the ecto-meso-interphase. To see the gb edge and yolk in movies of *srpHemo-3xH2A::mCherry*, either *Resille::GFP* labelling the outlines of all cells, or the auto-fluorescence of the yolk was used.
For analysis of gb migration in the *DfosDN* vs control macrophages*,* macrophages were tracked from when the first macrophage appeared between the ectoderm and the yolk sac until gb retraction started, typically 60 minutes. In the head and pre-gb, macrophage nuclei were extracted using the spot detection function, and tracks generated in 3D over time. The pre-gb and gb were defined as for macrophage counts described above. The mean position of the tracks in X- and Y restrict analysis to each migratory zones.
Cell speed and persistence were calculated from nuclei positions using custom Python scripts as described elsewhere (Smutny et al., 2017). Briefly, instantaneous velocities from single cell trajectories were averaged to obtain a mean instantaneous velocity value over the course of measurement. The directional persistence of a trajectory was calculated as the mean cosine of an angle between subsequent instantaneous velocities:

$$I\ (v_1, \dots, v_l) = \frac{1}{l-1} \sum_{k=1}^{l-1} \cos(v_k, v_{k+1}),$$

where l is duration of the trajectory and $v_1, \dots, v_l$ are its instantaneous velocities. Only trajectories with a minimal duration of 15 timeframes were used. Calculated persistence values were averaged over all trajectories to obtain a persistence index (I) for the duration of measurement (with -1 being the lowest and 1 the maximum). 3-6 embryos were recorded and analyzed for each genotype, numbers of control and perturbed embryos are equal in each pairwise comparison.

Measurement of junctional Phalloidin

The junctional intensity of F-actin (Phalloidin) was calculated using linescan analysis as previously described (Smutny et al., 2010) with the following changes. The line was ~5 µm and was always drawn in the middle slice of the Z stack (1 µm resolution) of the macrophage-macrophage junction. For every line, a Gaussian fit was applied and maximum intensities across the cell junction were then normalized against average intensities of F-actin (Phalloidin) staining in the stereotypical gb area of ~50x50µm^2 in each embryo. Analyses were carried out using standard Fiji software. 4-5 embryos were analysed per genotype. Macrophages in the pre-gb or gb entry zones were analyzed.

Measurement of F-actin reporters

To quantify cortical F-actin intensity in living embryos, a *srpHemo-moe::3xmCherry* reporter line (Gyoergy et al., 2018) was crossed into a background of macrophages expressing *DfosDN*, *cher RNAi*, or *TM4SF* RNAi. Embryos were collected for 5h 30min at 29°C, de-chorionated in 50% bleach for 5 min, rinsed thoroughly with water, and aligned laterally side by side under a stereomicroscope using a fluorescence lamp to check for the presence of mCherry. Aligned embryos were then mounted as described in the live imaging section above. To image Moe::3xmCherry, a Zeiss LSM800 inverted microscope was used with the following settings:

Plan-APOCHROMAT 40x/1.4 Oil, DIC, WD=0.13 objective, 1.5x zoom, 1025x1025 pixel, speed 8, heating chamber set to 29°C, z-interval 1µm. Laser settings were kept constant in all experiments. Images were acquired during macrophage invasion into the gb (St 12). Pseudo-coloring was conducted for the mCherry red channel. Each pixel in the image has a color ascribed to it via the fire "Look Up Table" translating the level of intensity of the mCherry channel into a defined amount of each color. The highest intensity of the image is represented as very bright yellow and all other grey values are depicted as colors on the scale accordingly. For quantification of Moe::3xmCherry intensity, an ROI was drawn in Fiji software around macrophages at the germband entry site in 20 z-stacks for each embryo. The area mean intensity was measured in all ROIs and the average/embryo was calculated. To normalize fluorescence intensities per batch, the average intensity/embryo of all ROIs in each sample was divided by the arithmetic mean of the average intensity/embryo of all ROIs in the control per batch. The normalized average intensities/embryo were then compared to each other using a t-test with Welch's correction for *DfosDN* and one way-ANOVA for *cher RNAi* and *TM4SF RNAi*.

Quantification of membrane localization of DiaRBD::GFP and Dia::GFP

Methanol fixed St 11 embryos were mounted either after staining with GFP antibody (Dia::GFP) or without staining(DiaRBD::GFP) and imaged with a Zeiss Inverted LSM800, Plain-Apochromat 63X/1.4 Oil Objective at an XY-resolution of 0.1 µm and a Z-resolution of 1 µm (~15 µm total stack). All macrophages within 40µm of the germband were analysed. For the quantification of the levels of DiaRBD or the complete Dia protein at the plasma membrane versus the cytoplasm, confocal images were processed using Fiji and MATLAB-R2017b (MathWorks). Individual focal planes were used to segment a profile corresponding to an 8 pixel wide line drawn across the single outer membrane of individual macrophages chosen such that the extracellular portion of the line extended into surrounding tissue or space and not another macrophage. The corresponding intensity profiles of the mem::Tomato and Dia::GFP or DiaRBD::GFP channels were extracted in Fiji using a custom macro and analyzed further using a custom MATLAB script. The membrane region was defined by finding the maximal value in the Tomato intensity profile and centering a 0.8 µm interval around it. The background was calculated for each GFP profile as the mean intensity in the 2 µm outside the cell, flanking the membrane region, and substracted from the entire profile. The integrated Dia::GFP or DiaRBD::GFP intensity at the membrane was calculated within the 0.8 µm interval defined above. The integrated cytoplasmic Dia::GFP or DiaRBD::GFP level was calculated as the mean intensity of 2 µm of the GFP profile inside the cell flanking the membrane region. Image analysis scripts are publicly available at https://github.com/Axmasha/Image_analysis_scripts.

Cell aspect ratio analysis and imaging actin dynamics

Laterally oriented embryos were used to measure the maximal length and width of macrophages expressing *UAS-CLIP::GFP* under the control of *srpHemoGal4*. Briefly, 3D-stacks with 1 µm Z resolution were acquired every 35-45 seconds for approximately 1 hour. As the strength of the GAL4 expression increased over time, laser power was adjusted during acquisition to reach the best possible quality of visualization. Images acquired from mutiphoton microscopy were initially processed with ImSpector software (LaVision Bio Tec) to compile channels from the imaging data.

We started measuring from the time the cell body of the first macrophage fully appeared at the interface between the ectoderm and mesoderm and yolk sac until it had moved 30 µm along the ectoderm mesoderm interface. At each timeframe, a line was drawn in Fiji along the longest dimension of the macrophage in the direction of its front-rear polarization axis, denoted the maximal cell length, and along the orthologonal longest dimension, which was considered maximal cell width. We did not observe long CLIP::GFP protrusions, but when a small protrusion was present, it was not included in the length measurement; within this gb region the front of the first macrophage was clearly outlined with CLIP::GFP. The border between the first and second entering macrophages was drawn based on the uninterrupted intense line of CLIP::GFP at the base of the first macrophage; only cells with a clearly visible border were measured. The length to width ratio was quantified for each timeframe and a probability density function was plotted: 5 embryos were recorded for each genotype.

Imaging the actin protrusion

Laterally oriented embryos expressing *srpHemo-Gal4 UAS-LifeAct::GFP* were used to image macrophage actin live with a 3D-stack resolution of 1µm. See above description of CLIP::GFP labeled macrophage imaging for laser power and image compilation. Laser power was also increased further in the DfosDN samples to enhance actin visualization. We measured the length of the filopodia-like protrusion of the first entering macrophage with Imaris software (Bitplane) from the time when the protrusion was inserted into the ectoderm, mesoderm and yolk sac interface until the macrophage started to translocate its cell body into that location.

2.5.12 FACS sorting of macrophages

Adult flies of either *w;+;srpHemoGal4,srpHemo::3xmCherry/+* or *w;+; srpHemoGal4,srpHemo::3xmCherry /UASDfosDN* genotypes were placed into plastic cages closed with apple juice plates with applied yeast to enhance egg laying. Collections were performed at 29°C for 1 hour, then kept at 29°C for additional 5 hours 15 minutes to reach stage 11-early stage 12. Embryos were harvested for 2 days with 6-7 collections per day and stored meanwhile at +4°C to slow down development. Collected embryos were dissociated and the macrophages sorted as previously described (Gyoergy et al., 2018). About 1-1.5x10^5 macrophages were sorted within 30 minutes.

2.5.13 Sequencing of the macrophage transcriptome

Total RNA was isolated from FACS-sorted macrophages using Qiagen RNeasy Mini kit (Cat No. 74104). The quality and concentration of RNA was determined using Agilent 6000 Pico kit (Cat No. 5067-1513) on an Agilent 2100 Bioanalyzer: on average about 100 ng of total RNA was extracted from 1.5x10^5 macrophages. RNA sequencing was performed by the CSF facility of Vienna Biocenter according to standard procedures (https://www.vbcf.ac.at/facilities/next-generation-sequencing/) on three replicates. Briefly, the cDNA library was synthesized using QuantSeq 3’ mRNA-seq Library Prep kit and
sequenced on the Illumina HiSeq 2500 platform. The reads were mapped to the *Drosophila melanogaster* Ensembl BDGP6 reference genome with STAR (version 2.5.1b). The read counts for each gene were detected using HTSeq (version 0.5.4p3). Flybase annotation (r6.19) was

used in both mapping and read counting. Counts were normalised to arbitrary units using the TMM normalization from edgeR package in R. Prior to statistical testing the data was voom transformed and then the differential expression between the sample groups was calculated with limma package in R. The functional analyses were done using the topGO and gage packages in R (Anders, Pyl, & Huber, 2015; Dobin et al., 2013). RNA sequencing data has been deposited at GEO as GSE182470.

2.5.14 qRT-PCR analysis of mRNA levels in murine bones and osteosarcomas

RNA isolation and qPCR was performed from bones of wild-type C57BL/6 mice and from bones and osteosarcomas (OS) of H2-c-fosLTR as previously described with the below primers (Rüther et al., 1989).

Table 2-2: List of primers used in this study (Chapter 2)

Primer	Sequence
Fos fw	ATGGTGAAGACCGTGTCAGG
Fos_rv	GTTGATCTGTCTCCGCTTGGA
Flna_fw	GTCACAGTGTCAATCGGAGGT
Flna_rv	TTGCCTGCTGCTTTTGTGTC
Flnb_fw	TTCTACACTGCTGCCAAGCC
Flnb_rv	CTGTAACCCAGGGCCTGAATC
Flnc_fw	CATCACCCGGAGTCCTTTCC
Flnc_rv	CTCTGTGCCCTTTGGACCTT
Tspan6_fw	TCGAACTAGTTGCCGCCATT
Tspan6_rv	CCGCAACAATGCAACGTACT
Gstt3_fw	GGAGCTCTACCTGGACCTGA
Gstt3_rv	AAGATGGCCACACTCTCTGC
Eva1c_fw	GTTGCCTACGCATGTGTTCC
Eva1c_rv	CCGATGCAGACACTGGACAT
Tspo_fw	GTATTCAGCCATGGGGTATGG
Tspo_rv	AAGCAGAAGATCGGCCAAGG
Tbp_fw	GGGGAGCTGTGATGTGAAGT
Tbp_rv	CCAGGAAATAATTCTGGCTCAT

2.5.15 Statistics and Repeatability

Mouse experiments:

Data are shown as mean±SEM. One-way ANOVA followed by Tukey's multiple comparisons post-test was applied to compare experimental groups. Statistical analysis was performed using GraphPad Prism 6.0 software. A p-value <0.05 was considered statistically significant (*p<0.05, **p<0.01, ***p<0.001, ****p<0.0001).

Drosophila experiments:

Statistical tests as well as the number of embryos/cells/tracks/contacts assessed are listed in the Figure legends. All statistical analyses were performed using GraphPad PRISM or R Studio

and significance was determined using a 95% confidence interval. No statistical method was used to predetermine sample size.
Representative images of Dfos antibody staining were analyzed per replicate per genotype and *in situ* hybridization are from experiments that were repeated 2 times with many embryos with reproducible results. *Dfos* mutants analysis in Fig 1 and S1 Fig are from experiments that were repeated 2-3 times. In live imaging experiments in Fig 2 and S2 Fig, 3-7 embryos for each genotype were analyzed, each embryo was recorded on a separate day. FACS sorting of macrophages from embryos was conducted in three replicates, from which RNA samples were prepared for RNA sequencing. Experiments in Fig 4 and S4 Fig were repeated at least 3 times, with representative images and plots of phalloidin immunostaining from experiments that were repeated 4 times. In the LifeAct::GFP protrusion live imaging experiment in Fig 5 and S5 Fig, 3-5 embryos were analyzed for each genotype. In CLIP::GFP live imaging experiments in Fig 5 and S5 Fig, 5-6 embryos were analyzed for each genotype for the cell aspect ratio in the germband zone, and 2 embryos in the pre-germband zone and for tracking of the front vs rear speed. Each embryo was recorded on a separate day. The Lamin over expression in S5 Fig and the Lamin knockdown rescue experiments in Fig 5G were repeated at least 3 times. The gb rescue experiment in Fig 5H was repeated at least 4 times.

Acknowledgements

We thank the following for their contributions: The *Drosophila* Genomics Resource Center supported by NIH grant 2P40OD010949-10A1 for plasmids, K. Brueckner. B. Stramer, M. Uhlirova, O. Schuldiner, the Bloomington *Drosophila* Stock Center supported by NIH grant P40OD018537 and the Vienna *Drosophila* Resource Center for fly stocks, FlyBase (Thurmond et al., 2019) for essential genomic information, and the BDGP *in situ* database for data (Tomancak et al., 2002, 2007). For antibodies, we thank the Developmental Studies Hybridoma Bank, which was created by the Eunice Kennedy Shriver National Institute of Child Health and Human Development of the NIH, and is maintained at the University of Iowa, as well as J. Zeitlinger for her generous gift of Dfos antibody. We thank the Vienna BioCenter Core Facilities for RNA sequencing and analysis and the Life Scientific Service Units at IST Austria for technical support and assistance with microscopy and FACS analysis. We thank C. P. Heisenberg, P. Martin, M. Sixt and Siekhaus group members for discussions and T. Hurd, A. Ratheesh and P. Rangan for comments on the manuscript.

2.6 REFERENCES

Anders, S., Pyl, P. T., & Huber, W. (2015). HTSeq-A Python framework to work with high-throughput sequencing data. *Bioinformatics*, *31*(2), 166–169. https://doi.org/10.1093/bioinformatics/btu638

Abreu-Blanco, M.T., Verboon, J.M., & Parkhurst S.M. (2014) Coordination of Rho Family GTPase activities to orchestrate cytoskeleton responses during wound repair. *Current Biology*, *24*(2), 144-155. https://doi.org/10.1016/j.cub.2013.11.048

Andrés, V., & González, J. M. (2009). Role of A-type lamins in signaling, transcription, and chromatin organization. *Journal of Cell Biology*, *187*(7), 945–957. https://doi.org/10.1083/jcb.200904124

Bellanger, J. M., Astier, C., Sardet, C., Ohta, Y., Stossel, T. P., & Debant, A. (2000). The Rac1-

and RhoG-specific GEF domain of trio targets filamin to remodel cytoskeletal actin. *Nature Cell Biology*, *2*(12), 888–892. https://doi.org/10.1038/35046533

Benhra, N., Barrio, L., Muzzopappa, M., & Milán, M. (2018). Chromosomal Instability Induces Cellular Invasion in Epithelial Tissues. *Developmental Cell*, *47*(2), 161-174.e4. https://doi.org/10.1016/j.devcel.2018.08.021

Berditchevski, F., & Odintsova, E. (1999). Characterization of integrin-tetraspanin adhesion complexes: Role of tetraspanins in integrin signaling. *Journal of Cell Biology*, *146*(2), 477–492. https://doi.org/10.1083/jcb.146.2.477

Bershadsky, A. D., Balaban, N. Q., & Geiger, B. (2003). Adhesion-Dependent Cell Mechanosensitivity. *Annual Review of Cell and Developmental Biology*, *19*(1), 677–695. https://doi.org/10.1146/annurev.cellbio.19.111301.153011

Bilancia, C. G., Winkelman, J. D., Tsygankov, D., Nowotarski, S. H., Sees, J. A., Comber, K., … Peifer, M. (2014). Enabled negatively regulates diaphanous-driven actin dynamics in vitro and in vivo. *Developmental Cell*, *28*(4), 394–408. https://doi.org/10.1016/j.devcel.2014.01.015

Bosch, P.S., Makhijani, K., Herboso, L., Gold, K.S., Baginsky, R., Woodcock, K.J., Alexander, B., Kukar, K., Corcoran, S., Jacobs, T., Ouyang, D., Wong, C., Ramond, E.J.V., Rhiner, C., Moreno, E., Lemaitre, B., Geissmann, F., & Brueckner, K. (2019). Adult *Drosophila* lack hematopoiesis but rely on a blood cell reservoir at the respiratory epithelia to relay infection signals to surrounding tissues. *Developmental Cell*, *51*(6)787-803. https://doi.org/10.1016/j.devcel.2019.10.017

Brock, A. R., Wang, Y., Berger, S., Renkawitz-Pohl, R., Han, V. C., Wu, Y., & Galko, M. J. (2012). Transcriptional regulation of profilin during wound closure in Drosophila larvae. *Journal of Cell Science*, *125*(23), 5667–5676. https://doi.org/10.1242/jcs.107490

Brückner, K., Kockel, L., Duchek, P., Luque, C. M., Rørth, P., & Perrimon, N. (2004). The PDGF/VEGF receptor controls blood cell survival in Drosophila. *Developmental Cell*, *7*(1), 73–84. https://doi.org/10.1016/j.devcel.2004.06.007

Brzozowski, J. S., Bond, D. R., Jankowski, H., Goldie, B. J., Burchell, R., Naudin, C., … Weidenhofer, J. (2018). Extracellular vesicles with altered tetraspanin CD9 and CD151 levels confer increased prostate cell motility and invasion. *Scientific Reports*, *8*(1). https://doi.org/10.1038/s41598-018-27180-z

Butcher, D.T., Alliston, T. & Weaver, V.M.(2009). A tense situation: forcing tumour progression. *Nature Reviews Cancer, 9*(2), 108-22. . https://doi.org/10.11038/nrc2544

Cho, N. K., Keyes, L., Johnson, E., Heller, J., Ryner, L., Karim, F., & Krasnow, M. A. (2002). Developmental control of blood cell migration by the Drosophila VEGF pathway. *Cell*, *108*(6). https://doi.org/10.1016/S0092-8674(02)00676-1

Chugh, P., Clark, A. G., Smith, M. B., Cassani, D. A. D., Dierkes, K., Ragab, A., … Paluch, E. K. (2017). Actin cortex architecture regulates cell surface tension. *Nature Cell Biology*, *19*(6), 689–697. https://doi.org/10.1038/ncb3525

Danuser, G., Allard, J., & Mogilner, A. (2013). Mathematical Modeling of Eukaryotic Cell Migration: Insights Beyond Experiments. *Annual Review of Cell and Developmental*

Biology, *29*(1). https://doi.org/10.1146/annurev-cellbio-101512-122308

Davidson, A. J., Millard, T. H., Evans, I. R., & Wood, W. (2019). Ena orchestrates remodelling within the actin cytoskeleton to drive robust Drosophila macrophage chemotaxis. *Journal of Cell Science*, *132*(5). https://doi.org/10.1242/jcs.224618

Davidson, P.M., Denais, C., Bakshi, M., & Lammerding, J. (2014).. Nuclear deformability constitutes a rate-limiting step during cell migration in 3-D environments. *Cellular and Molecular Bioengineering, 7*(3)293-306. https://doi.org/10.1007/s12195-014-0342-y

Davis, J. R., Luchici, A., Miodownik, M., Stramer, B. M., Davis, J. R., Luchici, A., … Stramer, B. M. (2015). Inter-Cellular Forces Orchestrate Contact Inhibition of Locomotion Article Inter-Cellular Forces Orchestrate Contact Inhibition of Locomotion. *Cell*, *161*(2), 361–373. https://doi.org/10.1016/j.cell.2015.02.015

Delaguillaumie, A., Lagaudrière-Gesbert, C., Popoff, M. R., & Conjeaud H., H. (2002). Rho GTPase link cytoskeletal rearrangements and activation processes induced via the tetraspanin CD82 in T lymphocytes. *Journal of Cell Science*, *115*(2). https://doi.org/10.1242/jcs.115.2.433

Deluca, T. F., Cui, J., Jung, J. Y., St. Gabriel, K. C., & Wall, D. P. (2012). Roundup 2.0: Enabling comparative genomics for over 1800 genomes. *Bioinformatics*, *28*(5). https://doi.org/10.1093/bioinformatics/bts006

Del Valle-Perez, B., Martinez, V.G., Casa-Salavert, C., Figueras, A., Shapiro, S.S., Takafuta T., Casanovas, O., Capella, G., Ventura, F., & Vinals, F. (2010) Filamin B plays a key role in vascular endothelial growth factor-induced endothelial cell motility through its interaction with Rac-1 and Vav-2. Journal of Biological Chemistry, *285*(14), 10748-60. https://doi.org/10.1074/jbc.M109.062984

Dobin, A., Davis, C. A., Schlesinger, F., Drenkow, J., Zaleski, C., Jha, S., … Gingeras, T. R. (2013). STAR: Ultrafast universal RNA-seq aligner. *Bioinformatics*, *29*(1), 15–21. https://doi.org/10.1093/bioinformatics/bts635

Duffy, J. B. (2002). GAL4 system in Drosophila: A fly geneticist's Swiss army knife. *Genesis*, *34*(1–2), 1–15. https://doi.org/10.1002/gene.10150

Edwards, K. A., Demsky, M., Montague, R. A., Weymouth, N., & Kiehart, D. P. (1997). GFP-moesin illuminates actin cytoskeleton dynamics in living tissue and demonstrates cell shape changes during morphogenesis in Drosophila. *Developmental Biology*, *191*(1). https://doi.org/10.1006/dbio.1997.8707

Ehrlicher, A. J., Nakamura, F., Hartwig, J. H., Weitz, D. A., & Stossel, T. P. (2011). Mechanical strain in actin networks regulates FilGAP and integrin binding to filamin A. *Nature*, *478*(7368), 260–263. https://doi.org/10.1038/nature10430

Eresh, S., Riese, J., Jackson, D. B., Bohmann, D., & Bienz, M. (1997). A CREB-binding site as a target for decapentaplegic signalling during Drosophila endoderm induction. *EMBO Journal*, *16*(8), 2014–2022. https://doi.org/10.1093/emboj/16.8.2014

Evans, I. R., & Wood, W. (2011). Drosophila embryonic hemocytes. *Current Biology*, *21*(5), R173–R174. https://doi.org/10.1016/j.cub.2011.01.061

Franck, Z., Gary, R., & Bretscher, A. (1993). Moesin, like ezrin, colocalizes with actin in the

cortical cytoskeleton in cultured cells, but its expression is more variable. *Journal of Cell Science*, *105*(1).

Fujita, M., Mitsuhashi, H., Isogai, S., Nakata, T., Kawakami, A., Nonaka, I., … Kudo, A. (2012). Filamin C plays an essential role in the maintenance of the structural integrity of cardiac and skeletal muscles, revealed by the medaka mutant zacro. *Developmental Biology*, *361*(1), 79–89. https://doi.org/10.1016/j.ydbio.2011.10.008

García-Echeverría, C. Methionine-containing zipper peptides. *Lett Pept Sci* **4,** 135–140 (1997). https://doi.org/10.1007/BF02443525

Ginhoux, F.& Guilliams, M. (2016). Tissue-resident macrophage ontogeny and homeostasis. *Immunity 44*(3), 439-449. https://doi.org/10.1016/j.immuni.2016.02.024

Glogauer, M., Arora, P., Chou, D., Janmey, P. A., Downey, G. P., & McCulloch, C. A. G. (1998). The role of actin-binding protein 280 in integrin-dependent mechanoprotection. *Journal of Biological Chemistry*, *273*(3), 1689–1698. https://doi.org/10.1074/jbc.273.3.1689

Glover, J.N.M. and Harrison, S.C. (1005). Crystal structure of the heterodimeric bZIP transcritpion factor c-Fos-c-Jun bound to DNA. *Nature, 373*(6511):257-261. https://doi.org/10.1038/373257a0

Goldmann, W. H., Tempel, M., Sprenger, I., Isenberg, G., & Ezzell, R. M. (1997). Viscoelasticity of actin-gelsolin networks in the presence of filamin. *European Journal of Biochemistry*, *246*(2), 373–379. https://doi.org/10.1111/j.1432-1033.1997.00373.x

Goode, B.L. & Eck. M. (2007) Mechanism and Function of Formins in the Control of Actin Assembly. *Annual Review of Biochemistry 78*, 593-627. https://doi.org/10.1146/annurev.biochem.75.103004.142647

Greten, F.R. & Grovennikov, S.I. (2019). Inflammation and Cancer: Triggers, Mechanisms and Consequences. *Immunity 51*(1), 27-41. j.immuni.2019.06.025

Großhans, J., Wenzl, C., Herz, H. M., Bartoszewski, S., Schnorrer, F., Vogt, N., … Müller, H. A. (2005). RhoGEF2 and the formin Dia control the formation of the furrow canal by directed actin assembly during Drosophila cellularisation. *Development*, *132*(5), 1009–1020. https://doi.org/10.1242/dev.01669

Guilliams, M., Thierry, G.R., Bonnardel, J., & Bajenoff, M. (2020). Establishment and Maintenance of the Macrophage Niche. *Immunity 52*(3), 434-451. https://doi.org/10.1016/j.immuni.2020.02.015

Gyoergy, A., Roblek, M., Ratheesh, A., Valoskova, K., Belyaeva, V., Wachner, S., … Siekhaus, D. E. (2018). Tools allowing independent visualization and genetic manipulation of Drosophila melanogaster macrophages and surrounding tissues. *G3: Genes, Genomes, Genetics*, *8*(3). https://doi.org/10.1534/g3.117.300452

Hammonds, A. A. S., Bristow, C. C. a, Fisher, W. W., Weiszmann, R., Wu, S., Hartenstein, V., … Celniker, S. E. (2013). Spatial expression of transcription factors in Drosophila embryonic organ development. *Genome Biology*, *14*(12), R140. https://doi.org/10.1186/gb-2013-14-12-r140

Harada, T., Swift, J., Irianto, J., Shin, J, Spinler, K.R., Athirasala, A., Diegmiller, R., Dingal, P.C.D.P., Ivanovska, I.L., & Discher, D.E. (2014). Nuclear lamin stiffness is a barrier to 3D

migration, but softness can limit survival. *J. Cell Biology,* (5)669-82. https://doi.org/10.1083/jcb.201308029.

Hattori, A., Mizuno, T., Akamatsu, M., Hisamoto, N., Matsumoto, K. (2013). The Caenorhabditis elegans JNK signaling pathway activates expression of stress response genes by depressing the Fos/HDAC repressor complex. *Plos Genetics 9*(2):e1003315. https://doi.org/10.1371/journal.pgen.1003315

Heer, N. C., & Martin, A. C. (2017). Tension, contraction and tissue morphogenesis. *Development (Cambridge)*, *144*(23)4249-4260. https://doi.org/10.1242/dev.151282

Holz, A., Bossinger, B., Strasser, T., Janning, W., & Klapper, R. (2003). The two origins of hemocytes in *Drosophila. Development, 130*(20), 4955-62. https://doi.org/10.1242/dev.007202

Homem, C.C., Peifer, M. (2008) Diaphanous regulates myosin and adherens junctions to control cell contractility and protrusive behavior during morphogenesis. *Development*, *135*(6)1005-1018. https://doi.org/10.1242/dev.151282

Homem, C.C., Peifer, M. (2009) Exploring the roles of Diaphanous and Enabled activity in shaping the balance between filopodia and lamellipodia. Molecular Biology of the Cell, *20*(24) 5138-55. https://doi.org/10.1091/mbc.e09-02-0144

Hong, I. K., Jeoung, D. Il, Ha, K. S., Kim, Y. M., & Lee, H. (2012). Tetraspanin CD151 stimulates adhesion-dependent activation of Ras, Rac, and Cdc42 by facilitating molecular association between β1 integrins and small GTPases. *Journal of Biological Chemistry*, *287*(38), 32027–32039. https://doi.org/10.1074/jbc.M111.314443

Hu, J., Lu, J., Lian, G., Ferland, R. J., Dettenhofer, M., & Sheen, V. L. (2014). Formin 1 and filamin B physically interact to coordinate chondrocyte proliferation and differentiation in the growth plate. *Human Molecular Genetics*, *23*(17), 4663–4673. https://doi.org/10.1093/hmg/ddu186

Kasza, K. E., Broedersz, C. P., Koenderink, G. H., Lin, Y. C., Messner, W., Millman, E. A., … Weitz, D. A. (2010). Actin filament length tunes elasticity of flexibly cross-linked actin networks. *Biophysical Journal*, *99*(4), 1091–1100. https://doi.org/10.1016/j.bpj.2010.06.025

Kessenbrock, K., Plaks, V., & Werb, Z. (2010). Matrix metalloproteinases: regulators of the tumor microenvironment. *Cell 141*(1), 52-67. https://doi.org/10.1016/j.cell.2010.03.015

Külshammer, E., Mundorf, J., Kilinc, M., Frommolt, P., Wagle, P., & Uhlirova, M. (2015). Interplay among Drosophila transcription factors Ets21c, Fos and Ftz-F1 drives JNK-mediated tumor malignancy. *DMM Disease Models and Mechanisms*, *8*(10), 1279–1293. https://doi.org/10.1242/dmm.020719

Külshammer, E., & Uhlirova, M. (2013). The actin cross-linker Filamin/Cheerio mediates tumor malignancy downstream of JNK signaling. *Journal of Cell Science*, *126*(4), 927–938. https://doi.org/10.1242/jcs.114462

Kumar, A., Shutova, M. S., Tanaka, K., Iwamoto, D. V., Calderwood, D. A., Svitkina, T. M., & Schwartz, M. A. (2019). Filamin A mediates isotropic distribution of applied force across the actin network. *Journal of Cell Biology*, *218*(8), 2481–2491. https://doi.org/10.1083/jcb.201901086

Lehmann, R., & Tautz, D. (1994). In Situ Hybridization to RNA. *Methods in Cell Biology*, *44*(C), 575–596. https://doi.org/10.1016/S0091-679X(08)60933-4

Lemaitre, B., & Hoffmann, J. (2007). The Host Defense of *Drosophila melanogaster*. *Annual Review of Immunology*, *25*(1), 697–743. https://doi.org/10.1146/annurev.immunol.25.022106.141615

Lesch, C., Jo, J., Wu, Y., Fish, G. S., & Galko, M. J. (2010). A Targeted *UAS-RNAi* Screen in Drosophila Larvae Identifies Wound Closure Genes Regulating Distinct Cellular Processes. *Genetics*, *186*(3), 943–957. https://doi.org/10.1534/genetics.110.121822

Lian, G., Dettenhofer, M., Lu, J., Downing, M., Chenn, A., Wong, T., & Sheen, V. (2016). Filamin A- and formin 2-dependent endocytosis regulates proliferation via the canonical wnt pathway. *Development (Cambridge)*, *143*(23). https://doi.org/10.1242/dev.139295

Linder, M., Glitzner, E., Srivatsa, S., Bakiri, L., Matsuoka, K., Shahrouzi, P., … Sibilia, M. (2018). EGFR is required for FOS-dependent bone tumor development via RSK2/CREB signaling. *EMBO Molecular Medicine*, *10*(11). https://doi.org/10.15252/emmm.201809408

Luster, A. D., Alon, R., & von Andrian, U. H. (2005). Immune cell migration in inflammation: Present and future therapeutic targets. *Nature Immunology*, *6*(12), 1182–1190. https://doi.org/10.1038/ni1275

Makhijani, K., Alexander, B., Tanaka, T., Rulfson, E., & Brückner, K. (2011). The peripheral nervous system supports blood cell homing and survival in the Drosophila larva. *Development, 138*(24), 5379-91. https://doi.org/10.1242/dev.067322

Matsubayashi, Y., Louani, A., Dragu, A., Sánchez-Sánchez, B. J., Serna-Morales, E., Yolland, L., … Stramer, B. M. (2017). A Moving Source of Matrix Components Is Essential for De Novo Basement Membrane Formation. *Current Biology*, *27*(22), 3526-3534.e4. https://doi.org/10.1016/j.cub.2017.10.001

Mitchison, T.J., and Cramer, L.P. (1996) Actin-based cell motility and cell locomotion. *Cell 84*(3)371-9). https://doi.org/10.1016/s0092-8864(00)81281-7.

Muñoz-Alarcón, A., Pavlovic, M., Wismar, J., Schmitt, B., Eriksson, M., Kylsten, P., & Dushay, M. S. (2007). Characterization of lamin mutation phenotypes in Drosophila and comparison to human laminopathies. *PloS One*, *2*(6). https://doi.org/10.1371/journal.pone.0000532

Ohta, Y., Suzuki, N., Nakamura, S., Hartwig, J. H., & Stossel, T. P. (1999). The small GTPase RalA targets filamin to induce filopodia. *Proceedings of the National Academy of Sciences of the United States of America*, *96*(5), 2122–2128. https://doi.org/10.1073/pnas.96.5.2122

Paluch, E. K., Aspalter, I. M., & Sixt, M. (2016). Focal Adhesion–Independent Cell Migration. *Annual Review of Cell and Developmental Biology*, *32*(1), 469–490. https://doi.org/10.1146/annurev-cellbio-111315-125341

Perez-Hernandez, D., Gutiérrez-Vázquez, C., Jorge, I., López-Martín, S., Ursa, A., Sánchez-Madrid, F., … Yañez-Mó, M. (2013). The intracellular interactome of tetraspanin-enriched microdomains reveals their function as sorting machineries toward exosomes. *Journal of Biological Chemistry*, *288*(17), 11649–11661.

https://doi.org/10.1074/jbc.M112.445304

Perkins, L. A., Holderbaum, L., Tao, R., Hu, Y., Sopko, R., McCall, K., … Perrimon, N. (2015). The transgenic RNAi project at Harvard medical school: Resources and validation. *Genetics*, *201*(3), 843–852. https://doi.org/10.1534/genetics.115.180208

Popowicz, G. M., Schleicher, M., Noegel, A. A., & Holak, T. A. (2006). Filamins: promiscuous organizers of the cytoskeleton. *Trends in Biochemical Sciences*, *31*(7), 411–419. https://doi.org/10.1016/j.tibs.2006.05.006

Raab, M., Gentili, M., de Belly, H., Thiam, H.R., Vargas, P., Jimenez, A.J., Lautenschlaeger, F., Voituriez, R., Lennon-Duménil, A.M., Manel, N, Piel, M. (2016). ESCRT III repairs nuclear envelope ruptures during cell migration to limit DNA damage and cell death. Science, 352(6283), 359-62. https://doi.org/10.1126/science.aad7611

Ratheesh, A., Belyaeva, V., & Siekhaus, D. E. (2015). Drosophila immune cell migration and adhesion during embryonic development and larval immune responses. *Current Opinion in Cell Biology*, *36*, 71–79. https://doi.org/10.1016/j.ceb.2015.07.003

Ratheesh, A., Biebl, J., Vesela, J., Smutny, M., Papusheva, E., Krens, S. F. G., … Siekhaus, D. E. (2018). Drosophila TNF Modulates Tissue Tension in the Embryo to Facilitate Macrophage Invasive Migration. *Developmental Cell*, *45*(3), 331-346.e7. https://doi.org/10.1016/j.devcel.2018.04.002

Razinia, Z., Mäkelä, T., Ylänne, J., & Calderwood, D. A. (2012). Filamins in Mechanosensing and Signaling. *Annual Review of Biophysics*, *41*(1), 227–246. https://doi.org/10.1146/annurev-biophys-050511-102252

Riesgo-Escovar, J. R., & Hafen, E. (1997). Common and distinct roles of DFos and DJun during Drosophila development. *Science (New York, N.Y.)*, *278*(5338), 669–672. https://doi.org/10.1126/science.278.5338.669

Riveline, D., Zamir, E., Balaban, N. Q., Schwarz, U. S., Ishizaki, T., Narumiya, S., … Bershadsky, A. D. (2001). Focal contacts as mechanosensors: Externally applied local mechanical force induces growth of focal contacts by an mDia1-dependent and ROCK-independent mechanism. *Journal of Cell Biology*, *153*(6), 1175–1185. https://doi.org/10.1083/jcb.153.6.1175

Rose, R., Weyand, M., Lammers, M., Ishizaki, T., Ahmadian, M. R., & Wittinghofer, A. (2005). Structural and mechanistic insights into the interaction between Rho and mammalian Dia. *Nature*, *435*(7041), 513–518. https://doi.org/10.1038/nature03604

Rousso, T., Shewan, A. M., Mostov, K. E., Schejter, E. D., & Shilo, B. Z. (2013). Apical targeting of the formin diaphanous in Drosophila tubular epithelia. *ELife*, *2013*(2). https://doi.org/10.7554/eLife.00666

Sánchez-Sánchez, B. J., Urbano, J. M., Comber, K., Dragu, A., Wood, W., Stramer, B., & Martín-Bermudo, M. D. (2017). Drosophila Embryonic Hemocytes Produce Laminins to Strengthen Migratory Response. *Cell Reports*, *21*(6), 1461–1470. https://doi.org/10.1016/j.celrep.2017.10.047

Seth, A., Otomo, C., & Rosen, M. K. (2006). Autoinhibition regulates cellular localization and actin assembly activity of the diaphanous-related formins FRLα and mDia1. *Journal of*

Cell Biology, *174*(5), 701–713. https://doi.org/10.1083/jcb.200605006

Sharma, P. & Allison, J.P. (2015) The future of immune checkpoint therapy. *Science 348*(6230), 56-61. https://doi.org/10.1126/science.aaa8172.

Siekhaus, D., Haesemeyer, M., Moffitt, O., & Lehmann, R. (2010). RhoL controls invasion and Rap1 localization during immune cell transmigration in Drosophila. *Nature Cell Biology*, *12*(6), 605–610. https://doi.org/10.1038/ncb2063

Smutny, M., Ákos, Z., Grigolon, S., Shamipour, S., Ruprecht, V., Čapek, D., … Heisenberg, C. P. (2017). Friction forces position the neural anlage. *Nature Cell Biology*, *19*(4), 306–317. https://doi.org/10.1038/ncb3492

Sokol, N. S., & Cooley, L. (2003). Drosophila filamin is required for follicle cell motility during oogenesis. *Developmental Biology*, *260*(1), 260–272. https://doi.org/10.1016/S0012-1606(03)00248-3

Somogyi, K., & Rørth, P. (2004). Evidence for tension-based regulation of Drosophila MAL and SRF during invasive cell migration. *Developmental Cell*, *7*(1), 85–93. https://doi.org/10.1016/j.devcel.2004.05.020

Stossel, T. P., Condeelis, J., Cooley, L., Hartwig, J. H., Noegel, A., Schleicher, M., & Shapiro, S. S. (2001). Filamins as integrators of cell mechanics and signalling. *Nature Reviews Molecular Cell Biology*, *2*(2), 138–145. https://doi.org/10.1038/35052082

Szabo, P.A., Miron, M., & Farber, D.L. (2019). Location, location, location: Tissue residence memory T cells in mice and humans. *Science Immunology 4*(34), https://doi.org/10.1126/scieimunol.aas9673

Szalóki, N., Krieger, J. W., Komáromi, I., Tóth, K., & Vámosi, G. (2015). Evidence for Homodimerization of the c-Fos Transcription Factor in Live Cells Revealed by Fluorescence Microscopy and Computer Modeling. *Molecular and Cellular Biology*, *35*(21). https://doi.org/10.1128/mcb.00346-15

Tejera, E., Rocha-Perugini, V., López-Martín, S., Prez-Hernández, D., Bachir, A. I., Horwitz, A. R., … Yáñez-Mo, M. (2013). CD81 regulates cell migration through its association with Rac GTPase. *Molecular Biology of the Cell*, *24*(3), 261–273. https://doi.org/10.1091/mbc.E12-09-0642

Termini, C. M., & Gillette, J. M. (2017). Tetraspanins Function as Regulators of Cellular Signaling. *Frontiers in Cell and Developmental Biology*, *5*, 34. https://doi.org/10.3389/fcell.2017.00034

Theret, M., Mounier, R., & Rossi, F. (2019). The origins and non-canonical functions of macrophages in development and regeneration. *Development, 146*(9). https://doi.org/10.1242/dev.156000

Thiam, H., Vargas, P., Carpi, N., Crespo, C.L., Raab, M., Terriac, E., King, M.C., Jacobelli, J., Alberts, A.S., Stradal, T., Lennon-Dumenil, A., Piel, M. (2016). Perinuclear Arp2/3-driven actin polymerization enables nuclear deformation to facilitate cell migration through complex environments. Stremmel:10997, https://doi.org/10.1038/ncomms10997

Thurmond, J., Goodman, J. L., Strelets, V. B., Attrill, H., Gramates, L. S., Marygold, S. J., … Baker, P. (2019). FlyBase 2.0: The next generation. *Nucleic Acids Research*, *47*(D1).

https://doi.org/10.1093/nar/gky1003

Tomancak, P., Beaton, A., Weiszmann, R., Kwan, E., Shu, S. Q., Lewis, S. E., … Rubin, G. M. (2002). Systematic determination of patterns of gene expression during Drosophila embryogenesis. *Genome Biology*, *3*(12). https://doi.org/10.1186/gb-2002-3-12-research0088

Tomancak, P., Berman, B. P., Beaton, A., Weiszmann, R., Kwan, E., Hartenstein, V., … Rubin, G. M. (2007). Global analysis of patterns of gene expression during Drosophila embryogenesis. *Genome Biology*, *8*(7). https://doi.org/10.1186/gb-2007-8-7-r145

Tseng, Y., An, K. M., Esue, O., & Wirtz, D. (2004). The Bimodal Role of Filamin in Controlling the Architecture and Mechanics of F-actin Networks. *Journal of Biological Chemistry*, *279*(3), 1819–1826. https://doi.org/10.1074/jbc.M306090200

Uhlirova, M., & Bohmann, D. (2006). JNK- and Fos-regulated Mmp1 expression cooperates with Ras to induce invasive tumors in Drosophila. *EMBO Journal*, *25*(22), 5294–5304. https://doi.org/10.1038/sj.emboj.7601401

Vadlamudi, R. K., Li, F., Adam, L., Nguyen, D., Ohta, Y., Stossel, T. P., & Kumar, R. (2002). Filamin is essential in actin cytoskeletal assembly mediated by p21-activated kinase 1. *Nature Cell Biology*, *4*(9), 681–690. https://doi.org/10.1038/ncb838

Valoskova, K., Biebl, J., Roblek, M., Emtenani, S., Gyoergy, A., Misova, M., … Siekhaus, D. E. (2019). A conserved major facilitator superfamily member orchestrates a subset of O-glycosylation to aid macrophage tissue invasion. *ELife*, *8*. https://doi.org/10.7554/eLife.41801

Vetter, I.R., & Wittinghofer, A. (2001). The guanine nucleotide-binding switch in three dimensions. *Science 294(*5545),1299-1304. https://doi.org/10.1126/science.1062023

Warner, S. J., & Longmore, G. D. (2009). Cdc42 antagonizes Rho1 activity at adherens junctions to limit epithelial cell apical tension. *Journal of Cell Biology*, *187*(1), 119–133. https://doi.org/10.1083/jcb.200906047

Weavers, H., Evans, I. R., Martin, P., & Wood, W. (2016). Corpse Engulfment Generates a Molecular Memory that Primes the Macrophage Inflammatory Response. *Cell*. https://doi.org/10.1016/j.cell.2016.04.049

Williams, M. J., Habayeb, M. S., & Hultmark, D. (2007). Reciprocal regulation of Rac1 and Rho1 in Drosophila circulating immune surveillance cells. *Journal of Cell Science*, *120*(3), 502–511. https://doi.org/10.1242/jcs.03341

Wintner, O., Hirsch-Attas, N., Schlossberg, M., Brofman, F., Friedman, R., Kupervaser, M., … Buxboim, A. (2020). A Unified Linear Viscoelastic Model of the Cell Nucleus Defines the Mechanical Contributions of Lamins and Chromatin. *Advanced Science*, *7*(8). https://doi.org/10.1002/advs.201901222

Wood, W., Faria, C., & Jacinto, A. (2006). Distinct mechanisms regulate hemocyte chemotaxis during development and wound healing in Drosophila melanogaster. *Journal of Cell Biology*, *173*(3). https://doi.org/10.1083/jcb.200508161

Yeung, L., Hickey, M.J., & Wright, M.D. (2018) The many and varied roles of tetraspanins in immune cell recrutment and migration. Frontiers in Immunology.9:1644 .https:// doi:

10.3389/fimmu.2018.01644.

Zeitlinger, J., Kockel, L., Peverali, F. A., Jackson, D. B., Mlodzik, M., & Bohmann, D. (1997). Defective dorsal closure and loss of epidermal decapentaplegic expression in Drosophila fos mutants. *EMBO Journal*, *16*(24), 7393–7401. https://doi.org/10.1093/emboj/16.24.7393

Zhang, X. A., Bontrager, A. L., & Hemler, M. E. (2001). Transmembrane-4 Superfamily Proteins Associate with Activated Protein Kinase C (PKC) and Link PKC to Specific β1 Integrins. *Journal of Biological Chemistry*, *276*(27), 25005–25013. https://doi.org/10.1074/jbc.M102156200

Zhou, J., Kim, H. Y., & Davidson, L. A. (2009). Actomyosin stiffens the vertebrate embryo during crucial stages of elongation and neural tube closure. *Development*, *136*(4), 677–688. https://doi.org/10.1242/dev.026211

Zhuang, S., Kelo, L., Nardi, J., & Kanost, M.R. (2007). An Integrin-Tetraspanin Interaction Required for Cellular Innate Immune Responses of an Insect, *Manduca sexta. Journal of Biological Chemistry*. *282*(31)22563-22572. https://doi.org/10.1074/jbc.M700341200

Zwerger, M., Jaalouk, D. E., Lombardi, M. L., Isermann, P., Mauermann, M., Dialynas, G., … Lammerding, J. (2013). Myopathic lamin mutations impair nuclear stability in cells and tissue and disrupt nucleo-cytoskeletal coupling. *Human Molecular Genetics*, *22*(12), 2335–2349. https://doi.org/10.109

2.7 SUPPLEMENTARY INFORMATION

The following supplemental raw data can be accessed via the original publication (Belyaeva et al., 2022) here: https://doi.org/10.1371/journal.pbio.3001494

S1_raw_images. Raw images of Western blots shown in S4A,A Fig

S1 Data. Data used to plot all graphs and to perform statistical analyses

S2 Data. RNA sequencing data

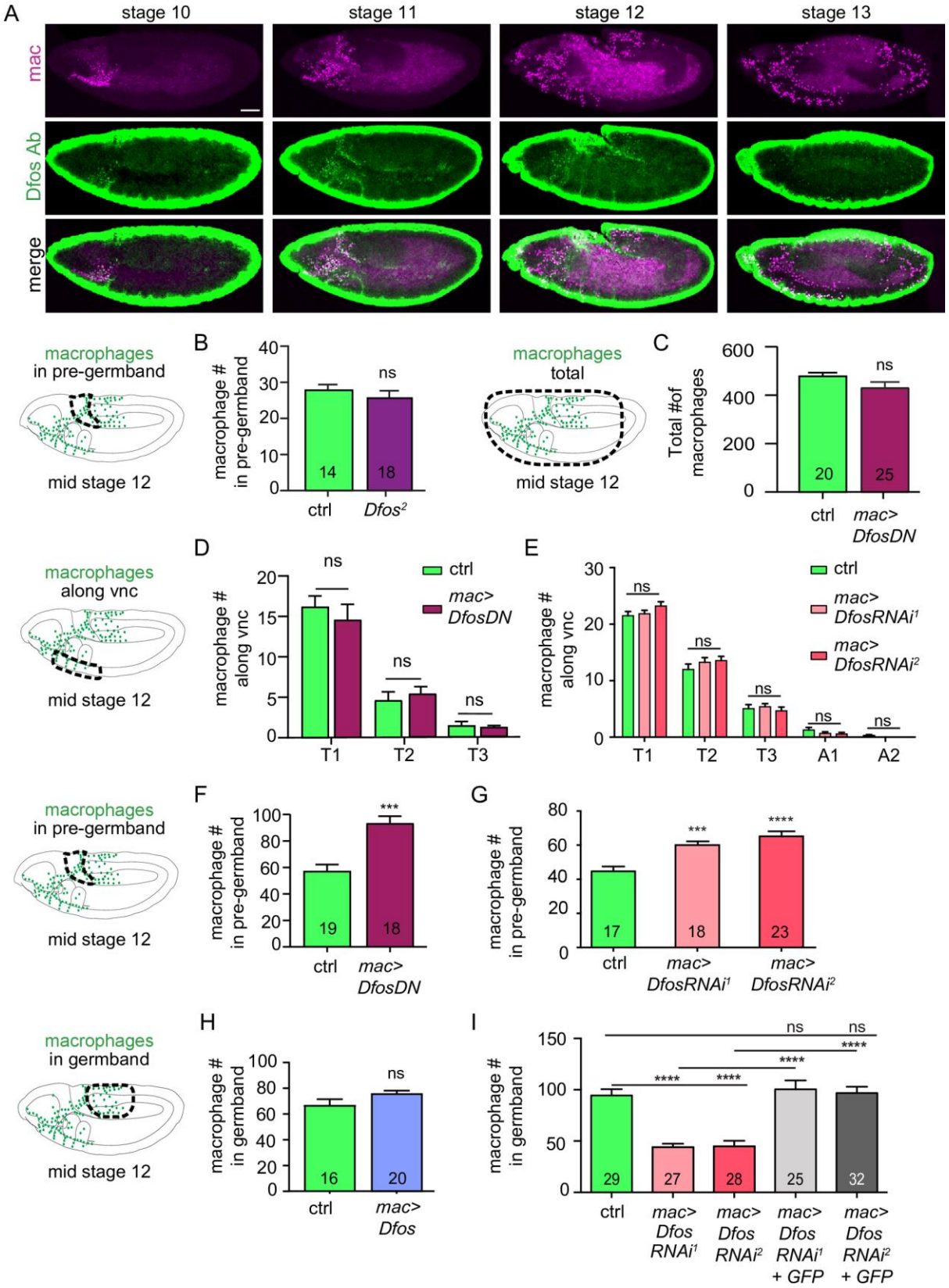

Chapter 2 Fig. S 1. Dfos does not affect the total number of macrophages, or their number in the pre-gb zone and along the vnc

(A) Dfos protein (red) is detected with an antibody in macrophages (green) in embryos from the stages as indicated. (B-I) Quantification in mid St 12 embryos. (B) The number of macrophages (green) in the pre-gb zone (outlined by a black dotted line in the schematic on the left) showed no significant change in *Dfos²* mutant

embryos compared to the control (p=0.37) SD: 6,7. (C) The total number of macrophages (see schematic at left) was not altered from that in the control embryos expressing DfosDN in macrophages (p=0.12). SD: 60, 120. (D-E) The number of macrophages (green) along the vnc (outlined by black dotted line in the schematic on the left) shows no significant difference between the control and (D) macrophages that express DfosDN or (E) either of two RNAi lines against *Dfos*. (D) *DfosDN* p=0.88, 0.99, >0.99. *Dfos RNAi*^{1} (TRiP HMS00254) p=0.21, 0.06, 0.11, 0.072, 0.033, 0.30, 0.56. *Dfos RNAi*^{2} (TRiP JF02804) p=0.34, 0.15, 0.83, 0.27, 0.47, 1.0, 0.45. (D) SD: Ctrl 3, 3, 3, 0.8; *DfosDN* 6, 3, 0.7. (E) SD: Ctrl 6, 3, 3, 3, 2, 0.3; *Dfos RNAi*^{1} 6, 3, 3, 3, 2, 2, 0.3; *Dfos RNAi*^{2} 6, 2, 3, 2, 3, 1, 0.4. (F, G) Macrophage numbers in the pre-gb (see schematic at left) are increased compared to the control for lines expressing (F) DfosDN or (G) one of two different *UAS-Dfos RNAi* constructs in macrophages under *srpHemo-GAL4* control. (F) p=.04, SD: 19, 29. (G) *Dfos RNAi*^{1} p<0.0009, *Dfos RNAi*^{2} p<0.0001. SD: 12, 9, 14. (H) Macrophage numbers in the germband are not significantly altered compared to the control upon overexpression of Dfos in macrophages (p=0.14). SD: 22, 14. (I) Macrophage numbers in the gb for lines expressing one of two different *UAS-Dfos RNAi* constructs in macrophages under *srpHemo-GAL4* control and lines which additionally express *UAS-GFP*. Control vs. *mac>Dfos RNAi*^{1} (TRiP HMS00254) or Control vs. *mac>Dfos RNAi*^{2} (TRiP JF02804), p<0.0001. *mac>Dfos RNAi*^{1} vs. *mac>Dfos RNAi*^{1} *+ GFP* or *mac>Dfos RNAi*^{2} vs. *mac>Dfos RNAi*^{2} *+ GFP*, p>0.99. SD: 33, 47, 34. The effect of each *Dfos RNAi* was eliminated upon simultaneous expression of another UAS construct. Macrophages are labeled using either *srpHemo-Gal4* driving *UAS-GFP* or *srpHemo-H2A::3xmCherry*. "*mac>*" indicates *srpHemo-GAL4* driver expressing UAS constructs specifically in macrophages. Histograms show mean + SEM ***p<0.005, **p<0.01, *p<0.05. Unpaired t-test was used for statistics, except for G, I, which used One-Way ANOVA. The number of embryos analysed for that genotype is shown within each column in the graphs. In D n=6 embryos for the control and n=9 for Dfos DN. In E n=9 embryos for control, 15 and 11 for *Dfos RNAis*. Scale bar in A: 10 µm.

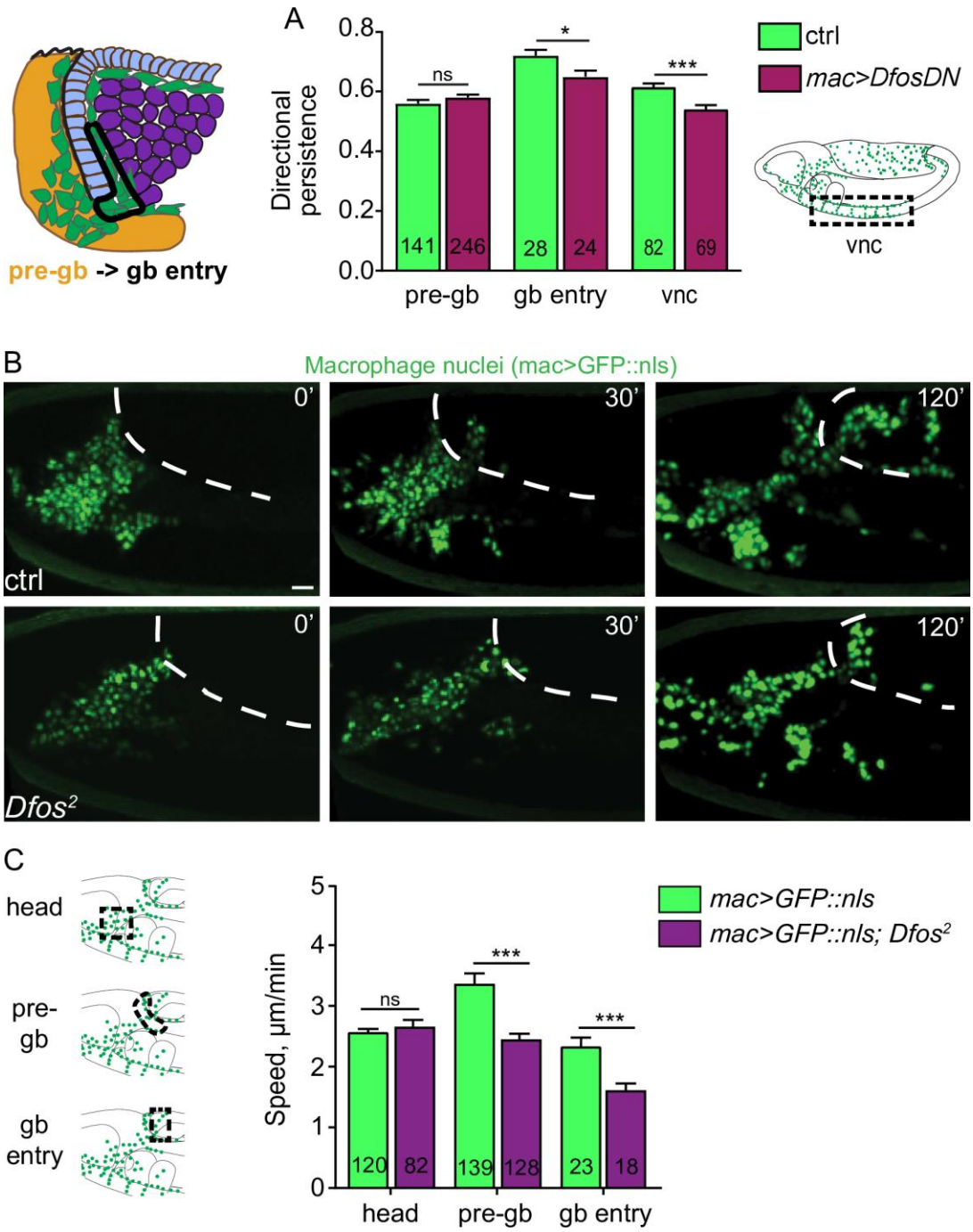

Chapter 2 Fig. S 2. Dfos facilitates macrophage motility during initial invasion into the tissue

(A) Quantification reveals that the directional persistence of macrophages expressing DfosDN (0.58) is unchanged (0.56) in the pre-gb area (p=0.66) but decreased during gb entry (0.65) (0.72), p=0.038 and along the vnc (0.54) compared to the control (0.61), p=0.00026. Left schematic shows pre-gb area in yellow, gb entry outlined in solid line. Boxed area in right schematic shows analyzed area of vnc. **(B)** Movie stills showing wild type and *Dfos*^{2} macrophages entering the gb (outlined by the dashed line). Time in min shown in the top right corner of each image. **(C)** Quantification of macrophage speed shows a significant reduction in the speed of *Dfos*^{2} macrophages in the pre-gb zone and at gb entry, but none in the head. Regions analysed indicated in left schematic. Speed in head: control=2.59 µm/min, *Dfos*^{2}=2.68 µm/min, p=0.40; speed in pre-gb=3.38 µm/min, *Dfos*^{2}=2.47 µm/min, p=2.38e^{-06}; speed in gb entry: control=2.35 µm/min, *Dfos*^{2}=1.62 µm/min, p= 0.0003. Macrophages are labeled using *srpHemo-H2A::3xmCherry*. Histograms show mean±SEM ***p<0.005, **p<0.01, *p<0.05. Unpaired t-test was used for statistics. The number of analyzed macrophages for each genotype shown within each graph column. Tracks were obtained from movies of 3 embryos each for control and *mac>DfosDN* for pre gb entry in **A**, 4 each for gb entry in **A**, 3 each for the vnc in **A**, 4 each of control and 4 *Dfos*^{2} embryos for head and pre-gb in **C**, and 3 embryos each for gb entry in **C**. Scale bars: 10 µm.

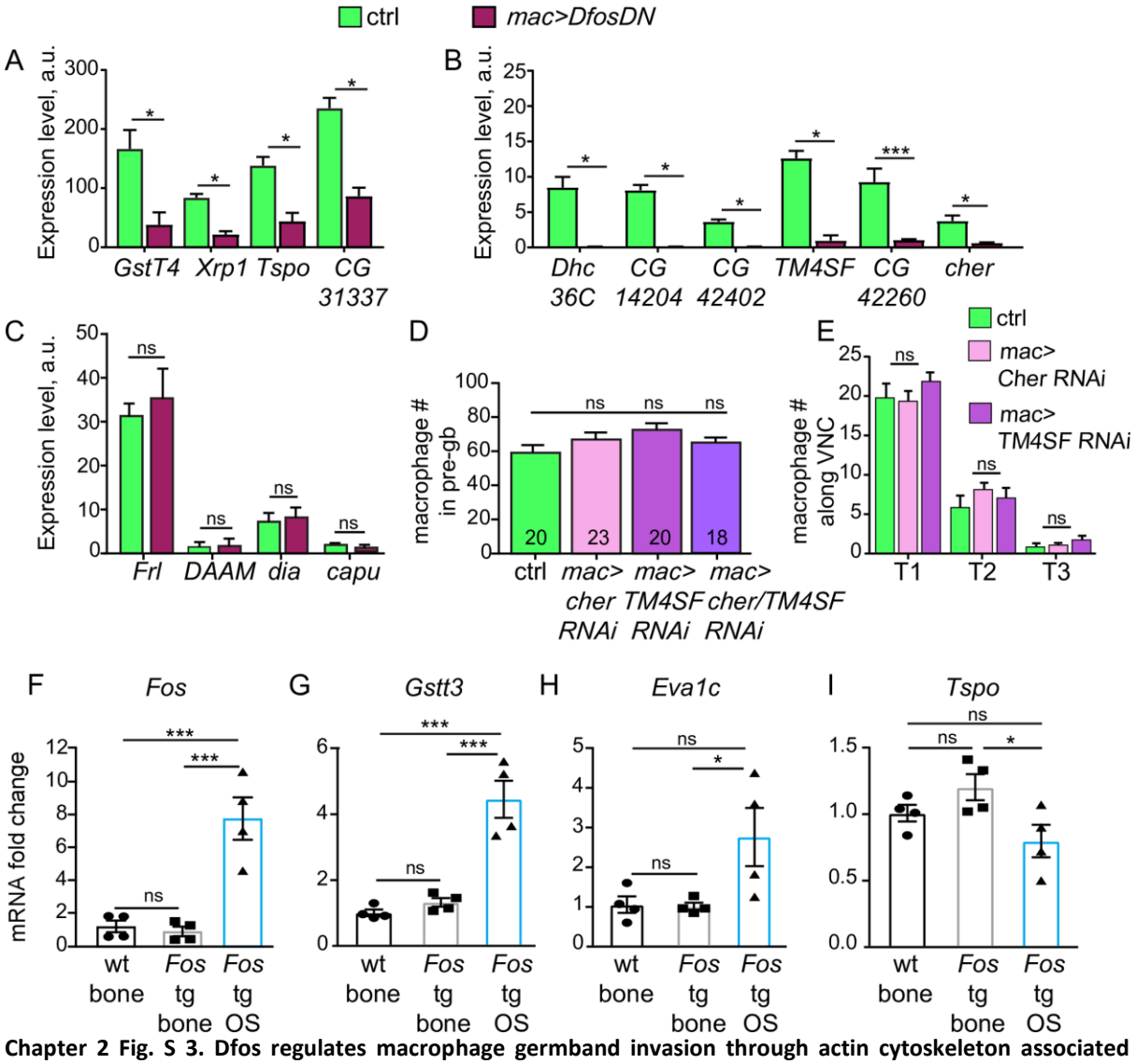

Chapter 2 Fig. S 3. Dfos regulates macrophage germband invasion through actin cytoskeleton associated proteins

(A-C) Comparative mRNA expression levels as determined from RNA sequencing analysis of FACS sorted wild type macrophages and those expressing DfosDN, n=3 biological replicates. (A-B) Genes down-regulated in macrophages expressing DfosDN are shown, separated into those with (A) strong and (B) moderate expression in wild type macrophages. (C) Expression levels of *Drosophila* formin family genes are unchanged. Fold enrichment is normalized. p-values: *Dhc36C* 0.02, *CG14204* 0.03, *CG42402* 0.04, *CR43767* 0.046, *TM4SF* 0.03, *CG42260* 0.0011, *cher* 0.046, *GstT4* 0.018, *Xrp1* 0.0011, *Tspo* 0.046, CG31337_0.046. *Frl*, *DAAM*, *dia*, *capu* all >0.99. (D-E) Quantification of the macrophage numbers in (D) the pre-gb zone and (E) along the vnc from embryos expressing RNAi against *cher* (*KK 107451*), or *TM4SF* in macrophages (*KK 102206*) driven by *srpHemo-Gal4* shows no significant alteration. The number in the column in (D) corresponds to the number of embryos analyzed. Control vs. *cher RNAi* p=0.33. Control vs. *TM4SF RNAi* p=0.05. Control vs. *cher/TM4SF RNAi* p=0.67. (D) SD: 20, 20, 19, 13. For (E) n=13 embryos for control and n=15 for each *cher RNAi* and *TM4SF RNAi*. Control vs. *cher RNAi* p=0.97 for T1, p=0.33 for T2, p=0.88 for T3. Control vs. *TM4SF RNAi* p=0.52 for T1, p=0.76 for T2, p=0.35 for T3. SD: ctrl 6.5, 5.4, 0.6; *cher RNAi* 5.0, 3.3, 0.8; *TM4SF RNAi* 4.4, 4.9, 1.9. (F-I) q-PCR analysis of mRNA extracted from the bones of mice that are wild type, transgenic (tg) for MHC c-fos, viral 3'UTR, and those in which c-fos transgenesis has led to an osteosarcoma (OS). Analysis of mRNA expression shows that (F) higher *Fos* levels in osteosarcomas correlate with hgher levels of (G) the glutathione S transferase *Gstt3*, and (H) the slit receptor *Eva1c*. but not (I) *Tspo*. Bone and osteosarcoma RNA isolated from the same transgenic mouse, n=4 mice per group, age 5 to 6 months. p-values= 0.86, 0.0028, 0.0013 in (F), 0.79, 0.0001, 0.0003 in (G), 1.0, 0.054, 0.049 in (H), 0.37, 0.33, 0.040 in (I). SD: 0.7, 0.6, 2.6 in (F); 0.2, 0.3, 1.1 in (G); 0.4, 0.2, 1.5 in (H); 0.1, 0.2, 0.2 in (I). Histograms show mean + SEM ***p<0.005, **p<0.01, *p<0.05. Unpaired t-test or one-way ANOVA with Tukey post hoc were used for statistics of quantifications. Significance is based on adjusted p values.

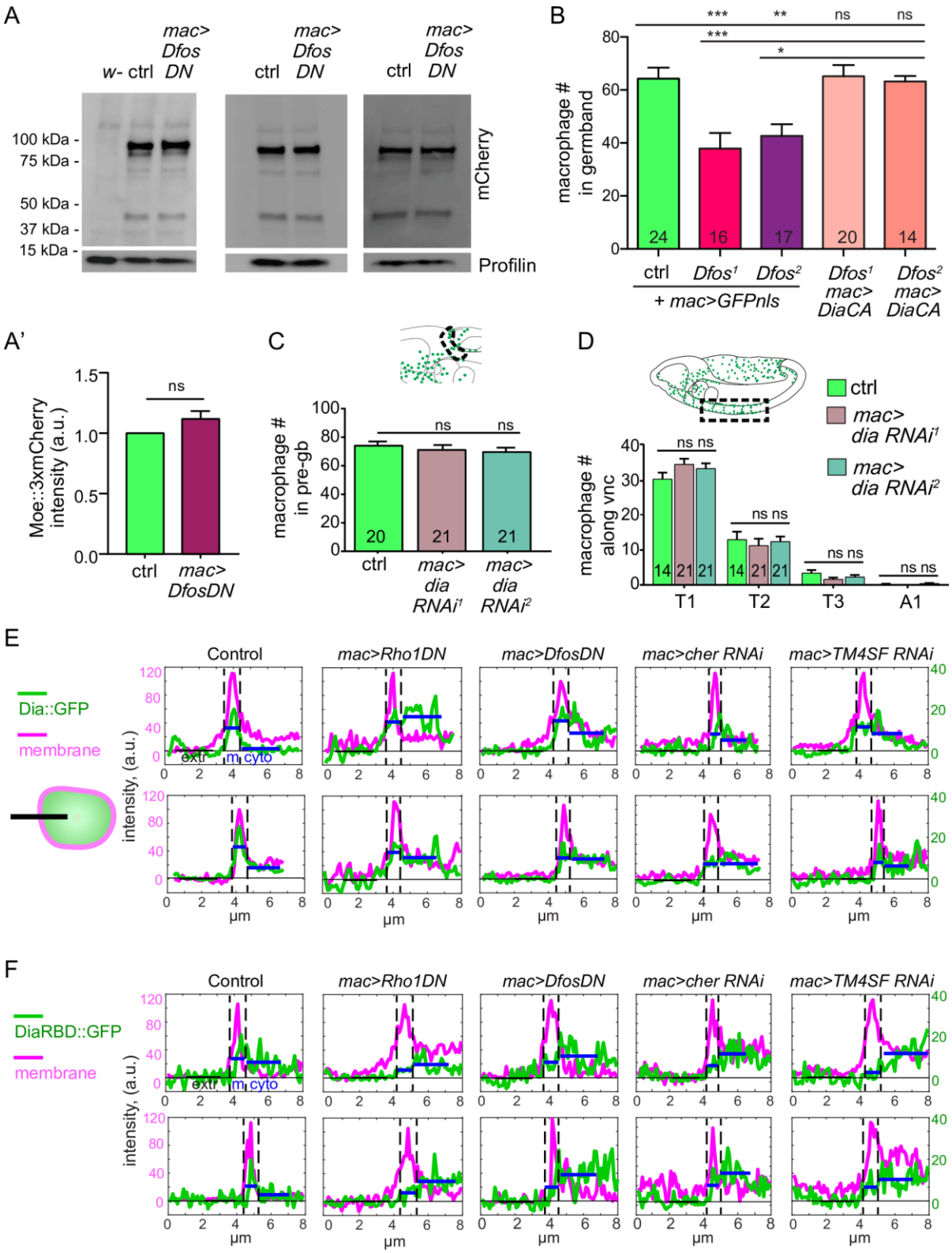

Chapter 2 Fig. S 4. Dia does not affect macrophage numbers in the pre-gb zone and along the vnc

(A) Three Western blots probed with an mCherry antibody of St 11 embryo extracts from *srpHemo-moe::3xmCherry* expressing either *CD8::GFP* (ctrl) or *DfosDN* in macrophages. Left Western blot also contains *w-* lane. Original uncropped Western blots can be found in S1_raw_images. (A') Quantitation of the Western blots. We observed no significant change in the expression of the Moe protein reporter when Dfos function is inhibited. (B) Expressing Dia-CA in macrophages in *Dfos*^{1} or *Dfos*^{2} embryos completely rescued the macrophage germband invasion defect. p-values: Control vs. *Dfos*^{1} or vs. *Dfos*^{2} p=0.0004 or p=0.0055 respectively; Control vs. *Dfos*^{1} *mac>DiaCA* or vs. *Dfos*^{2} *mac>DiaCA* p >0.999; *Dfos*^{1} vs. *Dfos*^{1} *mac>DiaCA* p=0.0005; *Dfos*^{2} vs. *Dfos*^{2}

mac>DiaCA p=0.035. SD: 20, 23, 18, 19, 7.8. (C-D) There was no significant change in the number of macrophages in (C) the pre-gb zone or (D) along the vnc in embryos expressing either of two different RNAi lines against *dia* expressed in macrophages. Pre-gb: Control vs. *dia RNAi*^{1} p=0.54, Control vs. *dia RNAi*^{2} p=0.77. vnc: Control vs. *dia RNAi*^{1} p=0.99, Control vs. *dia RNAi*^{2} p=0.95. *RNAi*^{1} =TRiP HMS05027, *RNAi*^{2} = TRiP HMS00308. (C) SD: 9, 12, 13. (D) SD: Ctrl 5.2, 6.4, 2.5, 0.4; *dia RNAi*^{1} 5.6, 6.8, 1.7, 0.2; *dia RNAi*^{2} 5.1, 4.9, 2.1, 0.6. (E-F) Two further examples of line profiles used for the determination of the membrane-to-cytoplasmic ratios in Fig 4N, P. Line intensity profiles of (E) *Dia::GFP* or (F) *DiaRBD::GFP* (green) and *membrane myr::Tomato* (magenta) across the edge of macrophages expressing either *lacZ* (Control), *RhoDN*, *DfosDN*, *cher RNAi*, or *TM4SF RNAi* as shown in the schematic in E. Line length ~ 8µm. Blue lines indicate mean GFP intensity on the membrane and in cytoplasm. Histograms show mean + SEM ***p<0.005, **p<0.01, *p<0.05. One way ANOVA with Tukey post hoc was used for statistics of quantification. The number in each column corresponds to the number of analysed embryos. "mac>" indicates *srpHemo-GAL4* driver expressing *UAS* constructs in macrophages. Macrophages are labeled using *srpHemo-H2A::3xmCherry.*

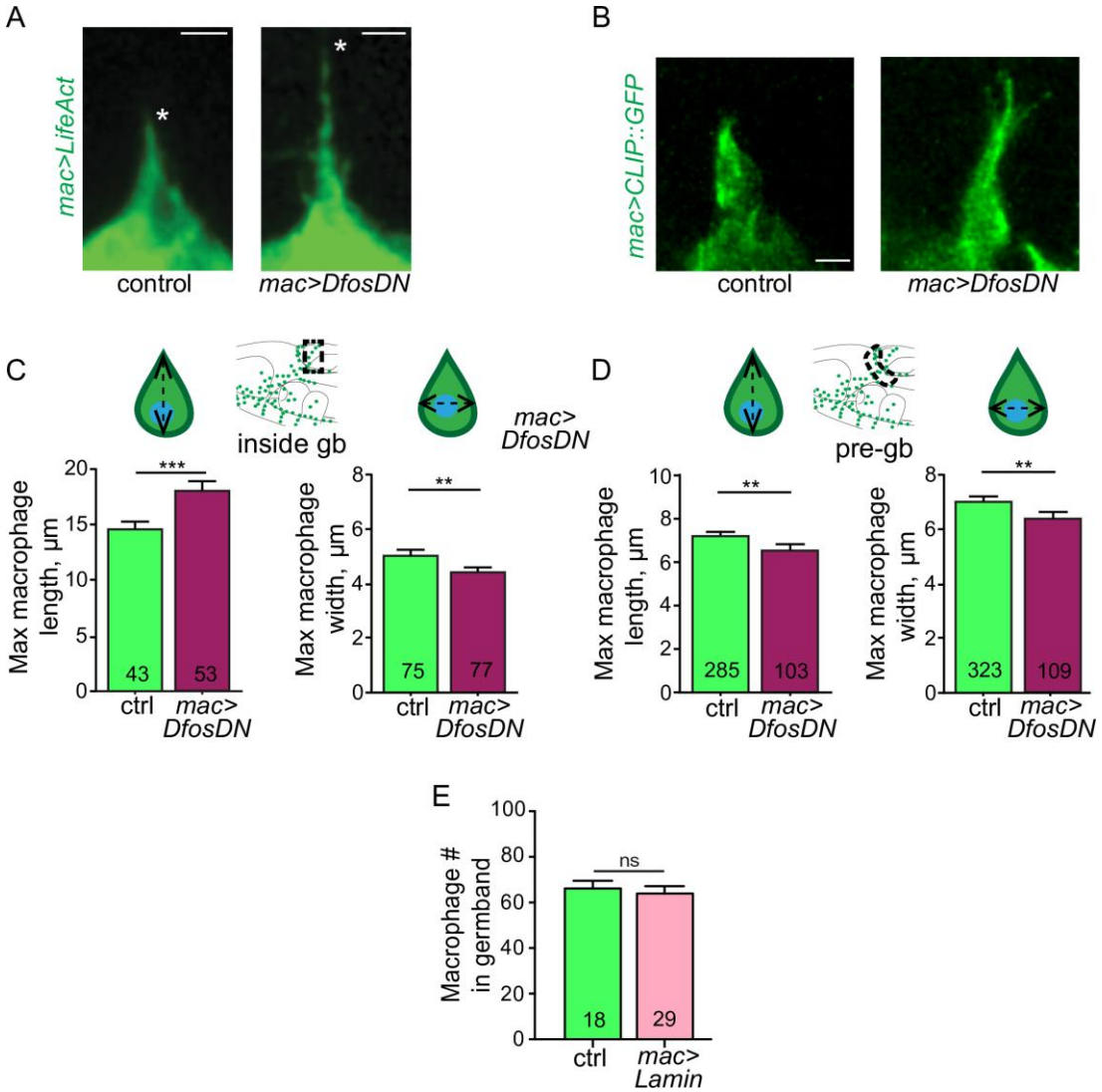

Chapter 2 Fig. S 5. Dfos controls cell shape in macrophages

(A) Representative image showing actin protrusions of the first macrophage entering the germband in the control and in lines expressing DfosDN in macrophages. Actin was visualized by *srpHemo-Gal4* ("mac>") driving *UAS-LifeActGFP*. White stars indicate the tip of each actin protrusion. Scale bar 5µm. (B) Microtubules are labeled with *srpHemo-Gal4* driving *UAS-CLIP::GFP*. Spatially matched stills of the first macrophage expressing DfosDN and control extending protrusions into the gb slightly before entering with the body of the cell. As DfosDN macrophages have a delay in entry, the stills from the DfosDN movie are from a later developmental time point

than the control. (C) Quantification of macrophage maximum length and maximum width shows that DfosDN expressing macrophages are 23% longer and 12% thinner than wild type macrophages inside the gb (indicated in schematic above by dashed box). Control vs. *DfosDN* maximum length p=0.0005, SD: 3.4, 5.7; control vs. *DfosDN* maximum width p=0.0025, SD: 1.3, 1.0. (D) Quantification of the maximum length and maximum width of macrophages in the pre-gb zone (indicated in schematic by dashed box) shows that macrophages expressing DfosDN are 9% shorter and 9% thinner than wild type macrophages. Control vs. *DfosDN* maximum length p=0.0095, SD: 2.2, 2.0; control vs. *DfosDN* maximum width p=0.005, SD: 2.3, 1.9. (E) Overexpression of *UAS-Lam* in macrophages through *srpHemo-Gal4* (*mac>*) causes no change in their number in the gb compared to the control. p=0.65, SD: 15, 18. Histograms show mean + SEM ***p<0.005, **p<0.01, *p<0.05. Unpaired t-test was used for statistics of quantification. The number of measurements per genotype is shown in each columns.

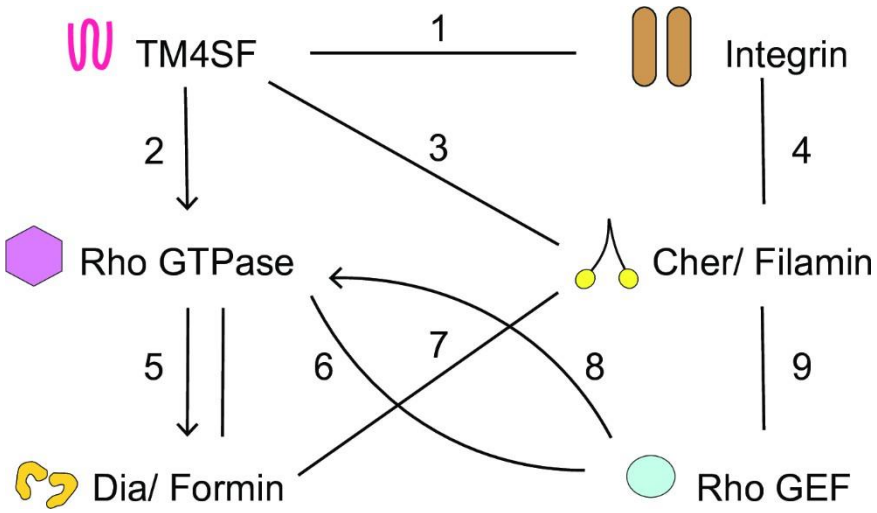

Chapter 2 Fig. S 6. Model of protein interactions at the macrophage cortex
Proposed interactions of proteins at the cell cortex in wildtype macrophages during gb infiltration as shown in Fig 6. Direct binding between two proteins is indicated by a line, signaling between the interaction partners is represented as an arrow. These interactions and the resulting model in Figure 6 are based on the papers at the end of this legend next to the corresponding number shown for each linkage. The Tetraspanin TM4SF can cluster adhesion receptors such as Integrins at the membrane and lead to the recruitment and activation of Rho GTPases. Rho GTPases can bind and activate the formin Dia leading to F-actin polymerization. In addition, Integrin can bind filamins (Cher), which can bind to and thereby recruit RhoGEF to the membrane. Rho GEFs can in turn bind to and activate Rho GTPases. References for listed interactions: 1, Tetraspanins-Integrin) Zhuang et al, 2007; Berditchevski & Odintsova, 1999. 2, Tetraspanins-Rho GTPases) Delaguillaumie, et al., 2002; Hong et al., 2012; Tejera et al., 2013. 3, Tetraspanins-Filamins) Brzozowski et al., 2018; Perez-Hernandez et al., 2013. 4, Integrin-Filamins) Razinia et al., 2012; Ehrlicher et al., 2011. 5, Rho1 GTPase-Dia in *Drosophila)* Großhans et al., 2005; Rose et al., 2005. 6 & 8, Rho GEF-Rho GTPases) Vetter & Wittinghofer, 2001. 7, Formins-Filamins) Hu et al., 2014; Lian et al., 2016. 9, Filamins-RhoGEFs) Bellanger et al., 2000; Del-Valle Perez, 2010.

S1 Movie. Dfos facilitates macrophage motility during initial invasion into the germband tissue
Movies corresponding to stills shown in **Fig 2A**. Macrophages (green) labelled using *srpHemo-H2A::3xmCherry* are imaged while entering the gb in control embryos (left) and embryos in which macrophages express a dominant negative (DN) version of Dfos (DfosDN) (right). Time in minutes is indicated in the upper right corner. Scale bar: 10 µm.

S2 Movie. Dfos does not affect macrophage migration along the vnc
Movies corresponding to stills shown in **Fig 2G**. Macrophages (green) labelled by *srpHemo-Gal4* driving *UAS-GFP::nls* are imaged during their migration along the segments of the vnc in control embryos (left) and embryos in which *DfosDN* is expressed in macrophages (right). Time in minutes is indicated in the upper right corner. Scale bar: 10 µm.

S3 Movie. Macrophages in $Dfos^2$ mutants invade germband more slowly
Movies corresponding to stills shown in S2B Fig. Macrophages (green) labelled by srpHemo-Gal4 driving UAS-GFP::nls are imaged while entering the gb in control embryos (left) and *$Dfos^2$* mutant embryos (right). Time is indicated in minutes. Scale bar: 10 µm.

S4 Movie. DfosDN expressing macrophages make long actin protrusions during germband entry
Movies corresponding to stills shown in **S5A Fig**. F-actin in macrophages (green) labelled with *srpHemo-Gal4* driving *UAS-LifeAct::GFP* is imaged during gb entry in control embryos (left) and embryos with macrophages expressing *DfosDN* (right). Note the extended protrusion of the *DfosDN* expressing macrophages. Time is indicated in minutes. Scale bar: 10 µm.

S5 Movie. Dfos controls cell shape in macrophages
Movies corresponding to stills shown in **Fig 5B-C** and **S5B Fig**. Microtubules of macrophages are labelled with *srpHemo-Gal4* driving *UAS-CLIP::GFP*. They are imaged during gb entry in control embryos (left) and embryos with macrophages expressing DfosDN (right). Note the extended shape of the *DfosDN* expressing macrophages. Time is indicated in minutes. Scale bar: 10 µm.

2.8 AUTHOR CONTRIBUTION

The following list gives a detailed overview on my contributions to the manuscript in Chapter 2 of this thesis.

Table 2-3 Contribution of Stephanie Wachner to the Chapter 2 publication

	Super-vision/ Training	*Crosses*	*Fixation*	*Staining*	*Microscopy*	*Analysis*	*Figure preparation*	*sample preparation*
Figure 1								
A							X	
B							X	
C							X	
D							X	
E							X	
F							X	
G							X	
H							X	
I							X	
J							X	
K							X	
L							X	
M							X	
N							X	
O		X	X	X	X	X	X	X
P		X	X	X	X	X	X	X
Q		X	X	X	X	X	X	X
R								
Figure S1								
A	X	X	X	X	X	X	X	X
B							X	
C		X	X	X	X	X	X	X
D							X	
E							X	
F		X	X	X	X	X	X	X
G								
H							X	
I								
Figure 2								
A							X	
B							X	
C							X	
D						X	X	
E							X	

F							X	
G							X	
Figure S2								
A							X	
B							X	
C							X	
D							X	
Figure 3								
A							X	
B							X	
C		X	X	X	X	X	X	X
D		X	X	X	X	X	X	X
E		X	X	X	X	X	X	X
F		X	X	X	X	X	X	X
G		X	X	X	X	X	X	X
H		X	X	X	X	X	X	X
I		X	X	X	X	X	X	X
J		X	X	X	X	X	X	X
K		X	X	X	X	X	X	X
L		X	X	X	X	X	X	X
M							X	
N							X	
N'							X	
N''							X	
O							X	
Figure S3								
A							X	
B							X	
C							X	
D		X	X	X	X	X	X	X
E		X	X	X	X	X	X	X
F							X (+statistic)	
G							X (+statistic)	
H							X (+statistic)	
I							X (+statistic)	
Figure 4								
A		X	X	X	X	X	X	X
B	X	X			X	X	X	X
C	X	X			X	X	X	X
D	X	X			X	X	X	X
E	X	X			X	X	X	X
F	X	X			X	X	X	X
G	X	X			X	X	X	X

H	X	X			X	X	X	X
I		X	X	X	X	X	X	X
J		X	X	X	X	X	X	X
K						X	X	
L						X	X	
M								
N	X (concept)							
O								
P	X (concept)							
Figure S4								
A	X	X					X	X
B							X	
C							X	
D						X	X	
E	X							
F	X							
Figure 5								
A						X	X	
B	X						X	
C	X						X	
D							X	
E		X	X	X	X	X	X	X
E'		X	X	X	X	X	X	X
E''		X	X	X	X	X	X	X
E'''		X	X	X	X	X	X	X
F		X	X	X	X	X	X	X
F'		X	X	X	X	X	X	X
F''		X	X	X	X	X	X	X
F'''		X	X	X	X	X	X	X
G	X	X	X	X	X	X	X	X
H		X	X	X	X	X	X	X
Figure S5								
A	X						X	
B	X						X	
C						X	X	
D						X	X	
E							X	
Figure 6							X	
Figure S6							X (incl. lit. review)	

3 Paper Draft: BMP activates a subpopulation of macrophages that lead efficient tissue infiltration in *Drosophila* embryos

Stephanie Wachner[1,2], Pierre Cattenoz[3], Vera Belyaeva[1,6], Aleksandr Bykov[4,5], Attila Gyoergy[1,4], Angela Giangrande[3], Luisa Cochella[4,5], Daria Siekhaus[1*]

*- Corresponding author: daria.siekhaus@ist.ac.at

1 – Institute of Science and Technology Austria, Am Campus 1, 3400 Klosterneuburg, Austria

2 – Current address: Pfizer Corporation GmbH, Floridsdorfer Hauptstraße 1, 1210 Vienna, Austria

3–Université de Strasbourg, Illkirch, France

4 –Campus-Vienna-BioCenter 1, 1030 Vienna, Austria

5– Current address: Johns Hopkins University School of Medicine, Baltimore, MD 21205, USA

6 – Current address: Molecular Devices, Urstein Süd 17, 5412, Austria

3.1 ABSTRACT

Recent studies have shown that *Drosophila* immune cells (hemocytes) invade a tissue barrier during their colonization of the embryo in a manner akin to mammalian immune cell extravasation from the vasculature, introducing them as a new model for tissue barrier penetration. Here, we reveal a novel hemocyte subpopulation, one in which BMP signaling is active during early migratory steps prior to their penetration of the tissue barrier of the germband. BMP^+ hemocytes predominantly populate the germband tissue and lead germband invasion. The BMP type I receptor *thickveins* (*tkv*) is crucial for regulating the persistent migration of leading hemocytes specifically at the tissue entry site. Surprisingly, leading hemocytes inside the germband belong to a previously unknown cluster enriched in the expression of enhancer of split complex (*E(spl)C*) genes, which we identify by single-cell RNA-Sequencing of hemocytes throughout early embryonic stages. This E(spl)C cluster shows higher expression of putative BMP target genes *Fasciclin2*, *Fasciclin3*, *Tsp39D*, and *Pvf3* that regulate th efficiency of hemocyte invasion into the germband tissue, a process independent of Notch signaling. As such, our findings extend the current view of embryonic hemocyte heterogeneity and point toward a conserved role for canonical BMP signaling in specifying the subpopulation that leads migration of tissue-resident macrophages during embryogenesis.

3.2 INTRODUCTION

Blood cells not only play an important role in immune responses and tissue repair, but tissue-resident macrophages are also crucial for normal embryonic development, such as the formation of the eye, the brain, fetal testis, and mammary glands (Chaplin, 2010; DeFalco et al., 2014; Fantin et al., 2010; Gouon-Evans et al., 2000; Ingman et al., 2006; Rymo et al., 2011; Wynn et al., 2013; Yosef et al., 2018). Advantages in lineage tracing and RNA-Sequencing have allowed for deeper insights into the complexity of the vertebrate immune system, leading to a paradigm shift in the view of tissue-resident macrophages (Gautiar et al., 2012; Wynn et al., 2013). Previously believed to solely originate from bone marrow-derived monocytes, they are now defined as independent yolk-sac-derived erythro-myeloid lineages which are predicted to be a heterogeneous population themselves (Dzierzak & Speck, 2008; S. J. Morrison & Scadden, 2014; van Furth et al., 1972; Yamane, 2018). Different organs harbor specific types of tissue-resident macrophages, and their colonization during early embryogenesis is controlled by different signaling pathways such as TGFβ and BMP signaling for the microglia population of the brain and the Langerhans cells in the skin (T. Borkowski et al., 1997; T. A. Borkowski et al., 1996; Butovsky et al., 2014; Kel et al., 2010; Utz et al., 2020). While these studies clearly show an effect of TGFβ signaling in establishing a tissue-resident macrophage population, whether this plays a role during the macrophage tissue infiltration or at another point during embryonic development remains unclear. Moreover, the complexity of macrophage populations in the same tissue that can be differentially affected by TGFβ signaling complicates the interpretation of *in vivo* data in mice (Utz et al., 2020).

The immune system of *Drosophila melanogaster* is less complex, but shares functional characteristics and genetic factors with vertebrate immune cells. In both species, GATA and Runx factors control immune cell differentiation, and JAK/STAT, IMD, and Toll pathways mediate the immune response (Buchon et al., 2014; Lebestky et al., 2000). Additionally, the tissue infiltration of immune cells in the early embryo is regulated by Integrins and Rho-GTPases, similar to invasive immune cell migration in vertebrates, making them an ideal model to study the effects of BMP signaling on immune cell tissue invasion (Comber et al., 2013; Paladi & Tepass, 2004; Siekhaus et al., 2010; Wood & Jacinto, 2007).

Similar to vertebrates, there are two waves of hematopoiesis in the fly, with the first wave resembling primitive hematopoiesis in the embryo and the second wave in the lymph gland, the hematopoietic organ of the larva, giving rise to stem cell-like progenitors (Banerjee et al., 2019; Gold & Brückner, 2014; Makhijani et al., 2011). Embryonic hemocytes originate in the procephalic mesoderm and relate to the erythro-myeloid lineage of tissue-resident macrophages in vertebrates (de Velasco et al., 2006; Gold & Brückner, 2014; Tepass et al., 1994). The lymph gland lineage originates from cardiogenic mesoderm more similar to hematopoietic stem and progenitor cells of the vertebrate aorta-gonad-mesonephros (AGM) (Jung et al., 2005; Mandal et al., 2004). While lymph gland hemocytes are only released into circulation upon metamorphosis, embryonic hemocytes actively migrate via stereotyped routes (Siekhaus et al., 2010; Tepass et al., 1994). Similar to yolk-sac-derived vertebrate macrophages, they are crucial for the process of organ development, such as the positioning of renal tubules by localized amplification of BMP signaling through Collagen IV secretion and condensation of the nerve cord by engulfment of apoptotic midline glia (Olofsson & Page, 2005; Sears et al., 2003; Zhou et al., 1995).

The migration of embryonic hemocytes is regulated by the PDGF/VEGF-related ligands Pvf2 and Pvf3, known to be expressed along the future path of their migration (Cho et al., 2002; Heino et al., 2001), and the receptor Pvr, which is expressed in hemocytes themselves (N. K.

Cho et al., 2002; Heino et al., 2001; Parsons & Foley, 2013; Wood et al., 2006). Another PDGF/VEGF-related ligand, Pvf1, seems to be dispensable for embryonic hemocyte migration (N. K. Cho et al., 2002; Harris et al., 2007; Wood et al., 2006) but induces hemocyte proliferation in a *Drosophila* tumor model (Parisi et al., 2014). However, Pvr is also involved in hemocyte survival (Brückner et al., 2004), and individual Pvf ligands are not exclusively expressed along specific paths (N. K. Cho et al., 2002). Thus, it remains unknown how hemocytes decide between different routes. In the absence of Pvr, Pvf2 and Pvf3 were shown to be crucial for germband invasion when cell survival was restored. In contrast, migration from the side of origin in the head mesoderm up to the germband is Pvr-independent (N. K. Cho et al., 2002). Moreover, as hemocytes migrate in a stream of individual cells, additional mechanisms must exist that allow the leading cells to move beyond possible attractive signals while the following hemocytes still need to be able to sense guiding signals. This regulation was proposed to be either dependent on hemocyte interactions with the surrounding tissue or signaling from leading to following hemocytes, similar to Pvf gradient formation during lateral line migration in zebrafish (Donà et al., 2013; Ratheesh et al., 2015; Venkiteswaran et al., 2013). However, differences in embryonic hemocytes that could enable them to follow one another have yet to be investigated.

Despite the characterization of the precise origin of hemocytes from different zones of the head mesoderm (de Velasco et al., 2006), differences in gene expression in hemocyte subpopulations are just starting to be unraveled. One recent study identified functionally distinct subpopulations in late embryos at stage 15, a time when hemocytes have already dispersed through the embryo (Coates et al., 2021). These subpopulations showed characteristics of pro-inflammatory M1 macrophages of vertebrates with a faster migration towards wounds, and exhibited different localizations and dynamics throughout later fly development, demonstrating the complexity of embryonic hemocytes. However, during early embryonic development, hemocytes face very different tissue environments and display more characteristics of M2-like macrophages that shape tissue development.

Other studies utilized single-cell RNA-Sequencing of larval hemocytes and identified previously unknown subpopulations in *Drosophila* immune cells, different states of hemocytes upon inflammation and immune challenge, and novel subtypes of crystal cells and lamellocytes enriched in the FGF-receptor *breathless* and the ligand *branchless* that are crucial for parasite defense (Cattenoz et al., 2020; Fu et al., 2020; Tattikota et al., 2020). The very small population of primocytes was proposed as a novel hematopoietic precursor population labeled by the expression of transcription factors controlling cell fate specification and differentiation, including *Antennapedia*, *knot*, *hamlet*, *Mothers against dpp* (*Mad*), and *Z600* (Fu et al., 2020). However, a comparison between larval and embryonic hemocytes showed significant differences in their gene expression and highlighted the need for in-depth characterization of hemocytes throughout embryonic development.

In an attempt to describe the embryonic hemocyte population during the time of their specification, transcriptome data from larval and embryonic single-cell RNA-Sequencing from the early *Drosophila* embryo at Stage 5 have been used to generate a pseudo-transcriptome (Cattenoz et al., 2021). Therein, procephalic mesoderm cells that will go on to form hemocytes were verified to express the earliest hemocyte-specific transcription factors Glial Cell Missing/Glial Cell Deficient (Gcm) and the GATA factor Serpent (Srp). Pro-hemocytes highly correlated with the proliferative plasmatocyte subgroups of the larval lymph gland, indicating that proliferating embryonic hemocytes give rise to larval hemocytes (Cattenoz et al., 2021). However, factors regulating macrophage subpopulations to penetrate a tissue barrier as a

physiological developmental process similar to the migration of yolk-sac-derived tissue-resident macrophages in vertebrates remain unknown.
Recently, we have shown that the transcription factor DFos in *Drosophila* modulates cellular properties of embryonic hemocytes by transcriptional regulation to aid their migration within the constrained environment of the germband tissue (Belyaeva et al., 2022). Previously, Dfos was shown to genetically interact during *Drosophila* development with one of the major signaling pathways – BMP – to control the formation and migration of leader cells during dorsal closure (Perkins et al., 1988; Riesgo-escovar & Hafen, 1997; Riesgo-Escovar & Hafen, 1997; Zeitlinger et al., 1997). Here, we describe the role of BMP signaling in embryonic hemocyte migration, revealing a novel hemocyte subpopulation activated by BMP signaling that predominantly populates the germband tissue and leads germband invasion. The BMP type I receptor Thickveins (Tkv) is crucial for regulating the persistent migration of leading hemocytes specifically at the tissue entry site. Surprisingly, leading hemocytes inside the germband belong to a previously unknown cluster enriched in the expression of enhancer of split complex (*E(spl)C*) genes, which we identify by single-cell RNA-Sequencing of hemocytes throughout early embryonic stages. This E(spl)C cluster shows higher expression of putative BMP target genes *Fasciclin2*, *Fasciclin3*, *Tsp39D*, and *Pvf3* that regulate the efficiency of hemocyte invasion into the germband tissue, a process independent of Notch signaling. Thereby, our findings extend the current view of embryonic hemocyte heterogeneity and point toward a conserved role for canonical BMP signaling in specifying the subpopulation that leads migration of tissue-resident macrophages during embryogenesis.

3.3 RESULTS

3.3.1 Early *Drosophila* embryonic hemocytes contain a BMP$^+$ subpopulation

Recently, cellular properties of *Drosophila* hemocytes populating the embryo from their origin in the head mesoderm via conserved routes (Fig. 1A) were shown to be regulated by the transcription factor DFos, which has been linked to BMP signaling in different contexts (Belyaeva et al., 2022; Dequier et al., 2001; Perkins et al., 1988; Riesgo-escovar & Hafen, 1997; Riesgo-Escovar & Hafen, 1997). However, the role of BMP signaling in this process is not known. Therefore, we first visualized active BMP signaling by antibody staining against the activated form of the transcriptional regulator P-Mad. P-Mad staining can be found in the nucleus of hemocytes at stage 10, when they have started to spread out from the head mesoderm (Fig. 1C). P-Mad-positive hemocyte nuclei are not observed during their later migration into the germband. To our surprise, BMP-signaling was only active in a subpopulation of hemocytes at Stage 10, comprising about 25% of the total population (Mean=25.1%, lower 95% CI of mean=22.8%, upper 95% CI of mean=27.3%, minimum=17%, maximum=30%). Those hemocytes positively labeled for BMP signaling activity (BMP$^+$) are localized close to the outer epithelium of the head and typically form a stripe underneath the cephalic furrow at the edge between the head and gnathal segments. At this stage, dpp, the predominant ligand of BMP signaling shaping *Drosophila* embryonic development, is expressed throughout the lateral ectoderm, and in the head it is enriched in the area that abuts the BMP$^+$ hemocytes (François et al., 1994). Thus, Dpp diffusion from the ectoderm could be spatially restricted to affect only a subpopulation of hemocytes.
To examine if hemocytes that have experienced BMP signaling occupy any particular migration route during later stages, we made use of the fluorescent Dpp-signaling sensor *Dad-GFP* which is comprised of the conserved minimal *Dad* enhancer fused to GFP, which has been

frequently used to label canonical BMP-signaling activation at the transcriptional level (Hamaratoglu et al., 2011; Ninov et al., 2010; Weiss et al., 2010b).
As our previous results had shown a specific role for *Dfos* during hemocyte penetration of the germband tissue, we closely examined the *Dad-GFP* signal during the early phase of germband entry (Fig. 1E-F). At this stage, about 33 hemocytes on average have penetrated the germband; of these 41% were *Dad-GFP* positive (Fig. 1G, Mean=41.3%, lower 95% CI of mean=36.9%, upper 95% CI of mean=45.7%, minimum=21%, maximum=65%), indicating that a high fraction of hemocytes which invade into the germband tissue are BMP^+. Moreover, in the majority of embryos, the BMP^+ hemocytes were found among those farthest inside the germband (Fig. 1E, F). In 78% of embryos, the leading hemocyte showed *Dad-GFP* signal, and in another 19% of embryos either the second or third hemocyte showed marker expression (Fig. 1G). Precise discrimination of the second or third hemocyte inside the germband is not feasible, as they can overtake each other during migration and sometimes the two nuclei are located side by side. In one embryo, the precise order of the hemocytes inside the germband could not be assessed and was therefore categorized as unclear. These results indicate that hemocytes that have experienced BMP-activation are predominantly the leading cells inside the germband.
To examine the specificity of this linkage between previous BMP signaling and invasive migration, we assessed the *Dad-GFP* reporter's activity in hemocytes migrating along the vnc, an environment in which surrounding cells are less densely packed compared to inside the germband tissue (Evans et al., 2010; Ratheesh et al., 2018). In contrast to the germband, only one *Dad-GFP* positive hemocyte was found midway along the vnc in two out of 13 embryos (Fig. 1H-I). Thus, the majority of vnc hemocytes do not belong to the BMP^+ subpopulation. However, BMP^+ hemocytes do reside in the head area, especially anterior to the vnc segments in the labial gnathal segment (Fig. 1H, white asterisk).
Taken together, these results show a novel BMP^+ subpopulation of embryonic hemocytes at stage 10, which are localized in a stereotypic pattern. The majority of hemocytes inside the germband belong to this BMP^+ subpopulation at this developmental timepoint.

3.3.2 BMP signaling components regulate tissue invasion of embryonic hemocytes

We then sought to assess whether BMP signaling activation can affect hemocyte migration by counting the number of hemocytes that had invaded the germband of stage 12 embryos (marked by a black box in Fig. 2A) in BMP gain- and loss-of-function experiments. Down-regulation of the canonical BMP signaling pathway was achieved by expressing the full-length inhibitory Smad that is directly fused to the hemocyte-specific srpHemo promoter (*srpHemo-Dad*). Dad down-regulates BMP signaling by blocking the phosphorylation of Mad through the Tkv receptor and oligomerization of P-Mad (H. Inoue et al., 1998). Moreover, this inhibition has been shown to be targeted to Mad, but not the other transcriptional regulator in *Drosophila,* Smad2 (Kamiya et al., 2008). Compared to the control, 31% fewer *srpHemo-Dad* expressing hemocytes were found inside the germband at the same stage (Fig. 2A). However, this effect was only visible when *Dad* expression was directly driven by the *srpHemo* promoter and could not be observed for *Dad* over-expression using the Gal4 system (*srpHemo-Gal4, UAS-Dad*) (Fig. 2 S1A), indicating that the timing of BMP signaling is crucial for effects on hemocyte migration into the germband.

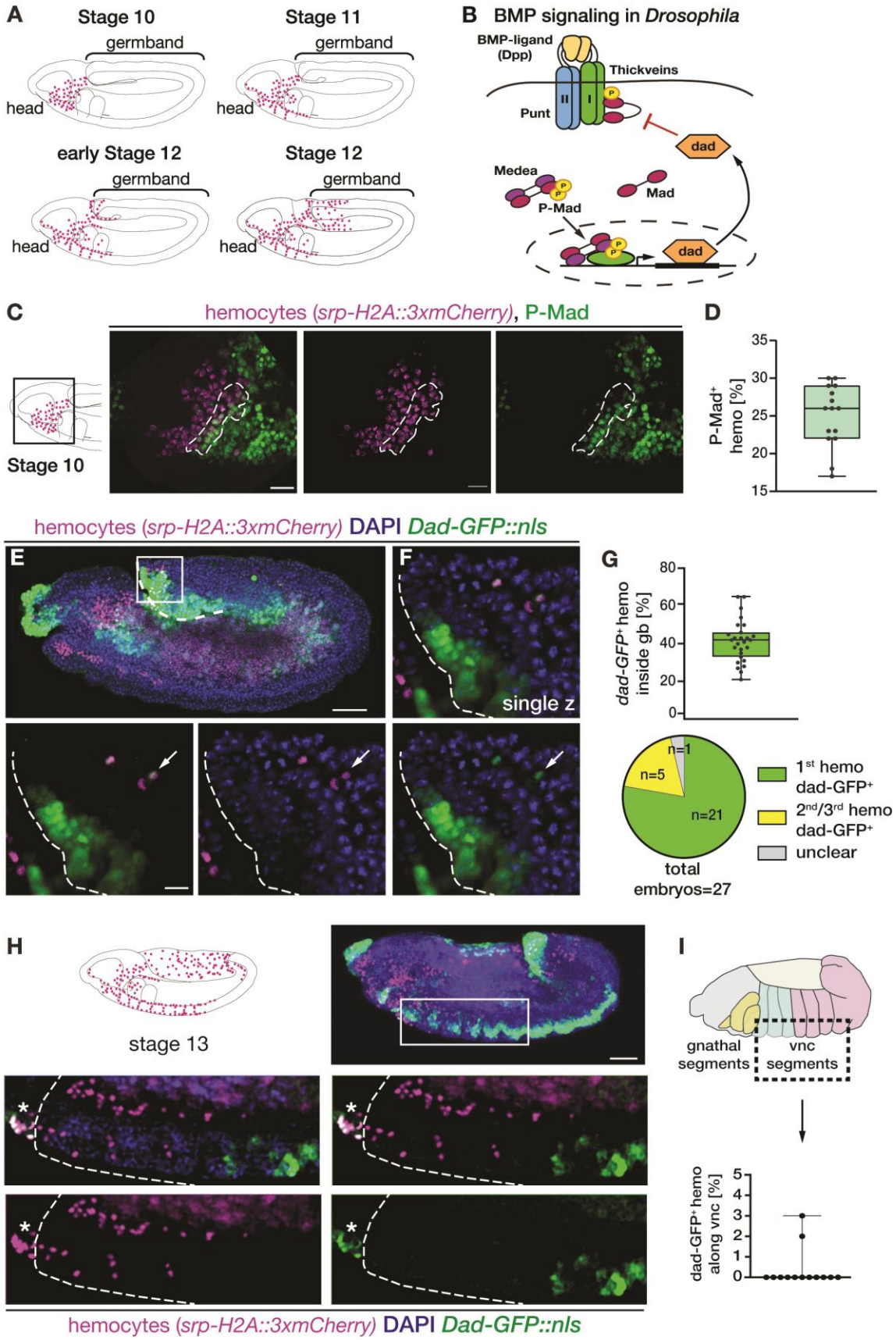

Chapter 3 Fig 1. A subpopulation of Drosophila embryonic immune cells show BMP-signaling activation

(A) Stages of Drosophila embryogenic development. At stage 10, characterized by germband retraction less than 29%, hemocytes are spreading out from head mesoderm. At stage 11 (germband retraction 29%-31%)

hemocytes approach germband border and align in a semi-circular arch, and start to migrate along vnc on the ventral side. At early stage 12 hemocytes invade into germband tissue. Later during stage 12 the germband retracts further to the posterior, hemocytes that did not invade into the germband reside in the pre-germband zone, whereas hemocytes at the ventral side migrate through vnc segments. **(B)** Schematic of BMP signaling in *Drosophila*: binding of the BMP-ligand (primarily Dpp) to type I (primarily Thickveins, Tkv) and type II (primarily Punt, Put) receptors leads to phosphorylation and activation of the transcriptional regulator Mad (P-Mad) by the hetero-receptor-complex. Upon binding of P-Mad to the transcriptional co-regulator Medea the complex translocates into the nucleus regulating transcription. Eventually, a negative feedback loop is initiated through Dad-mediated inhibition of Mad activation. **(C)** Representative images of a stage 10 embryo (maximum z-projection of 25 slices, inter-slice interval 1um) in which hemocyte nuclei (magenta) are labelled by *srpHemo-H2A::3xmCherry* and stained with an antibody against the phosphorylated form of Mad (P-Mad) shown in green. Black box in the schematic of stage 10 indicates position of imaged area of the anterior lateral embryo. Area of hemocytes closest to the overlying epidermis showing P-Mad positive hemocytes is indicated by a white dashed line. **(D)** Quantification of P-Mad positive hemocytes in stage 10 embryos shown in Fig. 1C. Number of total hemocytes and P-Mad positive hemocytes were quantified per embryo and shown in % for 15 individual embryos. Boxplot with mean=25.1%, lower 95% CI of mean=22.8%, upper 95% CI of mean=27.3%, minimum=17%, maximum=30%. (**E,F)** Analysis of BMP^+ hemocytes, which invaded into the germband. **(E)** Representative image of early stage 12 embryo imaged with 20x objective for measuring germband retraction used for quantification in Fig. 1E-E' with BMP^+ cells labelled by *Dad-GFP::nls* (green), hemocytes labelled by *srpHemo-H2A::3xmCherry* (magenta) and all cell nuclei labelled with DAPI (blue). Edge of germband tissue is indicated by a white dashed line. White box indicates analyzed area in Fig. 1E-E', and area imaged with a 63x objective shown in **(F)**. **(F)** showing a single z-slice with nuclei of the leading three hemocytes inside the germband. Note the arrow pointing towards the *Dad-GFP::nls* positive 1st hemocyte nucleus. 2nd hemocyte nucleus behind without GFP, and 3rd hemocyte nucleus following positive for *Dad-GFP::nls*. **(G)** Top panel showing quantification of BMP^+ hemocytes inside the germband of early stage 12 embryos by assessment of the BMP-signaling reporter *Dad-GFP::nls* in hemocytes labelled by *srpHemo-H2A::3xmCherry*. The number of BMP^+ hemocytes was divided by the number of hemocytes that had already invaded into the germband tissue for each embryo in a total of 27 embryos. Boxplot with mean= 41.3%, lower 95% CI of mean= 36.9%, upper 95% CI of mean= 45.7%, minimum=21%, maximum=65%. Bottom panel showing BMP-signaling activation of first 3 hemocytes invading into the germband tissue in embryos analyzed in top panel. Quantification of the number of embryos in which either the leader hemocyte (1st mac), or the following two hemocytes (2nd/3rd mac) were *Dad-GFP::nls* positive. For one embryo the order of invading hemocytes was unclear. Total n=27, 1st mac *Dad-GFP::nls* positive 78% (n=21), 2nd/3rd mac *Dad-GFP::nls* positive 19% (n=5), unclear 4% (n=1). **(H-I)** Analysis of BMP^+ hemocytes at the ventral side of stage 13 embryos. **(H)** Representative image of stage 13 embryo (see schematic in upper left panel) imaged with 20x objective for measuring germband retraction. BMP^+ cells labelled by *Dad-GFP::nls* (green), hemocytes labelled by *srpHemo-H2A::3xmCherry* (magenta) and all cell nuclei labelled with DAPI (blue). White box in upper right image showing zoomed area of hemocytes migrating along the vnc in middle and bottom panels; vnc segments indicated by a white dashed line. BMP^+ hemocytes are located anterior to vnc segments in gnathal segments of the head. **(I)** Quantification of stage 13 embryos with BMP^+ hemocytes along vnc in %, BMP^+ hemocytes were divided by total number of vnc hemocytes. Total embryos=13, average hemocytes along vnc=36.4 (s.e.m.=2.3), 11 embryos without BMP^+ hemocytes along vnc, 2 embryos with BMP^+ hemocytes along vnc (embryo 1= 1/56=2% and embryo 2= 1/32=3%), average BMP^+ hemocytes along vnc=0.4%. All embryos shown throughout this thesis are oriented laterally, with anterior to the left and posterior to the right. ns $p>0.05$, *$p\leq0.05$ **$p\leq0.01$ ***$p\leq0.001$ ****$p\leq0.0001$, Scale bars **C,G**=10µm, **F,H**=20µm.

Compared to the germband, where hemocytes are confined between closely apposing ectoderm and mesoderm cells (Belyaeva et al., 2022; Aparna Ratheesh et al., 2018), the segments of the vnc comprise a less confined environment (Iwan R. Evans et al., 2010; Aparna Ratheesh et al., 2018; Siekhaus et al., 2010) and can therefore be used as an approximation of possible effects on the general developmental migration of hemocytes. While *Dad*-expressing hemocytes accumulated in front of the germband (Fig. 2 S1B), we observed no strong effect on migration along the vnc nor on total hemocyte numbers (Fig. 2 S1C-D). These

results point toward a specific role for canonical BMP signaling in aiding hemocytes to overcome a tissue barrier during embryonic migration.

Next, we investigated if particular BMP receptors are involved in hemocyte germband invasion. The BMP type I receptor Tkv controls early *Drosophila* embryonic development, and embryos with maternal and zygotic mutations for *tkv* show developmental defects, including dorsoventral patterning (Affolter et al., 1994; Zeitlinger et al., 1997). However, maternal Tkv governs early development, and zygotic Tkv is only needed for developmental processes following germband retraction (Affolter et al., 1994). We therefore examined early stage 12 embryos that were zygotically mutant for the amorphic allele tkv^{4} and found the number of hemocytes inside the germband reduced by 28% (Fig. 2B). Moreover, hemocyte-specific down-regulation of *tkv* using three independent RNAi constructs decreased hemocyte germband numbers by 39%, 30%, and 48%, respectively (Fig. 2C). In *tkv* loss-of-function experiments, hemocytes were still able to migrate up to the germband, accumulating in the pre-germband area (Fig. 2 S1E, G), and *tkv* RNAi-expressing hemocytes migrated normally along the vnc (Fig. 2 S1H). Similar to *Dad* overexpression, there was no change in total hemocyte numbers in *tkv* loss-of-function (Fig. 2 S1F, I). In accordance with these results, overexpression of the dominant negative variant tkv^{DN} inside hemocytes also decreased their germband numbers by 24% without changes in the pre-germband and the vnc, while expression of the constitutively active tkv^{CA} did not affect hemocyte migration at the analyzed stage (Fig. 2D, Fig. 2 S1J-K), and neither changed the number of total hemocytes (Fig. 2 S1L). These results show a stronger effect of the dominant negative receptor variant over the *tkv* RNAi, possibly caused by additional changes in BMP receptor binding and sequestering. They further indicate that canonical BMP signaling aids hemocyte tissue invasion.

Another receptor in *Drosophila* that has been shown to transduce the signaling downstream of the BMP-like ligand Dpp is Sax, whose closest orthologue in mice is the Activin A receptor like kinase 1 (Acvr1) (Haerry et al., 1998). While *tkv* is expressed more strongly in particular regions, *sax* is expressed faintly throughout the early embryo, and ubiquitous expression of *tkv* can rescue *sax* loss-of-function mutants (T. J. Brummel et al., 1994). It is therefore assumed that Tkv is the primary BMP type I receptor for Dpp. Expression of two different RNAi constructs against *sax* reduced hemocyte numbers inside the germband by 39% and 34%, respectively (Fig. 1E), and resulted in hemocyte accumulation in the pre-germband (Fig. 2 S1M), while migration along the vnc was not strongly affected (Fi. 2 S1N). Total hemocyte numbers were increased in *sax* $RNAi^{2}$ at late stage 12/early stage 13 (Fig. 2 S1O). We also quantified the total hemocytes in earlier embryos used for germband counts and found more hemocytes in those embryos as well (Fig. 2 S1P). Normalization to the total numbers revealed that still more *sax* $RNAi^{2}$-expressing hemocytes accumulated in the pre-germband and did not enter the germband normally (Fig. 2 S1Q-R). This indicates that both BMP type I receptors regulate hemocyte germband invasion efficiency.

We also wanted to examine the role of BMP type II receptors. In *Drosophila*, two type II receptors can form a complex with Tkv and Sax to regulate BMP signaling. One of them is Wit; however, this receptor is first expressed at stage 12 in a subset of cells of the CNS (Marqués et al., 2002; Roy et al., 2010; Tomancak et al., 2002, 2007), so we did not examine it. The other BMP type II receptor is Put, which can respond to dpp (Ruberte et al., 1995), or Activin, which regulates hemocyte homing to hematopoietic pockets in the larva (Makhijani et al., 2017).

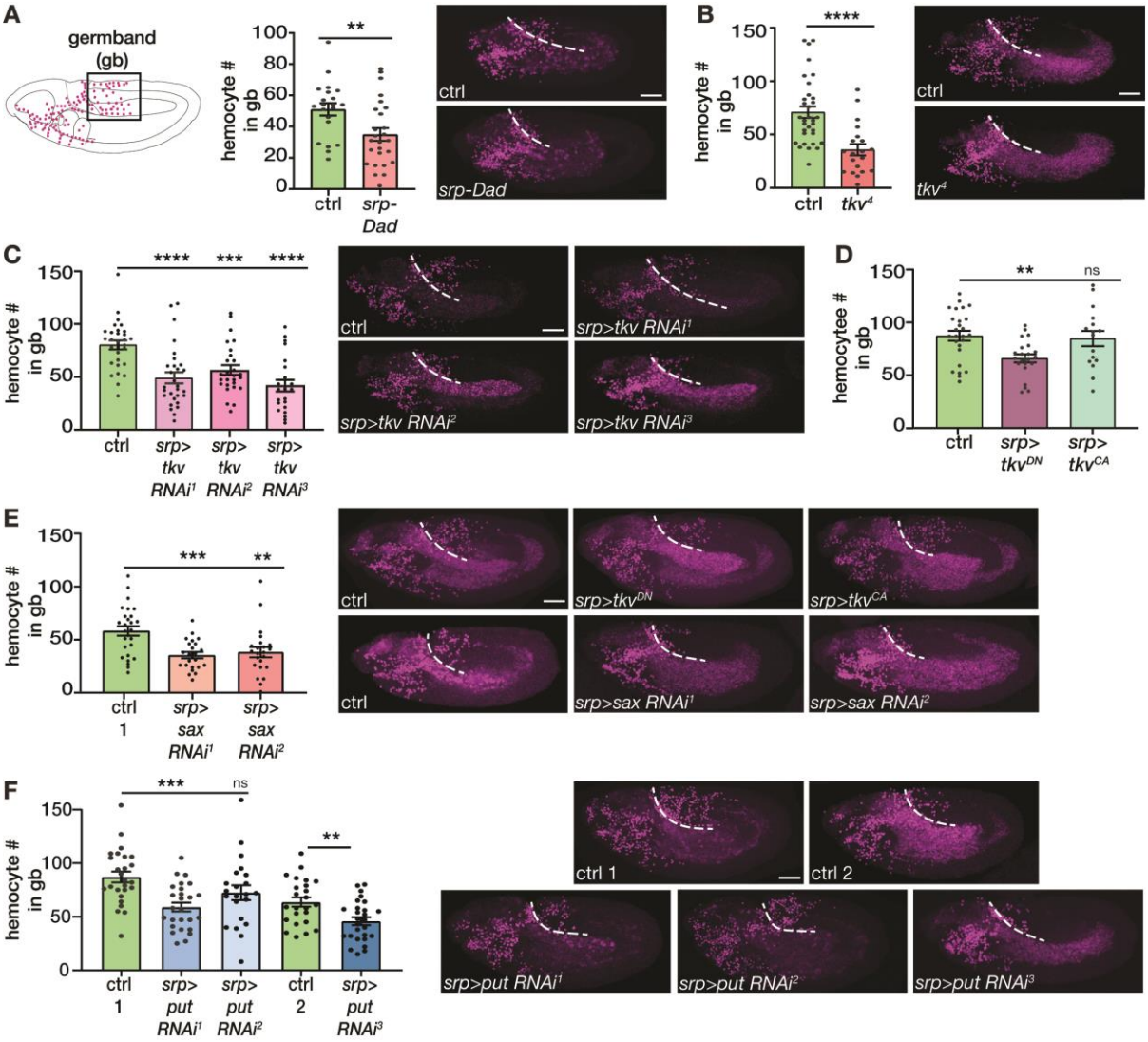

G

	# in gb	# in pre-gb	total #	# along vnc
srp-Dad	↓	↑	↔	↑
tkv⁴	↓	↑	↔	\
srp> tkv RNAi¹	↓	↑	↔	↔
srp>tkv RNAi²	↓	↑	↔	↔
srp>tkv RNAi³	↓	↑	↔	↔
srp>tkv^{DN}	↓	↔	↔	↑
srp>tkv^{CA}	↔	↔	↔	\
srp>sax RNAi¹	↓	↑	↔	↓
srp>sax RNAi²	↓	↑	↑	↔
srp>put RNAi¹	↓	↔	↔*	↔
srp>put RNAi²	↔	↔	↔	\
srp>put RNAi³	↓	↔	↔	↔

Chapter 3 Fig 2. Loss of BMP signaling activation impairs ability of immune cells to invade into the germband tissue

(A) Number of hemocytes inside the germband (gb) was quantified for all samples in stage 12 embryos, area indicated by a black box in the schematic on the left. Hemocytes were labeled using *srpHemo-H2A::3xmCherry* shown in magenta. Representative images of maximum z-projections shown for each genotype as indicated in the image, white dashed line indicating edge of germband tissue. Expression of the full length *Dad* by a direct

fusion construct to the hemocyte specific *srpHemo* promoter (*srp-Dad*) leads to reduced numbers of hemocytes in the germband compared to the control. n=21 (ctrl), n=26 (srp-Dad), p=0.0071. **(B)** Embryos homozygous for the amorphic mutation of the BMP receptor type I Thickveins (tkv^4) show strongly reduced numbers of hemocytes inside the germband. n=33 (ctrl), n=20 (tkv^4), p<0.0001. **(C)** Hemocyte-specific loss of function of BMP receptor type I *tkv* by expression of three independent RNAi lines (*tkv* $RNAi^1$=*TRiP.GLV21018*, *tkv* $RNAi^2$=*TRiP.GL00035*, *tkv* $RNAi^3$=*TRiP.GL01338*) under the hemocyte driver *srpHemo-Gal4* strongly decreases hemocyte numbers in the germband. n=29 (ctrl), n=29 (mac> *tkv* $RNAi^1$) p<0.0001, n=27 (mac> *tkv* $RNAi^2$) p=0.001, n=23 (mac> *tkv* $RNAi^3$) p<0.0001. **(D)** Expression of a dominant negative version of tkv in hemocytes (*mac>*tkv^{DN}) leads to reduced hemocytes inside the germband. Expression of a constitutively active version of *tkv* in hemocytes (*mac>*tkv^{DA}) does not change germband invasion efficiency of hemocytes. n=26 (ctrl), n=22 (*mac>*tkv^{DN}) p=0.0019, n=16 (*mac>*tkv^{DA}) p=0.94. **(E)** Hemocyte-specific loss of function of another BMP receptor type I *sax* by expression of two independent RNAi lines (*sax* $RNAi^1$=*TRiP.JF03431* and *sax* $RNAi^2$=*TRiP.HMC04135*) under the hemocyte driver *srpHemo-Gal4* decreases hemocyte numbers in the germband similar to loss of *tkv*. n=27 (ctrl), n=23 (*mac>sax* $RNAi^1$) p=0.0002, n=23 (*mac>sax* $RNAi^2$) p=0.0074. **(F)** Hemocyte-specific loss of function of BMP receptor type II *put* by expression of three independent RNAi lines (*put* $RNAi^1$=*TRiP.GL00069,* *put* $RNAi^2$=*TRiP.JF02664*, *put* $RNAi^3$=*P{GD49}v848*) under the hemocyte driver *srpHemo-Gal4* decreases hemocyte numbers in the germband significantly in two of them. n=26 (ctrl 1), n=26 (*mac>put* $RNAi^1$) p=0.0002, n=22 (*mac>put* $RNAi^2$) p=0.17, n=24 (ctrl 2), n=27 (*mac>put* $RNAi^3$) p=0.0029. **(G)** Summary of hemocyte quantification in different areas in BMP-signaling loss and gain of function experiments shown in Figure 2 and Figure 2 Supplement 1. Arrow pointing down indicating decreased numbers of hemocytes (mac#) in this specific area, arrow pointing up indicating increased hemocyte numbers, two arrows pointing left and right indicating no significant change compared to control, slash indicating no assessment. Total numbers of hemocytes were increased in embryos used for vnc quantification in *put* $RNAi^1$. Scale bars=20µm.

However, expression of Activin only begins in later stages and is then restricted to the developing CNS and PNS (Graveley et al., 2010; Roy et al., 2010). Knockdown of *put* in hemocytes with RNAi constructs led to comparable results to knockdown of *tkv* and *sax*. Hemocyte migration into the germband tissue was reduced by 32% and 28% in *mac>put* $RNAi^1$ and *mac>put* $RNAi^3$, respectively (Fig. 1F) and not significantly changed by a third RNAi line (*mac>put* $RNAi^2$). However, hemocytes did not accumulate in front of the germband (Fig. 2 S1S). Knock down of *put* did not change hemocyte numbers along the vnc (Fig. 2 S1T), and did not strongly affect total hemocyte numbers; an increase in hemocyte numbers for *put* $RNAi^1$ observed at late stage 12/early stage 13 (Fig. 2 S1U) was not found in the stage 12 embryos used for germband quantifications (Fig. 2 S1V). These results suggest a function for BMP receptor type II Put in the regulation of hemocyte migration up to the pre-germband.
Taken together, these experiments show the necessity of functional canonical BMP-signaling to allow for proper germband invasion of hemocytes. However, quantification of hemocytes in fixed embryos gives only a static image of the involvement of BMP signaling in migration efficiency while leaving the effects on dynamic hemocyte migration parameters unexplored.

3.3.3 Tkv in hemocytes is crucial for directional migration specifically during germband entry

We therefore were eager to observe hemocytes live during their migration out of the head towards the germband and during germband entry upon reductions in Tkv function. The bright *srpHemo-H2A::3xmCherry* reporter generated in our lab allowed us to record a time series for several hours of development without bleaching or damaging the embryo (Gyoergy et al., 2018). Previous studies have described different phases of the hemocyte migratory route through the embryo. In the first phase, which is independent from the PDGF/VEGF receptor Pvr, hemocytes migrate out from their origin in the head mesoderm over the yolk towards the germband tissue (Brückner et al., 2004; N. K. Cho et al., 2002; Parsons & Foley,

2013; Siekhaus et al., 2010). They then face the tissue barrier of the germband ectoderm, clearly visible by their alignment outside the edge of the germband (Belyaeva et al., 2022; Aparna Ratheesh et al., 2018; Sánchez-Sánchez et al., 2017; Siekhaus et al., 2010; Valoskova et al., 2019). During germband entry, they face closely apposed ectoderm and mesoderm cells (Fig. 3A) and must push them apart to create space for their further migration (Belyaeva et al., 2022; Aparna Ratheesh et al., 2018). In contrast to the first phase, phase 2 is described as the Pvr-dependent step of hemocyte penetration into the germband tissue (N. K. Cho et al., 2002). This is later followed by phase 3 when hemocytes disperse throughout the embryo, which is again Pvr-independent.

We specifically aimed to investigate the invasion of hemocytes into the germband tissue. Therefore, we first analyzed the time span for germband crossing of *tkv* RNAi-expressing hemocytes. We define the time span for germband crossing as the time between the alignment of all hemocytes in front of the germband (Fig. 3B-C, upper left panel) and the time point when the first hemocyte pushes its nucleus into the germband (Fig. 3B, upper middle panel, white arrowhead). Knockdown of *tkv* in hemocytes leads to a strong delay of hemocyte germband invasion (Fig. 3B and Movie 1) with a 2.1 fold increase of germband crossing time compared to the control (Fig. 3B-C, control=32min, n=3 vs. *tkv RNAi*^{2}=67min, n=7). Thus, Tkv affects hemocyte germband invasion at the first step of germband crossing.

Next, we aimed to identify changes in their migration behavior specifically during tissue invasion by analyzing the first 30-35µm inside the germband, before they join hemocytes invading from the other side to migrate along the dorsal midline. While *tkv*-RNAi expressing hemocytes showed no difference in their speed (Fig. 3D, control=3µm/min, n=3 vs. *tkv RNAi*^{2}=3µm/min, n=5), the average persistence of the first 3-4 hemocytes was reduced by 41% (Fig. 3E, control=0.64, n=3 vs. *tkv RNAi*^{2}=0.38, n=5). Consistent with our observations in fixed embryos, there was no change in the speed and persistence of *tkv* RNAi expressing hemocytes during their migration from the head to the germband (Fig. 3F-G).

Individual analysis of the persistence of the first, second, and third hemocyte entering the germband showed a negative trend for all three (Fig. 3H). However, there was a higher variability in the persistence measurements for the second hemocyte in different embryos compared to the data for the first and third hemocyte. Upon *tkv* RNAi expression, the persistence of the first hemocyte entering the germband was reduced by 40% (control 0.6, n=3, tkv RNAi 0.36, n=5), and the persistence of the third was reduced by 48% (control 0.8, n=3, vs. *tkv* RNAi 0.42, n=4). These results indicate that Tkv regulates hemocyte germband invasion by affecting their persistence specifically at the entry site.

3.3.4 BMP^{+} hemocytes lead invasion into the germband tissue

These results, together with our observations from fixed embryos showing BMP signaling activation in the hemocytes furthest inside the germband in the great majority of embryos (Fig. 1E), suggest that BMP^{+} hemocytes lead efficient germband invasion by regulating the persistence of hemocytes. However, during germband entry, hemocytes can squeeze past one another and take over each other's position, complicating our analysis. Therefore, we performed live imaging of the *Dad-GFP::nls* reporter embryos in which hemocytes were labeled with *srpHemo-H2A::3xmCherry* (Fig. 3I).

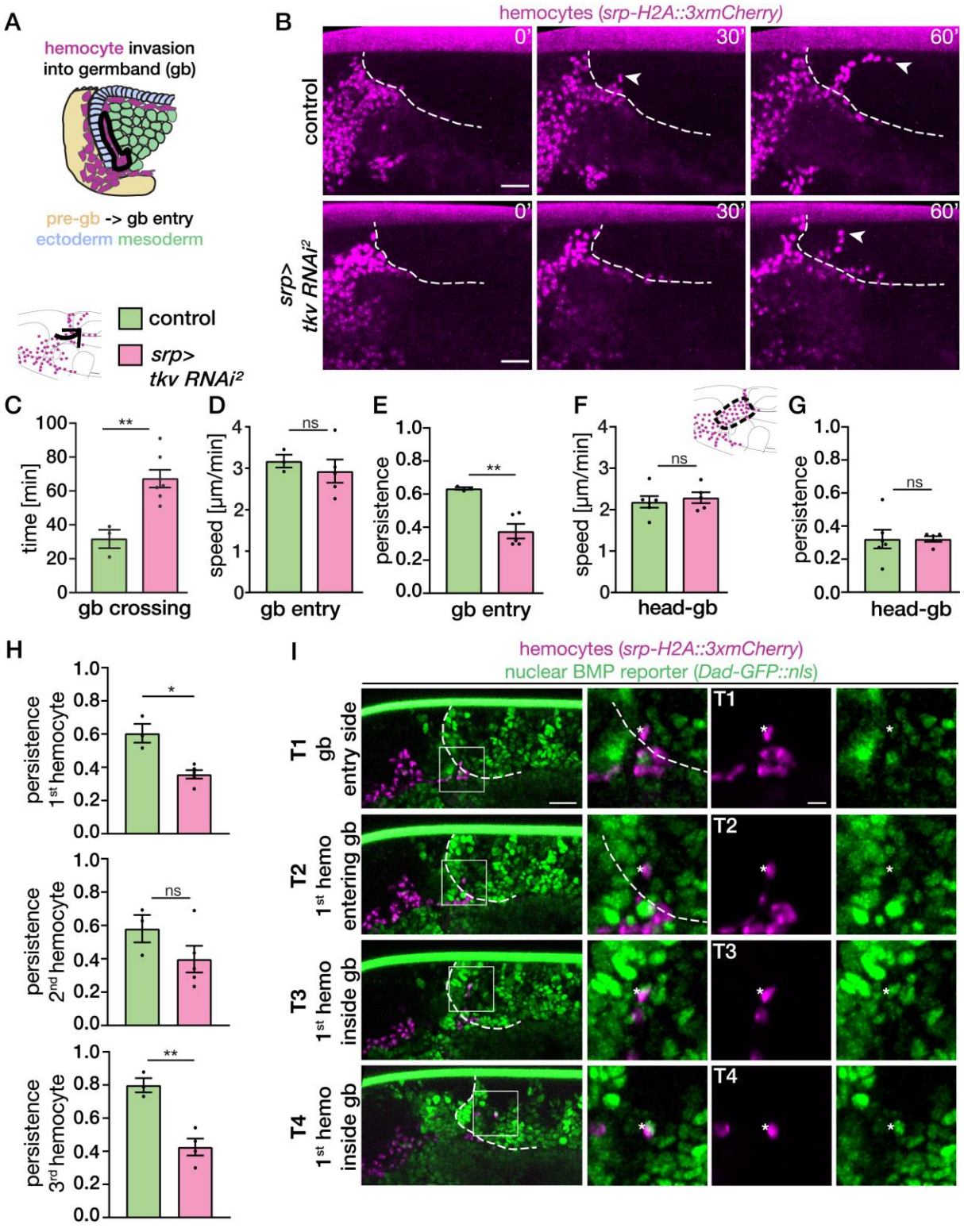

Chapter 3 Fig 3. BMP regulates persistence of hemocytes to allow efficient germband invasion

(A) Detailed illustration of the germband edge and hemocyte entry side into the germband. Hemocytes (magenta) migrate from the pre-germband zone (beige) into the germband comprised of closely opposed ectoderm (light blue) and mesoderm cells (light green). Hemocytes then migrate in between those tissues dorsally. Their migration within the first 30-35µm inside the germband was analyzed for speed and persistence in the germband entry zone (gb entry). **(B)** Stills of hemocyte nuclei labelled by *srpHemo-H2A::3xmCherry* (magenta) used for tracking during germband invasion *in vivo*. The germband edge is indicated by a white dashed line. Time in minutes is shown in upper right corners of each still image starting at 0' with hemocytes lining up

in front of the germband tissue in a typical semi-circle arch prior to further posterior migration between germband and yolk, and germband invasion between mesoderm and ectoderm, respectively. Hemocyte nuclei of control entering into the germband after 30' indicated by white arrowhead (top panel), followed by migration as a stream. Hemocyte nuclei expressing *tkv RNAi²* driven by *srpHemo-Gal4* (*mac>tkv RNAi²*) show delayed entry; at 60' the first hemocyte nuclei are present in the germband indicated by white arrowhead (bottom panel). Note that *tkv RNAi²* expressing hemocyte nuclei align in a bulk approaching germband entry at a further posterior position of the germband after 60' (white asterisk, bottom panel). **(C)** Time for hemocyte germband crossing was quantified in min for control and *tkv RNAi²* expressing hemocytes starting from the time point when hemocytes had migrated up to the germband aligning in front of the germband tissue in a typical semi-circular arch (T0). The time point of the first hemocyte nucleus moving into the germband by a typical step toward the dorsal side of the germband was taken as the time point of germband entry (T1). Schematic illustrates the analyzed area of the embryo. T1-T0 is shown for n=3 independent control embryos and n=7 embryos with hemocytes expressing *tkv RNAi²*, p=0.0037. **(D)** Hemocyte speed was similar in control and *tkv RNAi²* at the germband entry. The average of the first 3-4 hemocyte nuclei per embryo was used for analysis. n=3 embryos, total number of tracks=11 (control) and n=5 embryos, total number of tracks=18 (*mac>tkv RNAi²*), p=0.48. **(E)** Persistence of hemocyte nuclei was extracted from 3D tracks generated in IMARIS as track straightness, which is calculated from the total track distance divided by the total track length. The average of the first 3-4 hemocyte nuclei per embryo was used for analysis. *tkv RNAi²* expressing hemocytes showed decreased persistence at the germband entry compared to the control. n=3 embryos, total number of tracks=11 (control) and n=5 embryos, total number of tracks=18 (*mac>tkv RNAi²*), p=0.0036. **(F)** Speed of hemocytes during their migration towards the germband was not changed in *tkv RNAi²* expressing hemocytes compared to the control. Analyzed area marked by dashed black line in the schematic to the right. The average speed of all tracks per embryo was used for analysis. n=6 embryos, total number of tracks=463 (control) and n=5 embryos, total number of tracks=436 (*mac>tkv RNAi²*), p=0.62. **(G)** Persistence of hemocytes during their migration towards the germband was not changed in *tkv RNAi²* expressing hemocytes compared to the control. Analyzed area marked by dashed black line in the schematic to the left. The average speed of all tracks per embryo was used for analysis. n=6 embryos, total number of tracks=463 (control) and n=5 embryos, total number of tracks=436 (*mac>tkv RNAi²*), p=0.996. **(H)** The persistence of the first 3 hemocyte nuclei invading into the germband tissue was assessed individually. The leading and third hemocyte nucleus moved significantly less persistent compared to the control in *tkv RNAi²* expressing hemocytes. The second *tkv RNAi²* expressing hemocyte did not show a significantly reduced persistence. n=3 (control) and n=5 (*mac>tkv RNAi²*), persistence 1st mac p=0.031, persistence 2nd mac p=0.17, persistence 3rd mac p=0.0025. **(I)** Single z-plane images showing representative stills of two-photon movies from early stage 12 embryos during hemocyte germband invasion imaged with a 40x objective. Hemocytes were labeled with *srpHemo-H2A::3xmCherry* (magenta) and BMP signaling was visualized using a *Dad-GFP::nls* reporter (green). The edge of the germband tissue is indicated by a white dashed line. White boxes in left overview images indicate zoomed area shown in single color and merged in panels on the right next to corresponding overview images. First hemocyte (white asterisk) is approaching the germband entry side at T1 (top panel), and translocating into the germband at T2 showing weak reporter signal. T3 and T4 show stronger BMP reporter signal in the first hemocyte within the germband. At T4 the germband has already started to retract towards the posterior of the embryo. Stills from one representative movie are shown, total n=4 movies/embryos. Scale bar **A**=10µm, **I**=20µm left overview panels, 5µm single color zoom images

Here, we could observe the activation of the BMP reporter in the first hemocyte to enter the germband (Fig. 3I, white asterisk, germband indicated by white dashed line). The *Dad-GFP::nls* fluorescence inside hemocytes became stronger while they entered the germband tissue (Fig. 3I, T2, and T3, white asterisk). We did not observe a strong bias for BMP reporter activity in either the second or the third hemocytes following the leader into the germband. In two out of three movies, the first, second and third hemocyte showed *Dad-GFP::nls* fluorescence, and in one of them, the second hemocyte did not show BMP activation, unlike the first and third BMP^+ hemocytes (Supplemental Movie 2-4). Thus, our data support the hypothesis that BMP signaling activation is predominantly needed for the leading hemocyte to invade the germband.

3.3.5 Bulk RNA-Sequencing of BMP$^+$ hemocytes identifies regulators of germband invasion

We hypothesized that BMP signaling activated the transcription of target genes to enable invasion. This idea was based on two findings: the *Dad-GFP* reporter relies on the canonical BMP pathway and transcriptional signaling cascade to be activated, and we were able to inhibit invasion by expressing Dad, an inhibitor of the transcriptional arm of BMP responses. To identify target genes we first collected Stage 12 embryos expressing the *Dad-GFP* reporter and mCherry to mark hemocytes, and FACS isolated hemocytes as previously described (Belyaeva et al., 2022; Gyoergy et al., 2018). We gated for either mCherry-positive hemocytes, or GFP and mCherry double positive BMP$^+$ hemocytes (Fig. 4A). We conducted RNA-Sequencing on both populations and looked for differentially expressed genes (DEG). Among these, 31 genes showed significantly higher expression in the BMP$^+$ hemocytes compared to all other hemocytes at stage 12 (Fig. 4B). We selected five of these genes that had previously been shown to affect cell migration yet had not been examined in the context of hemocyte movement for further analysis.

We first investigated a potential effect of Mipp1, which aids the migration of leader cells during tracheal development (Cheng & Andrew, 2015). While expression of a dominant negative version of Mipp1 in hemocytes reduced the numbers inside the germband and increased their numbers in the pre-gb (Fig. 4C-D), it also affected total hemocyte numbers and migration along the vnc (Fig. 4 S2B, E). Furthermore, when normalized to the total number of hemocytes in the same stage, the decrease in germband numbers was not significant (Fig. 4 S2C). However, the increase in hemocytes in the pre-gb was still prominent (Fig. 4 S2D). These results likely point toward an effect of *Mipp1^{DN}* in hemocytes besides cell migration.

Fasciclin 2 (Fas2) is the *Drosophila* ortholog of the neural cell adhesion molecule (NCAM) and is known to control neuronal recognition of a specific axon type (Grenningloh et al., 1991). Further, Fas2 has been shown to regulate the migration of border cells by organizing cluster polarity and motility (Szafranski & Goode, 2004). Knockdown of Fas2 in hemocytes using two independent RNAi lines slightly decreased their numbers in the germband and led to higher hemocyte numbers in the pre-gb area (Fig. 4C-D and Fig. 4 S2A). However, only the reduction inside the germband for *Fas2 RNAi^2* was significant. The numbers along the vnc were unchanged, and total hemocyte numbers for *Fas2 RNAi^2* even increased (Fig. 4 S2B,E). Fasciclin 3 (Fas3) has been shown to be crucial for selective filopodia formation in distinct subtypes of cardioblasts to allow cell matching (S. Zhang et al., 2018). Interestingly, Fas3 has recently been identified in a sub-cluster of pro-hemocytes in the larval lymph gland, which is also high in the expression of enhancer of split complex (E(spl)C) genes (B. Cho et al., 2020). However, a role in hemocyte migration has not been identified so far. Knock-down of Fas3 in hemocytes strongly reduced their numbers inside the germband, and increased hemocyte numbers in the pre-gb zone without affecting their migration along the vnc or total hemocyte numbers (Fig. 4C-D and Fig. 4 S2A-B,E). Thus, Fas3 and potentially Fas2 appear to have specific roles in enhancing hemocyte germband invasion.

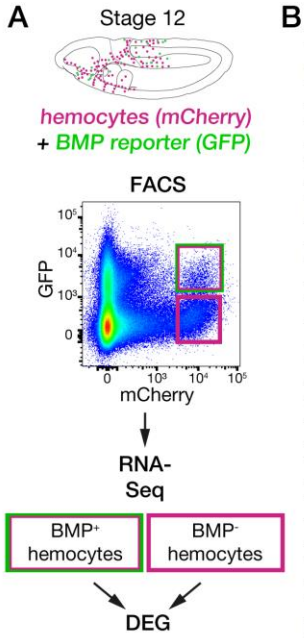

B

name	function	mouse ortholog	identity
CG14932	unknown	none	
CG31627	transcription factor (madf-bess domain)	none	
Fasciclin 3	cell adhesion	Cadm3	22%
Actin 57B	myofibrillar actin, embryonic muscle development	ActB	95%
CG12011	unknown	none	
abrupt	transcription factor, cell migration, oncogenesis, germ cell differentiation	Zbtb12	22%
Cystatin-like	cysteine-type endopeptidase	Cstl1	23%
astray	serine metabolism, nervous system development	Psph	50%
CG11876	acetyl-CoA biosynthesis	Pdhb	69%
Mipp 1	Multiple inositol polyphosphate phosphatase, generation of IP3	Minpp1	26%
mab-21	mab21 domain, embryonic development	Mab21l1	75%
Tetraspanin 39D	scaffolding protein, formation of tetraspanin-enriched microdomains	CD36	32%
arouser	adaptor protein interacting with Egfr and PI3K pathways, synapse formation	Eps8l2	26%
CG31121	cholesterol transporter activity, ATP-binding cassette transporter family	Abcg5	25%
Actin 87E	cytoskeleton formation, cell migration	ActB	96%
yellow-e3	Major royal jelly protein, melanization pathway	none	
CG13631	unknown	none	
Fasciclin 2	cell-cell adhesion, negative regulation of EGFR signaling, fibronectin type III	Ncam2	27%
Chitinase 6	hydrolysation in chitin polymers	Chit1	35%
varicose	tracheal system development, septate junction assembly	Mpp6	38%
rutabaga	cAMP synthesis	Adcy1	39%
CG7294	unknown	none	
uninflatable	negative regulation of Notch signaling, localization of Sara endosomes	Elapor1	21%
Megalin	EGF-like doamin, predicted to be involved in endocytosis	Lrp2	40%
crumbs	apico-basal cell polarity, negative regulator of Notch and Hippo pathway	Crb1	29%
grainy head	transcription factor, response to Branchless/FGF signaling	Grhl1	31%
frizzled	Wnt receptor, planar cell polarity pathway	Fzd1	47%
Myosin light chain 2	subunit of myosin complex, myofibril assembly	Myl2	37%
CG5080	unknown	none	
fat	tumor suppressor, receptor for Hippo signaling, planar cell polarity pathway	Fat4	36%
Pvf3	chemoattractant, macrophage migration	Pgf/Vegfa	26%/23%

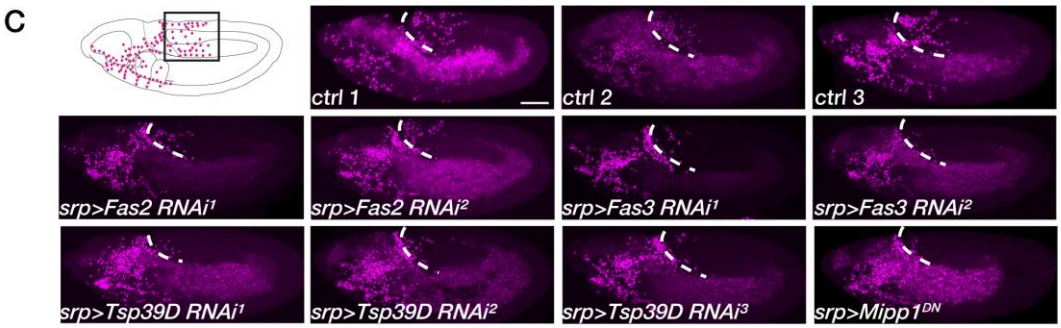

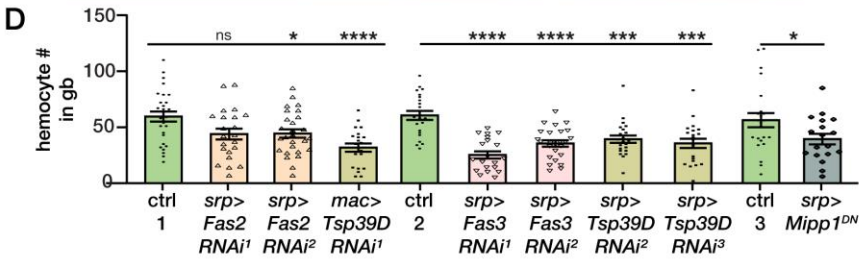

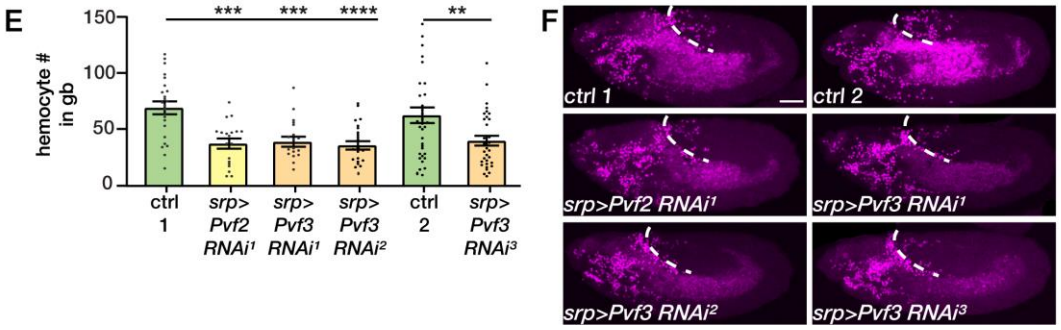

Chapter 3 Fig 4. Putative target genes up-regulated in BMP+ subpopulation can regulate germband invasion efficiency of hemocytes

(A) Workflow for identification of differentially expressed genes (DEG) in the BMP+ hemocyte subpopulation. Embryos with hemocytes labeled by srpHemo-3xmCherry and activated BMP signaling shown by the BMP signaling reporter Dad-GFP were collected at stage 12, when hemocytes had already invaded into the germband tissue and GFP reporter intensity in hemocytes was strong enough for detection. BMP^{+} and BMP^{-} hemocytes

were separated by FACS from a single cell suspension of pooled and homogenized embryos. Both populations were further processed for RNA-Sequencing and compared to identify DEG. n=3 samples for BMP^+ hemocytes and n=6 for BMP^- hemocytes. **(B)** List of identified DEG significantly up-regulated in BMP^+ hemocytes of stage 12 embryos showing name, function, mouse ortholog, and identity to mouse ortholog in % (comparison of *Drosophila m.* and mouse protein). Candidates highlighted in purple were used for further analysis of their effect on hemocyte germband invasion efficiency due to their function indicating a role for cell migration. **(C)** Representative images of loss of function of selected putative BMP regulated candidate genes in stage 12 embryos with hemocyte nuclei labeled by *srp-Hemo-H2A::3xmCherry*. Germband edge indicated by white dashed line. **(D)** Quantification of hemocyte numbers inside the germband in RNAi knock-down of selected putative BMP regulated candidate genes in hemocytes driven by *srpHemo-Gal4*. Knock-down of *Fas2* shows mild effect on hemocyte germband invasion with *Fas* $RNAi^1$ (*TRiP.JF02918*) not reaching significance, and *Fas* $RNAi^2$ (*TRiP.HMS01098*) showing mild reduction of hemocyte germband numbers. Three independent RNAi lines for *Tsp39D*, and two RNAi lines targeting *Fas3* all strongly decrease numbers of hemocytes inside the germband (*Tsp39D* $RNAi^1$=*TRiP.JF01847*, *Tsp39D* $RNAi^2$=*KK104661*, *Tsp39D* $RNAi^3$=*GD1796*, *Fas3* $RNAi^1$=*GD13161*, *Fas3* $RNAi^2$=*GD2576*). Expression of a dominant negative variant of *Mipp1* ($Mipp1^{DN}$) inside hemocytes mildly reduces their numbers inside the germband. n=28 (ctrl 1), n=22 (*mac>Fas2* $RNAi^1$) p=0.0666 ns, n=27 (*mac>Fas2* $RNAi^2$) p=0.038, n=21 (*mac>Tsp39D* $RNAi^1$) p<0.0001, n=22 (ctrl 2), n=20 (*mac>Fas3* $RNAi^1$) p<0.0001, n=24 (*mac>Fas3* $RNAi^2$) p<0.0001, n=22 (*mac>Tsp39D* $RNAi^2$) p=0.0009, n=21 (*mac>Tsp39D* $RNAi^3$) p=0.0004, n=23 (ctrl 3), n=18 (*mac>*$Mipp1^{DN}$) p=0.039. **(E)** Quantification of hemocyte numbers inside the germband in RNAi knock-down of chemoattractants *Pvf2* and *Pvf3* in hemocytes driven by *srpHemo-Gal4*. One RNAi line for *Pvf2* (*Pvf2* $RNAi^1$=*KK110608*) and three independent RNAi lines for *Pvf3* (*Pvf3* $RNAi^1$=*GD5238, Pvf3* $RNAi^2$=*KK112796, Pvf3* $RNAi^3$=*TRiP.HMS01876*) all lead to decreased numbers of hemocytes inside the germband in stage 12 embryos. **(F)** Representative images of *Pvf2* and *Pvf3* knock-down in stage 12 embryos with hemocyte nuclei labeled by *srp-Hemo-H2A::3xmCherry*. Germband edge indicated by white dashed line. Scale bar **C,F**= 20µm

Additionally, we selected the scaffolding protein Tetraspanin 39D (Tsp39), which is the fly ortholog of CD63, a marker for immune cells in mammals that regulates the secretion of von Willebrand Factor (vWF) and has been shown to interact with integrins (Mannion et al., 1996; Vischer & Wagner, 1993). Hemocyte-specific knockdown of Tsp39D strongly reduced their numbers inside the germband in three independent RNAi lines (Fig. 4C-D), and two of them also led to significantly increased hemocyte numbers in the pre-gb (Fig. 4 S2A) without affecting total hemocyte numbers (Fig. 4 S2B). However, knockdown using these two RNAi lines additionally slightly reduced hemocyte numbers in the first segment of the vnc (Fig. 4 S2E), indicating that Tsp39D plays a crucial role in invasion and potentially a small role in vnc migration.

Surprisingly, the chemoattractant Pvf3 was identified as one of the up-regulated genes in BMP^+ hemocytes. Together with the closely related Pvf2, Pvf3 is a well-known chemoattractant for *Drosophila* hemocytes and plays a crucial role during embryonic hemocyte migration and germband invasion (Brückner et al., 2004; N. K. Cho et al., 2002; Parsons & Foley, 2013; Sears et al., 2003; Wood et al., 2006). However, studies on this relationship did not identify expression in a hemocyte subpopulation and have either used full mutants for their analysis or knocked-down *pvf2* and *pvf3* ubiquitously by dsRNA injections into the embryo. Hemocyte-specific knock-down of *pvf2* and *pvf3* strongly decreased their germband invasion efficiency, and two out of three RNAi-mediated knockdowns also strongly increased hemocyte numbers in the pre-gb (Fig. 4E and Fig. 4 S2F). This indicates that Pvf3 and likely Pvf2 are not only expressed in surrounding tissues to guide hemocyte migration but that their expression is also needed in hemocytes to regulate their tissue invasion during early stage 12.

Taken together, three out of four of the selected potential BMP signaling target genes showed a specific invasion defect.

3.3.6 Single Cell RNA-Sequencing identifies subpopulations of hemocytes throughout embryogenesis

As far as we know, the BMP$^+$ hemocyte subpopulation is the earliest described subpopulation of *Drosophila* embryonic hemocytes. However, very recently different hemocyte populations were identified in stage 15 embryos (Coates et al., 2021), which inspired us to investigate the embryonic hemocyte population from stages 8, 10, 12, and 16 in greater depth using single cell RNA-Sequencing (scRNA-Seq).

We could identify distinct clusters of hemocytes already in stage 8 embryos (Fig. 5A), which showed differential expression of certain genes. Most of the top markers identified for stage 8-12, the time window when hemocytes disperse through the embryo and invade into the germband, are not exclusively expressed in hemocytes, but can be used for cluster identification (Fig.5A-C). During development, the number of identified hemocyte clusters increased from four in stage 8 to 10 in stage 12, indicating an increase in population complexity over the course of development. Additionally, when compared with previously identified proliferative markers from *Drosophila* lymph gland data, stage 8 and stage 10 hemocytes are enriched in proliferative genes, whereas their expression is rapidly decreasing in stage 12 hemocytes (Fig. 5 S3B). We were especially curious if we could identify a cluster corresponding to the BMP$^+$ hemocytes at stage 12. At stage 12, two clusters stood out from all the others with a strong enrichment of *E(spl)C* gene expression (Fig. 5C-D cluster 0 and cluster 1). DEG in hemocytes at stage 12 identified from bulk RNA-Seq of the BMP reporter shows significant enrichment in the same clusters as the *E(spl)C* genes (Fig. 5E), compared to genes down-regulated in BMP$^+$ hemocytes (Fig. 5 S3A). We therefore hypothesized that there might be an overlap between the BMP$^+$ hemocytes and the E(spl)C enriched clusters. To test our hypothesis, we imaged embryos in which E(spl)m5 was labeled by GFP and found a stronger signal in the first hemocytes entering the germband (Fig. 5F), indicating a possible overlap of these markers.

Typically, *E(spl)C* genes are known to be Notch-responsive. However, Notch does not play a role in hemocyte germband invasion (Valoskova, 2019). However, *E(spl)mβ* has been shown to be expressed in response to dpp in pro-hemocytes of the larval lymph gland to keep them in a stem cell-like state (Dey et al., 2016). Thus, BMP could enhance E(spl)C gene expression to define a hitherto unknown hemocyte subpopulation in the *Drosophila* embryo that leads invasion into the germband tissue.

3.4 DISCUSSION

We have identified a novel subpopulation of early *Drosophila* embryonic immune cells that are leaders of tissue invasion *in vivo*. This subpopulation is defined by transient BMP signaling activation prior to hemocyte tissue invasion. BMP$^+$ hemocytes localize to distinct areas of the embryo and are especially prominent in the germband. They differ from the rest of the total immune cell population in their transcriptional profile and rely on those up-regulated genes for crossing the germband tissue barrier efficiently.

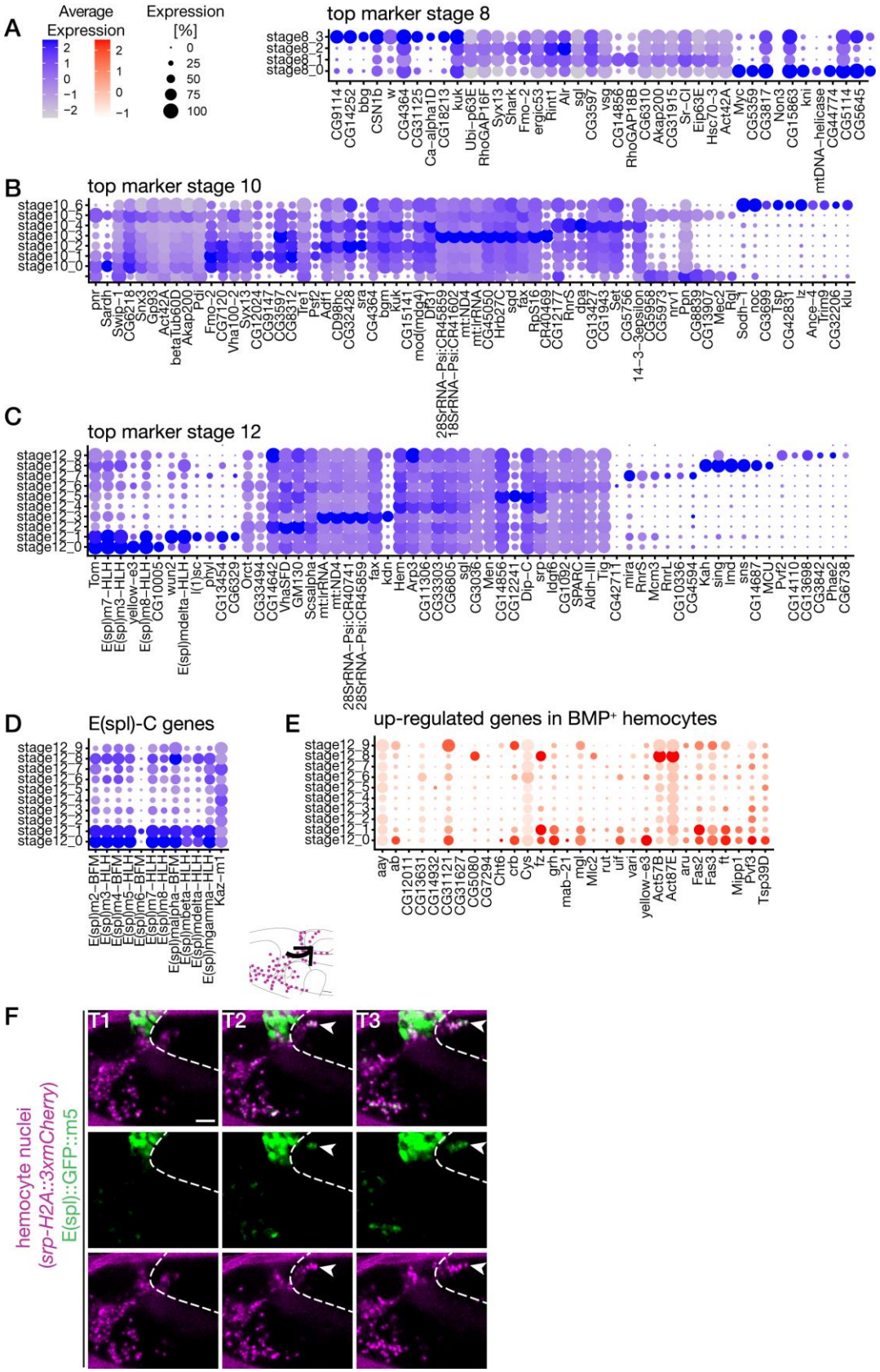

Chapter 3 Fig 5. Single Cell RNA-Seq identifies E(spl)C enriched hemocytes sharing overlapping characteristics with BMP+ subpopulation at stage 12

(A) Single Cell RNA-Sequencing of isolated hemocytes was performed from embryos of stage 8, 10, 12, and 16. Dotplots show relative average gene expression levels indicated by color code in purple and red with darkest

colors showing strongest gene expression. The fraction of cells in the identified cluster is represented by the size of each dot. Stage 8 embryos are comprised of hemocytes from 4 different clusters. The top markers characteristic for stage 8 clusters are shown. **(B)** A higher number of hemocytes clusters were identified for stage 10 embryos. Dotplot shows the top markers for each of the 7 clusters identified. **(C)** Hemocytes from stage 12 embryos can be clustered into 10 different populations with cluster 0 and 1 showing a strong enrichment of E(spl)C genes. Top markers for stage 12 are shown in dotplot. **(D)** Two clusters in stage 12 embryos are highly enriched in E(spl)C genes, all E(spl)C genes are shown in dotplot. **(E)** Putative target genes upregulated in BMP^+ hemocytes as identified by bulk RNA-Seq of BMP reporter embryos at early stage 12. They are predominantly enriched in cluster 0 and 1 characterized by higher levels of E(spl)C genes in the single cell RNA-Seq analysis. **(F)** Stills of hemocytes invading into the germband tissue in an early stage 12 embryo expressing *E(spl)::GFP::m5* shown in green. Hemocytes are labeled by *srpHemo-H2A::3xmCherry* shown in magenta. White dashed line indicating edge of the germband. At T1 hemocytes have already started to enter into the germband and *E(spl)::GFP::m5* is strongly expressed in the amnioserosa, and weakly in some hemocytes inside the head. At T2 the stream of hemocytes moves posterior along the dorsal midline of the germband with the leading hemocytes showing stronger *E(spl)::GFP::m5* expression (white arrowhead). Some hemocytes inside the head and at the ventral side of the embryo, at a location of the gnathal segments show strong *E(spl)::GFP::m5* signal intensity. At T3 the germband retracts further posterior showing leading hemocytes inside the germband with *E(spl)::GFP::m5* enrichment (white arrowhead). Scale bar= 20µm

Previously, BMP signaling has been shown to affect the second wave of *Drosophila* hematopoiesis through regulation of cardiogenic mesoderm formation and effects on the size of the lymph gland (Mandal et al., 2004; Pennetier et al., 2012b). Here, we identify a novel role for BMP signaling activation in the early embryo, one that is crucial for single immune cells leading penetration into the germband tissue. This function appears to be specifically required for tissue invasion, as loss of BMP signaling does not strongly affect hemocyte migration in the less confined environment of the vnc.

Using single cell RNA-Sequencing, we identify two distinct clusters of hemocytes from embryonic stage 12 that are strongly enriched in genes belonging to the Enhancer of Split complex (E(spl)C). The E(spl)C-enriched clusters share several up-regulated genes with hemocytes that received BMP signal in their earlier development. Surprisingly, leading hemocytes inside the germband become stronger in E(spl)m5 expression, indicating an overlap of BMP^+ hemocytes and E(spl)C enrichment in germband hemocytes.

Taken together, these data show a previously unidentified subpopulation of BMP-activated hemocytes crucial for embryonic tissue invasion. They further suggest that this subpopulation becomes enriched in E(spl)C expression during germband invasion, a process that is independent of Notch signaling.

3.4.1 Canonical BMP signaling primes a subpopulation of *Drosophila* immune cells of the myeloid lineage

BMP ligands are well-known morphogens that can control *Drosophila* development via short- or long-range signaling (Ferguson & Anderson, 1992; Nellen et al., 1996; Shimmi et al., 2005; Wharton et al., 1993). In the larval lymph gland, the BMP-related ligand Dpp was shown to maintain the stem cell-like identity of hematopoietic stem cells (HSCs) in the posterior signaling center (PSC) via short-range signaling of the niche cells to neighboring HSCs (Dey et al., 2016b). This process is reminiscent of the effect of the Dpp-related Activinβ (Actβ) ligand, which was shown to regulate the local proliferation of hemocytes in larval hematopoietic pockets (Makhijani et al., 2017). In the embryo, *dpp* is expressed in the lateral ectoderm and it is strongly enriched in the gnathal segments that overlay hemocytes, which start spreading

out from the head mesoderm (François et al., 1994). The same area also shows an enriched expression of the tolloid protease Tld that can accentuate the signaling ability of dpp (Canty et al., 2006; Childs & O'connor, 1994; Ferguson & Anderson, 1992; Marqués et al., 1997; Tomancak et al., 2002, 2007). It is therefore likely that Dpp in close proximity is the ligand that activates BMP signaling in the identified hemocyte subpopulation, and further affects migration of immune cells of the erythro-myeloid-like lineage. The BMP^{+} subpopulation can be visualized by antibody staining against the phosphorylated transcriptional regulator Mad, which functions in canonical BMP signaling downstream of dpp and Tkv (Kim et al., 1997; Newfeld et al., 1996, 1997). We cannot exclude a possible cross-reaction of the antibody with the Smad2/3-related transcriptional regulator Smox (also called dSmad2). However, the other ligands of the BMP/TGFβ and Activin family that exhibit transcriptional signaling via Smox, Activinβ, and Dawdle, are expressed either later in development or only in other tissues (Myoglianin) (Das et al., 1999; Kutty et al., 1998; Lee-Hoeflich et al., 2005; Lo & Frasch, 1999; Tomancak et al., 2002, 2007). Moreover, the *Dad-GFP* reporter used in this study labels the leading hemocytes of germband tissue invasion. *Dad*-expression is regulated by recruitment of the P-Mad/Medea complex to the Activating Element (AE), and was shown to be specific for Dpp signaling via the receptors Tkv and Sax, but not Babo (H. Inoue et al., 1998; Kamiya et al., 2008; Tsuneizumi et al., 1997; Weiss et al., 2010b). These arguments point towards activation of canonical BMP signaling in an embryonic hemocyte subpopulation by a local ligand source.

3.4.2 The BMP receptor type I Tkv exerts a crucial role in hemocyte tissue invasion

In *Drosophila* embryos, the BMP receptor type I-related Tkv has been shown to be the predominant receptor that binds dpp, whereas the ubiquitously expressed alternative type I receptor Sax acts rather redundantly, and has been proposed to fine-tune BMP signaling (T. J. Brummel et al., 1994). In loss-of function experiments we find that *tkv* mutants decrease hemocyte germband invasion efficiency leading to lower numbers inside the germband and increase hemocyte accumulation in the pre-germband with no effect on vnc migration or total hemocyte numbers. In contrast, type I receptor *sax* and type II receptor *put* can also affect total numbers. Knock down of *put* in hemocytes by RNAi, or expressing tkv^{DN} in hemocytes affected their numbers in the pre-germband. While Tkv^{DN} lacks its intracellular GS domain and kinase domain that exert signaling function in the wildtype Tkv receptor (Haerry et al., 1998), it can still bind ligands and form complexes with other receptors possibly causing pleiotropic effects. Moreover, BMP signaling corresponding to P-Mad nuclear localization is only active in 25% of hemocytes at stage 10. However, over-expression of Tkv^{DN} was performed in all hemocytes, which could lead to additional changes in hemocyte-hemocyte interactions.

Knock-down of Put was shown to affect hemocyte adhesion and proliferation in larvae together with the Actβ receptor Babo (Makhijani et al., 2017). In the early embryo, no function for *babo* has been shown, even though it is expressed throughout embryogenesis (T. Brummel et al., 1999). In contrast, expression of the ligand Actβ only starts in later stages of embryogenesis (Kutty et al., 1998). However, interfering with *put* expression could possibly cause additional effects on hemocyte proliferation, similar to what was shown in embryos for proliferation of progenitors in the germline, which is only affected by *put*, but not by *tkv* (Matunis et al., 1997). Moreover, Put was shown to be able to signal through a Mad-independent mechanism regulating neuronal development in larvae (Ng, 2008). This non-

canonical function of *put* remains unknown during embryogenesis. Nevertheless, it could be possible that *put* could affect general migration of embryonic hemocytes via unknown Mad-independent processes.
While we cannot exclude a functional role for related signaling pathways downstream of Put, we favor a mechanism in which Tkv-Mad-Dad signaling in the hemocyte subpopulation causes transcriptional changes specifically regulating hemocyte invasion into the germband.

3.4.3 Differentially expressed genes affecting cell-cell interactions allow efficient tissue invasion

The penetration of hemocytes into the germband tissue has been shown to rely on Integrin-dependent adhesion, similar to vertebrate monocytes moving through the vasculature (Abraham et al., 2009). In *Drosophila*, the hemocyte-specific GTPase RhoL controls proper localization of a GEF for Rap1 (*Dizzy*), leading to activation of α-Integrin (*inflated*) at the leading edge (Siekhaus et al., 2010). In the RhoL mutant, hemocytes cannot enter into the germband. Moreover, if Inflated is activated by expressing the constitutively active $Rap1^{CA}$ in hemocytes, they adhere to each other and build big clumps. This indicates that their adhesion to the tissue and to other hemocytes needs to be tightly controlled.
Our identification of higher expression of the adhesion molecules Fas2, Fas3 and Tsp39D in the BMP^+ hemocytes supports the argument that differential capacities of the BMP^+ subpopulation potentially have a positive impact on their tissue invasion. Fas2, the orthologue of NCAM, is also expressed in a distinct subset of *Drosophila* interneurons allowing homophilic clustering and fasciculation of Fas2-expressing axons (D. M. Lin et al., 1994). Fas3, an orthologue of the Nectin-family adhesion molecules, controls selective filopodia matching of cardioblasts during heart formation in *Drosophila* (S. Zhang et al., 2018) and was recently identified in a larval hemocyte subpopulation (B. Cho et al., 2020). In vertebrates, nectin-family members were shown to interact with PDGF and VEGF receptors as well as integrins to regulate angiogenesis and directional cell movement by localization at the leading edge (Kinugasa et al., 2012; Ogita et al., 2010). Furthermore, Nectin-2 is necessary for the localization of zyxin to cell-cell contacts *in vitro* (Gregory Call et al., 2011). In *Drosophila* embryos, zyxin-regulated contact inhibition of locomotion (CIL) is crucial for hemocyte dispersal on the ventral side (Davis et al., 2012), pointing towards a possible function of Fas3 for zyxin localization in hemocyte-hemocyte interaction during germband invasion in leading cells. CIL is also known to enhance efficient migration of leader cells during collective migration of *Xenopus* neural crest cells, which migrate along a chemokine gradient (Carmona-Fontaine et al., 2008). Moreover, we found the tetraspanin Tsp39D as an interesting putative BMP target gene in hemocytes that affects their ability of efficient tissue invasion. The vertebrate orthologue of Tsp39D (CD63) controls integrin-dependent leukocyte rolling and recruitment to endothelial cells (Doyle et al., 2011; Vischer & Wagner, 1993). In addition, *CD63* is not expressed at a similar level in all myeloid blood cells, but was recently shown to be enriched in one human monocyte subpopulation (Champion et al., 2018; Tippett et al., 2013). These findings highlight potential functions for BMP signaling to upregulate adhesion-related target genes in a subpopulation of hemocytes affecting cell-cell contacts, eventually leading to efficient germband tissue entry. Transient cell-cell adhesions could exert similar functions for the collectively migrating hemocytes like in neural crest cells.
Drosophila embryonic hemocytes migrate collectively, and BMP^+ hemocytes show increased expression of the chemokine Pvf3 and Fas2 pointing towards a possible signaling function

from leader to follower cells during tissue invasion. While previous studies identified the VEGF/PDGF ligands Pvf2/3 to be crucial for germband invasion, both ligands were thought to be expressed in the germband tissue raising the question of how other hemocytes can follow the pioneers, and how pioneering hemocytes can possibly move past the Pvf2/3 source. In *pvf2* and *pvf3* mutant embryos, hemocytes cannot enter into the germband, but this phenotype can be rescued by expression of *pvf2* inside the germband edge (Parsons & Foley, 2013). Signaling of Pvf2 from the germband edge could affect leading hemocytes, which themselves express Pvf3 and other cell-cell interaction candidates to migrate further into the germband and possibly signal back to following hemocytes. Along the vnc, Pvf2 and Pvf3 have different roles to control hemocyte migration and downregulation of *pvf2* along the dorsal midline is needed for lateral migration of hemocytes at stage 15 (Wood et al., 2006). Differences between Pvf2 and Pvf3 have not been identified in hemocytes during germband invasion. Recently, Pv3 and Pvf3 were shown to differentially affect larval hemocytes (Bakopoulos et al., 2022). Whereas a transient expression in a hemocyte subpopulation affected proliferation, Pvf3 was suggested to have an earlier effect, possibly in the embryo. This indicates that hemocyte subpopulations can express *pvf2/3* ligands themselves affecting the whole hemocyte population. Interestingly, we not only find *pvf3*-expression to be upregulated in the BMP^+ hemocytes, but also higher expression levels of *Fas2*. Recently, *Fas2* was also found to be expressed by *Drosophila* glia cells and proposed to exert adhesion-independent signaling functions in a secreted form, as glia expression of secreted *Fas2* could rescue the lethal *Fas2* mutant phenotype (Neuert et al., 2020). These findings point towards a role for BMP^+ hemocyte upregulated genes to provide signals to follower cells allowing the stream of hemocytes to migrate further along the germband route.

While hemocytes were proposed to migrate towards a source of Pvf2/3 chemokines, there seems to be a missing link that gives insights into their role during germband invasion. Expression of *pvf2* in an area through which hemocytes migrate leads to clumps of hemocytes, which was suggested to show that *pvf2* acts as a chemoattractant (N. K. Cho et al., 2002; Parsons & Foley, 2013). However, overexpression of the constitutively active receptor Pvr^{CA} did not block hemocyte migration. Furthermore, hemocytes expressing Pvr^{CA} in the *pvr* mutant background cannot be rescued for their inability to invade the germband (Parsons & Foley, 2013). These results point toward a role for Pvr in hemocyte adhesion, especially at the germband entry. Similar to the expression of Pvr^{CA}, we did not observe changes in the migration of Tkv^{CA} expressing hemocytes. However, expression of both active receptors was driven in all hemocytes. We observe that leading hemocytes belong to the BMP-activated subpopulation suggesting that they show advantages in their ability to invade the tissue. Strikingly, knockdown of *tkv* in hemocytes does not affect migration speed, but specifically lowers persistence at the germband entry, indicating a role for *tkv* signaling in leader cells to affect the entry of the collective. This differs from the effect of other regulators of hemocyte germband invasion, such as *minerva*, *atossa*, and *porthos*, as well as *Dfos*, which all lead to decreased migration speed (Belyaeva et al., 2022; Emtenani et al., 2021; Valoskova et al., 2019). Additionally, upregulation of *pvf3* and *Fas2* in the BMP^+ hemocytes suggests that they could possibly signal to follower hemocytes allowing efficient tissue entry of the collective. We hypothesize that activation of Pvr and BMP signaling pathways in hemocytes needs to be controlled in a spatio-temporal manner to allow efficient invasion of leading hemocytes into the germband and for other hemocytes to follow in a stream. We speculate that BMP^+ hemocyte show an advantage in their formation of the invading leading edge, such as through higher levels of factors enhancing integrin signaling. This allows them to move forward in a

more directional orientation, and signaling from leader to follower hemocytes ensures efficient invasion of the collective.

3.4.4 Could BMP$^+$ hemocytes resemble M2 macrophages in higher organisms?

Screening for possible counterparts of the BMP$^+$ hemocyte subpopulation in higher organisms led us to the pro-healing M2 macrophages, which share similarities with BMP$^+$ hemocytes in *Drosophila*. Macrophages in vertebrates can be functionally divided depending on their inflammatory state into pro-inflammatory M1 and anti-inflammatory/ pro-healing M2 macrophages. However, this binary classification should be handled with caution, as it might rather refer to extreme states of activation, and different grades of those states can likely be found in the complex *in vivo* environment (Wynn et al., 2013). M2 macrophages were proposed as the default program of resident tissue macrophages (Murray & Wynn, 2011), which are important drivers of tissue repair as they secrete components of the ECM such as collagen, drive fibrosis, and remodel the tissue (Italiani & Boraschi, 2014). Comparable to the M2 macrophage pro-healing function, larval hemocytes are needed for tissue repair after induction of a sterile wound, a process that is dependent on the JNK orthologue Basket (Wood & Martin, 2017). Their tissue remodeling functions are similar to the role of resident macrophages such as microglia, which regulate brain development (Paolicelli et al., 2011). In a similar way, *Drosophila* embryonic hemocytes are crucial for tissue development such as for the nervous system by providing components of the ECM, removing dead cells and remodeling other tissues (Olofsson & Page, 2005; Sears et al., 2003; Zhou et al., 1995). These aspects highlight shared characteristics of M2 macrophages and BMP$^+$ hemocytes during development.

Moreover, BMP and TGFβ pathway signaling components play a role for macrophage polarization towards an M2 phenotype in flies and higher organisms. One study in adult flies revealed differences in hemocyte functions during a sterile infection, reminiscent of M1 and M2 macrophage differences in higher organisms. There, Dpp signaling was necessary for a subset of immune cells in the adult fly to serve as anti-inflammatory regulators, repressing expression of anti-microbial peptides (Clark et al., 2011a). In contrast, another Activin-like ligand Dawdle was shown to be crucial for driving the inflammatory response. Additionally, Mad-Med-Shn silencer elements were identified near many anti-microbial peptide genes, suggesting that Dpp signaling induces M2-like characteristics in *Drosophila* immune cells. Similarly, Smad2/3 signaling was shown to promote the M2 state of macrophages in mice and humans (Gong et al., 2012; F. Zhang et al., 2016). Moreover, BMP-2 and BMP-4, orthologues of *Drosophila* Dpp, promote features of M2-like macrophages, enhance adhesion to endothelial cells and increase macrophage migration (Martínez et al., 2017; Pardali et al., 2018). While overexpression of an inhibitory Smad in mice can block expression of VEGF-A (Nakagawa et al., 2004), the BMP-4 induced shift towards M2-macrophages is associated with higher levels of VEGF-A, which is closely related to the Pvf ligands in *Drosophila* (N. K. Cho et al., 2002; Martínez et al., 2017). In contrast, a recent screen in *Drosophila* utilizing the VT-enhancer trap library identified functionally and molecularly distinct subpopulations of hemocytes in the later embryo at stage 15 (Coates et al., 2021). Those subpopulations show characteristics of M1 phenotypes with faster migration and wound response. However, these were not linked to Dpp signaling. These indications highlight similarities in the role of BMP signaling activation for the tissue-remodeling role of immune cells in flies and mammals. We therefore propose that BMP$^+$ hemocytes act similar to M2 macrophages.

3.4.5 BMP$^+$ hemocytes overlap with a novel E(spl)C-enriched cluster

The overlap of BMP signaling with functions of orthologues of E(spl)C genes in mammalian M2 macrophages suggests further similarities with the BMP$^+$ hemocyte subpopulation in *Drosophila* embryos. We identified two clusters of hemocytes strongly enriched in *E(spl)C* genes, and show enrichment of one of them in the leading hemocytes resembling the BMP$^+$ hemocyte subpopulation. *E(spl)C* genes are related to genes of the Hes/Hey family, and Hes1 was recently identified as a suppressor of inflammatory responses that promote M2 macrophage characteristics *in vitro* and *in vivo* (T. Inoue et al., 2019; Shang et al., 2016). Peritoneal M2-like macrophages that rapidly infiltrate tissue upon a sterile injury via a non-vascular route, to clear apoptotic cells without initiating an inflammatory response were shown to have a higher expression of Hes1 regulated by the transcription factor KLF4 (Roberts et al., 2017) and were characterized as M2 macrophages with yolk-sac origin (Bou Ghosn et al., 2010; J. Wang & Kubes, 2016). KLF4 has also been associated with gene expression patterns of tumor promoting macrophages leading to secretion of VEGF and other factors that help tumor cells to intravasate into surrounding tissues (Sica & Mantovani, 2012). As we see BMP$^+$ hemocytes secreting the VEGF-like ligand Pvf3, similar mechanisms could play a role in promoting the invasion of other hemocytes into the germband tissue in *Drosophila*.

The enrichment of E(spl)m5 in leading hemocytes during germband invasion visualized by *in vivo* live imaging suggests a potential role for BMP signaling in the regulation of *E(spl)C* gene expression. E(spl)C proteins are known to be signaling components downstream of Notch (Wurmbach et al., 1999). However, Notch does not play a role in hemocyte germband invasion and Notch protein was not found to be enriched in hemocytes prior to germband invasion (Valoskova et al., 2019). Nevertheless, another member of the E(spl)C gene family (E(spl)mβ) was shown to be activated via Dpp in the larval lymph gland (Dey et al., 2016b). In this process, Dpp is secreted from the hematopoietic niche (posterior signaling center, PSC) to keep adjacent hematopoietic stem cell (HSC)-like progenitors in an undifferentiated state, similar to the role of BMP4 for HSC maintenance in the vertebrate aorta-gonad mesonephros (AGM) (Drevon & Jaffredo, 2014; Durand et al., 2007). While the Notch pathway in *Drosophila* has been shown to regulate differentiation and maintenance of only crystal cell (Duvic et al., 2002; Lebestky et al., 2000), a recent publication revealed Notch signaling to be a binary regulator of both plasmatocyte and crystal cell fate depending on the presence of Notch-ligand Serrate in surrounding cells (Blanco-Obregon et al., 2020). For future studies, it will be interesting to take a closer look at possible functions linked to Notch signaling in the BMP$^+$ hemocytes after their germband entry.

We find BMP reporter activity and E(spl)C enrichment in leading hemocytes resembling the interaction of BMP and Notch signaling in sprouting morphogenesis. During angiogenesis, BMP signaling defines tip cells in the front, while synergistically signaling with Notch to regulate stalk cell identity (Moya et al., 2012). Combining results from myogenic cells shown to react to synergistic Notch and BMP signaling pathways (Blokzijl et al., 2003; Dahlqvist et al., 2003), Itoh and colleagues analyzed the relationship between Notch and BMP signaling during the migration of endothelial cells in different conditions. Interestingly, they showed that endothelial cells without cell-cell contacts express the target gene Id1 downstream of BMP ligands, thereby inducing cell migration. In contrast, upon contact with cells expressing components of Notch signaling (Jagged or Delta) the Hes-related gene Herp2 is synergistically up-regulated by BMP and Notch signaling pathways eventually inhibiting migration through Id1 degradation by Herp2 (Itoh et al., 2004). These results highlight the synergistic regulation of cell migration by BMP and Notch signaling.

3.4.6 BMP signaling during invasive migration in vertebrates

BMP and Notch signaling were shown to interact during the migration of epithelial sheets and collective migration of mesenchymal cells, but the role of leader cell formation in blood cells is not known. During mammalian angiogenesis, BMP type I receptors can take over distinct roles depending on the cellular context (Benn et al., 2017). Activation by the ligand BMP2 induces leader cell (tip cell) competence by driving the expression of tip cell–associated genes such as the Notch-activating delta-like ligand 4 (DLL4). Whereas signaling activated by BMP6 triggers collective cell migration and expression of follower cells (stalk cells), associated genes such as the *E(spl)C*-related genes *hairy* and *enhancer of split 1* (HES1) are activated by Smad1/5. In this process, expression levels and complex formation of different BMP type I receptors determine leader vs. follower cell identity. In zebrafish angiogenesis, BMP-activated leader cells form filopodia mediated by activation of Cdc42 in the front edge and actin assembly through Formin-like 3 (Wakayama et al., 2015). Moreover, BMP4 was shown to enhance epithelial-to-mesenchymal transition (EMT) of breast cancer cells via Notch signaling, which can induce migration of cancer cells *in vitro* (Choi et al., 2019).

The tissue invasion of BMP^+ hemocytes leading a stream of immune cells in *Drosophila* embryonic development shows similarities to the recently proposed role for BMP signaling for neural crest migration. The invasive front of cranial neural crest migration in chicken shows enrichment of BMP signature genes, which are also upregulated upon BMP-induced EMT via the transcription factor SNAIL1 in a human colorectal cancer model (Frey et al., 2020). This invasive front is defined by highly invasive neural crest Trailblazer cells with a specific transcriptional signature (McLennan et al., 2015; J. A. Morrison et al., 2017). Moreover, BMP was shown to induce faster mesenchymal migration of pre-osteoblastic cells via actin-rich membrane waves at the leader edge *in vitro* (Zouani et al., 2014). Additionally, in zebrafish lateral mesoderm migration *in vivo*, BMP signaling is crucial for regulation of cell-cell adhesions (Myers et al., 2002; von der Hardt et al., 2007). These indications lead us to hypothesize that BMP signaling activation might have similar functions for inducing leading hemocytes during the invasion of the germband tissue in *Drosophila* embryos. We believe that our findings will pave the way for a deeper understanding of BMP-induced cellular mechanisms of immune cell invasive migration.

3.5 MATERIALS AND METHODS

3.5.1 Fly strains and genetics

Flies were raised on standard food bought from IMBA (Vienna, Austria) which contained agar, cornmeal, and molasses with the addition of 1.5% Nipagin. For cage crosses, adult flies were placed in cages in a Percival DR 36VL incubator maintained at 29°C and 65% humidity; embryos were collected on standard plates prepared in house from apple juice, sugar, agar and Nipagin supplemented with normal baking yeast on the plate surface. For stock maintenance, flies were kept at 18°C or 25°C in humidified rooms, or at 29°C in a humidified incubator. Cage crosses and embryo collections for RNA interference experiments (7-8 hour collection) as well as live imaging (4-5 hour collection), and for bulk RNA-sequencing of the *dad-GFP* reporter positive macrophages were conducted at 29°C. Collection of embryos for single cell RNA-sequencing of isolated macrophages was performed at 25°C.

3.5.2 Fly stocks and genotypes

srpHemo-GAL4 and *UAS-Dad* were kindly provided by K. Brückner (Brückner et al., 2004). *Dad-GFP::nls* and *Dad-GFP* lines were kindly provided by T. Kornberg (UCSF, USA). *UAS-tkv^{DN}* and *UAS-tkv^{QD}* were a gift from G. Pyrowolakis (Freiburg, Germany). *E(spl)::GFP::m5* was a gift from F. Schweisguth (Paris, France).
The RNA lines tested in this PhD thesis were obtained from the Bloomington *Drosophila* Stock Centre (Bloomington, USA) and the Vienna *Drosophila* Resource Center (VDRC, Vienna, Austria), see Table 1 for exact genotypes. Lines *w-*; *P{w[+mC]; srpHemo-3xmCherry}*, *w-*; *P{w[+mC]; srpHemo-H2A::3xmCherry}* were published previously (Gyoergy et al., 2018).

Table 3-1: List of genotypes used in this study (Chapter 3)

name in thesis	**genotype**	**obtained from**
tkv^{4}	*w[]; tkv[4] P{ry[+t7.2]n=eoFRT}40A/CyO*	Bloomington Stock Center (USA)
tkv RNAi^{1}	*y1 sc v1; P{TRiP.GLV21018}attP2*	Bloomington Stock Center (USA)
tkv RNAi^{2}	*y1 sc v1; P{TRiP.GL00035}attP2*	Bloomington Stock Center (USA)
tkv RNAi^{3}	*y1 sc v1; P{TRiP.GL01338}attP2*	Bloomington Stock Center (USA)
sax RNAi^{1}	*y1 v1; P{TRiP.JF03431}attP2*	Bloomington Stock Center (USA)
sax RNAi^{2}	*y1 v1; P{TRiP.HMC04135}attP2*	Bloomington Stock Center (USA)
put RNAi^{1}	*y[1] sc[] v[1] sev[21]; P{y[+t7.7]v[+t1.8]=TRiP.GL00069}attP2*	Bloomington Stock Center (USA)
put RNAi^{2}	*y[1] v[1]; P{y[+t7.7] v[+t1.8]=TRiP.JF02664}attP2*	Bloomington Stock Center (USA)
Mad RNAi	*y[1] v[1]; P{y[+t7.7] v[+t1.8]=TRiP.JF01264}attP2*	Bloomington Stock Center (USA)

Fas2 RNAi[1]	*y[1] v[1]; P{y[+t7.7] v[+t1.8]=TRiP.JF02918}attP2 e[]*	Bloomington Stock Center (USA)
Fas2 RNAi[2]	*y[1] sc[] v[1] sev[21]; P{y[+t7.7] v[+t1.8]=TRiP.HMS01098}attP2*	Bloomington Stock Center (USA)
Tsp39D RNAi[1]	*y[1] v[1]; P{y[+t7.7] v[+t1.8]=TRiP.JF01847}attP2*	Bloomington Stock Center (USA)
Mipp1[DN]	*w[]; P{w[+mC]=UAS-Mipp1.H67A}2*	Bloomington Stock Center (USA)
Pvf3 RNAi[3]	*y1 v1; P{TRiP.HMS01876}attP40/CyO*	Bloomington Stock Center (USA)
attP2 ctrl	*y[1] v[1]; P{y[+t7.7]=CaryP}attP2*	Bloomington Stock Center (USA)
attP40 ctrl	*y[1] v[1]; P{y[+t7.7]=CaryP}attP40*	Bloomington Stock Center (USA)
put RNAi[3]	*w[1118]; P{GD49}v848*	Vienna Drosophila Resource Center (VDRC), Austria
Tsp39D RNAi[2]	*P{KK104661}VIE-260B*	Vienna Drosophila Resource Center (VDRC), Austria
Tsp39D RNAi[3]	*w1118; P{GD1796}v37127*	Vienna Drosophila Resource Center (VDRC), Austria
Fas3 RNAi[1]	*w1118; P{GD13161}v26850*	Vienna Drosophila Resource Center (VDRC), Austria
Fas3 RNAi[2]	*w1118; P{GD2576}v3091*	Vienna Drosophila Resource Center (VDRC), Austria
Pvf2 RNAi[2]	*P{KK110608}VIE-260B*	Vienna Drosophila Resource Center (VDRC), Austria
Pvf3 RNAi[1]	*w1118; P{GD5238}v37933*	Vienna Drosophila Resource Center (VDRC), Austria
Pvf3 RNAi[2]	*P{KK112796}VIE-260B*	Vienna Drosophila Resource Center (VDRC), Austria

3.5.3 Exact genotypes of *Drosophila* lines used in each Figure:

Figure1
Fig. 1C-D *w⁻;+;srpHemo-H2A::3xmCherry,* **Fig. 1E-I** *w⁻;Dad-GFP::nls;srpHemo-H2A::3xmCherry*

Figure 2 and Figure 2 Supplement 1
Fig. 2A, **Fig. 2S1B-D,** *w⁻;+; srpHemo-H2A::3xmCherry* (ctrl) and *w⁻;srpHemo-Dad; srpHemo-H2A::3xmCherry* (*srp-Dad*), **Fig. 2B, Fig. 2S1E,F** *w⁻;+; srpHemo-H2A::3xmCherry* (ctrl), *w⁻; tkv[4] P{ry[+t7.2]=neoFRT}40A; srpHemo-H2A::3xmCherry* (tkv[4]), **Fig. 2C, Fig. 2S1G-I** *w⁻/y[1] v[1];+; srpHemo-Gal4,srpHemo-H2A::3xmCherry/P{y[+t7.7]=CaryP}attP2* (ctrl), *w⁻/y1 sc v1;+; srpHemo-Gal4,srpHemo-H2A::3xmCherry/P{TRiP.GLV21018}attP2 (mac>tkv RNAi[1]), w⁻/ y1 sc v1;+; srpHemo-Gal4,srpHemo-H2A::3xmCherry/*P{TRiP.GL00035}attP2 *(mac>tkv RNAi[2]), w⁻/ y1 sc v1;+; srpHemo-Gal4,srpHemo-H2A::3xmCherry/P{TRiP.GL01338}attP2 (mac>tkv RNAi[3])*, **Fig. 2D, Fig. 2S1J-L** *w⁻; P{10XUAS-IVS-myr::GFP}su(Hw)attP5/+;srpHemo-Gal4,srpHemo-*

H2A::3xmCherry/+ (ctrl), *w⁻;+;srpHemo-Gal4,srpHemo-H2A::3xmCherry/UAS-tkv^{DN}* (*mac>tkv^{DN}*), *w⁻;+;srpHemo-Gal4,srpHemo-H2A::3xmCherry/UAS-tkv^{QD}* (*mac>tkv^{DA}*),
Fig. 2E, Fig. 2S1M-R *w⁻/y[1] v[1];+; srpHemo-Gal4,srpHemo-H2A::3xmCherry/P{y[+t7.7]=CaryP}attP2* (ctrl), *w⁻/y1 sc v1;+; srpHemo-Gal4,srpHemo-H2A::3xmCherry/P{TRiP. JF03431}attP2 (mac>sax RNAi^{1}), w⁻/ y1 sc v1;+; srpHemo-Gal4,srpHemo-H2A::3xmCherry/P{TRiP.HMC04135}attP2 (mac>sax RNAi^{2})***,* **Fig. 2F, Fig. 2S1S-V** *w⁻/y[1] v[1];+; srpHemo-Gal4,srpHemo-H2A::3xmCherry/P{y[+t7.7]=CaryP}attP2* (ctrl 1), *w⁻/y1 sc v1;+; srpHemo-Gal4,srpHemo-H2A::3xmCherry/P{TRiP. GL00069}attP2 (mac>put RNAi^{1}), w⁻/ y1 sc v1;+; srpHemo-Gal4,srpHemo-H2A::3xmCherry/P{TRiP. JF02664}attP2 (mac>put RNAi^{2}), w⁻;+;srpHemo-H2A::3xmCherry/+* (ctrl 2), *w[1118]; P{GD49}v848 (mac>put RNAi^{3})* **Fig. 2S1A** *w⁻;+;srpHemo-Gal4,srpHemo-H2A::3xmCherry/+* (ctrl), *w⁻;UAS-Dad/+;srpHemo-H2A::3xmCherry/+* (*mac>Dad*)

Figure 3
Fig. 3B-H *w⁻/ y[1] v[1];+; srpHemo-Gal4,srpHemo-H2A::3xmCherry/ P{y[+t7.7]=CaryP}attP2* (control), *w⁻/ y1 sc v1;+; srpHemo-Gal4,srpHemo-H2A::3xmCherry/ P{TRiP.GL00035}attP2 (mac>tkv RNAi^{2}),* **Fig. 3 I** *w⁻; Dad-GFP::nls; srpHemo-H2A::3xmCherry*

Figure 4 and Figure 4 Supplement 2
Fig. 4A *w⁻;Dad-GFP; srpHemo-3xmCherry* (for FACS), **Fig. 4C-D, Fig. 4S2A-E** *w⁻/ y[1] v[1];+; srpHemo-Gal4, srpHemo-H2A::3xmCherry/ P{y[+t7.7]=CaryP}attP2* (ctrl 1), *w⁻;+; srpHemo-Gal4,srpHemo-H2A::3xmCherry/ +* (ctrl 2), *w⁻; P{10XUAS-IVS-myr::GFP}su(Hw)attP5/ +; srpHemo-Gal4, srpHemo-H2A::3xmCherry/ +* (ctrl3), *w⁻/ y[1] v[1]; +; srpHemo-Gal4, srpHemo-H2A::3xmCherry/P{y[+t7.7] v[+t1.8]=TRiP.JF02918}attP2 e[]* (*mac>Fas2 RNAi^{1}*), *w⁻ /y[1] sc[] v[1] sev[21];+; srpHemo-Gal4, srpHemo-H2A::3xmCherry/ P{y[+t7.7] v[+t1.8]=TRiP.HMS01098}attP2* (*mac>Fas2 RNAi^{2}*), *w⁻ /w[1118]; P{GD13161}v26850/ +; srpHemo-Gal4, srpHemo-H2A::3xmCherry/+*
(*mac>Fas3 RNAi^{1}*), *w⁻/ w[1118]; P{GD2576}v3091/ +; srpHemo-Gal4,srpHemo-H2A::3xmCherry /+* (*mac>Fas3 RNAi^{2}*), *w⁻/ y[1] v[1];+; srpHemo-Gal4, srpHemo-H2A::3xmCherry/ P{y[+t7.7] v[+t1.8]=TRiP.JF01847}attP2* (*mac>Tsp39D RNAi^{1}*), *w⁻/ + ; P{KK104661}VIE-260B/ +; srpHemo-Gal4, srpHemo-H2A::3xmCherry/ +* (*mac>Tsp39D RNAi^{2}*), *w⁻/w[1118]; P{GD1796}v37127/ +; srpHemo-Gal4,srpHemo-H2A::3xmCherry/+* (*mac>Tsp39D RNAi^{3}*), *w⁻; P{w[+mC]=UAS-Mipp1.H67A}2/ +; srpHemo-Gal4,srpHemo-H2A::3xmCherry /+* (*mac>Mipp1^{DN}*), **Fig. 4E-F, Fig. 4S2G** *w⁻; + ; srpHemo-Gal4, srpHemo-H2A::3xmCherry/ +* (ctrl 1), *w⁻/ +; P{KK110608}VIE-260B/ +; srpHemo-Gal4, srpHemo-H2A::3xmCherry/ +* (*mac>Pvf2 RNAi^{1}*), *w⁻/ [w1118]; P{GD5238}v37933/ +; srpHemo-Gal4,srpHemo-H2A::3xmCherry/ +* (*mac>Pvf3 RNAi^{1}*), *w/ +; P{KK112796}VIE-260B/ +; srpHemo-Gal4, srpHemo-H2A::3xmCherry/ +* (*mac>Pvf3 RNAi^{2}*), *w⁻/ y[1] v[1]; P{attP,y[+],w[3`]}/ +; srpHemo-Gal4, srpHemo-H2A::3xmCherry /+* (ctrl2), *w⁻ /y[1] v[1]; P{TRiP.HMS01876}attP40/ +; srpHemo-Gal4, srpHemo-H2A::3xmCherry/+* (*mac>Pvf3 RNAi^{3}*)

Figure 5
Fig. 5A-C,E *w⁺; +; srpHemo-3xmCherry* (for all single cell RNA-Sequencing samples), **D** *srpHemo-H2A::3xmCherry/ + ; E(spl)::GFP::m5/+*

3.5.4 Cloning and generation of *srp-Dad* line

Standard molecular biology methods were used and constructs were sequenced by Mycrosynth (Vienna, Austria) before injection into flies. *NotI* was obtained from New England Biolabs. PCR amplifications were performed with Clone Amp polymerase (Clontech) using a PCR machine from Bio-Rad Laboratories. All Infusion cloning was conducted using an Infusion HD Cloning kit (Clontech's European distributer). The relevant oligo sequences were chosen using the Infusion primer Tool at the Clontech website (http://bioinfo.clontech.com/infusion/convertPcr sInit.do). Generation of the line was performed by Attila György. A 1707 bp fragment containing the full length Dad CDS was amplified from a plasmid containing cDNA of Dad (stock number DSPL418, BDGP plasmid LD47465) using the primers for further infusion cloning additionally introducing an N-terminal HA-tag:
5'
AGTTCTAGAGCGGCCGCATGTACCCATACGATGTTCCAGATTACGCTGCCGCCGCCATGATATTCCC
AAG3'
5' ACCGCGGTGGCGGCCGCTCACCGCAGATGACTAAAGTG 3'.
The fragment was cloned into the srpWattB plasmid (stock number DSPL336) after linearization with *NotI*, using an Infusion HD cloning kit (Clontech's European distributor). The final construct was then injected into flies carrying the attP2 landing site.

3.5.5 DNA isolation from single flies

Single male flies were frozen overnight before being ground with a pellet homogenizer (VWR, Radnor, USA) and plastic pestles (VWR, Radnor, USA) in 50µl of homogenizing buffer (100 mM Tris-HCl, 100 mM EDTA, 100 mM NaCL, and 0.5% SDS). Lysates were incubated at 65°C for 30 minutes. Then 5M KAc and 6M LiCl were added at a ratio of 1:2.5 and lysates were incubated on ice for 10 min. Lysates were centrifuged for 15 minutes at 20,000xg, supernatant was isolated and mixed with Isopropanol. Lysates were centrifuged again for 15 minutes at 20,000xg, the supernatant was discarded and the DNA pellet was washed in 70% ethanol and subsequently dissolved in distilled water.

3.5.6 Embryo staging

Embryos were staged for imaging based on the invagination of the stomodeum as well as germband retraction away from the anterior in a lateral orientation as described previously (Ratheesh et al., 2018). In brief, embryos which showed stomodeal invagination and a germband retraction of less than 29% were classified as Stage 10 and embryos with germband retractions between 29-31% as Stage 11 and 35-45% as Stage 12.

3.5.7 Embryo fixation and immunohistochemistry

Embryos were collected on apple juice plates for between 5-8 hours at 29°C. The chorion was removed by incubation in 50% Chlorox (DanClorix) for 5 min following rinsing with cold tap water. Embryos were fixed with 4% formaldehyde/heptane for 20 min followed by methanol devitellinization. Fixed embryos were blocked in BBT (0.1M PBS + 0.1% Triton X-100 + 0.1% BSA) for 2 hours at RT and then incubated with primary antibodies rotating overnight at 4°C. Antibodies were used at the following dilutions: Chicken Anti-GFP (Abcam, ab13970, dilution

1:500) and Rabbit Anti-Smad3 phospho S423+S425 [eP823Y] (Abcam, ab52903, Lot GR128879-63, dilution 1:200). Afterwards, embryos were washed in BBT for 2 hours, incubated with secondary antibodies Anti-Chicken 488 Alexa (Thermo Fisher Scientific, A-11039) at RT for 2 hours, and washed again with PBST for 2 hours. Alexa fluor 488 labelled secondary antibodies were used at a dilution of 1:500. The embryos were mounted overnight at 4°C in Vectashield mounting medium (Vector Laboratories, Burlingame, USA) containing DAPI. Embryos were placed on a slide and imaged with a Zeiss Inverted LSM800 or Zeiss Upright LSM900 Confocal Microscope using a Plain-Apochromat 20X/0.8 Air Objective or a Plain-Apochromat 63X/1.4 Oil Objective as required.

3.5.8 FACS sorting of macrophages

FACS sorting was performed to isolate total RNA from embryonic macrophages as described previously (György et al., 2018). For bulk RNA-Sequencing of BMP^+ macrophages, embryos were collected from *srpHemo-3xmCherry; Dad-GFP* reporter flies, as well as wildtype and *srpHemo-10xsf::EGFP* as negative controls for setting the gates. To obtain embryos from the correctly synchronized stages, flies were added to big collection cages topped with apple juice agar plates and sprinkled with yeast 2 days prior to collection. They were allowed to adjust to the cages by keeping them at the desired collection temperature (29°C for bulk RNA-Sequencing of dad-GFP positive vs. dad-GFP negative macrophages) in a 8AM-8PM light-dark cycle for 2days while changing plates at least 4x per day.
On the collection day, flies were pre-fed for 2h changing plates with yeast every 30min. Afterwards, embryos were allowed to lay for 1h. The isolated plates were further incubated at 29°C for a total of 6h30min to reach early stage 12, when macrophages have already started to invade into the germband tissue and the *dad-GFP* reporter reaches an intensity that can be clearly separated in the FACS gating. Embryos were collected for 1 day with about 8-9 collections per day and meanwhile stored at 4°C to slow down development. Collected embryos were dissociated and macrophages were sorted according to the procedure described in (Gyoergy et al., 2018). The cells were sorted using a FACS Aria III (BD) flow cytometer. Emission filters were 600LP, 610/20 and 502 LP, 510/50. Data was analyzed with FloJo software (Tree Star). Approximately 1-1.5x10^5 macrophages were sorted within 30 minutes.
For isolation of macrophages for single cell RNAseq, the procedure was slightly adjusted, using a temperature of 25°C for collection. Additionally, to decrease the time embryos were incubated at 4°C, collection and sorting were performed on one day using 12 large cages for parallel collection. Embryos were allowed to develop for a total of 3h30min for stage 8, 5h for stage 10, 8h30min for stage 12, and 13h for stage 16.

3.5.9 Total RNA-Sequencing of *Drosophila* embryonic hemocytes

Bulk RNA-Seq from pooled embryonic macrophages of *dad-GFP* reporter flies
Isolated macrophages from early stage 12 embryos were FACS sorted and separated according to GFP fluorescence intensity. 3 replicates of BMP^+ macrophages and 6 replicates of BMP^- macrophages of the genotype *dad-GFP; srpHemo-3xmCherry* had total RNA isolated from the FACS-sorted macrophages using Qiagen RNeasy Mini kit

(Cat No. 74104). The quality and concentration of RNA was determined using an Agilent 6000 Pico kit (Cat No. 5067-1513) on an Agilent 2100 Bioanalyzer: about 100ng of total RNA was extracted from $1.5x10^5$ macrophages. RNA sequencing was performed by the CSF facility of Vienna Biocenter according to the standard procedures (https://www.vbcf.ac.at/facilities/next-generation-sequencing/). Briefly, cDNA libraries were synthesized using QuantSeq 3' mRNA-seq Library Prep kit and sequenced on the Illumina HiSeq 2500 platform. The reads were mapped to the *Drosophila melanogaster* Ensembl BDGP6 reference genome with STAR (version 2.5.1b). The read counts for each gene were detected using HTSeq (version 0.5.4p3). The Flybase annotation (r6.19) was used in both mapping and read counting. The counts were normalised using the TMM normalization from edgeR package in R. Prior to statistical testing the data was transformed and then the differential expression between the sample groups was calculated with limma package in R. The functional analyses were done using the topGO and gage packages in R (Anders, Pyl, & Huber, 2015; Dobin et al., 2013).

Single Cell RNA-Sequencing of embryonic *Drosophila* hemocytes

To increase the precision of embryonic stage assignments, all embryos were additionally hand-picked on an ice cold metal plate under a fluorescent microscope after dechorionisation of each staged collection to remove slightly older, younger, or unfertilized embryos. Total RNA was then isolated from the FACS-sorted single hemocytes from stage 8, 10, 12, and 16 embryos of *w^+; +; srpHemo-3xmCherry* flies to identify different subpopulations during embryonic development. The following amounts of single cells were sorted per stage: stage 8=61, stage 10=279, stage 12=239, stage 16=290.

RNA sequencing was performed by Aleksandr Bykov (Luisa Cochella group, IMP Vienna) using SMART Seq2 as described previously (Picelli et al., 2014). To increase efficiency, the protocol was slightly adjusted. As the most critical step for the adapted protocol during the RT the plate was cooled down to 42°C after the incubation at 72°C to prevent oligo dT annealing to rRNA. Additionally, homemade tn5 was used. After tagmentation a pre-incubation step at 72°C was introduced during PCR to improve efficiency. Further, different oligos were used:

Oligo dT:AATGATACGGCGACCACCGAGATCTACACTTTTTTTTTTTTTTTTTTTTTTTTTTTTTVN

Custom template-switching oligos (TSO) were ordered as RNA oligos (Sigma).

TSO=[dA][dA][dG][dC][dA][dG][dT][dG][dG][dT][dA][dT][dC][dA][dA][dC][dG][dC][dA][dG][dA][dG][d T][dA][dC][dA][dT]GGG

Biotinylation at the 3'end avoided several template switching events in a row leading to several TSO sequences at the 3' end of the first cDNA strand.

Additionally pre-amplification primers were used as sequences of oligodT and TSO differed from the original protocol.

ISPCR:AAGCAGTGGTATCAACGCAGAGT

P5PCR:AATGATACGGCGACCACCGAGATCTACAC

The original smartSeq protocol has the overhang which is present on the TSO also on the oligoDT, therefore we only used ISPCR for amplifying the cDNA.

Following, all samples were sequenced using Illumina NextSeq550 high throughput with single reads of 75b. Subsequent data analysis was performed by Pierre Cattenoz and Tao Ye (Angela Giangrande group, IGBMC, Paris) as described previously (Cattenoz et al. 2020). In brief, reads were preprocessed in order to remove adapter, polyA and low-quality sequences (Phred quality score below 20). After this preprocessing, reads shorter than 40 bases were discarded

for further analysis. These preprocessing steps were performed using cutadapt (Martin, 2011) version 1.10.
Adapters were trimmed using trim_galore version 0.4.3. Reads were mapped onto the BDGP6 assembly of Drosophila melanogaster genome and quantified using STAR Solo (Dobin et al., 2013) version 2.7.7a with default filtering and annotations from Ensembl release 95. For further analysis and clustering, PCA was used for dimension reduction setting 500 variable features and 15 dimensions. In FindClusters function SLM algorithm was used with a resolution of 2 to not make too many clusters because of the low number of cells for each stage. Gene markers were tested by the default method using Wilcoxon rank sum test.

3.5.10 Statistics and Repeatability

Statistical tests as well as the number of embryos/ cells assessed are listed in the figure legends. All statistical analyses were performed using GraphPad Prism and significance was determined using a 95% confidence interval. Data points from individual experiments/ embryos were pooled to estimate mean and SEM. No statistical method was used to predetermine sample size and the experiments were not randomized. Unpaired t-test or Mann-Whitney was used to calculate the significance in differences between two groups and One-way Anova followed by Tukey post-test followed by Conover or Dunn's post-test for multiple comparisons. All measurements were performed in 3-34 embryos. Representative images shown in Figure1C, F-H were from separate experiments that were repeated at least 3 and up to 7 times. Stills shown in Figure 3B,I and Figure 5F are representative images from movies, which were repeated at least 3 times.

3.5.11 Time-Lapse Imaging

For time lapse imaging and further tracking of macrophage nuclei, embryos were dechorionated in 50% bleach for 5 min, washed with water, and mounted in
halocarbon oil 27 (Sigma) between a coverslip and an oxygen permeable membrane (YSI).
The anterior dorsolateral region of the embryo was imaged on an inverted multiphoton
microscope (TrimScope, LaVision) equipped with a UApo N340 40xW, NA 1.15 objective (Olympus). GFP and mCherry were imaged at 860 nm and 1150 nm excitation wavelengths, respectively, using a Ti-Sapphire femtosecond laser system (Coherent Chameleon Ultra) combined with optical parametric oscillator technology (Coherent Chameleon Compact OPO). Excitation intensity profiles were adjusted to tissue penetration depth and z-sectioning for imaging was set at 1 µm for tracking. For long-term imaging, movies were acquired for 180-200 minutes with a frame rate of 40-42 seconds. Embryos were imaged with a temperature control unit set to either 29°C.

3.5.12 Image Analysis

Macrophage cell counts:
To determine the stage of each embryo stomodeal invagination as well as germband retraction was assessed. DAPI staining and autofluorescence of the yolk were used to distinguish the germband edge and measure the distance from head to germband for analysis of fixed samples. Germband retraction away from the anterior was used to classify embryos into Stage 11 or Stage 12. Embryos with germband retraction of between 29-31% were

assigned to Stage 11. Embryos with 35-45% retraction of the tip of the germband (Stage 12) were analysed for the number of macrophages that had entered the germband. The macrophage numbers inside the germband were counted manually using the Cell Counter Plugin from Fiji. Embryos with 50-75% retraction were used for the number along the ventral nerve cord (vnc) and in the number of total macrophages inside the whole embryo, except for *mac>tkv^{QD}* and *mac>tkv^{DN}* in Fig. 2S1K, as well as for *mac>put RNAi^{1}* in Fig. 2S1T, in which the total number of macrophages was counted manually from embryos with germband retraction of 38%-45%. Additionally, in Fig. 4S2 C-D the number of total macrophages for mac>Mipp1DN was counted in embryos used for germband and pre-gb counts. For each embryo the number of macrophages inside the germband (#gb) or in the pre-germband zone (#pre-gb) was then divided by the number of total macrophages for that embryo. The results are shown in %. Macrophages were visualized using confocal microscopy with a Z-resolution of 2 µm and the number of macrophages within the germband or the segments of the vnc was calculated in individual slices (and then aggregated) using the Cell Counter plugin in FIJI. Total macrophage numbers for all embryos excluding the mentioned exceptions were obtained using Imaris (Bitplane) by detecting all the macrophage nuclei as spots.

Macrophage tracking, speed, persistence and time for macrophage entry analysis

Embryos in which the macrophage nuclei were labeled with *srpHemo-H2A::3XmCherry* were imaged and 250X130X35µm 3D-stacks were typically acquired with a constant 0.5X0.5X1µm voxel size at every 40-42 seconds for approximately 3 hours. Images acquired from multiphoton microscopy were initially processed with ImSpector software (LaVision Bio Tec) to compile channels from the imaging data. Afterwards, the exported files were further processed using Imaris software (Bitplane) to visualize the recorded channels in 3D and the movie from each imaged embryo was rotated and aligned along the AP axis for further tracking analysis.

To analyze the movies by Imaris, the following steps were applied:

i. To calculate the migration parameters while macrophages migrated from the head mesoderm to the edge of the germband tissue, movies were cropped in time to that period (typically 60 minutes from the original movie prior to germband entry of the first macrophage were used for analysis).

ii. To calculate the migration parameters of the macrophage moving from the pre-germband zone into the germband (germband entry), movies were recorded from the time point of the first macrophage appearing in the pre-germband zone until the onset of germband retraction.

iii. Macrophage nuclei were extracted using the spot detection function and tracks generated in 3D over time. We could not detect all macrophages in the head mesoderm as spots because of limitations in our imaging parameters. Tracks of macrophages, which migrate towards the dorsal vessel, ventral nerve cord (vnc) and to the anterior of the head were omitted. The edge of the germband was detected using autofluorescence from the yolk and the mean position of the tracks in X- and Y-axis was used to restrict analysis to before macrophages reach the edge of the germband.

iv. Nuclei positions in XYZ-dimensions were determined for each time point and used for further quantitative analysis.

v. The time point when the macrophage nuclei reached the germband edge aligning in a typical semi-circular arch was defined as T0 and the time point when the macrophage nuclei were within the germband and moved forward along the route between the ectoderm and mesoderm was taken as T1. T1-T0 was defined as the time for macrophage germband crossing. T0 and T1 were determined by precisely examining macrophage position in xy and z dimensions (examination of individual 1 micron slices) over time.

vi. To measure the speed and persistence at the germband entry, tracks were generated from the time when the first macrophages started to approach the germband tissue border comprised of ectoderm and mesoderm, which can typically be distinguished by macrophage nuclei appearing in a triangular form. Tracks were obtained from the first macrophage nuclei invading into the germband towards the dorsal side until they started to reach the dorsal midline and migrating further towards the posterior of the embryo.

vii. To calculate the speed of migration and persistence of the first, second, and third macrophage inside the germband the track generated for the first, second, or third macrophage alone was used to obtain the nuclei position in XYZ-dimensions. Moreover, the average speed of the first three macrophages moving along the same route was also measured. Speed and persistence were calculated within the first 30- 35 µm of the path between the germband ectoderm and mesoderm. The mean position of the tracks in X- and Y-axis was used to restrict analysis to either of the migratory zones (head-germband, germband crossing, germband entry=route along the germband ectoderm and mesoderm).
Embryos from the control (*w^-/y[1] v[1];+; srpHemo-Gal4,srpHemo-H2A::3xmCherry/ P{y[+t7.7]=CaryP}attP2)* and *mac>tkv RNAi^2* (*w^-/y1 sc v1;+; srpHemo-Gal4,srpHemo-H2A::3xmCherry/ P{TRiP.GL00035}attP2*) were used for calculating the time for macrophage germband crossing, speed and persistence at the germband entry, and during their migration from head to germband, respectively, as well as for the first three macrophages entering into the germband separately. Speed values were extracted from IMARIS directly in µm/sec, saved as Excel file, and the average speed of all analyzed tracks per embryo was converted into µm/min and used for statistical analysis in GraphPad/PRISM. Persistence values were extracted from IMARIS as "track straightness" values, which are calculated from the track displacement divided by the total track length.

Acknowledgements

We thank the following for their contributions: The *Drosophila* Genomics Resource Center supported by NIH grant 2P40OD010949-10A1 for plasmids, K. Brückner, G. Pyrowolakis, F. Schweisguth, D. Andrew, the Bloomington *Drosophila* Stock Center supported by NIH grant P40OD018537 and the Vienna *Drosophila* Resource Center for fly stocks, FlyBase (Thurmond et al., 2019) for essential genomic information, and the BDGP *in situ* database for data (Tomancak et al., 2002, 2007). For antibodies, we thank the Developmental Studies Hybridoma Bank, which was created by the Eunice Kennedy Shriver National Institute of Child Health and Human Development of the NIH, and is maintained at the University of Iowa. We thank the Vienna BioCenter Core Facilities for RNA sequencing and analysis and the Life

Scientific Service Units at IST Austria for technical support and assistance with microscopy and FACS analysis.

3.6 Author contributions

Stephanie Wachner
Roles: Conceptualization, Formal analysis, Data curation, Funding acquisition, Investigation, Methodology, Supervision, Resources, Validation, Visualization, Writing – original draft
All experiments shown were performed by S.W.; A.György assisted S.W. with embryo collection and fixation for RNAi-mediated knock down of *pvf2* and *pvf3* in hemocytes. P.C. with supervision of A.G., and L.C. performed formal data analysis of scRNA-Seq data and generated corresponding graphs in consultation with S.W.. The original draft was written by S.W. and edited by D.S..

Pierre Cattenoz
Roles: Conceptualization, Formal analysis, Data curation, Methodology, Supervision, Visualization
P.C. performed analysis of scRNA-Seq data, and generated corresponding graphs (Fig. 5A-E, Fig. 5S1 A-B).

Vera Belyaeva
Roles: Conceptualization, Methodology, Resources
V.B. established P-Mad antibody staining methodology in the lab, crossed *Dad-GFP::nls* fly lines, and performed preliminary experiments of BMP reporter movie recording, and analysis of *tkv* RNAi in hemocytes in fixed embryos.

Aleksandr Bykov
Roles: Data curation, Methodology, Supervision
A.B. and S.W. performed sample preparation of hemocytes and FACS for scRNA-Seq, A.B. performed library preparation for scRNA-Seq.

Attila György (A.György)
Roles: Methodology, Resources
A.György generated the *srp-Dad* fly line with help of S.W., and assisted with embryo collection and fixation of RNAi-meditated knock down of *pvf2* and *pvf3* in hemocytes (Fig. 4E-F; Fig. 4 S1G).

Angela Giangrande (A.G.)
Roles: Conceptualization, Funding acquisition, Methodology, Supervision

Luisa Cochella
Roles: Conceptualization, Funding acquisition, Methodology (scRNA-Seq, library preparation), Supervision (scRNA-Seq)

Daria Siekhaus

Roles: Conceptualization, Data curation, Funding acquisition, Methodology, Project administration, Supervision, Writing – original draft

3.7 REFERENCES

Abercrombie, M., Heaysman, J. E. M., & Pegrum, S. M. (1970). The locomotion of fibroblasts in culture. 3. Movements of particles on the dorsal surface of the leading lamella. *Experimental Cell Research*, *62*(2), 389–398. https://doi.org/10.1016/0014-4827(70)90570-7

Abraham, S., Yeo, M., Montero-Balaguer, M., Paterson, H., Dejana, E., Marshall, C. J., & Mavria, G. (2009). VE-Cadherin-mediated cell-cell interaction suppresses sprouting via signaling to MLC2 phosphorylation. *Current Biology : CB*, *19*(8), 668–674. https://doi.org/10.1016/J.CUB.2009.02.057

Affolter, M., Nellen, D., Nussbaumer, U., & Basler, K. (1994). Multiple requirements for the receptor serine/threonine kinase thick veins reveal novel functions of TGF beta homologs during Drosophila embryogenesis. *Development*, *120*(11), 3105–3117. http://dev.biologists.org/content/120/11/3105.abstract

Afik, R., Zigmond, E., Vugman, M., Klepfish, M., Shimshoni, E., Pasmanik-Chor, M., Shenoy, A., Bassat, E., Halpern, Z., Geiger, T., Sagi, I., & Varol, C. (2016). Tumor macrophages are pivotal constructors of tumor collagenous matrix. *The Journal of Experimental Medicine*, *213*(11), 2315. https://doi.org/10.1084/JEM.20151193

Akhmanova, M., Gyoergy, A., Vlasov, M., Vlasov, F., Krueger, D., Akopian, A., Emtenani, S., Ratheesh, A., Renzis, S. De, & Siekhaus, D. E. (2021). Cell division in tissues enables macrophage infiltration. *BioRxiv*, 2021.04.19.438995. https://doi.org/10.1101/2021.04.19.438995

Alfonso, T. B., & Jones, B. W. (2002). gcm2 promotes glial cell differentiation and is required with glial cells missing for macrophage development in Drosophila. *Developmental Biology*, *248*(2), 369–383. https://doi.org/10.1006/dbio.2002.0740

Amigo, J. D., Ackermann, G. E., Cope, J. J., Yu, M., Cooney, J. D., Ma, D., Langer, N. B., Shafizadeh, E., Shaw, G. C., Horsely, W., Trede, N. S., Davidson, A. J., Barut, B. A., Zhou, Y., Wojiski, S. A., Traver, D., Moran, T. B., Kourkoulis, G., Hsu, K., … Paw, B. H. (2009). The role and regulation of friend of GATA-1 (FOG-1) during blood development in the zebrafish. *Blood*, *114*(21), 4654. https://doi.org/10.1182/BLOOD-2008-12-189910

Awasaki, T., Lai, S. L., Ito, K., & Lee, T. (2008). Organization and Postembryonic Development of Glial Cells in the Adult Central Brain of Drosophila. *Journal of Neuroscience*, *28*(51), 13742–13753. https://doi.org/10.1523/JNEUROSCI.4844-08.2008

Bakopoulos, D., Whisstock, J. C., Warr, C. G., & Johnson, T. K. (2022). Macrophage self-renewal is regulated by transient expression of PDGF- and VEGF-related factor 2. *The FEBS Journal*. https://doi.org/10.1111/FEBS.16364

Banerjee, U., Girard, J. R., Goins, L. M., & Spratford, C. M. (2019). Drosophila as a Genetic Model for Hematopoiesis. *Genetics*, *211*(2), 367. https://doi.org/10.1534/GENETICS.118.300223

Bataillé, L., Augé, B., Ferjoux, G., Haenlin, M., & Waltzer, L. (2005). Resolving embryonic blood cell fate choice in Drosophila:interplay of GCM and RUNX factors. *Development*, *132*(20), 4635–4644. https://doi.org/10.1242/DEV.02034

Belele, C. L., English, M. A., Chahal, J., Burnetti, A., Finckbeiner, S. M., Gibney, G., Kirby, M.,

Sood, R., & Liu, P. P. (2009). Differential requirement for Gata1 DNA binding and transactivation between primitive and definitive stages of hematopoiesis in zebrafish. *Blood*, *114*(25), 5162. https://doi.org/10.1182/BLOOD-2009-05-224709

Belyaeva, V., Wachner, S., Gyoergy, A., Emtenani, S., Gridchyn, I., Akhmanova, M., Linder, M., Roblek, M., Sibilia, M., & Siekhaus, D. (2022). Fos regulates macrophage infiltration against surrounding tissue resistance by a cortical actin-based mechanism in Drosophila. *PLoS Biology*, *20*(1), e3001494. https://doi.org/10.1371/JOURNAL.PBIO.3001494

Benhra, N., Barrio, L., Muzzopappa, M., & Milán, M. (2018). Chromosomal Instability Induces Cellular Invasion in Epithelial Tissues. *Developmental Cell*, *47*(2), 161-174.e4. https://doi.org/10.1016/j.devcel.2018.08.021

Benn, A., Hiepen, C., Osterland, M., Schütte, C., Zwijsen, A., & Knaus, P. (2017). Role of bone morphogenetic proteins in sprouting angiogenesis: Differential BMP receptor-dependent signaling pathways balance stalk vs. tip cell competence. *FASEB Journal*, *31*(11), 4720–4733. https://doi.org/10.1096/FJ.201700193RR/-/DC1

Berke, B., Wittnam, J., McNeill, E., Van Vactor, D. L., & Keshishian, H. (2013). Retrograde BMP signaling at the synapse: a permissive signal for synapse maturation and activity-dependent plasticity. *The Journal of Neuroscience : The Official Journal of the Society for Neuroscience*, *33*(45), 17937–17950. https://doi.org/10.1523/JNEUROSCI.6075-11.2013

Bernardoni, R., Vivancos, V., & Giangrande, a. (1997). Glide/Gcm Is Expressed and Required in the Scavenger Cell Lineage. *Developmental Biology*, *191*(1), 118–130. https://doi.org/10.1006/dbio.1997.8702

Bhatia, M., Bonnet, D., Wu, D., Murdoch, B., Wrana, J., Gallacher, L., & Dick, J. E. (1999). Bone Morphogenetic Proteins Regulate the Developmental Program of Human Hematopoietic Stem Cells. *The Journal of Experimental Medicine*, *189*(7), 1139. https://doi.org/10.1084/JEM.189.7.1139

Blanco-Obregon, D., Katz, M. J., Durrieu, L., Gándara, L., & Wappner, P. (2020). Context-specific functions of Notch in Drosophila blood cell progenitors. *Developmental Biology*, *462*(1), 101–115. https://doi.org/10.1016/J.YDBIO.2020.03.018

Blaser, H., Reichman-Fried, M., Castanon, I., Dumstrei, K., Marlow, F. L. L., Kawakami, K., Solnica-Krezel, L., Heisenberg, C. P., & Raz, E. (2006). Migration of Zebrafish Primordial Germ Cells: A Role for Myosin Contraction and Cytoplasmic Flow. *Developmental Cell*, *11*(5), 613–627. https://doi.org/10.1016/J.DEVCEL.2006.09.023

Blokzijl, A., Dahlqvist, C., Reissmann, E., Falk, A., Moliner, A., Lendahl, U., & Ibáñez, C. F. (2003). Cross-talk between the Notch and TGF-beta signaling pathways mediated by interaction of the Notch intracellular domain with Smad3. *The Journal of Cell Biology*, *163*(4), 723–728. https://doi.org/10.1083/JCB.200305112

Borkowski, T. A., Letterio, J. J., Farr, A. G., & Udey, M. C. (1996). A role for endogenous transforming growth factor beta 1 in Langerhans cell biology: the skin of transforming growth factor beta 1 null mice is devoid of epidermal Langerhans cells. *J.Exp.Med.*, *184*(0022–1007), 2417–2422.

Borkowski, T., Letterio, J., Mackall, C., Saitoh, A., Wang, X., Roop, D., Gress, R., & Udey, M. (1997). A Role for TGFb1 in Langerhans Cell Biology. *The Journal of Clinical Investigation*, *100*(3), 575–581.

Bou Ghosn, E. E., Cassado, A. A., Govoni, G. R., Fukuhara, T., Yang, Y., Monack, D. M., Bortoluci, K. R., Almeida, S. R., Herzenberg, L. A., & Herzenberg, L. A. (2010). Two physically, functionally, and developmentally distinct peritoneal macrophage subsets. *Proceedings of the National Academy of Sciences of the United States of America*, *107*(6), 2568–2573.

https://doi.org/10.1073/PNAS.0915000107

Boulet, M., Renaud, Y., Lapraz, F., Benmimoun, B., Vandel, L., & Waltzer, L. (2021). Characterization of the Drosophila Adult Hematopoietic System Reveals a Rare Cell Population With Differentiation and Proliferation Potential. *Frontiers in Cell and Developmental Biology*, *9*, 2863. https://doi.org/10.3389/FCELL.2021.739357/BIBTEX

Brock, A. R., Wang, Y., Berger, S., Renkawitz-Pohl, R., Han, V. C., Wu, Y., & Galko, M. J. (2012). Transcriptional regulation of profilin during wound closure in Drosophila larvae. *Journal of Cell Science*, *125*(23), 5667–5676. https://doi.org/10.1242/jcs.107490

Brückner, K., Kockel, L., Duchek, P., Luque, C. M., Rorth, P., & Perrimon, N. (2004). The PDGF/VEGF receptor controls blood cell survival in Drosophila. *Developmental Cell*, *7*(1), 73–84.

Brummel, T., Abdollah, S., Haerry, T. E., Shimell, M. J., Merriam, J., Raftery, L., Wrana, J. L., & O'Connor, M. B. (1999). The Drosophila activin receptor Baboon signals through dSmad2 and controls cell proliferation but not patterning during larval development. *Genes and Development*, *13*(1), 98–111. https://doi.org/10.1101/gad.13.1.98

Brummel, T. J., Twombly, V., Marqués, G., Wrana, J. L., Newfeld, S. J., Attisano, L., Massagué, J., O'Connor, M. B., & Gelbart, W. M. (1994). Characterization and relationship of Dpp receptors encoded by the saxophone and thick veins genes in Drosophila. *Cell*, *78*(2), 251–261. https://doi.org/10.1016/0092-8674(94)90295-X

Bruveris, F. F., Ng, E. S., Leitoguinho, A. R., Motazedian, A., Vlahos, K., Sourris, K., Mayberry, R., McDonald, P., Azzola, L., Davidson, N. M., Oshlack, A., Stanley, E. G., & Elefanty, A. G. (2021). Human yolk sac-like haematopoiesis generates RUNX1-, GFI1- and/or GFI1B-dependent blood and SOX17-positive endothelium. *Development (Cambridge)*, *147*(20). https://doi.org/10.1242/DEV.193037/VIDEO-1

Buchon, N., Silverman, N., & Cherry, S. (2014). Immunity in Drosophila melanogaster — from microbial recognition to whole-organism physiology. *Nature Reviews Immunology 2014 14:12*, *14*(12), 796–810. https://doi.org/10.1038/nri3763

Bunt, S., Hooley, C., Hu, N., Scahill, C., Weavers, H., & Skaer, H. (2010). Hemocyte-secreted type IV collagen enhances BMP signaling to guide renal tubule morphogenesis in Drosophila. *Developmental Cell*, *19*(2), 296–306. https://doi.org/10.1016/j.devcel.2010.07.019

Butovsky, O., Jedrychowski, M. P., Moore, C. S., Cialic, R., Lanser, A. J., Gabriely, G., Koeglsperger, T., Dake, B., Wu, P. M., Doykan, C. E., Fanek, Z., Liu, L., Chen, Z., Rothstein, J. D., Ransohoff, R. M., Gygi, S. P., Antel, J. P., & Weiner, H. L. (2014). Identification of a Unique TGF-β Dependent Molecular and Functional Signature in Microglia. *Nature Neuroscience*, *17*(1), 131. https://doi.org/10.1038/NN.3599

Calero-Cuenca, F. J., Janota, C. S., & Gomes, E. R. (2018). Dealing with the nucleus during cell migration. *Current Opinion in Cell Biology*, *50*, 35–41. https://doi.org/10.1016/J.CEB.2018.01.014

Campos, I., Geiger, J. A., Santos, A. C., Carlos, V., & Jacinto, A. (2010). Genetic screen in Drosophila melanogaster uncovers a novel set of genes required for embryonic epithelial repair. *Genetics*, *184*(1), 129–140. https://doi.org/10.1534/GENETICS.109.110288

Canty, E. G., Garrigue-Antar, L., & Kadler, K. E. (2006). A Complete Domain Structure of Drosophila Tolloid Is Required for Cleavage of Short Gastrulation *. *Journal of Biological Chemistry*, *281*(19), 13258–13267. https://doi.org/10.1074/JBC.M510483200

Carmona-Fontaine, C., Matthews, H. K., Kuriyama, S., Moreno, M., Dunn, G. A., Parsons, M., Stern, C. D., & Mayor, R. (2008). Contact inhibition of locomotion in vivo controls neural

crest directional migration. *Nature*, *456*(7224), 957–961. https://doi.org/10.1038/NATURE07441

Cattenoz, P. B., Monticelli, S., Pavlidaki, A., & Giangrande, A. (2021). Toward a Consensus in the Repertoire of Hemocytes Identified in Drosophila Supplement. *Frontiers in Cell and Developmental Biology*, *9*. https://doi.org/10.3389/FCELL.2021.643712/FULL

Cattenoz, P. B., Sakr, R., Pavlidaki, A., Delaporte, C., Riba, A., Molina, N., Hariharan, N., Mukherjee, T., & Giangrande, A. (2020). Temporal specificity and heterogeneity of Drosophila immune cells. *The EMBO Journal*, *39*(12), e104486. https://doi.org/10.15252/EMBJ.2020104486

Caussinus, E., Colombelli, J., & Affolter, M. (2008). Tip-cell migration controls stalk-cell intercalation during Drosophila tracheal tube elongation. *Current Biology : CB*, *18*(22), 1727–1734. https://doi.org/10.1016/J.CUB.2008.10.062

Champion, T. C., Partridge, L. J., Ong, S. M., Malleret, B., Wong, S. C., & Monk, P. N. (2018). Monocyte Subsets Have Distinct Patterns of Tetraspanin Expression and Different Capacities to Form Multinucleate Giant Cells. *Frontiers in Immunology*, *9*(JUN). https://doi.org/10.3389/FIMMU.2018.01247

Chaplin, D. D. (n.d.). *Overview of the Immune Response*. *845*, 35294–2170. https://doi.org/10.1016/j.jaci.2009.12.980

Cheng, Y. L., & Andrew, D. J. (2015). Extracellular Mipp1 Activity Confers Migratory Advantage to Epithelial Cells during Collective Migration. *Cell Reports*, *13*(10), 2174–2188. https://doi.org/10.1016/j.celrep.2015.10.071

Childs, S. R., & O'connor, M. B. (1994). Two domains of the tolloid protein contribute to its unusual genetic interaction with decapentaplegic. *Developmental Biology*, *162*(1), 209–220. https://doi.org/10.1006/DBIO.1994.1079

Chiu, Y. H., & Chen, H. (2016). GATA3 inhibits GCM1 activity and trophoblast cell invasion. *Scientific Reports*, *6*. https://doi.org/10.1038/SREP21630

Cho, B., Yoon, S. H., Lee, D., Koranteng, F., Tattikota, S. G., Cha, N., Shin, M., Do, H., Hu, Y., Oh, S. Y., Lee, D., Vipin Menon, A., Moon, S. J., Perrimon, N., Nam, J. W., & Shim, J. (2020). Single-cell transcriptome maps of myeloid blood cell lineages in Drosophila. *Nature Communications*, *11*(1), 1–18. https://doi.org/10.1038/s41467-020-18135-y

Cho, N. K., Keyes, L., Johnson, E., Heller, J., Ryner, L., Karim, F., & Krasnow, M. A. (2002). Developmental control of blood cell migration by the drosophila VEGF pathway. *Cell*, *108*(6), 865–876. https://doi.org/10.1016/S0092-8674(02)00676-1

Choi, S., Yu, J., Park, A., Dubon, M. J., Do, J., Kim, Y., Nam, D., Noh, J., & Park, K. S. (2019). BMP-4 enhances epithelial mesenchymal transition and cancer stem cell properties of breast cancer cells via Notch signaling. *Scientific Reports 2019 9:1*, *9*(1), 1–14. https://doi.org/10.1038/s41598-019-48190-5

Clark, R. I., Woodcock, K. J., Geissmann, F., Trouillet, C., & Dionne, M. S. (2011a). Multiple TGF-β superfamily signals modulate the adult drosophila immune response. *Current Biology*, *21*(19), 1672–1677. https://doi.org/10.1016/J.CUB.2011.08.048/ATTACHMENT/6D330300-938F-4589-AACA-EAFF7D173691/MMC1.PDF

Clark, R. I., Woodcock, K. J., Geissmann, F., Trouillet, C., & Dionne, M. S. (2011b). Multiple TGF-β Superfamily Signals Modulate the Adult Drosophila Immune Response. *Current Biology*, *21*(19), 1672. https://doi.org/10.1016/J.CUB.2011.08.048

Coates, J. A., Brooks, E., Brittle, A. L., Armitage, E. L., Zeidler, M. P., & Evans, I. R. (2021). Identification of functionally distinct macrophage subpopulations in Drosophila. *ELife*,

10. https://doi.org/10.7554/ELIFE.58686

Comber, K., Huelsmann, S., Evans, I., Sánchez-Sánchez, B., Chalmers, a, Reuter, R., Wood, W., & Martín-Bermudo, M. (2013). A dual role for the βPS integrin myospheroid in mediating Drosophila embryonic macrophage migration. *Journal of Cell Science*, *126*(Pt 15), 3475–3484. https://doi.org/10.1242/jcs.129700

Couturier, L., Mazouni, K., Corson, F., & Schweisguth, F. (2019). Regulation of Notch output dynamics via specific E(spl)-HLH factors during bristle patterning in Drosophila. *Nature Communications*, *10*(1), 1–13. https://doi.org/10.1038/s41467-019-11477-2

Cramer, L. P. (1997). Molecular mechanism of actin-dependent retrograde flow in lamellipodia of motile cells. *Frontiers in Bioscience : A Journal and Virtual Library*, *2*. https://doi.org/10.2741/A189

Crozatier, M., Glise, B., & Vincent, A. (2004). Patterns in evolution: Veins of the Drosophila wing. *Trends in Genetics*, *20*(10), 498–505. https://doi.org/10.1016/j.tig.2004.07.013

Cunningham, C. L., Martínez-Cerdeño, V., & Noctor, S. C. (2013). Microglia Regulate the Number of Neural Precursor Cells in the Developing Cerebral Cortex. *Journal of Neuroscience*, *33*(10), 4216–4233. https://doi.org/10.1523/JNEUROSCI.3441-12.2013

Daga, A., Karlovich, C. A., Dumstrei, K., & Banerjee, U. (1996). Patterning of cells in the Drosophila eye by Lozenge, which shares homologous domains with AML1. *Genes & Development*, *10*(10), 1194–1205. https://doi.org/10.1101/GAD.10.10.1194

Dahlqvist, C., Blokzijl, A., Chapman, G., Falk, A., Dannaeus, K., Ibâñez, C. F., & Lendahl, U. (2003). Functional Notch signaling is required for BMP4-induced inhibition of myogenic differentiation. *Development (Cambridge, England)*, *130*(24), 6089–6099. https://doi.org/10.1242/DEV.00834

Das, P., Inoue, H., Baker, J. C., Beppu, H., Kawabata, M., Harland, R. M., Miyazono, K., & Padgett, R. W. (1999). Drosophila dSmad2 and Atr-I transmit activin/TGFβ signals. *Genes to Cells*, *4*(2), 123–134. https://doi.org/10.1046/J.1365-2443.1999.00244.X

Davies, L. C., Jenkins, S. J., Allen, J. E., & Taylor, P. R. (2013). Tissue-resident macrophages. *Nature Immunology 2013 14:10*, *14*(10), 986–995. https://doi.org/10.1038/ni.2705

Davis, J. R., Huang, C. Y., Zanet, J., Harrison, S., Rosten, E., Cox, S., Soong, D. Y., Dunn, G. A., & Stramer, B. M. (2012). Emergence of embryonic pattern through contact inhibition of locomotion. *Development (Cambridge)*, *139*(24), 4555–4560. https://doi.org/10.1242/DEV.082248/-/DC1

Davis, J. R., Luchici, A., Miodownik, M., Stramer, B. M., Davis, J. R., Luchici, A., Mosis, F., Thackery, J., Salazar, J. A., Mao, Y., Dunn, G. A., Betz, T., Miodownik, M., & Stramer, B. M. (2015). Inter-Cellular Forces Orchestrate Contact Inhibition of Locomotion Article Inter-Cellular Forces Orchestrate Contact Inhibition of Locomotion. *Cell*, *161*(2), 361–373. https://doi.org/10.1016/j.cell.2015.02.015

Davis, J. R., Luchici, A., Mosis, F., Thackery, J., Salazar, J. A., Mao, Y., Dunn, G. A., Betz, T., Miodownik, M., & Stramer, B. M. (2015). Inter-cellular forces orchestrate contact inhibition of locomotion. *Cell*, *161*(2), 361–373. https://doi.org/10.1016/j.cell.2015.02.015

Dawson, C. A., Pal, B., Vaillant, F., Gandolfo, L. C., Liu, Z., Bleriot, C., Ginhoux, F., Smyth, G. K., Lindeman, G. J., Mueller, S. N., Rios, A. C., & Visvader, J. E. (2020). Tissue-resident ductal macrophages survey the mammary epithelium and facilitate tissue remodelling. *Nature Cell Biology*, *22*(5), 546–558. https://doi.org/10.1038/S41556-020-0505-0

de Velasco, B., Mandal, L., Mkrtchyan, M., & Hartenstein, V. (2006). Subdivision and developmental fate of the head mesoderm in Drosophila melanogaster. *Development*

Genes and Evolution, *216*(1), 39–51. https://doi.org/10.1007/s00427-005-0029-4

DeFalco, T., Bhattacharya, I., Williams, A. V., Sams, D. M., & Capel, B. (2014). Yolk-sac-derived macrophages regulate fetal testis vascularization and morphogenesis. *Proceedings of the National Academy of Sciences of the United States of America*, *111*(23), E2384–E2393. https://doi.org/10.1073/PNAS.1400057111/-/DCSUPPLEMENTAL

Dequier, E., Souid, S., Pál, M., Maróy, P., Lepesant, J.-A., & Yanicostas, C. (2001). Top–DER- and Dpp-dependent requirements for the Drosophila fos/kayak gene in follicular epithelium morphogenesis. *Mechanisms of Development*, *106*(1–2), 47–60. https://doi.org/10.1016/S0925-4773(01)00418-X

Dey, N. S., Ramesh, P., Chugh, M., Mandal, S., & Mandal, L. (2016a). Dpp dependent hematopoietic stem cells give rise to Hh dependent blood progenitors in larval lymph gland of Drosophila. *ELife*, *5*(OCTOBER2016). https://doi.org/10.7554/ELIFE.18295

Dey, N. S., Ramesh, P., Chugh, M., Mandal, S., & Mandal, L. (2016b). Dpp dependent hematopoietic stem cells give rise to Hh dependent blood progenitors in larval lymph gland of Drosophila. *ELife*, *5*(OCTOBER2016). https://doi.org/10.7554/ELIFE.18295

Diz-Muñoz, A., Romanczuk, P., Yu, W., Bergert, M., Ivanovitch, K., Salbreux, G., Heisenberg, C. P., & Paluch, E. K. (2016). Steering cell migration by alternating blebs and actin-rich protrusions. *BMC Biology*, *14*(1), 1–13. https://doi.org/10.1186/S12915-016-0294-X/FIGURES/5

Dobin, A., Davis, C. A., Schlesinger, F., Drenkow, J., Zaleski, C., Jha, S., Batut, P., Chaisson, M., & Gingeras, T. R. (2013). STAR: Ultrafast universal RNA-seq aligner. *Bioinformatics*, *29*(1), 15–21. https://doi.org/10.1093/bioinformatics/bts635

Donà, E., Barry, J. D., Valentin, G., Quirin, C., Khmelinskii, A., Kunze, A., Durdu, S., Newton, L. R., Fernandez-Minan, A., Huber, W., Knop, M., & Gilmour, D. (2013). Directional tissue migration through a self-generated chemokine gradient. *Nature*, *503*(7475), 285–289. https://doi.org/10.1038/NATURE12635

Doyle, E. L., Ridger, V., Ferraro, F., Turmaine, M., Saftig, P., & Cutler, D. F. (2011). CD63 is an essential cofactor to leukocyte recruitment by endothelial P-selectin. *Blood*, *118*(15), 4265–4273. https://doi.org/10.1182/BLOOD-2010-11-321489

Drevon, C., & Jaffredo, T. (2014). Cell interactions and cell signaling during hematopoietic development. *Experimental Cell Research*, *329*(2), 200–206. https://doi.org/10.1016/J.YEXCR.2014.10.009

Dudzic, J. P., Kondo, S., Ueda, R., Bergman, C. M., & Lemaitre, B. (2015). Drosophila innate immunity: regional and functional specialization of prophenoloxidases. *BMC Biology*, *13*(1). https://doi.org/10.1186/S12915-015-0193-6

Durand, C., Robin, C., Bollerot, K., Baron, M. H., Ottersbach, K., & Dzierzak, E. (2007). Embryonic stromal clones reveal developmental regulators of definitive hematopoietic stem cells. *Proceedings of the National Academy of Sciences*, *104*(52), 20838–20843. https://doi.org/10.1073/PNAS.0706923105

Duvic, B., Hoffmann, J. A., Meister, M., & Royet, J. (2002). Notch signaling controls lineage specification during Drosophila larval hematopoiesis. *Current Biology : CB*, *12*(22), 1923–1927. https://doi.org/10.1016/S0960-9822(02)01297-6

Dzierzak, E., & Speck, N. A. (2008). Of lineage and legacy – the development of mammalian hematopoietic stem cells. *Nature Immunology*, *9*(2), 129. https://doi.org/10.1038/NI1560

Elagib, K. E., Racke, F. K., Mogass, M., Khetawat, R., Delehanty, L. L., & Goldfarb, A. N. (2003). RUNX1 and GATA-1 coexpression and cooperation in megakaryocytic differentiation.

Blood, *101*(11), 4333–4341. https://doi.org/10.1182/BLOOD-2002-09-2708

Emtenani, S., Martin, E. T., Gyoergy, A., Bicher, J., Genger, J.-W., Hurd, T. R., Köcher, T., Bergthaler, A., Rangan, P., & Siekhaus, D. E. (2021). A genetic program boosts mitochondrial function to power macrophage tissue invasion. *BioRxiv*, 2021.02.18.431643. https://doi.org/10.1101/2021.02.18.431643

Eresh, S., Riese, J., Jackson, D. B., Bohmann, D., & Bienz, M. (1997). A CREB-binding site as a target for decapentaplegic signalling during Drosophila endoderm induction. *EMBO Journal*, *16*(8), 2014–2022. https://doi.org/10.1093/emboj/16.8.2014

Etienne-Manneville, S. (2008). Polarity proteins in migration and invasion. *Oncogene*, *27*(55), 6970–6980. https://doi.org/10.1038/ONC.2008.347

Evans, C. J., Hartenstein, V., & Banerjee, U. (2003). Thicker than blood: Conserved mechanisms in Drosophila and vertebrate hematopoiesis. In *Developmental Cell* (Vol. 5, Issue 5, pp. 673–690). Cell Press. https://doi.org/10.1016/S1534-5807(03)00335-6

Evans, C. J., Sinenko, S. A., Mandal, L., Martinez-Agosto, J. A., Hartenstein, V., & Banerjee, U. (2007). Genetic Dissection of Hematopoiesis Using Drosophila as a Model System. *Advances in Developmental Biology*, *18*(07), 259–299. https://doi.org/10.1016/S1574-3349(07)18011-X

Evans, Iwan R., Hu, N., Skaer, H., & Wood, W. (2010). Interdependence of macrophage migration and ventral nerve cord development in Drosophila embryos. *Development*, *137*(10), 1625–1633. https://doi.org/10.1242/dev.046797

Evans, Iwan Robert, & Wood, W. (2011). Drosophila embryonic hemocytes. *Current Biology*, *21*(5), R173–R174. https://doi.org/10.1016/j.cub.2011.01.061

Fantin, A., Vieira, J. M., Gestri, G., Denti, L., Schwarz, Q., Prykhozhij, S., Peri, F., Wilson, S. W., & Ruhrberg, C. (2010). Tissue macrophages act as cellular chaperones for vascular anastomosis downstream of VEGF-mediated endothelial tip cell induction. *Blood*, *116*(5), 829–840. https://doi.org/10.1182/BLOOD-2009-12-257832

Ferguson, E. L., & Anderson, K. V. (1992). Decapentaplegic acts as a morphogen to organize dorsal-ventral pattern in the Drosophila embryo. *Cell*, *71*(3), 451–461. https://doi.org/10.1016/0092-8674(92)90514-D

Fernández, B. G., Arias, A. M., & Jacinto, A. (2007). Dpp signalling orchestrates dorsal closure by regulating cell shape changes both in the amnioserosa and in the epidermis. *Mechanisms of Development*, *124*(11–12), 884–897. https://doi.org/10.1016/J.MOD.2007.09.002

Fossett, N., Hyman, K., Gajewski, K., Orkin, S. H., & Schulz, R. A. (2003). Combinatorial interactions of serpent, lozenge, and U-shaped regulate crystal cell lineage commitment during Drosophila hematopoiesis. *Proceedings of the National Academy of Sciences of the United States of America*, *100*(20), 11451–11456. https://doi.org/10.1073/PNAS.1635050100

François, V., Solloway, M., O'Neill, J. W., Emery, J., & Bier, E. (1994). Dorsal-ventral patterning of the Drosophila embryo depends on a putative negative growth factor encoded by the short gastrulation gene. *Genes & Development*, *8*(21), 2602–2616. https://doi.org/10.1101/GAD.8.21.2602

Frey, P., Devisme, A., Schrempp, M., Andrieux, G., Boerries, M., & Hecht, A. (2020). Canonical BMP Signaling Executes Epithelial-Mesenchymal Transition Downstream of SNAIL1. *Cancers*, *12*(4). https://doi.org/10.3390/CANCERS12041019

Friedl, P., & Alexander, S. (2011). Cancer Invasion and the Microenvironment: Plasticity and Reciprocity. *Cell*, *147*(5), 992–1009. https://doi.org/10.1016/J.CELL.2011.11.016

Friedl, P., & Weigelin, B. (2008). Interstitial leukocyte migration and immune function. *Nat Immunol*, *9*(9), 960–969. http://dx.doi.org/10.1038/ni.f.212

Fu, Y., Huang, X., Zhang, P., van de Leemput, J., & Han, Z. (2020). Single-cell RNA sequencing identifies novel cell types in Drosophila blood. *Journal of Genetics and Genomics*, *47*(4), 175–186. https://doi.org/10.1016/j.jgg.2020.02.004

Fujiwara, Y., Chang, A. N., Williams, A. M., & Orkin, S. H. (2004). Functional overlap of GATA-1 and GATA-2 in primitive hematopoietic development. *Blood*, *103*(2), 583–585. https://doi.org/10.1182/blood-2003-08-2870

Gautiar, E. L., Shay, T., Miller, J., Greter, M., Jakubzick, C., Ivanov, S., Helft, J., Chow, A., Elpek, K. G., Gordonov, S., Mazloom, A. R., Ma'Ayan, A., Chua, W. J., Hansen, T. H., Turley, S. J., Merad, M., Randolph, G. J., Best, A. J., Knell, J., … Benoist, C. (2012). Gene-expression profiles and transcriptional regulatory pathways that underlie the identity and diversity of mouse tissue macrophages. *Nature Immunology*, *13*(11), 1118–1128. https://doi.org/10.1038/NI.2419

Ghabrial, A. S., & Krasnow, M. A. (2006). Social interactions among epithelial cells during tracheal branching morphogenesis. *Nature*, *441*(7094), 746–749. https://doi.org/10.1038/NATURE04829

Gold, K. S., & Brückner, K. (2014). Drosophila as a model for the two myeloid blood cell systems in vertebrates. *Experimental Hematology*, *42*(8), 717–727. https://doi.org/10.1016/j.exphem.2014.06.002

Gong, D., Shi, W., Yi, S. ju, Chen, H., Groffen, J., & Heisterkamp, N. (2012). TGFβ signaling plays a critical role in promoting alternative macrophage activation. *BMC Immunology*, *13*(1), 1–10. https://doi.org/10.1186/1471-2172-13-31/FIGURES/3

Gouon-Evans, V., Rothenberg, M. E., & Pollard, J. W. (2000). Postnatal mammary gland development requires macrophages and eosinophils. *Development*, *127*(11), 2269–2282. https://doi.org/10.1242/DEV.127.11.2269

Gout, S., & Huot, J. (2008). Role of cancer microenvironment in metastasis: Focus on colon cancer. *Cancer Microenvironment*, *1*(1), 69–83. https://doi.org/10.1007/s12307-008-0007-2

Graveley, B. R., Brooks, A. N., Carlson, J. W., Duff, M. O., Landolin, J. M., Yang, L., Artieri, C. G., Van Baren, M. J., Boley, N., Booth, B. W., Brown, J. B., Cherbas, L., Davis, C. A., Dobin, A., Li, R., Lin, W., Malone, J. H., Mattiuzzo, N. R., Miller, D., … Celniker, S. E. (2010). The developmental transcriptome of Drosophila melanogaster. *Nature 2010 471:7339*, *471*(7339), 473–479. https://doi.org/10.1038/nature09715

Gregory Call, S., Brereton, D., Bullard, J. T., Chung, J. Y., Meacham, K. L., Morrell, D. J., Reeder, D. J., Schuler, J. T., Slade, A. D., & Hansen, M. D. H. (2011). A zyxin–nectin interaction facilitates zyxin localization to cell–cell adhesions. *Biochemical and Biophysical Research Communications*, *415*(3), 485–489. https://doi.org/10.1016/J.BBRC.2011.10.099

Grenningloh, G., Jay Rehm, E., & Goodman, C. S. (1991). Genetic analysis of growth cone guidance in drosophila: Fasciclin II functions as a neuronal recognition molecule. *Cell*, *67*(1), 45–57. https://doi.org/10.1016/0092-8674(91)90571-F

Grimaldi, C., Schumacher, I., Boquet-Pujadas, A., Tarbashevich, K., Vos, B. E., Bandemer, J., Schick, J., Aalto, A., Olivo-Marin, J. C., Betz, T., & Raz, E. (2020). E-cadherin focuses protrusion formation at the front of migrating cells by impeding actin flow. *Nature Communications 2020 11:1*, *11*(1), 1–15. https://doi.org/10.1038/s41467-020-19114-z

Gyoergy, A., Roblek, M., Ratheesh, A., Valoskova, K., Belyaeva, V., Wachner, S., Matsubayashi, Y., Sánchez-Sánchez, B. J., Stramer, B., & Siekhaus, D. E. (2018). Tools allowing

independent visualization and genetic manipulation of Drosophila melanogaster macrophages and surrounding tissues. *G3: Genes, Genomes, Genetics*, *8*(3). https://doi.org/10.1534/g3.117.300452

Haerry, T. E., Khalsa, O., O'Connor, M. B., & Wharton, K. A. (1998). Synergistic signaling by two BMP ligands through the SAX and TKV receptors controls wing growth and patterning in Drosophila. *Development*, *125*(20), 3977–3987. https://doi.org/10.1242/DEV.125.20.3977

Hamaratoglu, F., de Lachapelle, A. M., Pyrowolakis, G., Bergmann, S., & Affolter, M. (2011). Dpp Signaling Activity Requires Pentagone to Scale with Tissue Size in the Growing Drosophila Wing Imaginal Disc. *PLoS Biology*, *9*(10). https://doi.org/10.1371/JOURNAL.PBIO.1001182

Harris, K. E., Schnittke, N., & Beckendorf, S. K. (2007). Two Ligands Signal Through the Drosophila PDGF/VEGF Receptor to Ensure Proper Salivary Gland Positioning. *Mechanisms of Development*, *124*(6), 441. https://doi.org/10.1016/J.MOD.2007.03.003

Heino, T. I., Kärpänen, T., Wahlström, G., Pulkkinen, M., Eriksson, U., Alitalo, K., & Roos, C. (2001). The Drosophila VEGF receptor homolog is expressed in hemocytes. *Mechanisms of Development*, *109*(1), 69–77. https://doi.org/10.1016/S0925-4773(01)00510-X

Hellström, M., Phng, L. K., Hofmann, J. J., Wallgard, E., Coultas, L., Lindblom, P., Alva, J., Nilsson, A. K., Karlsson, L., Gaiano, N., Yoon, K., Rossant, J., Iruela-Arispe, M. L., Kalén, M., Gerhardt, H., & Betsholtz, C. (2007). Dll4 signalling through Notch1 regulates formation of tip cells during angiogenesis. *Nature*, *445*(7129), 776–780. https://doi.org/10.1038/NATURE05571

Heyder, C., Gloria-Maercker, E., Hatzmann, W., Niggemann, B., Zänker, K. S., & Dittmar, T. (2005). Role of the β1-integrin subunit in the adhesion, extravasation and migration of T24 human bladder carcinoma cells. *Clinical and Experimental Metastasis*, *22*(2), 99–106. https://doi.org/10.1007/s10585-005-4335-z

Hollmén, M., Karaman, S., Schwager, S., Lisibach, A., Christiansen, A. J., Maksimow, M., Varga, Z., Jalkanen, S., & Detmar, M. (2016). G-CSF regulates macrophage phenotype and associates with poor overall survival in human triple-negative breast cancer. *OncoImmunology*, *5*(3). https://doi.org/10.1080/2162402X.2015.1115177/SUPPL_FILE/KONI_A_1115177_SM2985.PDF

Holz, A., Bossinger, B., Strasser, T., Janning, W., & Klapper, R. (2003). The two origins of hemocytes in Drosophila. *Development*, *130*(20), 4955–4962. https://doi.org/10.1242/DEV.00702

Ingman, W. V., Wyckoff, J., Gouon-Evans, V., Condeelis, J., & Pollard, J. W. (2006). Macrophages promote collagen fibrillogenesis around terminal end buds of the developing mammary gland. *Developmental Dynamics : An Official Publication of the American Association of Anatomists*, *235*(12), 3222–3229. https://doi.org/10.1002/DVDY.20972

Inoue, H., Imamura, T., Ishidou, Y., Takase, M., Udagawa, Y., Oka, Y., Tsuneizumi, K., Tabata, T., Miyazono, K., & Kawabata, M. (1998). Interplay of Signal Mediators of Decapentaplegic (Dpp): Molecular Characterization of Mothers against dpp, Medea, and Daughters against dpp. *Molecular Biology of the Cell*, *9*(8), 2145. https://doi.org/10.1091/MBC.9.8.2145

Inoue, T., Abe, C., Kohro, T., Tanaka, S., Huang, L., Yao, J., Zheng, S., Ye, H., Inagi, R., Stornetta, R. L., Rosin, D. L., Nangaku, M., Wada, Y., & Okusa, M. D. (2019). Non-canonical

cholinergic anti-inflammatory pathway-mediated activation of peritoneal macrophages induces Hes1 and blocks ischemia/reperfusion injury in the kidney. *Kidney International*, *95*(3), 563. https://doi.org/10.1016/J.KINT.2018.09.020

Irving, P., Ubeda, J. M., Doucet, D., Troxler, L., Lagueux, M., Zachary, D., Hoffmann, J. A., Hetru, C., & Meister, M. (2005). New insights into Drosophila larval haemocyte functions through genome-wide analysis. *Cellular Microbiology*, *7*(3), 335–350. https://doi.org/10.1111/J.1462-5822.2004.00462.X

Italiani, P., & Boraschi, D. (2014). From monocytes to M1/M2 macrophages: Phenotypical vs. functional differentiation. *Frontiers in Immunology*, *5*(OCT), 514. https://doi.org/10.3389/FIMMU.2014.00514/BIBTEX

Itoh, F., Itoh, S., Goumans, M. J., Valdimarsdottir, G., Iso, T., Dotto, G. P., Hamamori, Y., Kedes, L., Kato, M., & Ten Dijke, P. (2004). Synergy and antagonism between Notch and BMP receptor signaling pathways in endothelial cells. *The EMBO Journal*, *23*(3), 541. https://doi.org/10.1038/SJ.EMBOJ.7600065

Johansson, B. M., & Wiles, M. V. (1995). Evidence for involvement of activin A and bone morphogenetic protein 4 in mammalian mesoderm and hematopoietic development. *Molecular and Cellular Biology*, *15*(1), 141–151. https://doi.org/10.1128/MCB.15.1.141

Jones, C. V., Williams, T. M., Walker, K. A., Dickinson, H., Sakkal, S., Rumballe, B. A., Little, M. H., Jenkin, G., & Ricardo, S. D. (2013). M2 macrophage polarisation is associated with alveolar formation during postnatal lung development. *Respiratory Research*, *14*(1). https://doi.org/10.1186/1465-9921-14-41

Jung, S. H., Evans, C. J., Uemura, C., & Banerjee, U. (2005). The Drosophila lymph gland as a developmental model of hematopoiesis. *Development (Cambridge, England)*, *132*(11), 2521–2533. https://doi.org/10.1242/DEV.01837

Kallio, J., Leinonen, A., Ulvila, J., Valanne, S., Ezekowitz, R. A., & Rämet, M. (2005). Functional analysis of immune response genes in Drosophila identifies JNK pathway as a regulator of antimicrobial peptide gene expression in S2 cells. *Microbes and Infection*, *7*(5–6), 811–819. https://doi.org/10.1016/J.MICINF.2005.03.014

Kamiya, Y., Miyazono, K., & Miyazawa, K. (2008). Specificity of the inhibitory effects of Dad on TGF-β family type I receptors, Thickveins, Saxophone, and Baboon in Drosophila. *FEBS Letters*, *582*(17), 2496–2500. https://doi.org/10.1016/J.FEBSLET.2008.05.052

Kel, J. M., Girard-Madoux, M. J. H., Reizis, B., & Clausen, B. E. (2010). TGF- Is Required To Maintain the Pool of Immature Langerhans Cells in the Epidermis. *The Journal of Immunology*, *185*(6), 3248–3255. https://doi.org/10.4049/jimmunol.1000981

Khadilkar, R. J., Ho, K. Y. L., Venkatesh, B., & Tanentzapf, G. (2020). Integrins Modulate Extracellular Matrix Organization to Control Cell Signaling during Hematopoiesis. *Current Biology*, *30*(17), 3316-3329.e5. https://doi.org/10.1016/J.CUB.2020.06.027/ATTACHMENT/F8C90D31-9CAC-4CF5-8328-BC99F9CCBD95/MMC1.PDF

Khalil, A. A., & Friedl, P. (2010). Determinants of leader cells in collective cell migrationw. *This Journal Is*, *2*, 568–574. https://doi.org/10.1039/c0ib00052c

Kim, J., Johnson, K., Chen, H. J., Carroll, S., & Laughon, A. (1997). Drosophila Mad binds to DNA and directly mediates activation of vestigial by Decapentaplegic. *Nature 1997 388:6639*, *388*(6639), 304–308. https://doi.org/10.1038/40906

Kinugasa, M., Amano, H., Satomi-Kobayashi, S., Nakayama, K., Miyata, M., Kubo, Y., Nagamatsu, Y., Kurogane, Y., Kureha, F., Yamana, S., Hirata, K. I., Miyoshi, J., Takai, Y., & Rikitake, Y. (2012). Necl-5/poliovirus receptor interacts with VEGFR2 and regulates VEGF-

induced angiogenesis. *Circulation Research*, *110*(5), 716–726. https://doi.org/10.1161/CIRCRESAHA.111.256834

Kirmizitas, A., Meiklejohn, S., Ciau-Uitz, A., Stephenson, R., & Patient, R. (2017). Dissecting BMP signaling input into the gene regulatory networks driving specification of the blood stem cell lineage. *Proceedings of the National Academy of Sciences of the United States of America*, *114*(23), 5814–5821. https://doi.org/10.1073/PNAS.1610615114

Kubo, A., Nagao, K., Yokouchi, M., Sasaki, H., & Amagai, M. (2009). External antigen uptake by Langerhans cells with reorganization of epidermal tight junction barriers. *Journal of Experimental Medicine*, *206*(13), 2937–2946. https://doi.org/10.1084/JEM.20091527

Külshammer, E., Mundorf, J., Kilinc, M., Frommolt, P., Wagle, P., & Uhlirova, M. (2015). Interplay among Drosophila transcription factors Ets21c, Fos and Ftz-F1 drives JNK-mediated tumor malignancy. *DMM Disease Models and Mechanisms*, *8*(10), 1279–1293. https://doi.org/10.1242/dmm.020719

Külshammer, E., & Uhlirova, M. (2013). The actin cross-linker Filamin/Cheerio mediates tumor malignancy downstream of JNK signaling. *Journal of Cell Science*, *126*(4), 927–938. https://doi.org/10.1242/jcs.114462

Kunwar, P. S., Siekhaus, D. E., & Lehmann, R. (2006). In vivo migration: a germ cell perspective. *Annual Review of Cell and Developmental Biology*, *22*, 237–265. https://doi.org/10.1146/ANNUREV.CELLBIO.22.010305.103337

Kuriyama, S., Theveneau, E., Benedetto, A., Parsons, M., Tanaka, M., Charras, G., Kabla, A., & Mayor, R. (2014). In vivo collective cell migration requires an LPAR2-dependent increase in tissue fluidity. *The Journal of Cell Biology*, *206*(1), 113–127. https://doi.org/10.1083/JCB.201402093

Kurucz, É., Váczi, B., Márkus, R., Laurinyecz, B., Vilmos, P., Zsámboki, J., Csorba, K., Gateff, E., Hultmark, D., & Andó, I. (2007). Definition of Drosophila hemocyte subsets by cell-type specific antigens. *Acta Biologica Hungarica*, *58 Suppl*(SUPPL. 1), 95–111. https://doi.org/10.1556/ABIOL.58.2007.SUPPL.8

Kutty, G., Kutty, R. K., Samuel, W., Duncan, T., Jaworski, C., & Wiggert, B. (1998). Identification of a New Member of Transforming Growth Factor-Beta Superfamily inDrosophila:The First Invertebrate Activin Gene. *Biochemical and Biophysical Research Communications*, *246*(3), 644–649. https://doi.org/10.1006/BBRC.1998.8678

Labernadie, A., Kato, T., Brugués, A., Serra-Picamal, X., Derzsi, S., Arwert, E., Weston, A., González-Tarragó, V., Elosegui-Artola, A., Albertazzi, L., Alcaraz, J., Roca-Cusachs, P., Sahai, E., & Trepat, X. (2017). A mechanically active heterotypic E-cadherin/N-cadherin adhesion enables fibroblasts to drive cancer cell invasion. *Nature Cell Biology 2017 19:3*, *19*(3), 224–237. https://doi.org/10.1038/ncb3478

Lämmermann, T., Bader, B. L., Monkley, S. J., Worbs, T., Wedlich-Söldner, R., Hirsch, K., Keller, M., Förster, R., Critchley, D. R., Fässler, R., & Sixt, M. (2008). Rapid leukocyte migration by integrin-independent flowing and squeezing. *Nature*, *453*(7191), 51–55. https://doi.org/10.1038/NATURE06887

Lebestky, T., Chang, T., Hartenstein, V., & Banerjee, U. (2000). Specification of Drosophila hematopoietic lineage by conserved transcription factors. *Science*, *288*(5463). https://doi.org/10.1126/science.288.5463.146

Lebreton, G., & Casanova, J. (2014). Specification of leading and trailing cell features during collective migration in the Drosophila trachea. *Development*, *141*(4), e407–e407. https://doi.org/10.1242/DEV.108464

Lee-Hoeflich, S. T., Zhao, X., Mehra, A., & Attisano, L. (2005). The Drosophila type II receptor,

Wishful thinking, binds BMP and myoglianin to activate multiple TGFbeta family signaling pathways. *FEBS Letters*, *579*(21), 4615–4621. https://doi.org/10.1016/J.FEBSLET.2005.06.088

Lenz, K. M., & Nelson, L. H. (2018). Microglia and beyond: Innate immune cells as regulators of brain development and behavioral function. *Frontiers in Immunology*, *9*(APR), 698. https://doi.org/10.3389/FIMMU.2018.00698/BIBTEX

Lesch, C., Jo, J., Wu, Y., Fish, G. S., & Galko, M. J. (2010). A Targeted UAS-RNAi Screen in Drosophila Larvae Identifies Wound Closure Genes Regulating Distinct Cellular Processes. *Genetics*, *186*(3), 943–957. https://doi.org/10.1534/GENETICS.110.121822

Letourneau, M., Lapraz, F., Sharma, A., Vanzo, N., Waltzer, L., & Crozatier, M. (2016). Drosophila hematopoiesis under normal conditions and in response to immune stress. *FEBS Letters*, *590*(22), 4034–4051. https://doi.org/10.1002/1873-3468.12327

Lin, D. M., Fetter, R. D., Kopczynski, C., Grenningloh, G., & Goodman, C. S. (1994). Genetic analysis of Fasciclin II in Drosophila: defasciculation, refasciculation, and altered fasciculation. *Neuron*, *13*(5), 1055–1069. https://doi.org/10.1016/0896-6273(94)90045-0

Lin, Y., Xu, J., & Lan, H. (2019). Tumor-associated macrophages in tumor metastasis: biological roles and clinical therapeutic applications. *Journal of Hematology & Oncology 2019 12:1*, *12*(1), 1–16. https://doi.org/10.1186/S13045-019-0760-3

Lo, P. C. H., & Frasch, M. (1999). Sequence and expression of myoglianin, a novel Drosophila gene of the TGF-β superfamily. *Mechanisms of Development*, *86*(1–2), 171–175. https://doi.org/10.1016/S0925-4773(99)00108-2

Lomakin, A. J., Cattin, C. J., Cuvelier, D., Alraies, Z., Molina, M., Nader, G. P. F., Srivastava, N., Saez, P. J., Garcia-Arcos, J. M., Zhitnyak, I. Y., Bhargava, A., Driscoll, M. K., Welf, E. S., Fiolka, R., Petrie, R. J., de Silva, N. S., González-Granado, J. M., Manel, N., Lennon-Duménil, A. M., … Piel, M. (2020). The nucleus acts as a ruler tailoring cell responses to spatial constraints. *Science (New York, N.Y.)*, *370*(6514). https://doi.org/10.1126/SCIENCE.ABA2894

Makhijani, K., Alexander, B., Rao, D., Petraki, S., Herboso, L., Kukar, K., Batool, I., Wachner, S., Gold, K. S., Wong, C., O'Connor, M. B., & Brückner, K. (2017). Regulation of Drosophila hematopoietic sites by Activin-β from active sensory neurons. *Nature Communications*, *8*, 15990. https://doi.org/10.1038/ncomms15990

Makhijani, K., Alexander, B., Tanaka, T., Rulifson, E., & Brückner, K. (2011). The peripheral nervous system supports blood cell homing and survival in the Drosophila larva. *Development (Cambridge, England)*, *138*(24), 5379–5391. https://doi.org/10.1242/DEV.067322

Mancini, E., Sanjuan-Pla, A., Luciani, L., Moore, S., Grover, A., Zay, A., Rasmussen, K. D., Luc, S., Bilbao, D., O'Carroll, D., Jacobsen, S. E., & Nerlov, C. (2012). FOG-1 and GATA-1 act sequentially to specify definitive megakaryocytic and erythroid progenitors. *The EMBO Journal*, *31*(2), 351. https://doi.org/10.1038/EMBOJ.2011.390

Mandal, L., Banerjee, U., & Hartenstein, V. (2004). Evidence for a fruit fly hemangioblast and similarities between lymph-gland hematopoiesis in fruit fly and mammal aorta-gonadal-mesonephros mesoderm. *Nature Genetics 2004 36:9*, *36*(9), 1019–1023. https://doi.org/10.1038/ng1404

Mannion, B. A., Berditchevski, F., Kraeft, S. K., Chen, L. B., & Hemler, M. E. (1996). Transmembrane-4 superfamily proteins CD81 (TAPA-1), CD82, CD63, and CD53 specifically associated with integrin alpha 4 beta 1 (CD49d/CD29). *The Journal of*

Immunology, *157*(5).

Marqués, G., Bao, H., Haerry, T. E., Shimell, M. J., Duchek, P., Zhang, B., & O'Connor, M. B. (2002). The Drosophila BMP Type II Receptor Wishful Thinking Regulates Neuromuscular Synapse Morphology and Function. *Neuron*, *33*(4), 529–543. https://doi.org/10.1016/S0896-6273(02)00595-0

Marqués, G., Musacchio, M., Shimell, M. J., Wünnenberg-Stapleton, K., Cho, K. W. Y., & O'Connor, M. B. (1997). Production of a DPP activity gradient in the early Drosophila embryo through the opposing actions of the SOG and TLD proteins. *Cell*, *91*(3), 417–426. https://doi.org/10.1016/S0092-8674(00)80425-0

Martin, M. (2011). Cutadapt removes adapter sequences from high-throughput sequencing reads. *EMBnet.Journal*, *17*(1), 10. https://doi.org/10.14806/EJ.17.1.200

Martínez, V. G., Rubio, C., Onica Martínez-Fern Andez, M., Segovia, C., Opez-Calder On, F. L., Garín, M. I., Teijeira, A., Munera-Maravilla, E., Varas, A., Saced On, R., Elix Guerrero, F., Villacampa, F., De La Rosa, F., Castellano, D., L Opez-Collazo, E., Us, J., Paramio, M., Vicente, A., & Due˜ Nas, M. (2017). *Biology of Human Tumors BMP4 Induces M2 Macrophage Polarization and Favors Tumor Progression in Bladder Cancer*. https://doi.org/10.1158/1078-0432.CCR-17-1004

Matunis, E., Tran, J., Gönczy, P., Caldwell, K., & DiNardo, S. (1997). punt and schnurri regulate a somatically derived signal that restricts proliferation of committed progenitors in the germline. *Development*, *124*(21), 4383–4391. https://doi.org/10.1242/DEV.124.21.4383

McLennan, R., Schumacher, L. J., Morrison, J. A., Teddy, J. M., Ridenour, D. A., Box, A. C., Semerad, C. L., Li, H., McDowell, W., Kay, D., Maini, P. K., Baker, R. E., & Kulesa, P. M. (2015). Neural crest migration is driven by a few trailblazer cells with a unique molecular signature narrowly confined to the invasive front. *Development (Cambridge)*, *142*(11), 2014–2025. https://doi.org/10.1242/DEV.117507/VIDEO-2

Milde-Langosch, K. (2005). The Fos family of transcription factors and their role in tumourigenesis. *European Journal of Cancer*, *41*(16), 2449–2461. https://doi.org/10.1016/j.ejca.2005.08.008

Monteiro, R., Pinheiro, P., Joseph, N., Peterkin, T., Koth, J., Repapi, E., Bonkhofer, F., Kirmizitas, A., & Patient, R. (2016). Transforming Growth Factor β Drives Hemogenic Endothelium Programming and the Transition to Hematopoietic Stem Cells. *Developmental Cell*, *38*(4), 358–370. https://doi.org/10.1016/j.devcel.2016.06.024

Morikawa, M., Derynck, R., & Miyazono, K. (2016). TGF-β and the TGF-β Family: Context-Dependent Roles in Cell and Tissue Physiology. *Cold Spring Harbor Perspectives in Biology*, *8*(5). https://doi.org/10.1101/cshperspect.a021873

Morrison, J. A., McLennan, R., Wolfe, L. A., Gogol, M. M., Meier, S., McKinney, M. C., Teddy, J. M., Holmes, L., Semerad, C. L., Box, A. C., Li, H., Hall, K. E., Perera, A. G., & Kulesa, P. M. (2017). Single-cell transcriptome analysis of avian neural crest migration reveals signatures of invasion and molecular transitions. *ELife*, *6*. https://doi.org/10.7554/ELIFE.28415

Morrison, S. J., & Scadden, D. T. (2014). The bone marrow niche for haematopoietic stem cells. *Nature*, *505*(7483), 327. https://doi.org/10.1038/NATURE12984

Moya, I. M., Umans, L., Maas, E., Pereira, P. N., Beets, K., Francis, A., Sents, W., Robertson, E. J., Mummery, C. L., Huylebroeck, D., & Zwijsen, A. (2012). *Article Stalk Cell Phenotype Depends on Integration of Notch and Smad1/5 Signaling Cascades*. https://doi.org/10.1016/j.devcel.2012.01.007

Muratoglu, S., Garratt, B., Hyman, K., Gajewski, K., Schulz, R. A., & Fossett, N. (2006).

Regulation of Drosophila friend of GATA gene, u-shaped, during hematopoiesis: a direct role for serpent and lozenge. *Developmental Biology*, *296*(2), 561–579. https://doi.org/10.1016/J.YDBIO.2006.04.455

Murray, P. J., & Wynn, T. A. (2011). Protective and pathogenic functions of macrophage subsets. *Nature Reviews Immunology 2011 11:11*, *11*(11), 723–737. https://doi.org/10.1038/nri3073

Myers, D. C., Sepich, D. S., & Solnica-Krezel, L. (2002). Bmp Activity Gradient Regulates Convergent Extension during Zebrafish Gastrulation. *Developmental Biology*, *243*(1), 81–98. https://doi.org/10.1006/DBIO.2001.0523

Nakagawa, T., Li, J. H., Garcia, G., Mu, W., Piek, E., Böttinger, E. P., Chen, Y., Zhu, H. J., Kang, D. H., Schreiner, G. F., Lan, H. Y., & Johnson, R. J. (2004). TGF-beta induces proangiogenic and antiangiogenic factors via parallel but distinct Smad pathways. *Kidney International*, *66*(2), 605–613. https://doi.org/10.1111/J.1523-1755.2004.00780.X

Nakayama, T., Cui, Y., & Christian, J. L. (2000). Regulation of BMP/Dpp signaling during embryonic development. *Cellular and Molecular Life Sciences : CMLS*, *57*(6), 943–956. https://doi.org/Doi 10.1007/Pl00000736

Nellen, D., Burke, R., Struhl, G., & Basler, K. (1996). Direct and Long-Range Action of a DPP Morphogen Gradient. *Cell*, *85*(3), 357–368. https://doi.org/10.1016/S0092-8674(00)81114-9

Neuert, H., Deing, P., Krukkert, K., Naffin, E., Steffes, G., Risse, B., Silies, M., & Klambt, C. (2020). The Drosophila NCAM homolog Fas2 signals independently of adhesion. *Development (Cambridge)*, *147*(2). https://doi.org/10.1242/DEV.181479/VIDEO-6

Newfeld, S. J., Chartoff, E. H., Graft, J. M., Melton, D. A., & Gelbart, W. M. (1996). Mothers against dpp encodes a conserved cytoplasmic protein required in DPP/TGF-beta responsive cells. *Development*, *122*(7), 2099–2108. https://doi.org/10.1242/DEV.122.7.2099

Newfeld, S. J., Mehra, A., Singer, M. A., Wrana, J. L., Attisano, L., & Gelbart, W. M. (1997). Mothers against dpp participates in a DDP/TGF-beta responsive serine-threonine kinase signal transduction cascade. *Development*, *124*(16), 3167–3176. https://doi.org/10.1242/DEV.124.16.3167

Ng, J. (2008). TGF-beta signals regulate axonal development through distinct Smad-independent mechanisms. *Development (Cambridge, England)*, *135*(24), 4025–4035. https://doi.org/10.1242/DEV.028209

Nguyen, M., Parker, L., & Arora, K. (2000). Identification of maverick, a novel member of the TGF-β superfamily in Drosophila. *Mechanisms of Development*, *95*(1–2), 201–206. https://doi.org/10.1016/S0925-4773(00)00338-5

Ninov, N., Menezes-Cabral, S., Prat-Rojo, C., Manjón, C., Weiss, A., Pyrowolakis, G., Affolter, M., & Martín-Blanco, E. (2010). Dpp Signaling Directs Cell Motility and Invasiveness during Epithelial Morphogenesis. *Current Biology*, *20*(6), 513–520. https://doi.org/10.1016/j.cub.2010.01.063

Nobs, S. P., & Kopf, M. (2021). Tissue-resident macrophages: guardians of organ homeostasis. *Trends in Immunology*, *42*(6), 495–507. https://doi.org/10.1016/J.IT.2021.04.007

Nourshargh, S., Hordijk, P. P. L., & Sixt, M. (2010). Breaching multiple barriers: leukocyte motility through venular walls and the interstitium. *Nature Reviews Molecular Cell Biology*, *11*(5), 366–378. https://doi.org/10.1038/nrm2889

O'Connor, M. B., Umulis, D., Othmer, H. G., & Blair, S. S. (2006). Shaping BMP morphogen gradients in the Drosophila embryo and pupal wing. *Development (Cambridge, England)*,

133(2), 183–193. https://doi.org/10.1242/dev.02214

Ogita, H., Rikitake, Y., Miyoshi, J., & Takai, Y. (2010). Cell adhesion molecules nectins and associating proteins: Implications for physiology and pathology. *Proceedings of the Japan Academy. Series B, Physical and Biological Sciences*, *86*(6), 621. https://doi.org/10.2183/PJAB.86.621

Ohneda, K., & Yamamoto, M. (2002). Roles of Hematopoietic Transcription Factors GATA-1 and GATA-2 in the Development of Red Blood Cell Lineage. *Acta Haematologica*, *108*(4), 237–245. https://doi.org/10.1159/000065660

Olofsson, B., & Page, D. T. (2005). Condensation of the central nervous system in embryonic Drosophila is inhibited by blocking hemocyte migration or neural activity. *Developmental Biology*, *279*(1), 233–243. https://doi.org/10.1016/j.ydbio.2004.12.020

Omata, Y., Yasui, T., Hirose, J., Izawa, N., Imai, Y., Matsumoto, T., Masuda, H., Tokuyama, N., Nakamura, S., Tsutsumi, S., Yasuda, H., Okamoto, K., Takayanagi, H., Hikita, A., Imamura, T., Matsuo, K., Saito, T., Kadono, Y., Aburatani, H., & Tanaka, S. (2015). Genomewide Comprehensive Analysis Reveals Critical Cooperation Between Smad and c-Fos in RANKL-Induced Osteoclastogenesis. *Journal of Bone and Mineral Research*, *30*(5), 869–877. https://doi.org/10.1002/JBMR.2418

Paladi, M., & Tepass, U. (2004). Function of Rho GTPases in embryonic blood cell migration in Drosophila. *Journal of Cell Science*, *117*(26), 6313–6326. https://doi.org/10.1242/jcs.01552

Paluch, E. K., & Raz, E. (2013). The role and regulation of blebs in cell migration. *Current Opinion in Cell Biology*, *25*(5), 582–590. https://doi.org/10.1016/J.CEB.2013.05.005

Paolicelli, R. C., Bolasco, G., Pagani, F., Maggi, L., Scianni, M., Panzanelli, P., Giustetto, M., Ferreira, T. A., Guiducci, E., Dumas, L., Ragozzino, D., & Gross, C. T. (2011). Synaptic pruning by microglia is necessary for normal brain development. *Science (New York, N.Y.)*, *333*(6048), 1456–1458. https://doi.org/10.1126/SCIENCE.1202529

Pardali, E., Makowski, L.-M., Leffers, M., Borgscheiper, A., & Waltenberger, J. (2018). BMP-2 induces human mononuclear cell chemotaxis and adhesion and modulates monocyte-to-macrophage differentiation. *Journal of Cellular and Molecular Medicine*, *22*(11), 5429–5438. https://doi.org/10.1111/jcmm.13814

Parisi, F., Stefanatos, R. K., Strathdee, K., Yu, Y., & Vidal, M. (2014). Transformed epithelia trigger non-tissue-autonomous tumor suppressor response by adipocytes via activation of Toll and Eiger/TNF signaling. *Cell Reports*, *6*(5), 855–867. https://doi.org/10.1016/J.CELREP.2014.01.039

Parsons, B., & Foley, E. (2013). The Drosophila platelet-derived growth factor and vascular endothelial growth factor-receptor related (Pvr) protein ligands Pvf2 and Pvf3 control hemocyte viability and invasive migration. *Journal of Biological Chemistry*, *288*(28), 20173–20183. https://doi.org/10.1074/jbc.M113.483818

Pearson, J. C., Juarez, M. T., Kim, M., & McGinnis, W. (2009). Multiple transcription factor codes activate epidermal wound–response genes in Drosophila. *Proceedings of the National Academy of Sciences*, *106*(7), 2224–2229. https://doi.org/10.1073/PNAS.0810219106

Pennetier, D., Oyallon, J., Morin-Poulard, I., Dejean, S., Vincent, A., & Crozatier, M. (2012a). Size control of the Drosophila hematopoietic niche by bone morphogenetic protein signaling reveals parallels with mammals. *Proceedings of the National Academy of Sciences of the United States of America*, *109*(9), 3389–3394. https://doi.org/10.1073/pnas.1109407109

Pennetier, D., Oyallon, J., Morin-Poulard, I., Dejean, S., Vincent, A., & Crozatier, M. (2012b). Size control of the Drosophila hematopoietic niche by bone morphogenetic protein signaling reveals parallels with mammals. In *Proceedings of the National Academy of Sciences of the United States of America* (Vol. 109, Issue 9, pp. 3389–3394). https://doi.org/10.1073/pnas.1109407109

Perkins, K. K., Dailey, G. M., & Tjian, R. (1988). Novel Jun-and Fos-related proteins in Drosophila are functionally homologous to enhancer factor AP-1. *The EMBO Journal*, *7*(13), 4265–4273.

Picelli, S., Faridani, O. R., Björklund, Å. K., Winberg, G., Sagasser, S., & Sandberg, R. (2014). Full-length RNA-seq from single cells using Smart-seq2. *Nature Protocols 2013 9:1*, *9*(1), 171–181. https://doi.org/10.1038/nprot.2014.006

Prasad, M., & Montell, D. J. (2007). Cellular and molecular mechanisms of border cell migration analyzed using time-lapse live-cell imaging. *Developmental Cell*, *12*(6), 997–1005. https://doi.org/10.1016/J.DEVCEL.2007.03.021

Quan, Q., Wang, X., Lu, C., Ma, W., Wang, Y., Xia, G., Wang, C., & Yang, G. (2020). Cancer stem-like cells with hybrid epithelial/mesenchymal phenotype leading the collective invasion. *Cancer Science*, *111*(2), 467–476. https://doi.org/10.1111/CAS.14285

Rae, F., Woods, K., Sasmono, T., Campanale, N., Taylor, D., Ovchinnikov, D. A., Grimmond, S. M., Hume, D. A., Ricardo, S. D., & Little, M. H. (2007). Characterisation and trophic functions of murine embryonic macrophages based upon the use of a Csf1r-EGFP transgene reporter. *Developmental Biology*, *308*(1), 232–246. https://doi.org/10.1016/j.ydbio.2007.05.027

Ratheesh, A, Belyaeva, V., & Siekhaus, D. E. (2015). Drosophila immune cell migration and adhesion during embryonic development and larval immune responses. *Curr Opin Cell Biol*, *36*, 71–79. https://doi.org/10.1016/j.ceb.2015.07.003

Ratheesh, Aparna, Biebl, J., Vesela, J., Smutny, M., Papusheva, E., Krens, S. F. G., Kaufmann, W., Gyoergy, A., Casano, A. M., & Siekhaus, D. E. (2018). Drosophila TNF Modulates Tissue Tension in the Embryo to Facilitate Macrophage Invasive Migration. *Developmental Cell*, *45*(3), 331-346.e7. https://doi.org/10.1016/j.devcel.2018.04.002

Renkawitz, J., Kopf, A., Stopp, J., de Vries, I., Driscoll, M. K., Merrin, J., Hauschild, R., Welf, E. S., Danuser, G., Fiolka, R., & Sixt, M. (2019). Nuclear positioning facilitates amoeboid migration along the path of least resistance. *Nature*, *568*(7753), 546. https://doi.org/10.1038/S41586-019-1087-5

Reversat, A., Gaertner, F., Merrin, J., Stopp, J., Tasciyan, S., Aguilera, J., de Vries, I., Hauschild, R., Hons, M., Piel, M., Callan-Jones, A., Voituriez, R., & Sixt, M. (2020). Cellular locomotion using environmental topography. *Nature*, *582*(7813), 582–585. https://doi.org/10.1038/S41586-020-2283-Z

Ridley, A. J. (2015). Rho GTPase signalling in cell migration. *Current Opinion in Cell Biology*, *36*, 103–112. https://doi.org/10.1016/J.CEB.2015.08.005

Ridley, A. J., Comoglio, P. M., & Hall, A. (1995). Regulation of Scatter Factor/Hepatocyte Growth Factor Responses by Ras, Rac, and Rho in MDCK Cells. *MOLECULAR AND CELLULAR BIOLOGY*, *15*(2), 1110–1122. https://journals.asm.org/journal/mcb

Riesgo-escovar, J. R., & Hafen, E. (1997). Drosophila JUN kinase regulates expression of decapentaplegic via the ETS-domain protein AOP and the AP-1 transcription factor DJUN during dorsal closure: Riesgo-Escovar, J. and Hafen. E. Genes Dev. 11, 1717–1727. *Trends in Genetics*, *13*(10), 392. https://doi.org/http://dx.doi.org/10.1016/S0168-9525(97)90015-9

Riesgo-Escovar, J. R., & Hafen, E. (1997). Common and distinct roles of DFos and DJun during Drosophila development. *Science (New York, N.Y.)*, *278*(5338), 669–672. https://doi.org/10.1126/science.278.5338.669

Rizki, T. M., & Rizki, R. M. (1992). Lamellocyte differentiation in Drosophila larvae parasitized by Leptopilina. *Developmental and Comparative Immunology*, *16*(2–3), 103–110. https://doi.org/10.1016/0145-305X(92)90011-Z

Roberts, A. W., Lee, B. L., Deguine, J., John, S., Shlomchik, M. J., & Barton, G. M. (2017). Tissue-Resident Macrophages Are Locally Programmed for Silent Clearance of Apoptotic Cells. *Immunity*, *47*(5), 913-927.e6. https://doi.org/10.1016/J.IMMUNI.2017.10.006

Rodríguez-Pascual, F., Redondo-Horcajo, M., & Lamas, S. (2003). Functional cooperation between Smad proteins and activator protein-1 regulates transforming growth factor-β - Mediated induction of endothelin-1 expression. *Circulation Research*, *92*(12), 1288–1295. https://doi.org/10.1161/01.RES.0000078491.79697.7F

Roy, S., Ernst, J., Kharchenko, P. V., Kheradpour, P., Negre, N., Eaton, M. L., Landolin, J. M., Bristow, C. A., Ma, L., Lin, M. F., Washietl, S., Arshinoff, B. I., Ay, F., Meyer, P. E., Robine, N., Washington, N. L., Di Stefano, L., Berezikov, E., Brown, C. D., … Lowdon, R. F. (2010). Identification of functional elements and regulatory circuits by Drosophila modENCODE. *Science (New York, N.Y.)*, *330*(6012), 1787–1797. https://doi.org/10.1126/SCIENCE.1198374

Ruberte, E., Marty, T., Nellen, D., Affolter, M., & Baslert, K. (1995). An Absolute Requirement for Both the Type II and Type I Receptors, Punt and Thick Veins, for Dpp Signaling In Vivo. *Cell*, *80*, 889–897.

Rusch, J., & Levine, M. (1997). Regulation of a dpp target gene in the Drosophila embryo. *Development*, *124*(2), 303–311. https://doi.org/10.1242/DEV.124.2.303

Rymo, S. F., Gerhardt, H., Sand, F. W., Lang, R., Uv, A., & Betsholtz, C. (2011). A two-way communication between microglial cells and angiogenic sprouts regulates angiogenesis in aortic ring cultures. *PloS One*, *6*(1). https://doi.org/10.1371/JOURNAL.PONE.0015846

Sahai, E., Astsaturov, I., Cukierman, E., DeNardo, D. G., Egeblad, M., Evans, R. M., Fearon, D., Greten, F. R., Hingorani, S. R., Hunter, T., Hynes, R. O., Jain, R. K., Janowitz, T., Jorgensen, C., Kimmelman, A. C., Kolonin, M. G., Maki, R. G., Powers, R. S., Puré, E., … Werb, Z. (2020). A framework for advancing our understanding of cancer-associated fibroblasts. *Nature Reviews Cancer 2020 20:3*, *20*(3), 174–186. https://doi.org/10.1038/s41568-019-0238-1

Sánchez-Sánchez, B. J., Urbano, J. M., Comber, K., Dragu, A., Wood, W., Stramer, B., & Martín-Bermudo, M. D. (2017). Drosophila Embryonic Hemocytes Produce Laminins to Strengthen Migratory Response. *Cell Reports*, *21*(6), 1461–1470. https://doi.org/10.1016/j.celrep.2017.10.047

Scarpa, E., & Mayor, R. (2016). Collective cell migration in development. *Journal of Cell Biology*, *212*(2), 143–155. https://doi.org/10.1083/jcb.201508047

Sears, H. C., Kennedy, C. J., & Garrity, P. a. (2003). Macrophage-mediated corpse engulfment is required for normal Drosophila CNS morphogenesis. *Development (Cambridge, England)*, *130*(15), 3557–3565. https://doi.org/10.1242/dev.00586

Shang, Y., Coppo, M., He, T., Ning, F., Yu, L., Kang, L., Zhang, B., Ju, C., Qiao, Y., Zhao, B., Gessler, M., Rogatsky, I., & Hu, X. (2016). The transcriptional repressor Hes1 attenuates inflammation by regulating transcription elongation. *Nature Immunology 2016 17:8*, *17*(8), 930–937. https://doi.org/10.1038/ni.3486

Shimmi, O., Umulis, D., Othmer, H., & O'Connor, M. B. (2005). Facilitated transport of a

Dpp/Scw heterodimer by Sog/Tsg leads to robust patterning of the Drosophila blastoderm embryo. *Cell*, *120*(6), 873–886. https://doi.org/10.1016/J.CELL.2005.02.009

Sica, A., & Mantovani, A. (2012). Macrophage plasticity and polarization: in vivo veritas. *The Journal of Clinical Investigation*, *122*(3), 787–795. https://doi.org/10.1172/JCI59643

Siekhaus, D., Haesemeyer, M., Moffitt, O., & Lehmann, R. (2010). RhoL controls invasion and Rap1 localization during immune cell transmigration in Drosophila. *Nature Publishing Group*, *12*(6), 605–610. https://doi.org/10.1038/ncb2063

Sousa, S., Brion, R., Lintunen, M., Kronqvist, P., Sandholm, J., Mönkkönen, J., Kellokumpu-Lehtinen, P. L., Lauttia, S., Tynninen, O., Joensuu, H., Heymann, D., & Määttä, J. A. (2015). Human breast cancer cells educate macrophages toward the M2 activation status. *Breast Cancer Research*, *17*(1), 1–14. https://doi.org/10.1186/S13058-015-0621-0/FIGURES/4

Squarzoni, P., Oller, G., Hoeffel, G., Pont-Lezica, L., Rostaing, P., Low, D., Bessis, A., Ginhoux, F., & Garel, S. (2014). Microglia modulate wiring of the embryonic forebrain. *Cell Reports*, *8*(5), 1271–1279. https://doi.org/10.1016/J.CELREP.2014.07.042

Suchting, S., Freitas, C., Le Noble, F., Benedito, R., Bréant, C., Duarte, A., & Eichmann, A. (2007). The Notch ligand Delta-like 4 negatively regulates endothelial tip cell formation and vessel branching. *Proceedings of the National Academy of Sciences*, *104*(9), 3225–3230. https://doi.org/10.1073/PNAS.0611177104

Sundqvist, A., Vasilaki, E., Voytyuk, O., Bai, Y., Morikawa, M., Moustakas, A., Miyazono, K., Heldin, C. H., ten Dijke, P., & van Dam, H. (2020). TGFβ and EGF signaling orchestrates the AP-1- and p63 transcriptional regulation of breast cancer invasiveness. *Oncogene 2020 39:22*, *39*(22), 4436–4449. https://doi.org/10.1038/s41388-020-1299-z

Svitkina, T. (2018). The Actin Cytoskeleton and Actin-Based Motility. *Cold Spring Harbor Perspectives in Biology*, *10*(1). https://doi.org/10.1101/CSHPERSPECT.A018267

Szafranski, P., & Goode, S. (2004). A Fasciclin 2 morphogenetic switch organizes epithelial cell cluster polarity and motility. *Development*, *131*(9), 2023–2036. https://doi.org/10.1242/dev.01097

Szüts, D., & Bienz, M. (2000). An autoregulatory function of Dfos during Drosophila endoderm induction. *Mechanisms of Development*, *98*(1–2), 71–76. https://doi.org/10.1016/S0925-4773(00)00455-X

Tattikota, S. G., Cho, B., Liu, Y., Hu, Y., Barrera, V., Steinbaugh, M. J., Yoon, S. H., Comjean, A., Li, F., Dervis, F., Hung, R. J., Nam, J. W., Sui, S. H., Shim, J., & Perrimon, N. (2020). A single-cell survey of Drosophila blood. *ELife*, *9*, 1–35. https://doi.org/10.7554/ELIFE.54818

Tepass, U., Fessler, L. I., Aziz, A., & Hartenstein, V. (1994). Embryonic origins of hemocytes and their relationship to cell death in Drosophila. *Development*, *120*, 1829–1837.

Theveneau, E., & Mayor, R. (2010). Integrating chemotaxis and contact-inhibition during collective cell migration: Small GTPases at work. *Small GTPases*, *1*(2), 113–117. https://doi.org/10.4161/SGTP.1.2.13673

Thurmond, J., Goodman, J. L., Strelets, V. B., Attrill, H., Gramates, L. S., Marygold, S. J., Matthews, B. B., Millburn, G., Antonazzo, G., Trovisco, V., Kaufman, T. C., Calvi, B. R., Perrimon, N., Gelbart, S. R., Agapite, J., Broll, K., Crosby, L., Dos Santos, G., Emmert, D., … Baker, P. (2019). FlyBase 2.0: The next generation. *Nucleic Acids Research*, *47*(D1). https://doi.org/10.1093/nar/gky1003

Tippett, E., Cameron, P. U., Marsh, M., & Crowe, S. M. (2013). Characterization of tetraspanins CD9, CD53, CD63, and CD81 in monocytes and macrophages in HIV-1 infection. *Journal of Leukocyte Biology*, *93*(6), 913–920. https://doi.org/10.1189/JLB.0812391

Tokusumi, T., Shoue, D. A., Tokusumi, Y., Stoller, J. R., & Schulz, R. A. (2009). New hemocyte-

specific enhancer-reporter transgenes for the analysis of hematopoiesis in Drosophila. *Genesis*, *47*(11), 771–774. https://doi.org/10.1002/DVG.20561

Tomancak, P., Beaton, A., Weiszmann, R., Kwan, E., Shu, S. Q., Lewis, S. E., Richards, S., Ashburner, M., Hartenstein, V., Celniker, S. E., & Rubin, G. M. (2002). Systematic determination of patterns of gene expression during Drosophila embryogenesis. *Genome Biology*, *3*(12). https://doi.org/10.1186/gb-2002-3-12-research0088

Tomancak, P., Berman, B. P., Beaton, A., Weiszmann, R., Kwan, E., Hartenstein, V., Celniker, S. E., & Rubin, G. M. (2007). Global analysis of patterns of gene expression during Drosophila embryogenesis. *Genome Biology*, *8*(7). https://doi.org/10.1186/gb-2007-8-7-r145

Trepat, X., Chen, Z., & Jacobson, K. (2012). Cell migration. *Comprehensive Physiology*, *2*(4), 2369–2392. https://doi.org/10.1002/CPHY.C110012

Tsai, F. Y., Keller, G., Kuo, F. C., Weiss, M., Chen, J., Rosenblatt, M., Alt, F. W., & Orkin, S. H. (1994). An early haematopoietic defect in mice lacking the transcription factor GATA-2. *Nature*, *371*(6494), 221–226. https://doi.org/10.1038/371221A0

Tsang, A. P., Visvader, J. E., Turner, C. A., Fujiwara, Y., Yu, C., Weiss, M. J., Crossley, M., & Orkin, S. H. (1997). FOG, a multitype zinc finger protein, acts as a cofactor for transcription factor GATA-1 in erythroid and megakaryocytic differentiation. *Cell*, *90*(1), 109–119. https://doi.org/10.1016/S0092-8674(00)80318-9

Tsuneizumi, K., Nakayama, T., Kamoshida, Y., Kornberg, T. B., Christian, J. L., & Tabata, T. (1997). Daughters against dpp modulates dpp organizing activity in Drosophila wing development. *Nature*, *389*(6651), 627–631. https://doi.org/10.1038/39362

Uhlirova, M., & Bohmann, D. (2006). JNK- and Fos-regulated Mmp1 expression cooperates with Ras to induce invasive tumors in Drosophila. *EMBO Journal*, *25*(22), 5294–5304. https://doi.org/10.1038/sj.emboj.7601401

Upadhyay, A., Moss-Taylor, L., Kim, M. J., Ghosh, A. C., & O'Connor, M. B. (2017). TGF-β Family Signaling in Drosophila. *Cold Spring Harbor Perspectives in Biology*, *9*(9). https://doi.org/10.1101/CSHPERSPECT.A022152

Utz, S. G., See, P., Mildenberger, W., Thion, M. S., Silvin, A., Lutz, M., Ingelfinger, F., Rayan, N. A., Lelios, I., Buttgereit, A., Asano, K., Prabhakar, S., Garel, S., Becher, B., Ginhoux, F., & Greter, M. (2020). Early Fate Defines Microglia and Non-parenchymal Brain Macrophage Development. *Cell*, *181*(3), 557-573.e18. https://doi.org/10.1016/j.cell.2020.03.021

Valentin, G., Haas, P., & Gilmour, D. (2007). The chemokine SDF1a coordinates tissue migration through the spatially restricted activation of Cxcr7 and Cxcr4b. *Current Biology : CB*, *17*(12), 1026–1031. https://doi.org/10.1016/J.CUB.2007.05.020

Valoskova, K., Biebl, J., Roblek, M., Emtenani, S., Gyoergy, A., Misova, M., Ratheesh, A., Reis-Rodrigues, P., Shkarina, K., Larsen, I. S. B., Vakhrushev, S. Y., Clausen, H., & Siekhaus, D. E. (2019). A conserved major facilitator superfamily member orchestrates a subset of O-glycosylation to aid macrophage tissue invasion. *ELife*, *8*. https://doi.org/10.7554/eLife.41801

van Furth, R., Cohn, Z. A., Hirsch, J. G., Humphrey, J. H., Spector, W. G., & Langevoort, H. L. (1972). The mononuclear phagocyte system: a new classification of macrophages, monocytes, and their precursor cells. *Bulletin of the World Health Organization*, *46*(6), 845. /pmc/articles/PMC2480884/?report=abstract

Venkiteswaran, G., Lewellis, S. W., Wang, J., Reynolds, E., Nicholson, C., & Knaut, H. (2013). Generation and Dynamics of an Endogenous, Self-Generated Signaling Gradient across a Migrating Tissue. *Cell*, *155*(3), 674–687. https://doi.org/10.1016/J.CELL.2013.09.046

Vilchez Mercedes, S. A., Bocci, F., Levine, H., Onuchic, J. N., Jolly, M. K., & Wong, P. K. (2021). Decoding leader cells in collective cancer invasion. *Nature Reviews Cancer 2021 21:9*, *21*(9), 592–604. https://doi.org/10.1038/s41568-021-00376-8

Vincent, S., Ruberte, E., Grieder, N. C., Chen, C. K., Haerry, T., Schuh, R., & Affolter, M. (1997). DPP controls tracheal cell migration along the dorsoventral body axis of the Drosophila embryo. *Development*, *124*(14).

Vischer, U., & Wagner, D. (1993). CD63 Is a Component of Weibel-Palade Bodies of Human Endothelial Cells. *Blood*, *82*(4), 1184–1191. https://doi.org/10.1182/BLOOD.V82.4.1184.1184

von der Hardt, S., Bakkers, J., Inbal, A., Carvalho, L., Solnica-Krezel, L., Heisenberg, C. P., & Hammerschmidt, M. (2007). The Bmp Gradient of the Zebrafish Gastrula Guides Migrating Lateral Cells by Regulating Cell-Cell Adhesion. *Current Biology*, *17*(6), 475–487. https://doi.org/10.1016/J.CUB.2007.02.013

Wakayama, Y., Fukuhara, S., Ando, K., Matsuda, M., & Mochizuki, N. (2015). Cdc42 Mediates Bmp-Induced Sprouting Angiogenesis through Fmnl3-Driven Assembly of Endothelial Filopodia in Zebrafish. *Developmental Cell*, *32*(1), 109–122. https://doi.org/10.1016/J.DEVCEL.2014.11.024

Waltzer, L., Ferjoux, G., Bataillé, L., & Haenlin, M. (2003). Cooperation between the GATA and RUNX factors Serpent and Lozenge during Drosophila hematopoiesis. *The EMBO Journal*, *22*(24), 6516. https://doi.org/10.1093/EMBOJ/CDG622

Wang, J., & Kubes, P. (2016). A Reservoir of Mature Cavity Macrophages that Can Rapidly Invade Visceral Organs to Affect Tissue Repair. *Cell*, *165*(3), 668–678. https://doi.org/10.1016/J.CELL.2016.03.009/ATTACHMENT/3A4D7476-07F0-4364-A0E2-5F417D13BEB3/MMC8.MP4

Wang, Q., Liu, H., Wang, Q., Zhou, F., Liu, Y., Zhang, Y., Ding, H., Yuan, M., Li, F., & Chen, Y. (2017). Involvement of c-Fos in cell proliferation, migration, and invasion in osteosarcoma cells accompanied by altered expression of Wnt2 and Fzd9. *PLoS ONE*, *12*(6). https://doi.org/10.1371/journal.pone.0180558

Wang, Y., Chaffee, T. S., Larue, R. S., Huggins, D. N., Witschen, P. M., Ibrahim, A. M., Nelson, A. C., Machado, H. L., & Schwertfeger, K. L. (2020). Tissue-resident macrophages promote extracellular matrix homeostasis in the mammary gland stroma of nulliparous mice. *ELife*, *9*, 1–27. https://doi.org/10.7554/ELIFE.57438

Wegner, M., & Riethmacher, D. (2001). Chronicles of a switch hunt: gcm genes in development. *Trends in Genetics*, *17*(5), 286–290. https://doi.org/10.1016/S0168-9525(01)02275-2

Weiss, A., Charbonnier, E., Ellertsdóttir, E., Tsirigos, A., Wolf, C., Schuh, R., Pyrowolakis, G., & Affolter, M. (2010a). A conserved activation element in BMP signaling during Drosophila development. *Nature Structural & Molecular Biology*, *17*(1), 69–77. https://doi.org/10.1038/NSMB.1715

Weiss, A., Charbonnier, E., Ellertsdóttir, E., Tsirigos, A., Wolf, C., Schuh, R., Pyrowolakis, G., & Affolter, M. (2010b). A conserved activation element in BMP signaling during Drosophila development. *Nature Structural & Molecular Biology*, *17*(1), 69–76. https://doi.org/10.1038/nsmb.1715

West, H. C., & Bennett, C. L. (2018). Redefining the role of langerhans cells as immune regulators within the skin. *Frontiers in Immunology*, *8*(JAN), 1941. https://doi.org/10.3389/FIMMU.2017.01941/BIBTEX

Wharton, K. A., Ray, R. P., & Gelbart, W. M. (1993). An activity gradient of decapentaplegic is

necessary for the specification of dorsal pattern elements in the Drosophila embryo. *Development*, *117*(2), 807–822. https://doi.org/10.1242/DEV.117.2.807

Wood, W., Faria, C., & Jacinto, A. (2006). *Distinct mechanisms regulate hemocyte chemotaxis during development and wound healing in*. *173*(3), 405–416. https://doi.org/10.1083/jcb.200508161

Wood, W., & Jacinto, A. (2007). Drosophila melanogaster embryonic haemocytes: masters of multitasking. *Nature Reviews. Molecular Cell Biology*, *8*(7), 542–551. https://doi.org/10.1038/nrm2202

Wood, W., & Martin, P. (2017). Macrophage Functions in Tissue Patterning and Disease: New Insights from the Fly. *Developmental Cell*, *40*(3), 221. https://doi.org/10.1016/J.DEVCEL.2017.01.001

Wu, C. Y., Lin, M. W., Wu, D. C., Huang, Y. B., Huang, H. T., & Chen, C. L. (2014). The role of phosphoinositide-regulated actin reorganization in chemotaxis and cell migration. *British Journal of Pharmacology*, *171*(24), 5541. https://doi.org/10.1111/BPH.12777

Wu, Y., Zhang, X., Salmon, M., Lin, X., & Zehner, Z. E. (2007). TGFβ1 regulation of vimentin gene expression during differentiation of the C2C12 skeletal myogenic cell line requires Smads, AP-1 and Sp1 family members. *Biochimica et Biophysica Acta (BBA) - Molecular Cell Research*, *1773*(3), 427–439. https://doi.org/10.1016/J.BBAMCR.2006.11.017

Wurmbach, E., Wech, I., & Preiss, A. (1999). The Enhancer of split complex of Drosophila melanogaster harbors three classes of Notch responsive genes. *Mechanisms of Development*, *80*(2), 171–180. https://doi.org/10.1016/S0925-4773(98)00212-3

Wynn, T. A., Chawla, A., & Pollard, J. W. (2013). Macrophage biology in development, homeostasis and disease. *Nature 2013 496:7446*, *496*(7446), 445–455. https://doi.org/10.1038/nature12034

Yamada, K. M., & Sixt, M. (2019). Mechanisms of 3D cell migration. *Nature Reviews Molecular Cell Biology*, *20*(12), 738–752. https://doi.org/10.1038/s41580-019-0172-9

Yamane, T. (2018). Mouse yolk sac hematopoiesis. *Frontiers in Cell and Developmental Biology*, *6*(JUL), 80. https://doi.org/10.3389/FCELL.2018.00080/BIBTEX

Yokomizo, T., Ogawa, M., Osato, M., Kanno, T., Yoshida, H., Fujimoto, T., Fraser, S., Nishikawa, S., Okada, H., Satake, M., Noda, T., Nishikawa, S. I., & Ito, Y. (2001). Requirement of Runx1/AML1/PEBP2alphaB for the generation of haematopoietic cells from endothelial cells. *Genes to Cells : Devoted to Molecular & Cellular Mechanisms*, *6*(1), 13–23. https://doi.org/10.1046/J.1365-2443.2001.00393.X

Yosef, N., Vadakkan, T. J., Park, J. H., Poché, R. A., Thomas, J. L., & Dickinson, M. E. (2018). The phenotypic and functional properties of mouse yolk-sac-derived embryonic macrophages. *Developmental Biology*, *442*(1), 138–154. https://doi.org/10.1016/J.YDBIO.2018.07.009

Yu, S., Luo, F., & Jin, L. H. (2021). Rab5 and rab11 maintain hematopoietic homeostasis by restricting multiple signaling pathways in drosophila. *ELife*, *10*, 1–23. https://doi.org/10.7554/ELIFE.60870

Zeitlinger, J., Kockel, L., Peverali, F. A., Jackson, D. B., Mlodzik, M., & Bohmann, D. (1997). Defective dorsal closure and loss of epidermal decapentaplegic expression in Drosophila fos mutants. *EMBO Journal*, *16*(24), 7393–7401. https://doi.org/10.1093/emboj/16.24.7393

Zhang, F., Wang, H., Wang, X., Jiang, G., Liu, H., Zhang, G., Wang, H., Fang, R., Bu, X., Cai, S., & Du, J. (2016). *TGF-β induces M2-like macrophage polarization via SNAIL-mediated suppression of a pro-inflammatory phenotype* (Vol. 7, Issue 32).

www.impactjournals.com/oncotarget

Zhang, S., Amourda, C., Garfield, D., & Saunders, T. E. (2018). Selective Filopodia Adhesion Ensures Robust Cell Matching in the Drosophila Heart. *Developmental Cell*, *46*(2), 189-203.e4. https://doi.org/10.1016/J.DEVCEL.2018.06.015/ATTACHMENT/1CE65205-B6D7-432B-A3C4-46E26954441D/MMC1.PDF

Zhang, Y., Feng, X. H., & Derynck, R. (1998). Smad3 and Smad4 cooperate with c-Jun/c-Fos to mediate TGF-β-induced transcription. *Nature 1998 394:6696*, *394*(6696), 909–913. https://doi.org/10.1038/29814

Zhou, L., Hashimi, H., Schwartz, L. M., & Nambu, J. R. (1995). Programmed cell death in the Drosophila central nervous system midline. *Current Biology*, *5*(7), 784–790. https://doi.org/10.1016/S0960-9822(95)00155-2

Zouani, O. F., Gocheva, V., & Durrieu, M. C. (2014). Membrane Nanowaves in Single and Collective Cell Migration. *PLOS ONE*, *9*(5), e97855. https://doi.org/10.1371/JOURNAL.PONE.0097855

3.8 SUPPLEMENTAL MATERIAL

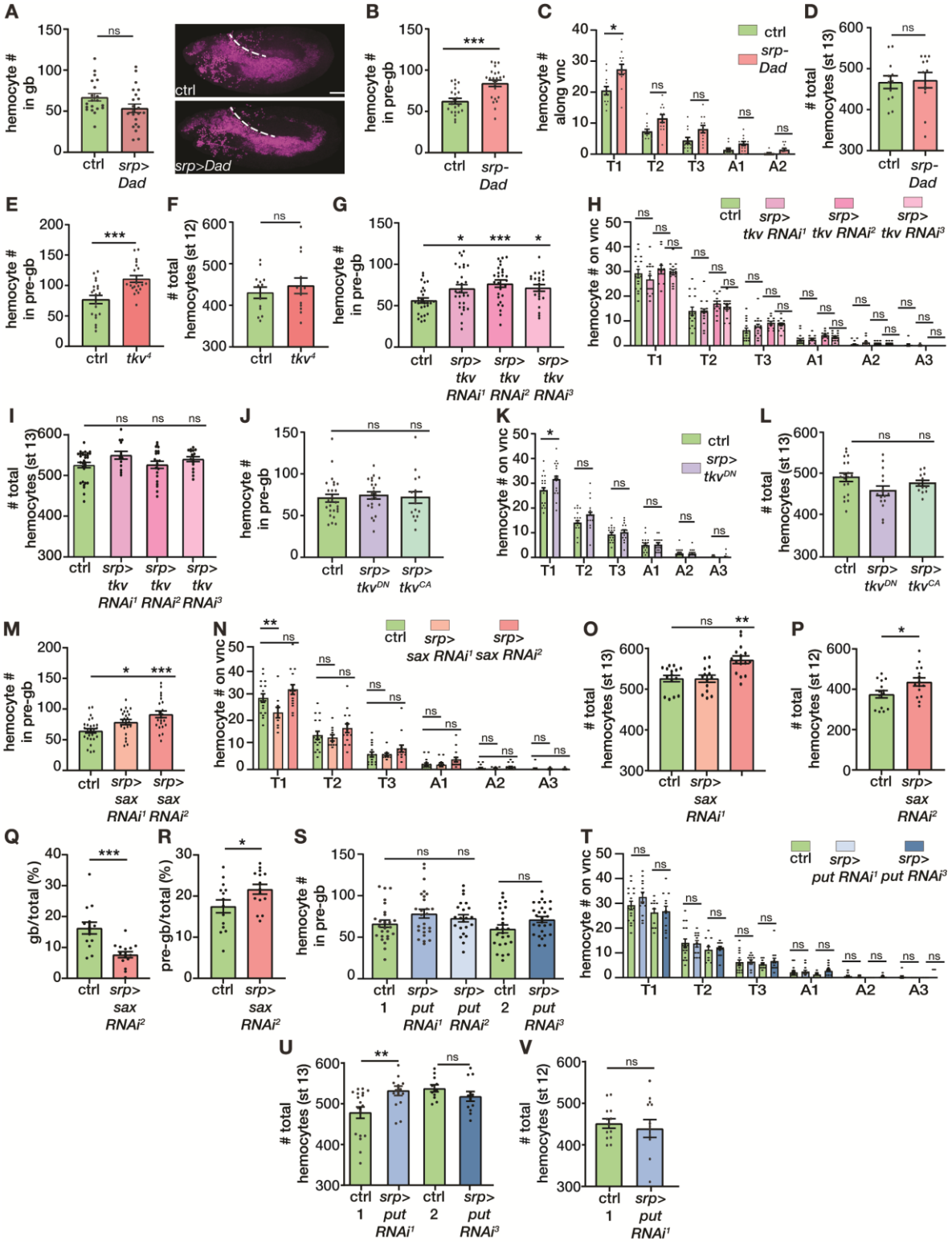

Chapter 3 Fig 2 S 1.BMP receptors in hemocytes predominantly affect germband tissue invasion
(A) Overexpression of the negative regulator of BMP signaling Dad using srpHemo-Gal4 does not significantly change hemocyte numbers invading into the germband. n=20 (ctrl), n=22 (*mac>Dad*) p=0.063 ns Representative images shown to the right. **(B-D)** Quantification of hemocytes in the pre-germband, vnc, and total hemocytes expressing full length *Dad* under the hemocyte promoter *srpHemo.* **(B)** Loss of function of BMP signaling by expressing full length *Dad* under the hemocyte promoter *srpHemo* increases hemocyte numbers in the pre-

germband zone. n=21 (ctrl), *srp-Dad* (n=24), p=0.0001. **(C)** Expression of the negative transcriptional BMP signaling regulator *Dad* under the *srpHemo* promoter has a mild effect on hemocyte numbers along vnc slightly increasing hemocyte numbers in the first vnc segment T1 without changes in the following segments. n=12 (ctrl in green), n=12 (*srp-Dad* in red) p=0.020 (T1), p=0.055 (T2) ns, p=0.14 (T3), p=0.096 (A1), p=0.10 (A2). **(D)** Expression of the negative transcriptional BMP signaling regulator *Dad* under the *srpHemo* promoter has no effect on total hemocyte numbers. n=12 (ctrl), n=12 (*srp-Dad*), p=0.85 **(E)** Hemocyte numbers in the pre-germband zone are strongly increased in tkv^4 mutant embryos. N=20 (ctrl), n=20 (tkv^4) p=0.0004 **(F)** tkv^4 mutation has no effect on total hemocyte numbers. n=13 (ctrl), n=13 (tkv^4) p=0.48 **(G-I)** Quantification of hemocytes in the pre-germband, vnc, and total hemocytes expressing three independent RNAi lines against *tkv*. **(G)** Three independent RNAi lines for *tkv* expressed in hemocytes by *srpHemo-Gal4* each increase pre-germband numbers of hemocytes. ctrl (n=29), *mac>tkv* $RNAi^1$ (n=29) p=0.039, *mac>tkv* $RNAi^2$ (n=27) p=0.001, *mac>tkv* $RNAi^3$ (n=23) p=0.012. **(H)** Numbers of hemocytes in vnc segments are similar to the control in three independent *tkv* RNAi expressing embryos. n=16 (ctrl in green), n=15 (*mac>tkv* $RNAi^1$ in purple) p=0.62 (T1), p=0.9972 (T2), p=0.64 (T3), p>0.9999 (A1), p=0.98 (A2), p=0.6428 (A3), n=12 (*mac>tkv* $RNAi^2$in pink) p=0.85 (T1), p=0.34 (T2), p=0.050 (T3), p=0.092 (A1), p=0.52 (A2), p=0.87 (A3), n=15 (*mac>tkv* $RNAi^3$ in light pink) p=0.99 (T1), p=0.70 (T2), p=0.1068 (T3), p=0.35 (A1), p=0.93 (A2), p=0.64 (A3). **(I)** Knock-down of *tkv* by three different RNAi lines driven in hemocytes by *srpHemo-Gal4* does not affect total numbers of hemocytes. n=31 (ctrl), n=13 (*mac>tkv* $RNAi^1$) p=0.14, n=21 (*mac>tkv* $RNAi^2$) p=0.9999, n=17 (*mac>tkv* $RNAi^3$) p=0.29. **(J-L)** Quantification of hemocytes in the pre-germband, vnc, and total hemocytes expressing dominant negative (tkv^{DN}) or constitutively activated tkv (tkv^{DA}). **(J)** Hemocyte-specific expression of dominant negative (tkv^{DN}) or constitutively activated tkv (tkv^{DA}) by *srpHemo-Gal4* does not affect pre-germband hemocyte numbers. ctrl (n=26), *mac>*tkv^{DN} (n=22) p=0.85, *mac>*tkv^{DA} (n=16) p=0.99. **(K)** Hemocyte-specific expression of dominant negative (tkv^{DN}) by *srpHemo-Gal4* has a mild effect on hemocyte numbers along vnc slightly increasing hemocyte numbers in the first vnc segment T1 without changes in the following segments. n=17 (ctrl in green), n=16 (*mac>*tkv^{DN} in blue), p=0.011 (T1), p=0.10 (T2), p=0.99 (T3), p=>0.9999 (A1), p=>0.9999 (A2) ns, p=0.9999 (A3). **(L)** Hemocyte-specific expression of dominant negative (tkv^{DN}) or constitutively activated tkv (tkv^{DA}) by *srpHemo-Gal4* does not affect total hemocyte numbers. n=19 (ctrl), n=16 (*mac>*tkv^{DN}) p=0.078, n=12 (*mac>*Tkv^{DA}) p=0.43. **(M-R)** Analysis of hemocytes expressing two independent RNAi lines against the alternative BMP type I receptor *sax*. **(M)** Two independent RNAi lines for *sax* expressed in hemocytes by *srpHemo-Gal4* each increase pre-germband numbers of hemocytes. ctrl (n=27), *mac>sax* $RNAi^1$ (n=23) p=0.030, *mac>sax* $RNAi^2$ (n=23) p=0.0004. **(N)** Knock-down of BMP receptor type I *sax* in hemocytes shows variable effect on their numbers along the vnc with *sax* $RNAi^1$ having a mild effect on hemocyte numbers along vnc, slightly decreasing hemocyte numbers in the first vnc segment T1 without changes in the following segments, and *sax* $RNAi^2$ showing no difference to the control. n=16 (ctrl in green), n=10 (*mac>sax* $RNAi^1$ in light orange) p=0.0022 (T1), p=0.79 (T2), p=0.997 (T3), p=0.997 (A1), p=0.991 (A2), p=0.995 (A3), n=15 (*mac>sax* $RNAi^2$ in dark orange) p=0.057 (T1), p=0.14 (T2), p=0.23 (T3), p=0.3578 (A1), p=0.96 (A2), p=0.99 (A3). **(O)** Knock-down of BMP receptor type I *sax* in hemocytes shows variable effect on their total numbers with one RNAi (*sax* $RNAi^1$) having no effect and another one (*sax* $RNAi^2$) even increasing total hemocyte numbers. n=15 (ctrl), n=14 (*mac>sax* $RNAi^1$) p>0.9999, n=15 (*mac>sax* $RNAi^2$) p=0.0016. **(P)** Total hemocytes expressing sax $RNAi^2$ are already increased at stage 12. n=14 (ctrl), n=15 (*mac>sax* $RNAi^2$) p=0.031. **(Q)** The numbers of hemocytes inside the germband at stage 12 shown in **Fig. 4 E** were normalized to the total hemocyte numbers in each embryo expressing *sax* $RNAi^2$ in hemocytes. Hemocyte numbers in the gb divided by all hemocytes per individual embryo (gb/total (%)) was strongly decreased. n=14 (ctrl), n=15 (*mac>sax* $RNAi^2$) p=0.0007.**(R)** Analysis of normalized hemocyte numbers corresponding to **M** shows increased fraction of *sax* $RNAi^2$ expressing hemocytes residing in the pre-germband zone in stage 12 embryos. n=14 (ctrl), n=15 (*mac>sax* $RNAi^2$) p=0.047. **(S-V)** Quantification of hemocytes in the pre-germband, vnc, and total hemocytes expressing two independent RNAi lines against the BMP type II receptor *put*. **(S)** Knock-down of *put* by three different RNAi lines driven in hemocytes by *srpHemo-Gal4* does not change numbers of hemocytes in the pre-germband zone. ctrl 1 (n=26), *mac>put* $RNAi^1$ (n=26) p=0.17, *mac>put* $RNAi^2$ (n=22) p=0.51, ctrl 2 (n=24), *mac>put* $RNAi^3$ (n=27) p=0.18. **(T)** Numbers of hemocytes in vnc segments are similar to the control for the two independent *put* RNAi expressing embryos that showed germband invasion efficiency effect. n=16 (ctrl 1 in green), n=12 (*mac>put* $RNAi^1$ in blue) p=0.22 (T1), p>0.9999 (T2), p>0.9999 (T3), p>0.9999 (A1), p>0.9999 (A2), p>0.9999 (A3), n=11 (ctrl 2 in green), n=12 (*mac>put* $RNAi^2$ in dark blue) p>0.9999 (T1), p>0.9999 (T2), p=0.93 (T3), p=0.36 (A1), p=0.72 (A2). **(U)** Of two independent RNAi lines for knock-down of the BMP receptor type II put that affect hemocyte germband invasion efficiency, one of them increases total hemocyte numbers (*put* $RNAi^1$), and one does not significantly change them (*put* $RNAi^2$). n=18 (ctrl 1), n=15 (*mac>put* $RNAi^1$) p=0.0056, n=11 (ctrl 2), n=12 (*mac> put* $RNAi^3$) p=0.19. **(V)** Total hemocyte numbers quantified in earlier embryos from stage 12 are not significantly changed in *put* $RNAi^1$. n=13 (ctrl 1 in green), n=13 (mac>*put* $RNAi^1$ in blue) p=0.62.

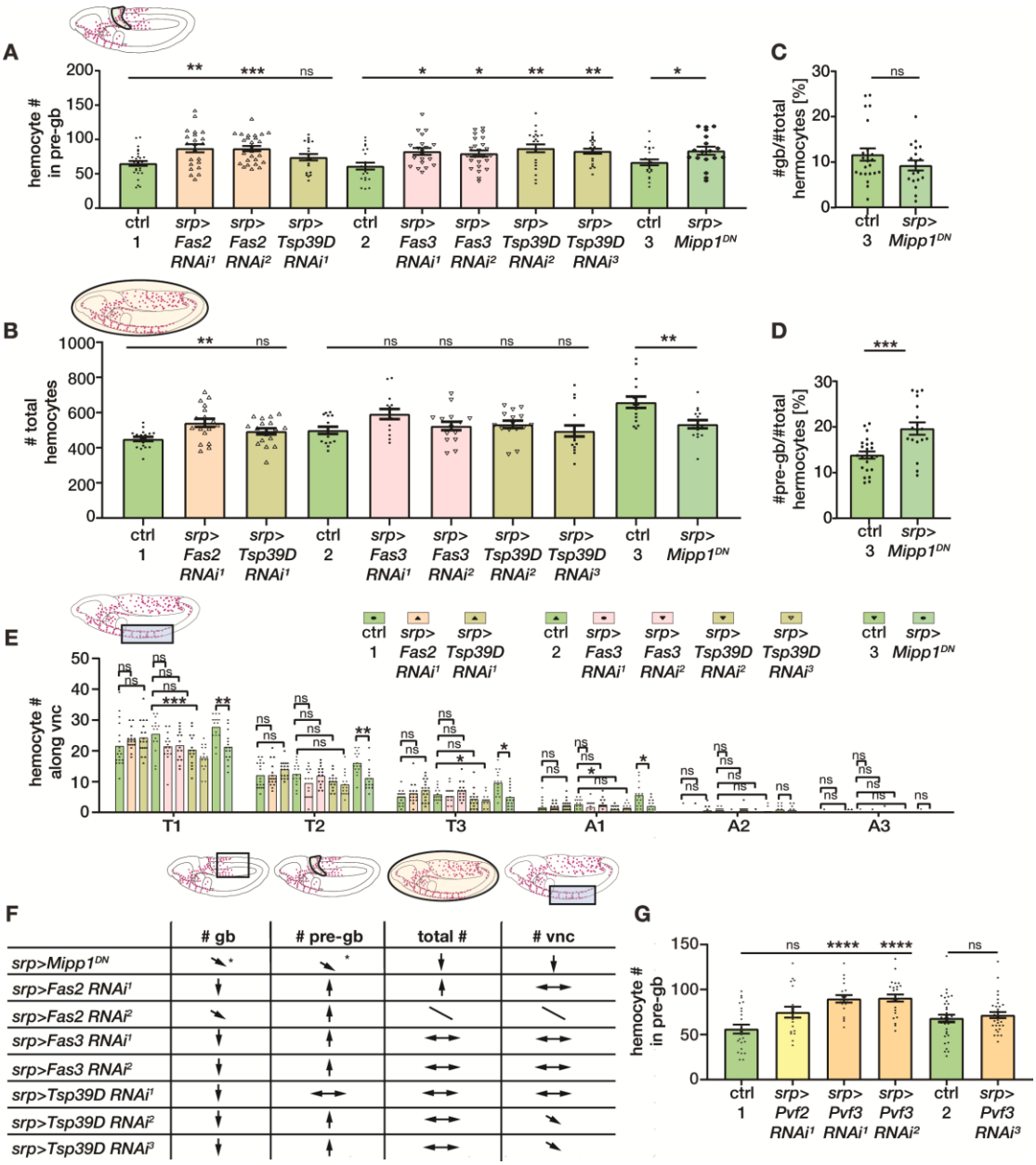

Chapter 3 Fig 4 S 1. Selected putative BMP target genes do not strongly regulate other routes of migration or total hemocyte numbers

(A) Quantification of hemocytes in the pre-germband zone next to the germband, in which hemocytes reside prior to germband invasion. Analyzed area shown in the schematic highlighted in light green with a thick black outline. Same embryos as in germband quantifications shown in Fig. 4 of corresponding indicated genotypes were used. Knock-down of nearly all selected putative BMP target genes except *Tsp39D RNAi*^{1}, as well as overexpression of a dominant negative *Mipp1* (*Mipp1*^{DN}) show increased numbers of hemocytes piling up in front of the germband. *Tsp39D RNAi*^{1} is similar to the control. n=28 (ctrl 1), n=22 (*mac>Fas2 RNAi*^{1}) p=0.0093, n=27 (*mac>Fas2 RNAi*^{2}) p=0.0004, n=21 (*mac>Tsp39D RNAi*^{1}) p=0.34, n=22 (ctrl 2), n=20 (*mac>Fas3 RNAi*^{1}) p=0.017, n=24 (*mac>Fas3 RNAi*^{2}) p=0.038, n=22 (*mac>Tsp39D RNAi*^{2}) p=0.0057 **, n=21 (*mac>Tsp39D RNAi*^{3}) p=0.0055, n=23 (ctrl 3), n=18 (*mac>Mipp1*^{DN}) p=0.025. **(B)** Total numbers of hemocytes in stage 13 embryos were increased in the hemocyte specific knock-down of *Fas2* that showed a germband invasion defect quantified in Fig.4D (*Fas2 RNAi*^{1}), and overexpression of the dominant negative *Mipp1*^{DN} decreases numbers of total hemocytes. All other RNAi are not changed in their total hemocyte numbers. n=18 (ctrl 1), n=18 (*mac>Fas2 RNAi*^{1}) p=0.0017, n=18 (*mac>Tsp39D RNAi*^{1}) p=0.19, n=15 (ctrl 2), n=15 (*mac>Fas3 RNAi*^{1}) p=0.054, n=15

(*mac>Fas3 RNAi*^{2}) p=0.94, n=15 (*mac>Tsp39D RNAi*^{2}) p=0.83, n=16 (*mac>Tsp39D RNAi*^{3}) p>0.9999, n=15 (ctrl 3), n=15 (*mac>Mipp1*^{DN}) p 0.0041. **(C)** The numbers of hemocytes inside the germband at stage 12 were normalized to the total hemocyte numbers in each embryo expressing *Mipp1*^{DN} in hemocytes. Hemocyte numbers divided by all hemocytes per individual embryo (#gb/#total mac [%]) did not differ from the control. n=23 (ctrl 3), n=18 (*mac>Mipp1*^{DN}) p=0.18. **(D)** Analysis of normalized hemocyte numbers corresponding to Fig. 4S2C shows increased fraction of *Mipp1*^{DN} expressing hemocytes residing in the pre-germband zone in stage 12 embryos. n=23 (ctrl 3), n=18 (*mac>Mipp1*^{DN}) p=0.0009. **(E)** Quantification of hemocytes inside segments of the vnc in stage 13 embryos. Knock-down of *Fas2* (*Fas2 RNAi*^{1}) and *Fas3* (*Fas3 RNAi*^{1} and *Fas3 RNAi*^{2}) did not affect hemocyte numbers along vnc. Knock-down of *Tsp39D* slightly reduces hemocyte numbers along the vnc with less hemocytes in the first vnc segment T1 for one RNAi (*Tsp39D RNAi*^{3}) and in segment T3 for another RNAi (*Tsp39D RNAi*^{2}), no change is observed for *Tsp39D RNAi*^{1}. Hemocytes expressing the dominant version of *Mipp1* show strong impairment in migration along the vnc. n=18 (ctrl 1), n=17 (*mac>Fas2 RNAi*^{2}) p=0.50 (T1), p>0.9999(T2), p=0.40 (T3), p=0.99 (A1), p=0.999 (A2), p=0.55 (A3), n=18 (*mac>Tsp39D RNAi*^{1}) p=0.37 (T1), p=0.21 (T2), p=0.053 (T3), p=0.50 (A1), p=0.49 (A2), p=0.52 (A3), ctrl 2 (n=15), n=15 (*mac>Fas3 RNAi*^{1}) p=0.15 (T1), p=0.20 (T2), p=0.97 (T3), p=0.53 (A1), p=0.065 (A2), p>0.9999 (A3), n=15 (*mac>Fas3 RNAi*^{2}) p=0.22 (T1), p=0.98 (T2), p=0.58 (T3), p=0.999 (A1), p>0.9999 (A2), p=0.99 (A3), n=15 (*mac>Tsp39D RNAi*^{2}) p=0.056 (T1), p=0.15 (T2), p=0.46 (T3), p=0.027 (A1), p=0.065 (A2), p=0.80 (A3), n=16 (*mac>Tsp39D RNAi*^{3}) p=0.0006 (T1), p=0.055 (T2), p=0.035 (T3), p=0.18 (A1), p=0.80 (A2), p=0.80 (A3), n=15 (ctrl 3), n=15 (*mac>Mipp1*^{DN}) p=0.0028 (T1), p= 0.0081 (T2), p=0.011 (T3), p=0.024 (A1), p=0.9997 (A2), p=0.91 (A3). **(F)** Summary of hemocyte quantification in different areas in BMP signaling loss and gain of function experiments shown in Figure 4 and Figure 4 Supplement1. Arrow pointing down indicating decreased numbers of hemocytes (mac#) in this specific area, arrow pointing up indicating increased hemocyte numbers, two arrows pointing left and right indicating no significant change compared to control, slash indicating no assessment. *Total numbers of hemocytes were decreased in embryos used for gb and pre-gb quantification in *Mipp1*^{DN}. **(G)** Quantification of hemocyte numbers in the pre-germband zone corresponding to analysis in **Fig. 4E**. Knock-down of *Pvf2* does not significantly show higher hemocyte numbers in the pre-germband zone; whereas knock-down of *Pvf3* by independent RNAi lines (*Pvf3 RNAi*^{1}*, Pvf3 RNAi*^{2}*, Pvf3 RNAi*^{3}) increases hemocyte numbers in that area. n=24 (ctrl 1), n=19 (*mac>Pvf2 RNAi*^{1}) p=0.062, n=19 (*mac>Pvf3 RNAi*^{1}) p<0.0001, n=25 (*mac>Pvf3 RNAi*^{2}) p<0.0001, n=34 (ctrl 2), n=32 (*mac>Pvf3 RNAi*^{3}) p=0.50.

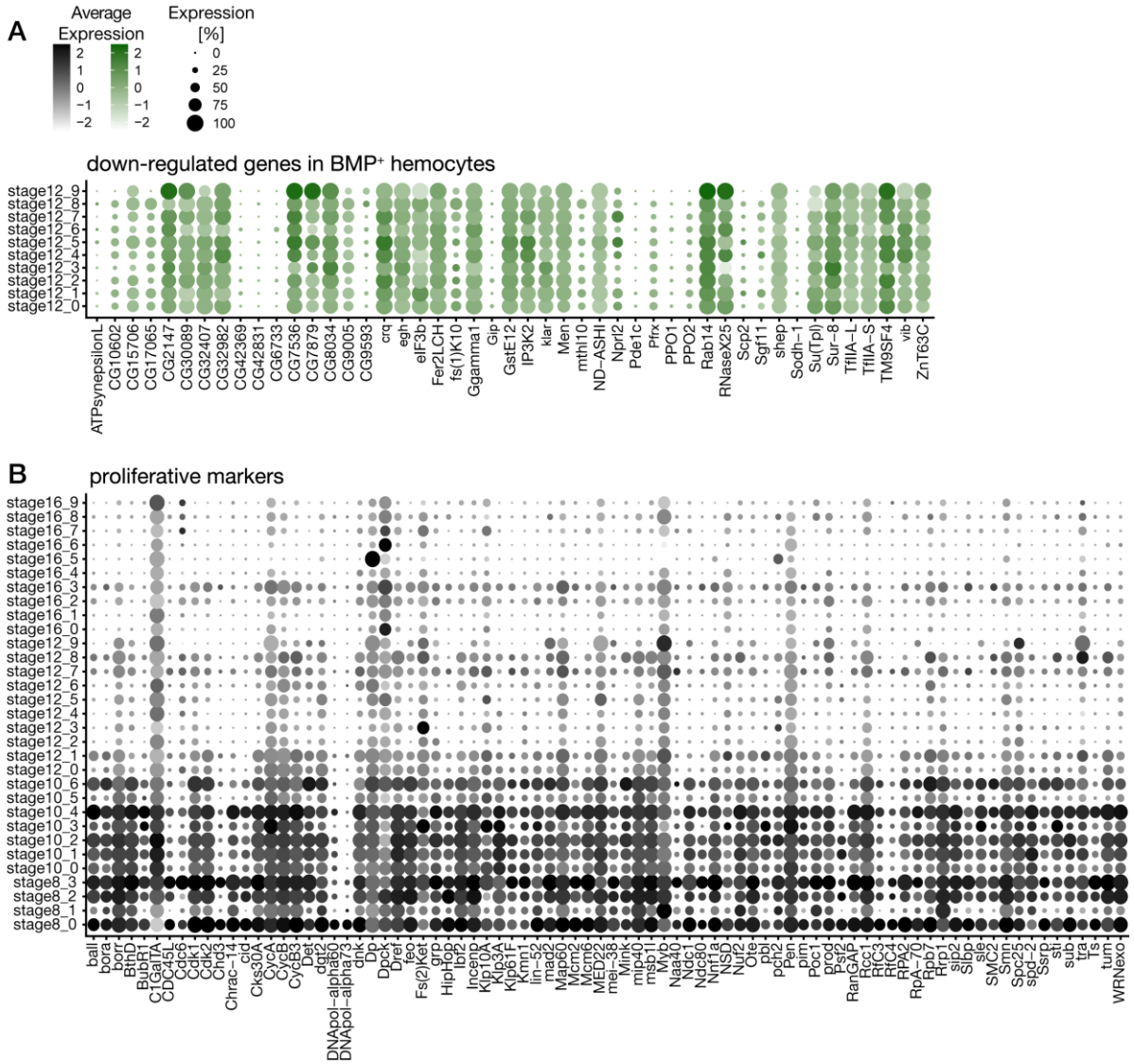

Chapter 3 Fig 5 S 1. Hemocyte clusters show no overlap with genes downregulated in BMP+ hemocytes, but enrichment of proliferation markers at early stages

(A) Dotplot shows expression in clusters of stage 12 hemocytes of down-regulated genes identified in bulk RNA-Sequencing of BMP^{+} hemocytes. There is no enrichment in specific clusters. **(B)** Dotplot shows proliferative markers for all stages in clusters of hemocyte single cell RNA-Sequencing. Hemocytes isolated from stage 8 and stage 10 embryos show enrichment of proliferative markers.

S1 Movie. BMP facilitates macrophage motility during initial invasion into the germband tissue

Movies corresponding to stills shown in **Fig 3B**. Macrophages (magenta) labelled using *srpHemo-H2A::3xmCherry* are imaged while entering the gb in control embryos (left) and embryos in which macrophages express *tkv RNAi*^{2} (right). Time in minutes is indicated in the upper right corner. Scale bar: 10 µm.

S2 Movie. BMP^{+} hemocytes lead germband invasion

Movies corresponding to stills shown in **Fig 3I**. Macrophages (magenta) labelled by *srpHemo-H2A::3xmCherry* are imaged during their invasion of the germband tissue. Activated BMP signaling is visualized using a *Dad-GFP::nls* reporter (green). Time in minutes is indicated in the upper right corner. Scale bar: 20 µm.

4 Future outlook

In this thesis, I describe two mechanisms that *Drosophila* immune cells rely on to overcome the barrier of the germband tissue. One strategy is the strengthening of the actin cortex through developmentally controlled transcriptional regulation induced by the *Drosophila* proto-oncogene family member Dfos. Dfos induces expression of the tetraspanin TM4SF and the filamin Cher, leading to higher levels of the activated formin Dia at the cortex and increased cortical F-actin. The enhanced cortical strength allows hemocytes to overcome the physical resistance of the surrounding tissue and translocate their nucleus to move forward. This mechanism affects the speed of migration when hemocytes face a confined environment *in vivo*. Another aspect is the initial step of the leading hemocytes entering the tissue that potentially guide the follower cells. In Chapter 3, I describe a novel subpopulation of hemocytes activated by BMP signaling prior to tissue invasion that lead penetration into the germband. Hemocytes deficient in BMP signaling activation show impaired persistence during their migration into the germband, while their migration speed remains unaffected. This suggests that there might be different mechanisms controlling immune cell migration within the confined environment *in vivo*, one of these being the general ability to overcome the resistance of the surrounding tissue and another affecting the order of hemocytes that collectively invade the tissue in a stream of individual cells. This opens up further questions regarding both aspects of regulation individually, as well as their interplay during this developmental process. In the following sections, I will give a short overview of future studies that could shed light on this process.

4.1 HOW DO DFOS AND BMP SIGNALING INTERACT DURING HEMOCYTE MIGRATION?

Dfos and BMP signaling both induce transcriptional changes in *Drosophila* embryonic hemocytes to allow efficient penetration into the confined environment of the germband tissue. However, their shared downstream mechanisms remain unknown. Previous experiments performed by Vera Belyaeva utilizing trans-heterogeneous mutant embryos for *tkv* and *Dfos* indicate their genetic interaction in hemocytes, which is reminiscent of their interaction in the developmental migration of epithelial sheets in *Drosophila* embryos. During dorsal closure, Dpp secreted from the leading edge cells regulates cell shape changes and cellular identity in more lateral ectoderm cells through signaling via Tkv/Put leading to changes in *Dfos* expression, which together with DJun regulates effector genes (Riesgo-Escovar & Hafen, 1997). Dpp was proposed to act as a relay signal inducing stretching of the more ventral cells in a Dfos-dependent manner (Perkins et al., 1988). Smad proteins were shown to regulate expression of genes, whose promoters are close to DNA binding sites for Fos-Jun family members, and Smad3 and Smad4 were shown to interact with AP-1 (c-Fos/c-Jun) in TGFβ signaling to synergistically induce gene expression (Omata et al., 2015; Rodríguez-Pascual et al., 2003; Y. Wu et al., 2007; Y. Zhang et al., 1998). It would be interesting to investigate a potential interaction between Dfos and Mad in *Drosophila* hemocytes and the effect on hemocyte invasive migration. Measuring the expression of the putative BMP target genes *Fas2, Fas3, Tsp39D,* and *Mipp1* in *Dfos*-RNAi expressing hemocytes via qPCR of FACS-isolated blood cells could give insights into possible synergistically controlled gene expression.

Additionally, antibody staining for Dfos in embryos with BMP loss of function in hemocytes could show if Dfos levels would potentially be affected by signals from BMP^+ hemocytes. Together, these experiments could contribute to a broader understanding of the still-unknown interaction of Fos and canonical BMP signaling for immune cell migration *in vivo*.

4.2 HOW DO HEMOCYTES INTERACT WITH EACH OTHER TO COORDINATE GERMBAND INVASION?

It is still unknown how immune cells interact with each other to orchestrate their migration during early tissue colonization. Hemocytes rely on Integrin localization to the leading edge through RhoL and the Rho GEF Dizzy for their migration into the germband (Siekhaus et al., 2010). Additionally, transplantation experiments demonstrated that they secrete the basement membrane component Laminin, and loss of Laminin hinders their tissue invasion (Sánchez-Sánchez et al., 2017). Moreover, our RNA-Sequencing identified the chemoattractant Pvf3 and proteins regulating cell-cell interactions to be higher expressed in a BMP^+ subpopulation of hemocytes leading tissue penetration. These findings point toward an orchestrated interaction of hemocytes during their embryonic migration into the germband. While Dia-dependent CIL through formation of a transient hemocyte-hemocyte interaction via an inter-cellular actin-clutch was shown to play a role in hemocyte distribution along the vnc (Davis, Luchici, Miodownik, et al., 2015), cell-cell interactions of hemocytes in a confined tissue remain unknown. Additionally, a direct effect of the Dfos targets TM4SF and Cher on the activation of Dia has not yet been demonstrated (Belyaeva et al., 2022). Future studies investigating the subcellular localization and potential role of putative BMP downstream target genes such as *Fas3*, *Fas2*, and *TM4SF* could shed light on inter-cellular mechanisms governing the collective migration of hemocytes and pave the way for investigations of their functions for tissue colonization by macrophages in higher organisms.

4.3 WHAT IS THE FUNCTION OF E(SPL)C FOR DROSOPHILA HEMOCYTES?

Surprisingly, leading hemocytes inside the germband belong to a previously unknown cluster enriched in the expression of enhancer of split complex *E(spl)C*) genes, which we identify by single cell RNA-Sequencing of hemocytes throughout early embryonic stages. This E(spl)C cluster shows higher expression of putative BMP target genes that regulate the efficient penetration of hemocytes into the germband. *E(spl)C* gene expression is induced downstream of Notch (Wurmbach et al., 1999) and does not play a role in hemocyte germband invasion (Valoskova, 2018). However, expression of one *E(spl)C* gene family member is activated through local Dpp signaling in the larval lymph regulating HSC-like identity (Dey et al., 2016). A direct link between *E(spl)C* expression and either BMP or Notch signaling in embryonic hemocytes has yet to be discovered. This could be investigated by analyzing *E(spl)C* gene activity in hemocytes expressing RNAi against *tkv* or *Notch* in hemocytes using recently generated tagged reporter lines (Couturier et al., 2019). Additionally, *E(spl)C* activity could be monitored in hemocytes expressing a constitutively active form of the Tkv receptor. Moreover, as Notch does not affect hemocyte tissue invasion, it would be very interesting to explore possible alternative effects, such as effects on proliferation similar to hemocytes in the larval lymph gland. Alternatively, *E(spl)C* enriched hemocytes might play specific roles for the further development, or localize to specific tissues similar to peritoneal M2 macrophages showing higher levels of the *E(spl)C* orthologue *Hes1* (Roberts et al., 2017; Shang et al., 2016).

Insights into potential BMP-dependent regulation of *E(spl)C* genes in immune cells would further strengthen similarities of anti-inflammatory M2-like tissue macrophages in *Drosophila* and higher organisms.

4.4 FURTHER INVESTIGATION OF THE DIFFERENT SUBPOPULATIONS

Hitherto, specific functions and localization throughout development of *Drosophila* embryonic immune cell subpopulations have not been well understood. However, *in silico* experiments correlated two subpopulations of unspecified immune cells (plasmatocyte clusters PL-1 and PL-3) with the larval eye disc, and two proliferative clusters of immune cells (plasmatocyte clusters PL-prolif and PL-Inos) with brain tissue (Cattenoz et al., 2021). Moreover, M1-like hemocyte subpopulations identified in late-stage embryos were recently shown to associate with distinct tissues (Coates et al., 2020). In larval hemocytes, immune cells reside in hematopoietic pockets, and they were suggested to adhere to those microenvironments because of local signals from the nervous system that triggers their local proliferation (Makhijani et al., 2011). These data, along with our findings of BMP^+ hemocytes predominantly populating the germband tissue, further suggest similarities between *Drosophila* hemocytes and tissue-resident macrophages in higher vertebrates. In the future, studies on the localization and additional functions of BMP+ hemocytes and other identified early embryonic hemocyte subpopulations will increase our understanding of hematopoietic complexity in flies, potentially revealing even more similarities with higher organisms. Over the past decade, mammalian macrophages have been shown to consist of several different types.

Similar to these findings and to what was suggested for other *Drosophila* hemocyte clusters, BMP^+ hemocytes could represent a population that also might have different features depending on their environment similar to tissue macrophages in higher organisms. In the larva, two plasmatocyte subpopulations showed similar gene expression patterns, and differed only in their level of proliferation markers. They were therefore suggested to reflect different states of the same plasmatocyte cell type (Cattenoz et al., 2020).

Recently, tissue-resident myeloid cells in the mouse brain were shown to be of several previously unknown subtypes expressing tissue-specific markers (Van Hove et al., 2019). Further, single-cell RNA-Seq combined with lab-on-a-chip live cell imaging demonstrated the complexity of macrophage ontogeny and tissue interaction that both account for macrophage heterogeneity (Wills et al., 2017). Combinations of such elegant *in vitro* studies with knowledge obtained from *Drosophila in vivo* could pave the way for a better understanding of the true mechanisms influencing the complexity of tissue resident macrophages, as well as their tissue infiltration ability during development and disease.

5 References

Abercrombie, M., Heaysman, J. E. M., & Pegrum, S. M. (1970). The locomotion of fibroblasts in culture. 3. Movements of particles on the dorsal surface of the leading lamella. *Experimental Cell Research*, *62*(2), 389–398. https://doi.org/10.1016/0014-4827(70)90570-7

Abraham, S., Yeo, M., Montero-Balaguer, M., Paterson, H., Dejana, E., Marshall, C. J., & Mavria, G. (2009). VE-Cadherin-mediated cell-cell interaction suppresses sprouting via signaling to MLC2 phosphorylation. *Current Biology : CB*, *19*(8), 668–674. https://doi.org/10.1016/J.CUB.2009.02.057

Affolter, M., Nellen, D., Nussbaumer, U., & Basler, K. (1994). Multiple requirements for the receptor serine/threonine kinase thick veins reveal novel functions of TGF beta homologs during Drosophila embryogenesis. *Development*, *120*(11), 3105–3117. http://dev.biologists.org/content/120/11/3105.abstract

Afik, R., Zigmond, E., Vugman, M., Klepfish, M., Shimshoni, E., Pasmanik-Chor, M., Shenoy, A., Bassat, E., Halpern, Z., Geiger, T., Sagi, I., & Varol, C. (2016). Tumor macrophages are pivotal constructors of tumor collagenous matrix. *The Journal of Experimental Medicine*, *213*(11), 2315. https://doi.org/10.1084/JEM.20151193

Akhmanova, M., Gyoergy, A., Vlasov, M., Vlasov, F., Krueger, D., Akopian, A., Emtenani, S., Ratheesh, A., Renzis, S. De, & Siekhaus, D. E. (2021). Cell division in tissues enables macrophage infiltration. *BioRxiv*, 2021.04.19.438995. https://doi.org/10.1101/2021.04.19.438995

Alfonso, T. B., & Jones, B. W. (2002). gcm2 promotes glial cell differentiation and is required with glial cells missing for macrophage development in Drosophila. *Developmental Biology*, *248*(2), 369–383. https://doi.org/10.1006/dbio.2002.0740

Amigo, J. D., Ackermann, G. E., Cope, J. J., Yu, M., Cooney, J. D., Ma, D., Langer, N. B., Shafizadeh, E., Shaw, G. C., Horsely, W., Trede, N. S., Davidson, A. J., Barut, B. A., Zhou, Y., Wojiski, S. A., Traver, D., Moran, T. B., Kourkoulis, G., Hsu, K., … Paw, B. H. (2009). The role and regulation of friend of GATA-1 (FOG-1) during blood development in the zebrafish. *Blood*, *114*(21), 4654. https://doi.org/10.1182/BLOOD-2008-12-189910

Awasaki, T., Lai, S. L., Ito, K., & Lee, T. (2008). Organization and Postembryonic Development of Glial Cells in the Adult Central Brain of Drosophila. *Journal of Neuroscience*, *28*(51), 13742–13753. https://doi.org/10.1523/JNEUROSCI.4844-08.2008

Bakopoulos, D., Whisstock, J. C., Warr, C. G., & Johnson, T. K. (2022). Macrophage self-renewal is regulated by transient expression of PDGF- and VEGF-related factor 2. *The FEBS Journal*. https://doi.org/10.1111/FEBS.16364

Banerjee, U., Girard, J. R., Goins, L. M., & Spratford, C. M. (2019). Drosophila as a Genetic Model for Hematopoiesis. *Genetics*, *211*(2), 367. https://doi.org/10.1534/GENETICS.118.300223

Bataillé, L., Augé, B., Ferjoux, G., Haenlin, M., & Waltzer, L. (2005). Resolving embryonic blood cell fate choice in Drosophila:interplay of GCM and RUNX factors. *Development*, *132*(20),

4635–4644. https://doi.org/10.1242/DEV.02034

Belele, C. L., English, M. A., Chahal, J., Burnetti, A., Finckbeiner, S. M., Gibney, G., Kirby, M., Sood, R., & Liu, P. P. (2009). Differential requirement for Gata1 DNA binding and transactivation between primitive and definitive stages of hematopoiesis in zebrafish. *Blood*, *114*(25), 5162. https://doi.org/10.1182/BLOOD-2009-05-224709

Belyaeva, V., Wachner, S., Gyoergy, A., Emtenani, S., Gridchyn, I., Akhmanova, M., Linder, M., Roblek, M., Sibilia, M., & Siekhaus, D. (2022). Fos regulates macrophage infiltration against surrounding tissue resistance by a cortical actin-based mechanism in Drosophila. *PLoS Biology*, *20*(1), e3001494. https://doi.org/10.1371/JOURNAL.PBIO.3001494

Benhra, N., Barrio, L., Muzzopappa, M., & Milán, M. (2018). Chromosomal Instability Induces Cellular Invasion in Epithelial Tissues. *Developmental Cell*, *47*(2), 161-174.e4. https://doi.org/10.1016/j.devcel.2018.08.021

Benn, A., Hiepen, C., Osterland, M., Schütte, C., Zwijsen, A., & Knaus, P. (2017). Role of bone morphogenetic proteins in sprouting angiogenesis: Differential BMP receptor-dependent signaling pathways balance stalk vs. tip cell competence. *FASEB Journal*, *31*(11), 4720–4733. https://doi.org/10.1096/FJ.201700193RR/-/DC1

Berke, B., Wittnam, J., McNeill, E., Van Vactor, D. L., & Keshishian, H. (2013). Retrograde BMP signaling at the synapse: a permissive signal for synapse maturation and activity-dependent plasticity. *The Journal of Neuroscience : The Official Journal of the Society for Neuroscience*, *33*(45), 17937–17950. https://doi.org/10.1523/JNEUROSCI.6075-11.2013

Bernardoni, R., Vivancos, V., & Giangrande, a. (1997). Glide/Gcm Is Expressed and Required in the Scavenger Cell Lineage. *Developmental Biology*, *191*(1), 118–130. https://doi.org/10.1006/dbio.1997.8702

Bhatia, M., Bonnet, D., Wu, D., Murdoch, B., Wrana, J., Gallacher, L., & Dick, J. E. (1999). Bone Morphogenetic Proteins Regulate the Developmental Program of Human Hematopoietic Stem Cells. *The Journal of Experimental Medicine*, *189*(7), 1139. https://doi.org/10.1084/JEM.189.7.1139

Blanco-Obregon, D., Katz, M. J., Durrieu, L., Gándara, L., & Wappner, P. (2020). Context-specific functions of Notch in Drosophila blood cell progenitors. *Developmental Biology*, *462*(1), 101–115. https://doi.org/10.1016/J.YDBIO.2020.03.018

Blaser, H., Reichman-Fried, M., Castanon, I., Dumstrei, K., Marlow, F. L. L., Kawakami, K., Solnica-Krezel, L., Heisenberg, C. P., & Raz, E. (2006). Migration of Zebrafish Primordial Germ Cells: A Role for Myosin Contraction and Cytoplasmic Flow. *Developmental Cell*, *11*(5), 613–627. https://doi.org/10.1016/J.DEVCEL.2006.09.023

Blokzijl, A., Dahlqvist, C., Reissmann, E., Falk, A., Moliner, A., Lendahl, U., & Ibáñez, C. F. (2003). Cross-talk between the Notch and TGF-beta signaling pathways mediated by interaction of the Notch intracellular domain with Smad3. *The Journal of Cell Biology*, *163*(4), 723–728. https://doi.org/10.1083/JCB.200305112

Borkowski, T. A., Letterio, J. J., Farr, A. G., & Udey, M. C. (1996). A role for endogenous transforming growth factor beta 1 in Langerhans cell biology: the skin of transforming growth factor beta 1 null mice is devoid of epidermal Langerhans cells. *J.Exp.Med.*,

184(0022–1007), 2417–2422.

Borkowski, T., Letterio, J., Mackall, C., Saitoh, A., Wang, X., Roop, D., Gress, R., & Udey, M. (1997). A Role for TGFb1 in Langerhans Cell Biology. *The Journal of Clinical Investigation*, *100*(3), 575–581.

Bou Ghosn, E. E., Cassado, A. A., Govoni, G. R., Fukuhara, T., Yang, Y., Monack, D. M., Bortoluci, K. R., Almeida, S. R., Herzenberg, L. A., & Herzenberg, L. A. (2010). Two physically, functionally, and developmentally distinct peritoneal macrophage subsets. *Proceedings of the National Academy of Sciences of the United States of America*, *107*(6), 2568–2573. https://doi.org/10.1073/PNAS.0915000107

Boulet, M., Renaud, Y., Lapraz, F., Benmimoun, B., Vandel, L., & Waltzer, L. (2021). Characterization of the Drosophila Adult Hematopoietic System Reveals a Rare Cell Population With Differentiation and Proliferation Potential. *Frontiers in Cell and Developmental Biology*, *9*, 2863. https://doi.org/10.3389/FCELL.2021.739357/BIBTEX

Brock, A. R., Wang, Y., Berger, S., Renkawitz-Pohl, R., Han, V. C., Wu, Y., & Galko, M. J. (2012). Transcriptional regulation of profilin during wound closure in Drosophila larvae. *Journal of Cell Science*, *125*(23), 5667–5676. https://doi.org/10.1242/jcs.107490

Brückner, K., Kockel, L., Duchek, P., Luque, C. M., Rorth, P., & Perrimon, N. (2004). The PDGF/VEGF receptor controls blood cell survival in Drosophila. *Developmental Cell*, *7*(1), 73–84.

Brummel, T., Abdollah, S., Haerry, T. E., Shimell, M. J., Merriam, J., Raftery, L., Wrana, J. L., & O'Connor, M. B. (1999). The Drosophila activin receptor Baboon signals through dSmad2 and controls cell proliferation but not patterning during larval development. *Genes and Development*, *13*(1), 98–111. https://doi.org/10.1101/gad.13.1.98

Brummel, T. J., Twombly, V., Marqués, G., Wrana, J. L., Newfeld, S. J., Attisano, L., Massagué, J., O'Connor, M. B., & Gelbart, W. M. (1994). Characterization and relationship of Dpp receptors encoded by the saxophone and thick veins genes in Drosophila. *Cell*, *78*(2), 251–261. https://doi.org/10.1016/0092-8674(94)90295-X

Bruveris, F. F., Ng, E. S., Leitoguinho, A. R., Motazedian, A., Vlahos, K., Sourris, K., Mayberry, R., McDonald, P., Azzola, L., Davidson, N. M., Oshlack, A., Stanley, E. G., & Elefanty, A. G. (2021). Human yolk sac-like haematopoiesis generates RUNX1-, GFI1- and/or GFI1B-dependent blood and SOX17-positive endothelium. *Development (Cambridge)*, *147*(20). https://doi.org/10.1242/DEV.193037/VIDEO-1

Buchon, N., Silverman, N., & Cherry, S. (2014). Immunity in Drosophila melanogaster — from microbial recognition to whole-organism physiology. *Nature Reviews Immunology 2014 14:12*, *14*(12), 796–810. https://doi.org/10.1038/nri3763

Bunt, S., Hooley, C., Hu, N., Scahill, C., Weavers, H., & Skaer, H. (2010). Hemocyte-secreted type IV collagen enhances BMP signaling to guide renal tubule morphogenesis in Drosophila. *Developmental Cell*, *19*(2), 296–306. https://doi.org/10.1016/j.devcel.2010.07.019

Butovsky, O., Jedrychowski, M. P., Moore, C. S., Cialic, R., Lanser, A. J., Gabriely, G., Koeglsperger, T., Dake, B., Wu, P. M., Doykan, C. E., Fanek, Z., Liu, L., Chen, Z., Rothstein,

J. D., Ransohoff, R. M., Gygi, S. P., Antel, J. P., & Weiner, H. L. (2014). Identification of a Unique TGF-β Dependent Molecular and Functional Signature in Microglia. *Nature Neuroscience*, *17*(1), 131. https://doi.org/10.1038/NN.3599

Calero-Cuenca, F. J., Janota, C. S., & Gomes, E. R. (2018). Dealing with the nucleus during cell migration. *Current Opinion in Cell Biology*, *50*, 35–41. https://doi.org/10.1016/J.CEB.2018.01.014

Campos, I., Geiger, J. A., Santos, A. C., Carlos, V., & Jacinto, A. (2010). Genetic screen in Drosophila melanogaster uncovers a novel set of genes required for embryonic epithelial repair. *Genetics*, *184*(1), 129–140. https://doi.org/10.1534/GENETICS.109.110288

Canty, E. G., Garrigue-Antar, L., & Kadler, K. E. (2006). A Complete Domain Structure of Drosophila Tolloid Is Required for Cleavage of Short Gastrulation *. *Journal of Biological Chemistry*, *281*(19), 13258–13267. https://doi.org/10.1074/JBC.M510483200

Carmona-Fontaine, C., Matthews, H. K., Kuriyama, S., Moreno, M., Dunn, G. A., Parsons, M., Stern, C. D., & Mayor, R. (2008). Contact inhibition of locomotion in vivo controls neural crest directional migration. *Nature*, *456*(7224), 957–961. https://doi.org/10.1038/NATURE07441

Cattenoz, P. B., Monticelli, S., Pavlidaki, A., & Giangrande, A. (2021). Toward a Consensus in the Repertoire of Hemocytes Identified in Drosophila Supplement. *Frontiers in Cell and Developmental Biology*, *9*. https://doi.org/10.3389/FCELL.2021.643712/FULL

Cattenoz, P. B., Sakr, R., Pavlidaki, A., Delaporte, C., Riba, A., Molina, N., Hariharan, N., Mukherjee, T., & Giangrande, A. (2020). Temporal specificity and heterogeneity of Drosophila immune cells. *The EMBO Journal*, *39*(12), e104486. https://doi.org/10.15252/EMBJ.2020104486

Caussinus, E., Colombelli, J., & Affolter, M. (2008). Tip-cell migration controls stalk-cell intercalation during Drosophila tracheal tube elongation. *Current Biology : CB*, *18*(22), 1727–1734. https://doi.org/10.1016/J.CUB.2008.10.062

Champion, T. C., Partridge, L. J., Ong, S. M., Malleret, B., Wong, S. C., & Monk, P. N. (2018). Monocyte Subsets Have Distinct Patterns of Tetraspanin Expression and Different Capacities to Form Multinucleate Giant Cells. *Frontiers in Immunology*, *9*(JUN). https://doi.org/10.3389/FIMMU.2018.01247

Chaplin, D. D. (n.d.). *Overview of the Immune Response*. *845*, 35294–2170. https://doi.org/10.1016/j.jaci.2009.12.980

Cheng, Y. L., & Andrew, D. J. (2015). Extracellular Mipp1 Activity Confers Migratory Advantage to Epithelial Cells during Collective Migration. *Cell Reports*, *13*(10), 2174–2188. https://doi.org/10.1016/j.celrep.2015.10.071

Childs, S. R., & O'connor, M. B. (1994). Two domains of the tolloid protein contribute to its unusual genetic interaction with decapentaplegic. *Developmental Biology*, *162*(1), 209–220. https://doi.org/10.1006/DBIO.1994.1079

Chiu, Y. H., & Chen, H. (2016). GATA3 inhibits GCM1 activity and trophoblast cell invasion. *Scientific Reports*, *6*. https://doi.org/10.1038/SREP21630

Cho, B., Yoon, S. H., Lee, D., Koranteng, F., Tattikota, S. G., Cha, N., Shin, M., Do, H., Hu, Y., Oh, S. Y., Lee, D., Vipin Menon, A., Moon, S. J., Perrimon, N., Nam, J. W., & Shim, J. (2020). Single-cell transcriptome maps of myeloid blood cell lineages in Drosophila. *Nature Communications*, *11*(1), 1–18. https://doi.org/10.1038/s41467-020-18135-y

Cho, N. K., Keyes, L., Johnson, E., Heller, J., Ryner, L., Karim, F., & Krasnow, M. A. (2002). Developmental control of blood cell migration by the drosophila VEGF pathway. *Cell*, *108*(6), 865–876. https://doi.org/10.1016/S0092-8674(02)00676-1

Choi, S., Yu, J., Park, A., Dubon, M. J., Do, J., Kim, Y., Nam, D., Noh, J., & Park, K. S. (2019). BMP-4 enhances epithelial mesenchymal transition and cancer stem cell properties of breast cancer cells via Notch signaling. *Scientific Reports 2019 9:1*, *9*(1), 1–14. https://doi.org/10.1038/s41598-019-48190-5

Clark, R. I., Woodcock, K. J., Geissmann, F., Trouillet, C., & Dionne, M. S. (2011). Multiple TGF-β Superfamily Signals Modulate the Adult Drosophila Immune Response. *Current Biology*, *21*(19), 1672. https://doi.org/10.1016/J.CUB.2011.08.048

Coates, J. A., Brooks, E., Brittle, A. L., Armitage, E. L., Zeidler, M. P., & Evans, I. R. (2021). Identification of functionally distinct macrophage subpopulations in Drosophila. *ELife*, *10*. https://doi.org/10.7554/ELIFE.58686

Comber, K., Huelsmann, S., Evans, I., Sánchez-Sánchez, B., Chalmers, a, Reuter, R., Wood, W., & Martín-Bermudo, M. (2013). A dual role for the βPS integrin myospheroid in mediating Drosophila embryonic macrophage migration. *Journal of Cell Science*, *126*(Pt 15), 3475–3484. https://doi.org/10.1242/jcs.129700

Couturier, L., Mazouni, K., Corson, F., & Schweisguth, F. (2019). Regulation of Notch output dynamics via specific E(spl)-HLH factors during bristle patterning in Drosophila. *Nature Communications*, *10*(1), 1–13. https://doi.org/10.1038/s41467-019-11477-2

Cramer, L. P. (1997). Molecular mechanism of actin-dependent retrograde flow in lamellipodia of motile cells. *Frontiers in Bioscience : A Journal and Virtual Library*, *2*. https://doi.org/10.2741/A189

Crozatier, M., Glise, B., & Vincent, A. (2004). Patterns in evolution: Veins of the Drosophila wing. *Trends in Genetics*, *20*(10), 498–505. https://doi.org/10.1016/j.tig.2004.07.013

Cunningham, C. L., Martínez-Cerdeño, V., & Noctor, S. C. (2013). Microglia Regulate the Number of Neural Precursor Cells in the Developing Cerebral Cortex. *Journal of Neuroscience*, *33*(10), 4216–4233. https://doi.org/10.1523/JNEUROSCI.3441-12.2013

Daga, A., Karlovich, C. A., Dumstrei, K., & Banerjee, U. (1996). Patterning of cells in the Drosophila eye by Lozenge, which shares homologous domains with AML1. *Genes & Development*, *10*(10), 1194–1205. https://doi.org/10.1101/GAD.10.10.1194

Dahlqvist, C., Blokzijl, A., Chapman, G., Falk, A., Dannaeus, K., Ibâñez, C. F., & Lendahl, U. (2003). Functional Notch signaling is required for BMP4-induced inhibition of myogenic differentiation. *Development (Cambridge, England)*, *130*(24), 6089–6099. https://doi.org/10.1242/DEV.00834

Das, P., Inoue, H., Baker, J. C., Beppu, H., Kawabata, M., Harland, R. M., Miyazono, K., & Padgett, R. W. (1999). Drosophila dSmad2 and Atr-I transmit activin/TGFβ signals. *Genes*

to Cells, *4*(2), 123–134. https://doi.org/10.1046/J.1365-2443.1999.00244.X

Davies, L. C., Jenkins, S. J., Allen, J. E., & Taylor, P. R. (2013). Tissue-resident macrophages. *Nature Immunology 2013 14:10*, *14*(10), 986–995. https://doi.org/10.1038/ni.2705

Davis, J. R., Huang, C. Y., Zanet, J., Harrison, S., Rosten, E., Cox, S., Soong, D. Y., Dunn, G. A., & Stramer, B. M. (2012). Emergence of embryonic pattern through contact inhibition of locomotion. *Development (Cambridge)*, *139*(24), 4555–4560. https://doi.org/10.1242/DEV.082248/-/DC1

Davis, J. R., Luchici, A., Miodownik, M., Stramer, B. M., Davis, J. R., Luchici, A., Mosis, F., Thackery, J., Salazar, J. A., Mao, Y., Dunn, G. A., Betz, T., Miodownik, M., & Stramer, B. M. (2015). Inter-Cellular Forces Orchestrate Contact Inhibition of Locomotion Article Inter-Cellular Forces Orchestrate Contact Inhibition of Locomotion. *Cell*, *161*(2), 361–373. https://doi.org/10.1016/j.cell.2015.02.015

Dawson, C. A., Pal, B., Vaillant, F., Gandolfo, L. C., Liu, Z., Bleriot, C., Ginhoux, F., Smyth, G. K., Lindeman, G. J., Mueller, S. N., Rios, A. C., & Visvader, J. E. (2020). Tissue-resident ductal macrophages survey the mammary epithelium and facilitate tissue remodelling. *Nature Cell Biology*, *22*(5), 546–558. https://doi.org/10.1038/S41556-020-0505-0

de Velasco, B., Mandal, L., Mkrtchyan, M., & Hartenstein, V. (2006). Subdivision and developmental fate of the head mesoderm in Drosophila melanogaster. *Development Genes and Evolution*, *216*(1), 39–51. https://doi.org/10.1007/s00427-005-0029-4

DeFalco, T., Bhattacharya, I., Williams, A. V., Sams, D. M., & Capel, B. (2014). Yolk-sac-derived macrophages regulate fetal testis vascularization and morphogenesis. *Proceedings of the National Academy of Sciences of the United States of America*, *111*(23), E2384–E2393. https://doi.org/10.1073/PNAS.1400057111/-/DCSUPPLEMENTAL

Dequier, E., Souid, S., Pál, M., Maróy, P., Lepesant, J.-A., & Yanicostas, C. (2001). Top–DER- and Dpp-dependent requirements for the Drosophila fos/kayak gene in follicular epithelium morphogenesis. *Mechanisms of Development*, *106*(1–2), 47–60. https://doi.org/10.1016/S0925-4773(01)00418-X

Dey, N. S., Ramesh, P., Chugh, M., Mandal, S., & Mandal, L. (2016). Dpp dependent hematopoietic stem cells give rise to Hh dependent blood progenitors in larval lymph gland of Drosophila. *ELife*, *5*(OCTOBER2016). https://doi.org/10.7554/ELIFE.18295

Diz-Muñoz, A., Romanczuk, P., Yu, W., Bergert, M., Ivanovitch, K., Salbreux, G., Heisenberg, C. P., & Paluch, E. K. (2016). Steering cell migration by alternating blebs and actin-rich protrusions. *BMC Biology*, *14*(1), 1–13. https://doi.org/10.1186/S12915-016-0294-X/FIGURES/5

Dobin, A., Davis, C. A., Schlesinger, F., Drenkow, J., Zaleski, C., Jha, S., Batut, P., Chaisson, M., & Gingeras, T. R. (2013). STAR: Ultrafast universal RNA-seq aligner. *Bioinformatics*, *29*(1), 15–21. https://doi.org/10.1093/bioinformatics/bts635

Donà, E., Barry, J. D., Valentin, G., Quirin, C., Khmelinskii, A., Kunze, A., Durdu, S., Newton, L. R., Fernandez-Minan, A., Huber, W., Knop, M., & Gilmour, D. (2013). Directional tissue migration through a self-generated chemokine gradient. *Nature*, *503*(7475), 285–289. https://doi.org/10.1038/NATURE12635

Doyle, E. L., Ridger, V., Ferraro, F., Turmaine, M., Saftig, P., & Cutler, D. F. (2011). CD63 is an essential cofactor to leukocyte recruitment by endothelial P-selectin. *Blood*, *118*(15), 4265–4273. https://doi.org/10.1182/BLOOD-2010-11-321489

Drevon, C., & Jaffredo, T. (2014). Cell interactions and cell signaling during hematopoietic development. *Experimental Cell Research*, *329*(2), 200–206. https://doi.org/10.1016/J.YEXCR.2014.10.009

Dudzic, J. P., Kondo, S., Ueda, R., Bergman, C. M., & Lemaitre, B. (2015). Drosophila innate immunity: regional and functional specialization of prophenoloxidases. *BMC Biology*, *13*(1). https://doi.org/10.1186/S12915-015-0193-6

Durand, C., Robin, C., Bollerot, K., Baron, M. H., Ottersbach, K., & Dzierzak, E. (2007). Embryonic stromal clones reveal developmental regulators of definitive hematopoietic stem cells. *Proceedings of the National Academy of Sciences*, *104*(52), 20838–20843. https://doi.org/10.1073/PNAS.0706923105

Duvic, B., Hoffmann, J. A., Meister, M., & Royet, J. (2002). Notch signaling controls lineage specification during Drosophila larval hematopoiesis. *Current Biology : CB*, *12*(22), 1923–1927. https://doi.org/10.1016/S0960-9822(02)01297-6

Dzierzak, E., & Speck, N. A. (2008). Of lineage and legacy – the development of mammalian hematopoietic stem cells. *Nature Immunology*, *9*(2), 129. https://doi.org/10.1038/NI1560

Elagib, K. E., Racke, F. K., Mogass, M., Khetawat, R., Delehanty, L. L., & Goldfarb, A. N. (2003). RUNX1 and GATA-1 coexpression and cooperation in megakaryocytic differentiation. *Blood*, *101*(11), 4333–4341. https://doi.org/10.1182/BLOOD-2002-09-2708

Emtenani, S., Martin, E. T., Gyoergy, A., Bicher, J., Genger, J.-W., Hurd, T. R., Köcher, T., Bergthaler, A., Rangan, P., & Siekhaus, D. E. (2021). A genetic program boosts mitochondrial function to power macrophage tissue invasion. *BioRxiv*, 2021.02.18.431643. https://doi.org/10.1101/2021.02.18.431643

Eresh, S., Riese, J., Jackson, D. B., Bohmann, D., & Bienz, M. (1997). A CREB-binding site as a target for decapentaplegic signalling during Drosophila endoderm induction. *EMBO Journal*, *16*(8), 2014–2022. https://doi.org/10.1093/emboj/16.8.2014

Etienne-Manneville, S. (2008). Polarity proteins in migration and invasion. *Oncogene*, *27*(55), 6970–6980. https://doi.org/10.1038/ONC.2008.347

Evans, C. J., Hartenstein, V., & Banerjee, U. (2003). Thicker than blood: Conserved mechanisms in Drosophila and vertebrate hematopoiesis. In *Developmental Cell* (Vol. 5, Issue 5, pp. 673–690). Cell Press. https://doi.org/10.1016/S1534-5807(03)00335-6

Evans, C. J., Sinenko, S. A., Mandal, L., Martinez-Agosto, J. A., Hartenstein, V., & Banerjee, U. (2007). Genetic Dissection of Hematopoiesis Using Drosophila as a Model System. *Advances in Developmental Biology*, *18*(07), 259–299. https://doi.org/10.1016/S1574-3349(07)18011-X

Evans, Iwan R., Hu, N., Skaer, H., & Wood, W. (2010). Interdependence of macrophage migration and ventral nerve cord development in Drosophila embryos. *Development*, *137*(10), 1625–1633. https://doi.org/10.1242/dev.046797

Evans, Iwan Robert, & Wood, W. (2011). Drosophila embryonic hemocytes. *Current Biology*, *21*(5), R173–R174. https://doi.org/10.1016/j.cub.2011.01.061

Fantin, A., Vieira, J. M., Gestri, G., Denti, L., Schwarz, Q., Prykhozhij, S., Peri, F., Wilson, S. W., & Ruhrberg, C. (2010). Tissue macrophages act as cellular chaperones for vascular anastomosis downstream of VEGF-mediated endothelial tip cell induction. *Blood*, *116*(5), 829–840. https://doi.org/10.1182/BLOOD-2009-12-257832

Ferguson, E. L., & Anderson, K. V. (1992). Decapentaplegic acts as a morphogen to organize dorsal-ventral pattern in the Drosophila embryo. *Cell*, *71*(3), 451–461. https://doi.org/10.1016/0092-8674(92)90514-D

Fernández, B. G., Arias, A. M., & Jacinto, A. (2007). Dpp signalling orchestrates dorsal closure by regulating cell shape changes both in the amnioserosa and in the epidermis. *Mechanisms of Development*, *124*(11–12), 884–897. https://doi.org/10.1016/J.MOD.2007.09.002

Fossett, N., Hyman, K., Gajewski, K., Orkin, S. H., & Schulz, R. A. (2003). Combinatorial interactions of serpent, lozenge, and U-shaped regulate crystal cell lineage commitment during Drosophila hematopoiesis. *Proceedings of the National Academy of Sciences of the United States of America*, *100*(20), 11451–11456. https://doi.org/10.1073/PNAS.1635050100

François, V., Solloway, M., O'Neill, J. W., Emery, J., & Bier, E. (1994). Dorsal-ventral patterning of the Drosophila embryo depends on a putative negative growth factor encoded by the short gastrulation gene. *Genes & Development*, *8*(21), 2602–2616. https://doi.org/10.1101/GAD.8.21.2602

Frey, P., Devisme, A., Schrempp, M., Andrieux, G., Boerries, M., & Hecht, A. (2020). Canonical BMP Signaling Executes Epithelial-Mesenchymal Transition Downstream of SNAIL1. *Cancers*, *12*(4). https://doi.org/10.3390/CANCERS12041019

Friedl, P., & Alexander, S. (2011). Cancer Invasion and the Microenvironment: Plasticity and Reciprocity. *Cell*, *147*(5), 992–1009. https://doi.org/10.1016/J.CELL.2011.11.016

Friedl, P., & Weigelin, B. (2008). Interstitial leukocyte migration and immune function. *Nat Immunol*, *9*(9), 960–969. http://dx.doi.org/10.1038/ni.f.212

Fu, Y., Huang, X., Zhang, P., van de Leemput, J., & Han, Z. (2020). Single-cell RNA sequencing identifies novel cell types in Drosophila blood. *Journal of Genetics and Genomics*, *47*(4), 175–186. https://doi.org/10.1016/j.jgg.2020.02.004

Fujiwara, Y., Chang, A. N., Williams, A. M., & Orkin, S. H. (2004). Functional overlap of GATA-1 and GATA-2 in primitive hematopoietic development. *Blood*, *103*(2), 583–585. https://doi.org/10.1182/blood-2003-08-2870

Gautier, E. L., Shay, T., Miller, J., Greter, M., Jakubzick, C., Ivanov, S., Helft, J., Chow, A., Elpek, K. G., Gordonov, S., Mazloom, A. R., Ma'Ayan, A., Chua, W. J., Hansen, T. H., Turley, S. J., Merad, M., Randolph, G. J., Best, A. J., Knell, J., … Benoist, C. (2012). Gene-expression profiles and transcriptional regulatory pathways that underlie the identity and diversity of mouse tissue macrophages. *Nature Immunology*, *13*(11), 1118–1128. https://doi.org/10.1038/NI.2419

Ghabrial, A. S., & Krasnow, M. A. (2006). Social interactions among epithelial cells during tracheal branching morphogenesis. *Nature*, *441*(7094), 746–749. https://doi.org/10.1038/NATURE04829

Gold, K. S., & Brückner, K. (2014). Drosophila as a model for the two myeloid blood cell systems in vertebrates. *Experimental Hematology*, *42*(8), 717–727. https://doi.org/10.1016/j.exphem.2014.06.002

Gong, D., Shi, W., Yi, S. ju, Chen, H., Groffen, J., & Heisterkamp, N. (2012). TGFβ signaling plays a critical role in promoting alternative macrophage activation. *BMC Immunology*, *13*(1), 1–10. https://doi.org/10.1186/1471-2172-13-31/FIGURES/3

Gouon-Evans, V., Rothenberg, M. E., & Pollard, J. W. (2000). Postnatal mammary gland development requires macrophages and eosinophils. *Development*, *127*(11), 2269–2282. https://doi.org/10.1242/DEV.127.11.2269

Gout, S., & Huot, J. (2008). Role of cancer microenvironment in metastasis: Focus on colon cancer. *Cancer Microenvironment*, *1*(1), 69–83. https://doi.org/10.1007/s12307-008-0007-2

Graveley, B. R., Brooks, A. N., Carlson, J. W., Duff, M. O., Landolin, J. M., Yang, L., Artieri, C. G., Van Baren, M. J., Boley, N., Booth, B. W., Brown, J. B., Cherbas, L., Davis, C. A., Dobin, A., Li, R., Lin, W., Malone, J. H., Mattiuzzo, N. R., Miller, D., … Celniker, S. E. (2010). The developmental transcriptome of Drosophila melanogaster. *Nature 2010 471:7339*, *471*(7339), 473–479. https://doi.org/10.1038/nature09715

Gregory Call, S., Brereton, D., Bullard, J. T., Chung, J. Y., Meacham, K. L., Morrell, D. J., Reeder, D. J., Schuler, J. T., Slade, A. D., & Hansen, M. D. H. (2011). A zyxin–nectin interaction facilitates zyxin localization to cell–cell adhesions. *Biochemical and Biophysical Research Communications*, *415*(3), 485–489. https://doi.org/10.1016/J.BBRC.2011.10.099

Grenningloh, G., Jay Rehm, E., & Goodman, C. S. (1991). Genetic analysis of growth cone guidance in drosophila: Fasciclin II functions as a neuronal recognition molecule. *Cell*, *67*(1), 45–57. https://doi.org/10.1016/0092-8674(91)90571-F

Grimaldi, C., Schumacher, I., Boquet-Pujadas, A., Tarbashevich, K., Vos, B. E., Bandemer, J., Schick, J., Aalto, A., Olivo-Marin, J. C., Betz, T., & Raz, E. (2020). E-cadherin focuses protrusion formation at the front of migrating cells by impeding actin flow. *Nature Communications 2020 11:1*, *11*(1), 1–15. https://doi.org/10.1038/s41467-020-19114-z

Gyoergy, A., Roblek, M., Ratheesh, A., Valoskova, K., Belyaeva, V., Wachner, S., Matsubayashi, Y., Sánchez-Sánchez, B. J., Stramer, B., & Siekhaus, D. E. (2018). Tools allowing independent visualization and genetic manipulation of Drosophila melanogaster macrophages and surrounding tissues. *G3: Genes, Genomes, Genetics*, *8*(3). https://doi.org/10.1534/g3.117.300452

Haerry, T. E., Khalsa, O., O'Connor, M. B., & Wharton, K. A. (1998). Synergistic signaling by two BMP ligands through the SAX and TKV receptors controls wing growth and patterning in Drosophila. *Development*, *125*(20), 3977–3987. https://doi.org/10.1242/DEV.125.20.3977

Hamaratoglu, F., de Lachapelle, A. M., Pyrowolakis, G., Bergmann, S., & Affolter, M. (2011).

Dpp Signaling Activity Requires Pentagone to Scale with Tissue Size in the Growing Drosophila Wing Imaginal Disc. *PLoS Biology*, *9*(10). https://doi.org/10.1371/JOURNAL.PBIO.1001182

Harris, K. E., Schnittke, N., & Beckendorf, S. K. (2007). Two Ligands Signal Through the Drosophila PDGF/VEGF Receptor to Ensure Proper Salivary Gland Positioning. *Mechanisms of Development*, *124*(6), 441. https://doi.org/10.1016/J.MOD.2007.03.003

Heino, T. I., Kärpänen, T., Wahlström, G., Pulkkinen, M., Eriksson, U., Alitalo, K., & Roos, C. (2001). The Drosophila VEGF receptor homolog is expressed in hemocytes. *Mechanisms of Development*, *109*(1), 69–77. https://doi.org/10.1016/S0925-4773(01)00510-X

Hellström, M., Phng, L. K., Hofmann, J. J., Wallgard, E., Coultas, L., Lindblom, P., Alva, J., Nilsson, A. K., Karlsson, L., Gaiano, N., Yoon, K., Rossant, J., Iruela-Arispe, M. L., Kalén, M., Gerhardt, H., & Betsholtz, C. (2007). Dll4 signalling through Notch1 regulates formation of tip cells during angiogenesis. *Nature*, *445*(7129), 776–780. https://doi.org/10.1038/NATURE05571

Heyder, C., Gloria-Maercker, E., Hatzmann, W., Niggemann, B., Zänker, K. S., & Dittmar, T. (2005). Role of the β1-integrin subunit in the adhesion, extravasation and migration of T24 human bladder carcinoma cells. *Clinical and Experimental Metastasis*, *22*(2), 99–106. https://doi.org/10.1007/s10585-005-4335-z

Hollmén, M., Karaman, S., Schwager, S., Lisibach, A., Christiansen, A. J., Maksimow, M., Varga, Z., Jalkanen, S., & Detmar, M. (2016). G-CSF regulates macrophage phenotype and associates with poor overall survival in human triple-negative breast cancer. *OncoImmunology*, *5*(3). https://doi.org/10.1080/2162402X.2015.1115177/SUPPL_FILE/KONI_A_1115177_SM2985.PDF

Holz, A., Bossinger, B., Strasser, T., Janning, W., & Klapper, R. (2003). The two origins of hemocytes in Drosophila. *Development*, *130*(20), 4955–4962. https://doi.org/10.1242/DEV.00702

Ingman, W. V., Wyckoff, J., Gouon-Evans, V., Condeelis, J., & Pollard, J. W. (2006). Macrophages promote collagen fibrillogenesis around terminal end buds of the developing mammary gland. *Developmental Dynamics : An Official Publication of the American Association of Anatomists*, *235*(12), 3222–3229. https://doi.org/10.1002/DVDY.20972

Inoue, H., Imamura, T., Ishidou, Y., Takase, M., Udagawa, Y., Oka, Y., Tsuneizumi, K., Tabata, T., Miyazono, K., & Kawabata, M. (1998). Interplay of Signal Mediators of Decapentaplegic (Dpp): Molecular Characterization of Mothers against dpp, Medea, and Daughters against dpp. *Molecular Biology of the Cell*, *9*(8), 2145. https://doi.org/10.1091/MBC.9.8.2145

Inoue, T., Abe, C., Kohro, T., Tanaka, S., Huang, L., Yao, J., Zheng, S., Ye, H., Inagi, R., Stornetta, R. L., Rosin, D. L., Nangaku, M., Wada, Y., & Okusa, M. D. (2019). Non-canonical cholinergic anti-inflammatory pathway-mediated activation of peritoneal macrophages induces Hes1 and blocks ischemia/reperfusion injury in the kidney. *Kidney International*, *95*(3), 563. https://doi.org/10.1016/J.KINT.2018.09.020

Irving, P., Ubeda, J. M., Doucet, D., Troxler, L., Lagueux, M., Zachary, D., Hoffmann, J. A., Hetru, C., & Meister, M. (2005). New insights into Drosophila larval haemocyte functions through genome-wide analysis. *Cellular Microbiology*, *7*(3), 335–350. https://doi.org/10.1111/J.1462-5822.2004.00462.X

Italiani, P., & Boraschi, D. (2014). From monocytes to M1/M2 macrophages: Phenotypical vs. functional differentiation. *Frontiers in Immunology*, *5*(OCT), 514. https://doi.org/10.3389/FIMMU.2014.00514/BIBTEX

Itoh, F., Itoh, S., Goumans, M. J., Valdimarsdottir, G., Iso, T., Dotto, G. P., Hamamori, Y., Kedes, L., Kato, M., & Ten Dijke, P. (2004). Synergy and antagonism between Notch and BMP receptor signaling pathways in endothelial cells. *The EMBO Journal*, *23*(3), 541. https://doi.org/10.1038/SJ.EMBOJ.7600065

Johansson, B. M., & Wiles, M. V. (1995). Evidence for involvement of activin A and bone morphogenetic protein 4 in mammalian mesoderm and hematopoietic development. *Molecular and Cellular Biology*, *15*(1), 141–151. https://doi.org/10.1128/MCB.15.1.141

Jones, C. V., Williams, T. M., Walker, K. A., Dickinson, H., Sakkal, S., Rumballe, B. A., Little, M. H., Jenkin, G., & Ricardo, S. D. (2013). M2 macrophage polarisation is associated with alveolar formation during postnatal lung development. *Respiratory Research*, *14*(1). https://doi.org/10.1186/1465-9921-14-41

Jung, S. H., Evans, C. J., Uemura, C., & Banerjee, U. (2005). The Drosophila lymph gland as a developmental model of hematopoiesis. *Development (Cambridge, England)*, *132*(11), 2521–2533. https://doi.org/10.1242/DEV.01837

Kallio, J., Leinonen, A., Ulvila, J., Valanne, S., Ezekowitz, R. A., & Rämet, M. (2005). Functional analysis of immune response genes in Drosophila identifies JNK pathway as a regulator of antimicrobial peptide gene expression in S2 cells. *Microbes and Infection*, *7*(5–6), 811–819. https://doi.org/10.1016/J.MICINF.2005.03.014

Kamiya, Y., Miyazono, K., & Miyazawa, K. (2008). Specificity of the inhibitory effects of Dad on TGF-β family type I receptors, Thickveins, Saxophone, and Baboon in Drosophila. *FEBS Letters*, *582*(17), 2496–2500. https://doi.org/10.1016/J.FEBSLET.2008.05.052

Kel, J. M., Girard-Madoux, M. J. H., Reizis, B., & Clausen, B. E. (2010). TGF- Is Required To Maintain the Pool of Immature Langerhans Cells in the Epidermis. *The Journal of Immunology*, *185*(6), 3248–3255. https://doi.org/10.4049/jimmunol.1000981

Khadilkar, R. J., Ho, K. Y. L., Venkatesh, B., & Tanentzapf, G. (2020). Integrins Modulate Extracellular Matrix Organization to Control Cell Signaling during Hematopoiesis. *Current Biology*, *30*(17), 3316-3329.e5. https://doi.org/10.1016/J.CUB.2020.06.027/ATTACHMENT/F8C90D31-9CAC-4CF5-8328-BC99F9CCBD95/MMC1.PDF

Khalil, A. A., & Friedl, P. (2010). Determinants of leader cells in collective cell migrationw. *This Journal Is*, *2*, 568–574. https://doi.org/10.1039/c0ib00052c

Kim, J., Johnson, K., Chen, H. J., Carroll, S., & Laughon, A. (1997). Drosophila Mad binds to DNA and directly mediates activation of vestigial by Decapentaplegic. *Nature 1997 388:6639*, *388*(6639), 304–308. https://doi.org/10.1038/40906

Kinugasa, M., Amano, H., Satomi-Kobayashi, S., Nakayama, K., Miyata, M., Kubo, Y., Nagamatsu, Y., Kurogane, Y., Kureha, F., Yamana, S., Hirata, K. I., Miyoshi, J., Takai, Y., & Rikitake, Y. (2012). Necl-5/poliovirus receptor interacts with VEGFR2 and regulates VEGF-induced angiogenesis. *Circulation Research*, *110*(5), 716–726. https://doi.org/10.1161/CIRCRESAHA.111.256834

Kirmizitas, A., Meiklejohn, S., Ciau-Uitz, A., Stephenson, R., & Patient, R. (2017). Dissecting BMP signaling input into the gene regulatory networks driving specification of the blood stem cell lineage. *Proceedings of the National Academy of Sciences of the United States of America*, *114*(23), 5814–5821. https://doi.org/10.1073/PNAS.1610615114

Kubo, A., Nagao, K., Yokouchi, M., Sasaki, H., & Amagai, M. (2009). External antigen uptake by Langerhans cells with reorganization of epidermal tight junction barriers. *Journal of Experimental Medicine*, *206*(13), 2937–2946. https://doi.org/10.1084/JEM.20091527

Külshammer, E., Mundorf, J., Kilinc, M., Frommolt, P., Wagle, P., & Uhlirova, M. (2015). Interplay among Drosophila transcription factors Ets21c, Fos and Ftz-F1 drives JNK-mediated tumor malignancy. *DMM Disease Models and Mechanisms*, *8*(10), 1279–1293. https://doi.org/10.1242/dmm.020719

Külshammer, E., & Uhlirova, M. (2013). The actin cross-linker Filamin/Cheerio mediates tumor malignancy downstream of JNK signaling. *Journal of Cell Science*, *126*(4), 927–938. https://doi.org/10.1242/jcs.114462

Kunwar, P. S., Siekhaus, D. E., & Lehmann, R. (2006). In vivo migration: a germ cell perspective. *Annual Review of Cell and Developmental Biology*, *22*, 237–265. https://doi.org/10.1146/ANNUREV.CELLBIO.22.010305.103337

Kuriyama, S., Theveneau, E., Benedetto, A., Parsons, M., Tanaka, M., Charras, G., Kabla, A., & Mayor, R. (2014). In vivo collective cell migration requires an LPAR2-dependent increase in tissue fluidity. *The Journal of Cell Biology*, *206*(1), 113–127. https://doi.org/10.1083/JCB.201402093

Kurucz, É., Váczi, B., Márkus, R., Laurinyecz, B., Vilmos, P., Zsámboki, J., Csorba, K., Gateff, E., Hultmark, D., & Andó, I. (2007). Definition of Drosophila hemocyte subsets by cell-type specific antigens. *Acta Biologica Hungarica*, *58 Suppl*(SUPPL. 1), 95–111. https://doi.org/10.1556/ABIOL.58.2007.SUPPL.8

Kutty, G., Kutty, R. K., Samuel, W., Duncan, T., Jaworski, C., & Wiggert, B. (1998). Identification of a New Member of Transforming Growth Factor-Beta Superfamily inDrosophila:The First Invertebrate Activin Gene. *Biochemical and Biophysical Research Communications*, *246*(3), 644–649. https://doi.org/10.1006/BBRC.1998.8678

Labernadie, A., Kato, T., Brugués, A., Serra-Picamal, X., Derzsi, S., Arwert, E., Weston, A., González-Tarragó, V., Elosegui-Artola, A., Albertazzi, L., Alcaraz, J., Roca-Cusachs, P., Sahai, E., & Trepat, X. (2017). A mechanically active heterotypic E-cadherin/N-cadherin adhesion enables fibroblasts to drive cancer cell invasion. *Nature Cell Biology 2017 19:3*, *19*(3), 224–237. https://doi.org/10.1038/ncb3478

Lämmermann, T., Bader, B. L., Monkley, S. J., Worbs, T., Wedlich-Söldner, R., Hirsch, K., Keller, M., Förster, R., Critchley, D. R., Fässler, R., & Sixt, M. (2008). Rapid leukocyte migration by integrin-independent flowing and squeezing. *Nature*, *453*(7191), 51–55.

https://doi.org/10.1038/NATURE06887

Lebestky, T., Chang, T., Hartenstein, V., & Banerjee, U. (2000). Specification of Drosophila hematopoietic lineage by conserved transcription factors. *Science*, *288*(5463). https://doi.org/10.1126/science.288.5463.146

Lebreton, G., & Casanova, J. (2014). Specification of leading and trailing cell features during collective migration in the Drosophila trachea. *Development*, *141*(4), e407–e407. https://doi.org/10.1242/DEV.108464

Lee-Hoeflich, S. T., Zhao, X., Mehra, A., & Attisano, L. (2005). The Drosophila type II receptor, Wishful thinking, binds BMP and myoglianin to activate multiple TGFbeta family signaling pathways. *FEBS Letters*, *579*(21), 4615–4621. https://doi.org/10.1016/J.FEBSLET.2005.06.088

Lenz, K. M., & Nelson, L. H. (2018). Microglia and beyond: Innate immune cells as regulators of brain development and behavioral function. *Frontiers in Immunology*, *9*(APR), 698. https://doi.org/10.3389/FIMMU.2018.00698/BIBTEX

Lesch, C., Jo, J., Wu, Y., Fish, G. S., & Galko, M. J. (2010). A Targeted UAS-RNAi Screen in Drosophila Larvae Identifies Wound Closure Genes Regulating Distinct Cellular Processes. *Genetics*, *186*(3), 943–957. https://doi.org/10.1534/GENETICS.110.121822

Letourneau, M., Lapraz, F., Sharma, A., Vanzo, N., Waltzer, L., & Crozatier, M. (2016). Drosophila hematopoiesis under normal conditions and in response to immune stress. *FEBS Letters*, *590*(22), 4034–4051. https://doi.org/10.1002/1873-3468.12327

Lin, D. M., Fetter, R. D., Kopczynski, C., Grenningloh, G., & Goodman, C. S. (1994). Genetic analysis of Fasciclin II in Drosophila: defasciculation, refasciculation, and altered fasciculation. *Neuron*, *13*(5), 1055–1069. https://doi.org/10.1016/0896-6273(94)90045-0

Lin, Y., Xu, J., & Lan, H. (2019). Tumor-associated macrophages in tumor metastasis: biological roles and clinical therapeutic applications. *Journal of Hematology & Oncology 2019 12:1*, *12*(1), 1–16. https://doi.org/10.1186/S13045-019-0760-3

Lo, P. C. H., & Frasch, M. (1999). Sequence and expression of myoglianin, a novel Drosophila gene of the TGF-β superfamily. *Mechanisms of Development*, *86*(1–2), 171–175. https://doi.org/10.1016/S0925-4773(99)00108-2

Lomakin, A. J., Cattin, C. J., Cuvelier, D., Alraies, Z., Molina, M., Nader, G. P. F., Srivastava, N., Saez, P. J., Garcia-Arcos, J. M., Zhitnyak, I. Y., Bhargava, A., Driscoll, M. K., Welf, E. S., Fiolka, R., Petrie, R. J., de Silva, N. S., González-Granado, J. M., Manel, N., Lennon-Duménil, A. M., … Piel, M. (2020). The nucleus acts as a ruler tailoring cell responses to spatial constraints. *Science (New York, N.Y.)*, *370*(6514). https://doi.org/10.1126/SCIENCE.ABA2894

Makhijani, K., Alexander, B., Rao, D., Petraki, S., Herboso, L., Kukar, K., Batool, I., Wachner, S., Gold, K. S., Wong, C., O'Connor, M. B., & Brückner, K. (2017). Regulation of Drosophila hematopoietic sites by Activin-β from active sensory neurons. *Nature Communications*, *8*, 15990. https://doi.org/10.1038/ncomms15990

Makhijani, K., Alexander, B., Tanaka, T., Rulifson, E., & Brückner, K. (2011). The peripheral

nervous system supports blood cell homing and survival in the Drosophila larva. *Development (Cambridge, England)*, *138*(24), 5379–5391. https://doi.org/10.1242/DEV.067322

Mancini, E., Sanjuan-Pla, A., Luciani, L., Moore, S., Grover, A., Zay, A., Rasmussen, K. D., Luc, S., Bilbao, D., O'Carroll, D., Jacobsen, S. E., & Nerlov, C. (2012). FOG-1 and GATA-1 act sequentially to specify definitive megakaryocytic and erythroid progenitors. *The EMBO Journal*, *31*(2), 351. https://doi.org/10.1038/EMBOJ.2011.390

Mandal, L., Banerjee, U., & Hartenstein, V. (2004). Evidence for a fruit fly hemangioblast and similarities between lymph-gland hematopoiesis in fruit fly and mammal aorta-gonadal-mesonephros mesoderm. *Nature Genetics 2004 36:9*, *36*(9), 1019–1023. https://doi.org/10.1038/ng1404

Mannion, B. A., Berditchevski, F., Kraeft, S. K., Chen, L. B., & Hemler, M. E. (1996). Transmembrane-4 superfamily proteins CD81 (TAPA-1), CD82, CD63, and CD53 specifically associated with integrin alpha 4 beta 1 (CD49d/CD29). *The Journal of Immunology*, *157*(5).

Marqués, G., Bao, H., Haerry, T. E., Shimell, M. J., Duchek, P., Zhang, B., & O'Connor, M. B. (2002). The Drosophila BMP Type II Receptor Wishful Thinking Regulates Neuromuscular Synapse Morphology and Function. *Neuron*, *33*(4), 529–543. https://doi.org/10.1016/S0896-6273(02)00595-0

Marqués, G., Musacchio, M., Shimell, M. J., Wünnenberg-Stapleton, K., Cho, K. W. Y., & O'Connor, M. B. (1997). Production of a DPP activity gradient in the early Drosophila embryo through the opposing actions of the SOG and TLD proteins. *Cell*, *91*(3), 417–426. https://doi.org/10.1016/S0092-8674(00)80425-0

Martin, M. (2011). Cutadapt removes adapter sequences from high-throughput sequencing reads. *EMBnet.Journal*, *17*(1), 10. https://doi.org/10.14806/EJ.17.1.200

Martínez, V. G., Rubio, C., Onica Martínez-Fern Andez, M., Segovia, C., Opez-Calder On, F. L., Garín, M. I., Teijeira, A., Munera-Maravilla, E., Varas, A., Saced On, R., Elix Guerrero, F., Villacampa, F., De La Rosa, F., Castellano, D., L Opez-Collazo, E., Us, J., Paramio, M., Vicente, A., & Due˜ Nas, M. (2017). *Biology of Human Tumors BMP4 Induces M2 Macrophage Polarization and Favors Tumor Progression in Bladder Cancer*. https://doi.org/10.1158/1078-0432.CCR-17-1004

Matunis, E., Tran, J., Gönczy, P., Caldwell, K., & DiNardo, S. (1997). punt and schnurri regulate a somatically derived signal that restricts proliferation of committed progenitors in the germline. *Development*, *124*(21), 4383–4391. https://doi.org/10.1242/DEV.124.21.4383

McLennan, R., Schumacher, L. J., Morrison, J. A., Teddy, J. M., Ridenour, D. A., Box, A. C., Semerad, C. L., Li, H., McDowell, W., Kay, D., Maini, P. K., Baker, R. E., & Kulesa, P. M. (2015). Neural crest migration is driven by a few trailblazer cells with a unique molecular signature narrowly confined to the invasive front. *Development (Cambridge)*, *142*(11), 2014–2025. https://doi.org/10.1242/DEV.117507/VIDEO-2

Milde-Langosch, K. (2005). The Fos family of transcription factors and their role in tumourigenesis. *European Journal of Cancer*, *41*(16), 2449–2461. https://doi.org/10.1016/j.ejca.2005.08.008

Monteiro, R., Pinheiro, P., Joseph, N., Peterkin, T., Koth, J., Repapi, E., Bonkhofer, F., Kirmizitas, A., & Patient, R. (2016). Transforming Growth Factor β Drives Hemogenic Endothelium Programming and the Transition to Hematopoietic Stem Cells. *Developmental Cell*, *38*(4), 358–370. https://doi.org/10.1016/j.devcel.2016.06.024

Morikawa, M., Derynck, R., & Miyazono, K. (2016). TGF-β and the TGF-β Family: Context-Dependent Roles in Cell and Tissue Physiology. *Cold Spring Harbor Perspectives in Biology*, *8*(5). https://doi.org/10.1101/cshperspect.a021873

Morrison, J. A., McLennan, R., Wolfe, L. A., Gogol, M. M., Meier, S., McKinney, M. C., Teddy, J. M., Holmes, L., Semerad, C. L., Box, A. C., Li, H., Hall, K. E., Perera, A. G., & Kulesa, P. M. (2017). Single-cell transcriptome analysis of avian neural crest migration reveals signatures of invasion and molecular transitions. *ELife*, *6*. https://doi.org/10.7554/ELIFE.28415

Morrison, S. J., & Scadden, D. T. (2014). The bone marrow niche for haematopoietic stem cells. *Nature*, *505*(7483), 327. https://doi.org/10.1038/NATURE12984

Moya, I. M., Umans, L., Maas, E., Pereira, P. N., Beets, K., Francis, A., Sents, W., Robertson, E. J., Mummery, C. L., Huylebroeck, D., & Zwijsen, A. (2012). *Article Stalk Cell Phenotype Depends on Integration of Notch and Smad1/5 Signaling Cascades*. https://doi.org/10.1016/j.devcel.2012.01.007

Muratoglu, S., Garratt, B., Hyman, K., Gajewski, K., Schulz, R. A., & Fossett, N. (2006). Regulation of Drosophila friend of GATA gene, u-shaped, during hematopoiesis: a direct role for serpent and lozenge. *Developmental Biology*, *296*(2), 561–579. https://doi.org/10.1016/J.YDBIO.2006.04.455

Murray, P. J., & Wynn, T. A. (2011). Protective and pathogenic functions of macrophage subsets. *Nature Reviews Immunology 2011 11:11*, *11*(11), 723–737. https://doi.org/10.1038/nri3073

Myers, D. C., Sepich, D. S., & Solnica-Krezel, L. (2002). Bmp Activity Gradient Regulates Convergent Extension during Zebrafish Gastrulation. *Developmental Biology*, *243*(1), 81–98. https://doi.org/10.1006/DBIO.2001.0523

Nakagawa, T., Li, J. H., Garcia, G., Mu, W., Piek, E., Böttinger, E. P., Chen, Y., Zhu, H. J., Kang, D. H., Schreiner, G. F., Lan, H. Y., & Johnson, R. J. (2004). TGF-beta induces proangiogenic and antiangiogenic factors via parallel but distinct Smad pathways. *Kidney International*, *66*(2), 605–613. https://doi.org/10.1111/J.1523-1755.2004.00780.X

Nakayama, T., Cui, Y., & Christian, J. L. (2000). Regulation of BMP/Dpp signaling during embryonic development. *Cellular and Molecular Life Sciences : CMLS*, *57*(6), 943–956. https://doi.org/Doi 10.1007/Pl00000736

Nellen, D., Burke, R., Struhl, G., & Basler, K. (1996). Direct and Long-Range Action of a DPP Morphogen Gradient. *Cell*, *85*(3), 357–368. https://doi.org/10.1016/S0092-8674(00)81114-9

Neuert, H., Deing, P., Krukkert, K., Naffin, E., Steffes, G., Risse, B., Silies, M., & Klambt, C. (2020). The Drosophila NCAM homolog Fas2 signals independently of adhesion. *Development (Cambridge)*, *147*(2). https://doi.org/10.1242/DEV.181479/VIDEO-6

Newfeld, S. J., Chartoff, E. H., Graft, J. M., Melton, D. A., & Gelbart, W. M. (1996). Mothers against dpp encodes a conserved cytoplasmic protein required in DPP/TGF-beta responsive cells. *Development*, *122*(7), 2099–2108. https://doi.org/10.1242/DEV.122.7.2099

Newfeld, S. J., Mehra, A., Singer, M. A., Wrana, J. L., Attisano, L., & Gelbart, W. M. (1997). Mothers against dpp participates in a DDP/TGF-beta responsive serine-threonine kinase signal transduction cascade. *Development*, *124*(16), 3167–3176. https://doi.org/10.1242/DEV.124.16.3167

Ng, J. (2008). TGF-beta signals regulate axonal development through distinct Smad-independent mechanisms. *Development (Cambridge, England)*, *135*(24), 4025–4035. https://doi.org/10.1242/DEV.028209

Nguyen, M., Parker, L., & Arora, K. (2000). Identification of maverick, a novel member of the TGF-β superfamily in Drosophila. *Mechanisms of Development*, *95*(1–2), 201–206. https://doi.org/10.1016/S0925-4773(00)00338-5

Ninov, N., Menezes-Cabral, S., Prat-Rojo, C., Manjón, C., Weiss, A., Pyrowolakis, G., Affolter, M., & Martín-Blanco, E. (2010). Dpp Signaling Directs Cell Motility and Invasiveness during Epithelial Morphogenesis. *Current Biology*, *20*(6), 513–520. https://doi.org/10.1016/j.cub.2010.01.063

Nobs, S. P., & Kopf, M. (2021). Tissue-resident macrophages: guardians of organ homeostasis. *Trends in Immunology*, *42*(6), 495–507. https://doi.org/10.1016/J.IT.2021.04.007

Nourshargh, S., Hordijk, P. P. L., & Sixt, M. (2010). Breaching multiple barriers: leukocyte motility through venular walls and the interstitium. *Nature Reviews Molecular Cell Biology*, *11*(5), 366–378. https://doi.org/10.1038/nrm2889

O'Connor, M. B., Umulis, D., Othmer, H. G., & Blair, S. S. (2006). Shaping BMP morphogen gradients in the Drosophila embryo and pupal wing. *Development (Cambridge, England)*, *133*(2), 183–193. https://doi.org/10.1242/dev.02214

Ogita, H., Rikitake, Y., Miyoshi, J., & Takai, Y. (2010). Cell adhesion molecules nectins and associating proteins: Implications for physiology and pathology. *Proceedings of the Japan Academy. Series B, Physical and Biological Sciences*, *86*(6), 621. https://doi.org/10.2183/PJAB.86.621

Ohneda, K., & Yamamoto, M. (2002). Roles of Hematopoietic Transcription Factors GATA-1 and GATA-2 in the Development of Red Blood Cell Lineage. *Acta Haematologica*, *108*(4), 237–245. https://doi.org/10.1159/000065660

Olofsson, B., & Page, D. T. (2005). Condensation of the central nervous system in embryonic Drosophila is inhibited by blocking hemocyte migration or neural activity. *Developmental Biology*, *279*(1), 233–243. https://doi.org/10.1016/j.ydbio.2004.12.020

Omata, Y., Yasui, T., Hirose, J., Izawa, N., Imai, Y., Matsumoto, T., Masuda, H., Tokuyama, N., Nakamura, S., Tsutsumi, S., Yasuda, H., Okamoto, K., Takayanagi, H., Hikita, A., Imamura, T., Matsuo, K., Saito, T., Kadono, Y., Aburatani, H., & Tanaka, S. (2015). Genomewide Comprehensive Analysis Reveals Critical Cooperation Between Smad and c-Fos in RANKL-Induced Osteoclastogenesis. *Journal of Bone and Mineral Research*, *30*(5), 869–877.

https://doi.org/10.1002/JBMR.2418

Paladi, M., & Tepass, U. (2004). Function of Rho GTPases in embryonic blood cell migration in Drosophila. *Journal of Cell Science*, *117*(26), 6313–6326. https://doi.org/10.1242/jcs.01552

Paluch, E. K., & Raz, E. (2013). The role and regulation of blebs in cell migration. *Current Opinion in Cell Biology*, *25*(5), 582–590. https://doi.org/10.1016/J.CEB.2013.05.005

Paolicelli, R. C., Bolasco, G., Pagani, F., Maggi, L., Scianni, M., Panzanelli, P., Giustetto, M., Ferreira, T. A., Guiducci, E., Dumas, L., Ragozzino, D., & Gross, C. T. (2011). Synaptic pruning by microglia is necessary for normal brain development. *Science (New York, N.Y.)*, *333*(6048), 1456–1458. https://doi.org/10.1126/SCIENCE.1202529

Pardali, E., Makowski, L.-M., Leffers, M., Borgscheiper, A., & Waltenberger, J. (2018). BMP-2 induces human mononuclear cell chemotaxis and adhesion and modulates monocyte-to-macrophage differentiation. *Journal of Cellular and Molecular Medicine*, *22*(11), 5429–5438. https://doi.org/10.1111/jcmm.13814

Parisi, F., Stefanatos, R. K., Strathdee, K., Yu, Y., & Vidal, M. (2014). Transformed epithelia trigger non-tissue-autonomous tumor suppressor response by adipocytes via activation of Toll and Eiger/TNF signaling. *Cell Reports*, *6*(5), 855–867. https://doi.org/10.1016/J.CELREP.2014.01.039

Parsons, B., & Foley, E. (2013). The Drosophila platelet-derived growth factor and vascular endothelial growth factor-receptor related (Pvr) protein ligands Pvf2 and Pvf3 control hemocyte viability and invasive migration. *Journal of Biological Chemistry*, *288*(28), 20173–20183. https://doi.org/10.1074/jbc.M113.483818

Pearson, J. C., Juarez, M. T., Kim, M., & McGinnis, W. (2009). Multiple transcription factor codes activate epidermal wound–response genes in Drosophila. *Proceedings of the National Academy of Sciences*, *106*(7), 2224–2229. https://doi.org/10.1073/PNAS.0810219106

Pennetier, D., Oyallon, J., Morin-Poulard, I., Dejean, S., Vincent, A., & Crozatier, M. (2012a). Size control of the Drosophila hematopoietic niche by bone morphogenetic protein signaling reveals parallels with mammals. *Proceedings of the National Academy of Sciences of the United States of America*, *109*(9), 3389–3394. https://doi.org/10.1073/pnas.1109407109

Pennetier, D., Oyallon, J., Morin-Poulard, I., Dejean, S., Vincent, A., & Crozatier, M. (2012b). Size control of the Drosophila hematopoietic niche by bone morphogenetic protein signaling reveals parallels with mammals. In *Proceedings of the National Academy of Sciences of the United States of America* (Vol. 109, Issue 9, pp. 3389–3394). https://doi.org/10.1073/pnas.1109407109

Perkins, K. K., Dailey, G. M., & Tjian, R. (1988). Novel Jun-and Fos-related proteins in Drosophila are functionally homologous to enhancer factor AP-1. *The EMBO Journal*, *7*(13), 4265–4273.

Picelli, S., Faridani, O. R., Björklund, Å. K., Winberg, G., Sagasser, S., & Sandberg, R. (2014). Full-length RNA-seq from single cells using Smart-seq2. *Nature Protocols 2013 9:1*, *9*(1),

171–181. https://doi.org/10.1038/nprot.2014.006

Prasad, M., & Montell, D. J. (2007). Cellular and molecular mechanisms of border cell migration analyzed using time-lapse live-cell imaging. *Developmental Cell*, *12*(6), 997–1005. https://doi.org/10.1016/J.DEVCEL.2007.03.021

Quan, Q., Wang, X., Lu, C., Ma, W., Wang, Y., Xia, G., Wang, C., & Yang, G. (2020). Cancer stem-like cells with hybrid epithelial/mesenchymal phenotype leading the collective invasion. *Cancer Science*, *111*(2), 467–476. https://doi.org/10.1111/CAS.14285

Rae, F., Woods, K., Sasmono, T., Campanale, N., Taylor, D., Ovchinnikov, D. A., Grimmond, S. M., Hume, D. A., Ricardo, S. D., & Little, M. H. (2007). Characterisation and trophic functions of murine embryonic macrophages based upon the use of a Csf1r-EGFP transgene reporter. *Developmental Biology*, *308*(1), 232–246. https://doi.org/10.1016/j.ydbio.2007.05.027

Ratheesh, A, Belyaeva, V., & Siekhaus, D. E. (2015). Drosophila immune cell migration and adhesion during embryonic development and larval immune responses. *Curr Opin Cell Biol*, *36*, 71–79. https://doi.org/10.1016/j.ceb.2015.07.003

Ratheesh, Aparna, Biebl, J., Vesela, J., Smutny, M., Papusheva, E., Krens, S. F. G., Kaufmann, W., Gyoergy, A., Casano, A. M., & Siekhaus, D. E. (2018). Drosophila TNF Modulates Tissue Tension in the Embryo to Facilitate Macrophage Invasive Migration. *Developmental Cell*, *45*(3), 331-346.e7. https://doi.org/10.1016/j.devcel.2018.04.002

Renkawitz, J., Kopf, A., Stopp, J., de Vries, I., Driscoll, M. K., Merrin, J., Hauschild, R., Welf, E. S., Danuser, G., Fiolka, R., & Sixt, M. (2019). Nuclear positioning facilitates amoeboid migration along the path of least resistance. *Nature*, *568*(7753), 546. https://doi.org/10.1038/S41586-019-1087-5

Reversat, A., Gaertner, F., Merrin, J., Stopp, J., Tasciyan, S., Aguilera, J., de Vries, I., Hauschild, R., Hons, M., Piel, M., Callan-Jones, A., Voituriez, R., & Sixt, M. (2020). Cellular locomotion using environmental topography. *Nature*, *582*(7813), 582–585. https://doi.org/10.1038/S41586-020-2283-Z

Ridley, A. J. (2015). Rho GTPase signalling in cell migration. *Current Opinion in Cell Biology*, *36*, 103–112. https://doi.org/10.1016/J.CEB.2015.08.005

Ridley, A. J., Comoglio, P. M., & Hall, A. (1995). Regulation of Scatter Factor/Hepatocyte Growth Factor Responses by Ras, Rac, and Rho in MDCK Cells. *MOLECULAR AND CELLULAR BIOLOGY*, *15*(2), 1110–1122. https://journals.asm.org/journal/mcb

Riesgo-escovar, J. R., & Hafen, E. (1997). Drosophila JUN kinase regulates expression of decapentaplegic via the ETS-domain protein AOP and the AP-1 transcription factor DJUN during dorsal closure: Riesgo-Escovar, J. and Hafen. E. Genes Dev. 11, 1717–1727. *Trends in Genetics*, *13*(10), 392. https://doi.org/http://dx.doi.org/10.1016/S0168-9525(97)90015-9

Riesgo-Escovar, J. R., & Hafen, E. (1997). Common and distinct roles of DFos and DJun during Drosophila development. *Science (New York, N.Y.)*, *278*(5338), 669–672. https://doi.org/10.1126/science.278.5338.669

Rizki, T. M., & Rizki, R. M. (1992). Lamellocyte differentiation in Drosophila larvae parasitized

by Leptopilina. *Developmental and Comparative Immunology*, *16*(2–3), 103–110. https://doi.org/10.1016/0145-305X(92)90011-Z

Roberts, A. W., Lee, B. L., Deguine, J., John, S., Shlomchik, M. J., & Barton, G. M. (2017). Tissue-Resident Macrophages Are Locally Programmed for Silent Clearance of Apoptotic Cells. *Immunity*, *47*(5), 913-927.e6. https://doi.org/10.1016/J.IMMUNI.2017.10.006

Rodríguez-Pascual, F., Redondo-Horcajo, M., & Lamas, S. (2003). Functional cooperation between Smad proteins and activator protein-1 regulates transforming growth factor-β - Mediated induction of endothelin-1 expression. *Circulation Research*, *92*(12), 1288–1295. https://doi.org/10.1161/01.RES.0000078491.79697.7F

Roy, S., Ernst, J., Kharchenko, P. V., Kheradpour, P., Negre, N., Eaton, M. L., Landolin, J. M., Bristow, C. A., Ma, L., Lin, M. F., Washietl, S., Arshinoff, B. I., Ay, F., Meyer, P. E., Robine, N., Washington, N. L., Di Stefano, L., Berezikov, E., Brown, C. D., … Lowdon, R. F. (2010). Identification of functional elements and regulatory circuits by Drosophila modENCODE. *Science (New York, N.Y.)*, *330*(6012), 1787–1797. https://doi.org/10.1126/SCIENCE.1198374

Ruberte, E., Marty, T., Nellen, D., Affolter, M., & Baslert, K. (1995). An Absolute Requirement for Both the Type II and Type I Receptors, Punt and Thick Veins, for Dpp Signaling In Vivo. *Cell*, *80*, 889–897.

Rusch, J., & Levine, M. (1997). Regulation of a dpp target gene in the Drosophila embryo. *Development*, *124*(2), 303–311. https://doi.org/10.1242/DEV.124.2.303

Rymo, S. F., Gerhardt, H., Sand, F. W., Lang, R., Uv, A., & Betsholtz, C. (2011). A two-way communication between microglial cells and angiogenic sprouts regulates angiogenesis in aortic ring cultures. *PloS One*, *6*(1). https://doi.org/10.1371/JOURNAL.PONE.0015846

Sahai, E., Astsaturov, I., Cukierman, E., DeNardo, D. G., Egeblad, M., Evans, R. M., Fearon, D., Greten, F. R., Hingorani, S. R., Hunter, T., Hynes, R. O., Jain, R. K., Janowitz, T., Jorgensen, C., Kimmelman, A. C., Kolonin, M. G., Maki, R. G., Powers, R. S., Puré, E., … Werb, Z. (2020). A framework for advancing our understanding of cancer-associated fibroblasts. *Nature Reviews Cancer 2020 20:3*, *20*(3), 174–186. https://doi.org/10.1038/s41568-019-0238-1

Sánchez-Sánchez, B. J., Urbano, J. M., Comber, K., Dragu, A., Wood, W., Stramer, B., & Martín-Bermudo, M. D. (2017). Drosophila Embryonic Hemocytes Produce Laminins to Strengthen Migratory Response. *Cell Reports*, *21*(6), 1461–1470. https://doi.org/10.1016/j.celrep.2017.10.047

Scarpa, E., & Mayor, R. (2016). Collective cell migration in development. *Journal of Cell Biology*, *212*(2), 143–155. https://doi.org/10.1083/jcb.201508047

Sears, H. C., Kennedy, C. J., & Garrity, P. a. (2003). Macrophage-mediated corpse engulfment is required for normal Drosophila CNS morphogenesis. *Development (Cambridge, England)*, *130*(15), 3557–3565. https://doi.org/10.1242/dev.00586

Shang, Y., Coppo, M., He, T., Ning, F., Yu, L., Kang, L., Zhang, B., Ju, C., Qiao, Y., Zhao, B., Gessler, M., Rogatsky, I., & Hu, X. (2016). The transcriptional repressor Hes1 attenuates inflammation by regulating transcription elongation. *Nature Immunology 2016 17:8*,

17(8), 930–937. https://doi.org/10.1038/ni.3486

Shimmi, O., Umulis, D., Othmer, H., & O'Connor, M. B. (2005). Facilitated transport of a Dpp/Scw heterodimer by Sog/Tsg leads to robust patterning of the Drosophila blastoderm embryo. *Cell*, *120*(6), 873–886. https://doi.org/10.1016/J.CELL.2005.02.009

Sica, A., & Mantovani, A. (2012). Macrophage plasticity and polarization: in vivo veritas. *The Journal of Clinical Investigation*, *122*(3), 787–795. https://doi.org/10.1172/JCI59643

Siekhaus, D., Haesemeyer, M., Moffitt, O., & Lehmann, R. (2010). RhoL controls invasion and Rap1 localization during immune cell transmigration in Drosophila. *Nature Publishing Group*, *12*(6), 605–610. https://doi.org/10.1038/ncb2063

Sousa, S., Brion, R., Lintunen, M., Kronqvist, P., Sandholm, J., Mönkkönen, J., Kellokumpu-Lehtinen, P. L., Lauttia, S., Tynninen, O., Joensuu, H., Heymann, D., & Määttä, J. A. (2015). Human breast cancer cells educate macrophages toward the M2 activation status. *Breast Cancer Research*, *17*(1), 1–14. https://doi.org/10.1186/S13058-015-0621-0/FIGURES/4

Squarzoni, P., Oller, G., Hoeffel, G., Pont-Lezica, L., Rostaing, P., Low, D., Bessis, A., Ginhoux, F., & Garel, S. (2014). Microglia modulate wiring of the embryonic forebrain. *Cell Reports*, *8*(5), 1271–1279. https://doi.org/10.1016/J.CELREP.2014.07.042

Suchting, S., Freitas, C., Le Noble, F., Benedito, R., Bréant, C., Duarte, A., & Eichmann, A. (2007). The Notch ligand Delta-like 4 negatively regulates endothelial tip cell formation and vessel branching. *Proceedings of the National Academy of Sciences*, *104*(9), 3225–3230. https://doi.org/10.1073/PNAS.0611177104

Sundqvist, A., Vasilaki, E., Voytyuk, O., Bai, Y., Morikawa, M., Moustakas, A., Miyazono, K., Heldin, C. H., ten Dijke, P., & van Dam, H. (2020). TGFβ and EGF signaling orchestrates the AP-1- and p63 transcriptional regulation of breast cancer invasiveness. *Oncogene 2020 39:22*, *39*(22), 4436–4449. https://doi.org/10.1038/s41388-020-1299-z

Svitkina, T. (2018). The Actin Cytoskeleton and Actin-Based Motility. *Cold Spring Harbor Perspectives in Biology*, *10*(1). https://doi.org/10.1101/CSHPERSPECT.A018267

Szafranski, P., & Goode, S. (2004). A Fasciclin 2 morphogenetic switch organizes epithelial cell cluster polarity and motility. *Development*, *131*(9), 2023–2036. https://doi.org/10.1242/dev.01097

Szüts, D., & Bienz, M. (2000). An autoregulatory function of Dfos during Drosophila endoderm induction. *Mechanisms of Development*, *98*(1–2), 71–76. https://doi.org/10.1016/S0925-4773(00)00455-X

Tattikota, S. G., Cho, B., Liu, Y., Hu, Y., Barrera, V., Steinbaugh, M. J., Yoon, S. H., Comjean, A., Li, F., Dervis, F., Hung, R. J., Nam, J. W., Sui, S. H., Shim, J., & Perrimon, N. (2020). A single-cell survey of Drosophila blood. *ELife*, *9*, 1–35. https://doi.org/10.7554/ELIFE.54818

Tepass, U., Fessler, L. I., Aziz, A., & Hartenstein, V. (1994). Embryonic origins of hemocytes and their relationship to cell death in Drosophila. *Development*, *120*, 1829–1837.

Theveneau, E., & Mayor, R. (2010). Integrating chemotaxis and contact-inhibition during collective cell migration: Small GTPases at work. *Small GTPases*, *1*(2), 113–117. https://doi.org/10.4161/SGTP.1.2.13673

Thurmond, J., Goodman, J. L., Strelets, V. B., Attrill, H., Gramates, L. S., Marygold, S. J., Matthews, B. B., Millburn, G., Antonazzo, G., Trovisco, V., Kaufman, T. C., Calvi, B. R., Perrimon, N., Gelbart, S. R., Agapite, J., Broll, K., Crosby, L., Dos Santos, G., Emmert, D., … Baker, P. (2019). FlyBase 2.0: The next generation. *Nucleic Acids Research*, *47*(D1). https://doi.org/10.1093/nar/gky1003

Tippett, E., Cameron, P. U., Marsh, M., & Crowe, S. M. (2013). Characterization of tetraspanins CD9, CD53, CD63, and CD81 in monocytes and macrophages in HIV-1 infection. *Journal of Leukocyte Biology*, *93*(6), 913–920. https://doi.org/10.1189/JLB.0812391

Tokusumi, T., Shoue, D. A., Tokusumi, Y., Stoller, J. R., & Schulz, R. A. (2009). New hemocyte-specific enhancer-reporter transgenes for the analysis of hematopoiesis in Drosophila. *Genesis*, *47*(11), 771–774. https://doi.org/10.1002/DVG.20561

Tomancak, P., Beaton, A., Weiszmann, R., Kwan, E., Shu, S. Q., Lewis, S. E., Richards, S., Ashburner, M., Hartenstein, V., Celniker, S. E., & Rubin, G. M. (2002). Systematic determination of patterns of gene expression during Drosophila embryogenesis. *Genome Biology*, *3*(12). https://doi.org/10.1186/gb-2002-3-12-research0088

Tomancak, P., Berman, B. P., Beaton, A., Weiszmann, R., Kwan, E., Hartenstein, V., Celniker, S. E., & Rubin, G. M. (2007). Global analysis of patterns of gene expression during Drosophila embryogenesis. *Genome Biology*, *8*(7). https://doi.org/10.1186/gb-2007-8-7-r145

Trepat, X., Chen, Z., & Jacobson, K. (2012). Cell migration. *Comprehensive Physiology*, *2*(4), 2369–2392. https://doi.org/10.1002/CPHY.C110012

Tsai, F. Y., Keller, G., Kuo, F. C., Weiss, M., Chen, J., Rosenblatt, M., Alt, F. W., & Orkin, S. H. (1994). An early haematopoietic defect in mice lacking the transcription factor GATA-2. *Nature*, *371*(6494), 221–226. https://doi.org/10.1038/371221A0

Tsang, A. P., Visvader, J. E., Turner, C. A., Fujiwara, Y., Yu, C., Weiss, M. J., Crossley, M., & Orkin, S. H. (1997). FOG, a multitype zinc finger protein, acts as a cofactor for transcription factor GATA-1 in erythroid and megakaryocytic differentiation. *Cell*, *90*(1), 109–119. https://doi.org/10.1016/S0092-8674(00)80318-9

Tsuneizumi, K., Nakayama, T., Kamoshida, Y., Kornberg, T. B., Christian, J. L., & Tabata, T. (1997). Daughters against dpp modulates dpp organizing activity in Drosophila wing development. *Nature*, *389*(6651), 627–631. https://doi.org/10.1038/39362

Uhlirova, M., & Bohmann, D. (2006). JNK- and Fos-regulated Mmp1 expression cooperates with Ras to induce invasive tumors in Drosophila. *EMBO Journal*, *25*(22), 5294–5304. https://doi.org/10.1038/sj.emboj.7601401

Upadhyay, A., Moss-Taylor, L., Kim, M. J., Ghosh, A. C., & O'Connor, M. B. (2017). TGF-β Family Signaling in Drosophila. *Cold Spring Harbor Perspectives in Biology*, *9*(9). https://doi.org/10.1101/CSHPERSPECT.A022152

Utz, S. G., See, P., Mildenberger, W., Thion, M. S., Silvin, A., Lutz, M., Ingelfinger, F., Rayan, N. A., Lelios, I., Buttgereit, A., Asano, K., Prabhakar, S., Garel, S., Becher, B., Ginhoux, F., & Greter, M. (2020). Early Fate Defines Microglia and Non-parenchymal Brain Macrophage Development. *Cell*, *181*(3), 557-573.e18. https://doi.org/10.1016/j.cell.2020.03.021

Valentin, G., Haas, P., & Gilmour, D. (2007). The chemokine SDF1a coordinates tissue migration through the spatially restricted activation of Cxcr7 and Cxcr4b. *Current Biology : CB*, *17*(12), 1026–1031. https://doi.org/10.1016/J.CUB.2007.05.020

Valoskova, K., Biebl, J., Roblek, M., Emtenani, S., Gyoergy, A., Misova, M., Ratheesh, A., Reis-Rodrigues, P., Shkarina, K., Larsen, I. S. B., Vakhrushev, S. Y., Clausen, H., & Siekhaus, D. E. (2019). A conserved major facilitator superfamily member orchestrates a subset of O-glycosylation to aid macrophage tissue invasion. *ELife*, *8*. https://doi.org/10.7554/eLife.41801

van Furth, R., Cohn, Z. A., Hirsch, J. G., Humphrey, J. H., Spector, W. G., & Langevoort, H. L. (1972). The mononuclear phagocyte system: a new classification of macrophages, monocytes, and their precursor cells. *Bulletin of the World Health Organization*, *46*(6), 845. /pmc/articles/PMC2480884/?report=abstract

Venkiteswaran, G., Lewellis, S. W., Wang, J., Reynolds, E., Nicholson, C., & Knaut, H. (2013). Generation and Dynamics of an Endogenous, Self-Generated Signaling Gradient across a Migrating Tissue. *Cell*, *155*(3), 674–687. https://doi.org/10.1016/J.CELL.2013.09.046

Vilchez Mercedes, S. A., Bocci, F., Levine, H., Onuchic, J. N., Jolly, M. K., & Wong, P. K. (2021). Decoding leader cells in collective cancer invasion. *Nature Reviews Cancer 2021 21:9*, *21*(9), 592–604. https://doi.org/10.1038/s41568-021-00376-8

Vincent, S., Ruberte, E., Grieder, N. C., Chen, C. K., Haerry, T., Schuh, R., & Affolter, M. (1997). DPP controls tracheal cell migration along the dorsoventral body axis of the Drosophila embryo. *Development*, *124*(14).

Vischer, U., & Wagner, D. (1993). CD63 Is a Component of Weibel-Palade Bodies of Human Endothelial Cells. *Blood*, *82*(4), 1184–1191. https://doi.org/10.1182/BLOOD.V82.4.1184.1184

von der Hardt, S., Bakkers, J., Inbal, A., Carvalho, L., Solnica-Krezel, L., Heisenberg, C. P., & Hammerschmidt, M. (2007). The Bmp Gradient of the Zebrafish Gastrula Guides Migrating Lateral Cells by Regulating Cell-Cell Adhesion. *Current Biology*, *17*(6), 475–487. https://doi.org/10.1016/J.CUB.2007.02.013

Wakayama, Y., Fukuhara, S., Ando, K., Matsuda, M., & Mochizuki, N. (2015). Cdc42 Mediates Bmp-Induced Sprouting Angiogenesis through Fmnl3-Driven Assembly of Endothelial Filopodia in Zebrafish. *Developmental Cell*, *32*(1), 109–122. https://doi.org/10.1016/J.DEVCEL.2014.11.024

Waltzer, L., Ferjoux, G., Bataillé, L., & Haenlin, M. (2003). Cooperation between the GATA and RUNX factors Serpent and Lozenge during Drosophila hematopoiesis. *The EMBO Journal*, *22*(24), 6516. https://doi.org/10.1093/EMBOJ/CDG622

Wang, J., & Kubes, P. (2016). A Reservoir of Mature Cavity Macrophages that Can Rapidly Invade Visceral Organs to Affect Tissue Repair. *Cell*, *165*(3), 668–678. https://doi.org/10.1016/J.CELL.2016.03.009/ATTACHMENT/3A4D7476-07F0-4364-A0E2-5F417D13BEB3/MMC8.MP4

Wang, Q., Liu, H., Wang, Q., Zhou, F., Liu, Y., Zhang, Y., Ding, H., Yuan, M., Li, F., & Chen, Y. (2017). Involvement of c-Fos in cell proliferation, migration, and invasion in

osteosarcoma cells accompanied by altered expression of Wnt2 and Fzd9. *PLoS ONE*, *12*(6). https://doi.org/10.1371/journal.pone.0180558

Wang, Y., Chaffee, T. S., Larue, R. S., Huggins, D. N., Witschen, P. M., Ibrahim, A. M., Nelson, A. C., Machado, H. L., & Schwertfeger, K. L. (2020). Tissue-resident macrophages promote extracellular matrix homeostasis in the mammary gland stroma of nulliparous mice. *ELife*, *9*, 1–27. https://doi.org/10.7554/ELIFE.57438

Wegner, M., & Riethmacher, D. (2001). Chronicles of a switch hunt: gcm genes in development. *Trends in Genetics*, *17*(5), 286–290. https://doi.org/10.1016/S0168-9525(01)02275-2

Weiss, A., Charbonnier, E., Ellertsdóttir, E., Tsirigos, A., Wolf, C., Schuh, R., Pyrowolakis, G., & Affolter, M. (2010a). A conserved activation element in BMP signaling during Drosophila development. *Nature Structural & Molecular Biology*, *17*(1), 69–77. https://doi.org/10.1038/NSMB.1715

Weiss, A., Charbonnier, E., Ellertsdóttir, E., Tsirigos, A., Wolf, C., Schuh, R., Pyrowolakis, G., & Affolter, M. (2010b). A conserved activation element in BMP signaling during Drosophila development. *Nature Structural & Molecular Biology*, *17*(1), 69–76. https://doi.org/10.1038/nsmb.1715

West, H. C., & Bennett, C. L. (2018). Redefining the role of langerhans cells as immune regulators within the skin. *Frontiers in Immunology*, *8*(JAN), 1941. https://doi.org/10.3389/FIMMU.2017.01941/BIBTEX

Wharton, K. A., Ray, R. P., & Gelbart, W. M. (1993). An activity gradient of decapentaplegic is necessary for the specification of dorsal pattern elements in the Drosophila embryo. *Development*, *117*(2), 807–822. https://doi.org/10.1242/DEV.117.2.807

Wood, W., Faria, C., & Jacinto, A. (2006). *Distinct mechanisms regulate hemocyte chemotaxis during development and wound healing in*. *173*(3), 405–416. https://doi.org/10.1083/jcb.200508161

Wood, W., & Jacinto, A. (2007). Drosophila melanogaster embryonic haemocytes: masters of multitasking. *Nature Reviews. Molecular Cell Biology*, *8*(7), 542–551. https://doi.org/10.1038/nrm2202

Wood, W., & Martin, P. (2017). Macrophage Functions in Tissue Patterning and Disease: New Insights from the Fly. *Developmental Cell*, *40*(3), 221. https://doi.org/10.1016/J.DEVCEL.2017.01.001

Wu, C. Y., Lin, M. W., Wu, D. C., Huang, Y. B., Huang, H. T., & Chen, C. L. (2014). The role of phosphoinositide-regulated actin reorganization in chemotaxis and cell migration. *British Journal of Pharmacology*, *171*(24), 5541. https://doi.org/10.1111/BPH.12777

Wu, Y., Zhang, X., Salmon, M., Lin, X., & Zehner, Z. E. (2007). TGFβ1 regulation of vimentin gene expression during differentiation of the C2C12 skeletal myogenic cell line requires Smads, AP-1 and Sp1 family members. *Biochimica et Biophysica Acta (BBA) - Molecular Cell Research*, *1773*(3), 427–439. https://doi.org/10.1016/J.BBAMCR.2006.11.017

Wurmbach, E., Wech, I., & Preiss, A. (1999). The Enhancer of split complex of Drosophila melanogaster harbors three classes of Notch responsive genes. *Mechanisms of*

Development, *80*(2), 171–180. https://doi.org/10.1016/S0925-4773(98)00212-3

Wynn, T. A., Chawla, A., & Pollard, J. W. (2013). Macrophage biology in development, homeostasis and disease. *Nature 2013 496:7446*, *496*(7446), 445–455. https://doi.org/10.1038/nature12034

Yamada, K. M., & Sixt, M. (2019). Mechanisms of 3D cell migration. *Nature Reviews Molecular Cell Biology*, *20*(12), 738–752. https://doi.org/10.1038/s41580-019-0172-9

Yamane, T. (2018). Mouse yolk sac hematopoiesis. *Frontiers in Cell and Developmental Biology*, *6*(JUL), 80. https://doi.org/10.3389/FCELL.2018.00080/BIBTEX

Yokomizo, T., Ogawa, M., Osato, M., Kanno, T., Yoshida, H., Fujimoto, T., Fraser, S., Nishikawa, S., Okada, H., Satake, M., Noda, T., Nishikawa, S. I., & Ito, Y. (2001). Requirement of Runx1/AML1/PEBP2alphaB for the generation of haematopoietic cells from endothelial cells. *Genes to Cells : Devoted to Molecular & Cellular Mechanisms*, *6*(1), 13–23. https://doi.org/10.1046/J.1365-2443.2001.00393.X

Yosef, N., Vadakkan, T. J., Park, J. H., Poché, R. A., Thomas, J. L., & Dickinson, M. E. (2018). The phenotypic and functional properties of mouse yolk-sac-derived embryonic macrophages. *Developmental Biology*, *442*(1), 138–154. https://doi.org/10.1016/J.YDBIO.2018.07.009

Yu, S., Luo, F., & Jin, L. H. (2021). Rab5 and rab11 maintain hematopoietic homeostasis by restricting multiple signaling pathways in drosophila. *ELife*, *10*, 1–23. https://doi.org/10.7554/ELIFE.60870

Zeitlinger, J., Kockel, L., Peverali, F. A., Jackson, D. B., Mlodzik, M., & Bohmann, D. (1997). Defective dorsal closure and loss of epidermal decapentaplegic expression in Drosophila fos mutants. *EMBO Journal*, *16*(24), 7393–7401. https://doi.org/10.1093/emboj/16.24.7393

Zhang, F., Wang, H., Wang, X., Jiang, G., Liu, H., Zhang, G., Wang, H., Fang, R., Bu, X., Cai, S., & Du, J. (2016). *TGF-β induces M2-like macrophage polarization via SNAIL-mediated suppression of a pro-inflammatory phenotype* (Vol. 7, Issue 32). www.impactjournals.com/oncotarget

Zhang, S., Amourda, C., Garfield, D., & Saunders, T. E. (2018). Selective Filopodia Adhesion Ensures Robust Cell Matching in the Drosophila Heart. *Developmental Cell*, *46*(2), 189-203.e4. https://doi.org/10.1016/J.DEVCEL.2018.06.015/ATTACHMENT/1CE65205-B6D7-432B-A3C4-46E26954441D/MMC1.PDF

Zhang, Y., Feng, X. H., & Derynck, R. (1998). Smad3 and Smad4 cooperate with c-Jun/c-Fos to mediate TGF-β-induced transcription. *Nature 1998 394:6696*, *394*(6696), 909–913. https://doi.org/10.1038/29814

Zhou, L., Hashimi, H., Schwartz, L. M., & Nambu, J. R. (1995). Programmed cell death in the Drosophila central nervous system midline. *Current Biology*, *5*(7), 784–790. https://doi.org/10.1016/S0960-9822(95)00155-2

Zouani, O. F., Gocheva, V., & Durrieu, M. C. (2014). Membrane Nanowaves in Single and Collective Cell Migration. *PLOS ONE*, *9*(5), e97855. https://doi.org/10.1371/JOURNAL.PONE.0097855